Investigating the regulation of B cell growth and survival genes by Epstein-Barr virus

Sarika Jayant Khasnis

A thesis submitted to the University of Sussex for the degree of Doctor of Philosophy

September 2018

UNIVERSITY OF SUSSEX

Declaration

I hereby declare that this thesis, whether in the same or different form, has not been previously submitted to this or any other University for the award of a degree. The work described here is my own except where otherwise stated.

Sarika Jayant Khasnis

September 2018

Acknowledgements

I'd like to thank my supervisor, Prof Michelle West, for giving me the opportunity to be a PhD student in her laboratory and for guiding me on my project. I also thank her for all the precious suggestions, useful criticism and encouragement she offered all through my work.

I extend my thanks to Prof Jane Endicott and Dr Helfrid Hochegger for giving useful insights into my project. I thank all my lab members and PhD friends Dr Michèle Brocard, Dr Andrea Gunnell, Helen Webb, Ankana, Stephy, Jake, Barak, Rob, Anja and Lina for all their support in the last four years.

I would like to extend my sincere gratitude to Yaqi Zhou, Dr Nisha Peter, Dr David Wood, Dr Rajaei Almohammed and Hilda Veenstra for making life in the lab more cherishable. You all made writing away from lab less stressful. A special thanks to Maria from Hochegger lab, who was always happy to answer my questions.

A big thank to Dr Muzaffar Ali and Dr Rajesh Ponnusamy for helping me out in difficult times and for all the brainstorming science sessions that we have had over coffee. Thank you for always motivating me and patiently answering my questions.

A special thank to my friend Amruta Shrikhande (PhD soulmate) who has always been there to guide and support me all through the years at Sussex right from the thought of applying for a PhD. Life at Sussex was never the same without her.

Finally, I thank my parents, brothers, my uncle (Ajay) and aunt (Sharmila) for their continuous support and encouragement. I would also like to thank my Fiancé Nithin Gangadhar for his everlasting love and faith in me and who helped me stay calm during stressful times over the last four years.

This work was funded by Chancellor's Research International Scholarship, University of Sussex.

UNIVERSITY OF SUSSEX

Sarika Jayant Khasnis

Doctor of Philosophy

Investigating the regulation of B cell growth and survival genes by Epstein-Barr virus

Summary

The cancer-associated Epstein Barr virus (EBV) infects and immortalises B cells and alters the expression of numerous cellular genes involved in the regulation of cell cycle and multiple growth and survival pathways. We investigated cell cycle regulation by EBV focusing on RGC-32, a cell cycle regulator that is translationally upregulated in EBV-infected cells. RGC-32 interacts with two mitotic kinases, cyclin-dependent kinase 1 (CDK1) and polo-like kinase 1 (PLK1) and overexpression of RGC-32 in B cells disrupts cell cycle arrest. Using Surface Plasmon Resonance and Microscale Thermophoresis (MST) and recombinant proteins, we demonstrated that RGC-32 directly interacts with CDK1. The affinity of this interaction is increased in the presence of Cyclin B1. Pull-down studies also identified the kinetochore subunit Spc24-25 as a new binding partner of RGC-32 and we confirmed this interaction using recombinant proteins and MST. The role of RGC-32 in regulating the G2/M transition was investigated using live-cell imaging. We generated a stable transgenic 'knock-in' RGC-32 inducible cell line in an ATP analogue-sensitive CDK1 background. Using this cell line arrested in G2 through CDK1 inhibition by the ATP analogue we demonstrated the ability of RGC-32 to promote mitotic entry and activate CDK1 *in vivo*. CDK1 activation was associated with decreased 'inactivating' phosphorylation on tyrosine 15 of CDK1.We also identified the B-cell receptor (BCR) signalling pathway to be potentially targeted by the EBV transcription factors Epstein-Barr virus nuclear antigens (EBNA) 2, 3A, 3B and 3C. To confirm regulation of BCR genes bound by these EBNAs, we performed gene expression profiling. We showed that *CD19, SYK, LYN, INPP5D, PIK3R1, PIK3R3, PIK3R5* are regulated by EBNA2 and EBNA3s. Our data demonstrated transcriptional repression of the PI3K-AKT pathway genes and decreased 'activating' phosphorylation of Akt by EBNA2, EBNA3A and EBNA3C.

Our data provide new insights into B cell reprogramming by EBV.

Abbreviations

ADP	Adenosine diphosphate
AS	ATP-analogue sensitive
ATM	Ataxia-telangiectasia-mutated
ATP	Adenosine triphosphate
ATR	Ataxia telangiectasia and Rad3-related
BAX	Bcl-2-associated x protein
BCR	B cell receptor
BL	Burkitt's lymphoma
bp	Base pairs
Ca^{2+}	Calcium
$CaCl_2$	Calcium chloride
CAK	CDK-activating kinase
CCAN	Constitutive centromere associated network
cdc	Cell division cycle
CDK	Cyclin-dependent Kinase
cDNA	Complimentary DNA
CENP	Centromere protein
ChIP	Chromatin Immunoprecipitation
ChIP-seq	Chromatin Immunoprecipitation sequencing
Chk	Checkpoint kinase
Cks	Cyclin dependent kinase subunit
CLL	Chronic lymphocytic leukemia
Cp	C promoter
CREB	cAMP response element-binding protein
CRS	Cytoplasmic retension sequence
DAPI	4',6-diamidino-2-phenylindole
DLBCL	Diffuse large B cell lymphoma
DMEM	Dulbecco modified eagles medium
DMSO	Dimethyl sulphoxide
DNA	Deoxyribonucleic acid
Dox	Doxycycline
DSB	Double strand break
E.Coli	Escherichia coli
EBER	Epstein-Barr virus encoded RNA
EBNA	Epstein-Barr nuclear antigen
EBNA LP	Epstein-Barr nuclear antigen leader protein
EBV	Epstein-Barr Virus
ECL	Enhnaced chemiluminescence
EDTA	Ethylene diamine tetraacetic acid
FACS	Fluorescence-activated cell sorting
FBS	Fetal bovine serum
FBS	Fetal bovine serum
g	Centrifugal force constant
GFP	Green fluorescent protein
gRNA	Guide RNA

GST	Glutathione-S-Transferase
H3K27ac	Histone 3 lysine 27 acetylation
H3K27me3	Histone 3 lysine 27 trimethylation
H3K4me3	Histone 3 lysine 4 trimethylation
HEK	Human embryonic kidney cells
HL	Hodgkin's lymphoma
HT	Hydroxytamoxifen
IgH	Immunoglobulin heavy chain
IgL	Immunoglobulin light chain
IM	Infectious mononucleosis
INK	Inhibitors of CDK
IP	Immunoprecipitation
IPTG	Isopropylthio-β-galactoside
ITAM	Immunoreceptor tyrosine-based inhibition motif
kDa	Kilo dalton
KMN	Knl1-Mis12 complex-Ndc80 complex
KO	Knockout
LCL	Lymphoblastoid cell line
LMP	Latent membrane protein
MDM2	Mouse double minute 2 homolog
$MgCl_2$	Magnesium chloride
MST	Microscale Thermophoresis
NES	Nuclear export signal
NLS	Nuclear localisation signal
NP-40	Nonident P40
NPC	Nasopharyngeal carcinoma
oriP	Origin of latent DNA replication
PAM	Protospacer adjacent motif
PBD	Polo box domain
PBS	Phosphate-buffered saline
PCR	Polymerase chain reaction
PHYRE	Protein homology/analogy recognition engine
PI3K	Phosphoinositide 3-kinase
PIC	Protease inhibitor Cocktail
PLK1	Polo-like kinase 1
PMSF	Phenylmethylsulphonyl fluoride
pRB	Retinoblastoma protein
PRC	Polycomb repressor complex
PTLD	Post transplant lymphoproliferative disease
Qp	Q promoter
Rev	Revertant
RGC-32	Response gene to complement 32
RNA	Ribonucleic acid
RNAi	RNA interference
RPE	Human retinal pigmented epithelium cells
rpm	Revolutions per minute
RU	Response units
SDS-PAGE	Sodium dodecyl sulphate polyacrylamide gel electrophoresis
Ser	Serine
siRNA	Small interfering RNA

Spc	Spindle pole component
SPR	Surface plasmon resonance
TCEP	Tris 2-carboxyethyl phosphine
TCL	Total cell lysate
Thr	Threonine
TRAF	TNF receptor interacting protein CNN-1
Tyr/Y	Tyrosine
Wp	W promoter
WT	Wild type
wtBAC	Wild type bacmid
X. laevis	*Xenopous Laevis*

Table of Contents

1 Introduction

1.1 The Cell Cycle

The cell cycle is a highly regulated series of events that allows a eukaryotic cell to reproduce. It consists of two main discrete stages called the Synthesis (S) phase and the Mitotic (M) phase. These two phases are separated by Gap (G1 & G2) phases. During the synthesis phase, DNA is duplicated by replication of its two complementary strands, a process that is regulated by the replication machinery (Meselson and Stahl, 1958). Duplicated chromosomes (sister chromatids) are held together by a ring-shaped protein complex called cohesin.

Mitosis is further subdivided into five different phases: prophase, prometaphase, metaphase, anaphase and telophase. In prophase, chromatids condense, and the centrosomes duplicate and migrate to the poles forming spindle poles. The transition into prometaphase is marked by nuclear envelope breakdown (NEB), which allows the microtubules to make contact with the chromosomes (Cheeseman and Desai, 2008). During metaphase, the sister chromatids align in a midzone called the metaphase plate. This is followed by the sister chromatids being pulled apart as a result of depolymerisation of kinetochore-microtubule complexes in anaphase. Lastly, anaphase is followed by telophase where the chromosomes de-condense and one of each sister chromatid pair is distributed to the daughter cell after that the nuclear envelope reforms (Morgan, 2007).

The gap (G1 & G2) phases provide time for cell growth and serve as an important regulatory transition in which the progression into the next stage is controlled. Cells cannot proceed into the next phase if the process from the previous phase is not

completed. During G1 phase, the cells decide whether to enter the next cell cycle and coordinate the molecular signals for DNA synthesis or choose to enter the G0 phase where they become senescent (reviewed in (Vermeulen *et al.*, 2003)). In G2 phase, the cells prepare to enter mitosis. During this phase, Cyclin A and Cyclin B are synthesised and any DNA damage that might have occurred during S phase is repaired. The cell cycle is highly regulated by four different checkpoints: G1/S, intra-S, G2/M and the mitotic spindle checkpoint (Barnum and O'Connell, 2014). Each of these checkpoints has an important role in the cell cycle which is discussed in the following paragraphs.

The G1/S checkpoint makes sure that the cells have achieved sufficient growth without any DNA damage. The intra S checkpoint ensures that DNA replicates without any faults. The G2/M checkpoint verifies the completion of DNA replication and determines whether there is any DNA damage before the cell proceeds into M phase. Finally, the mitotic spindle checkpoint verifies whether the spindle is completely assembled, and the kinetochores of sister chromatids have been attached correctly to the opposite spindle poles for segregation (reviewed in (Vermeulen *et al.*, 2003)).

The essential components involved in the cell cycle regulation are the cyclin-dependent kinases (Cdks) and cyclins. Cdks are serine/threonine kinases that are activated by binding to a specific cyclin (reviewed in (Malumbres and Pérez De Castro, 2014)). Various Cdks are present throughout the cell cycle but the oscillation in their activity is primarily due to the changes in the amounts of specific cyclins which are synthesised and subsequently degraded by ubiquitin-mediated proteolysis. For example, in G0 phase, expression of cyclin D needs to be upregulated for the quiescent cell to enter the cell cycle. It forms a complex with CDK 4/6 which induces the expression of cyclin E.

Binding of cyclin E to CDK2 promotes G1/S transition (Blagosklonny and Pardee, 2002). In S phase, however, CDK2 binds to cyclin A which is required for progression through S phase. Cyclin A also has the ability to bind CDK1 during the G2 phase which then dissociates and binds to cyclin B for the progression through the G2/M checkpoint (reviewed in (Vermeulen *et al.*, 2003)) (**Figure 1.1**).

Another important family of proteins that play a role in cell cycle regulation is the CDK inhibitors (CKI). These proteins negatively regulate CDK activity (Peter and Herskowitz, 1994). The CDKIs are classified into two families based on sequence homology and target inhibition: The CIP/KIP family comprising $p21^{WAF1/CIP1}$, $p27^{KIP1}$, $p57^{KIP2}$ and the INK4 family comprising $p16^{INK4A}$, $p15^{INK4C}$, $p19^{INK4D}$. The CIP/KIP inhibitors inhibit the activity of CDK-cyclin complex whereas INK4 inhibitors prevent the association of CDK with their cyclin partner (Morgan, 1997, Sherr and Roberts, 1999).

1.1.1 The G1/S Checkpoint

At the G1/S checkpoint, cell-cycle arrest induced by DNA damage occurs via ATM (ATR)/CHK2 (CHK1)–p53/MDM2-p21 pathway. The protein kinases, Ataxia-telangiectasia-mutated (ATM) and ATM-Rad3-related (ATR) are critical regulators of DNA damage response. ATR responds primarily to DNA damage mainly at the replication forks, whereas ATM is activated primarily to DNA double-strand breaks (DSBs). Upon DNA damage, these kinases are recruited at the break sites followed by

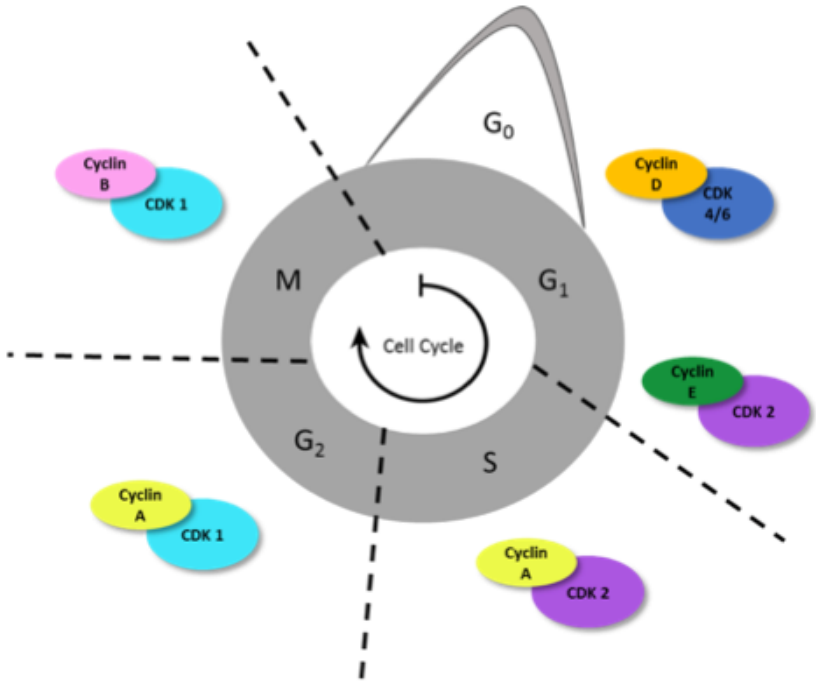

Figure 1.1 The mammalian cell cycle.
Cell cycle is a unidirectional event consisting of different phases. The cell grows in three phases. In G1 & G2 phase the cell grows in size whereas, in S phase, DNA is replicated. In M phase, the cell divides into two daughter cells. The unidirectional progression of cells from one phase to the other is dependent on the association of specific Cyclins with Cyclin Dependent Kinase (CDKs).

cell cycle arrest and DNA repair (reviewed in (Awasthi *et al.*, 2016)). ATM and ATR further phosphorylate p53 to activate downstream signalling cascade. Phosphorylated p53 cannot bind to ubiquitin ligase MDM2 resulting in stabilisation and accumulation of p53 protein (reviewed in (Kastan and Bartek, 2004)). p53 acts as a transcriptional activator of various genes such as $p21^{WAF1/CIP1}$, MDM2 (Mouse Double Minute 2 homolog) and BAX (Bcl-2-associated X protein) (Agarwal *et al.*, 1998). Active p53 induces $p21^{WAF1/CIP1}$ transcription which then silences CDK2/cyclin E complex and results in G1 arrest (Sherr and Roberts, 1999). Furthermore, silencing of CDK2/ cyclin E keeps the Retinoblastoma (Rb) protein activated which associates with the E2F transcription factor causing sustained G1 blockade (reviewed in (Kastan and Bartek, 2004)).

1.1.2 Activation of the CDK1-Cyclin B complex

The CDK1-Cyclin B complex plays a key role in the regulation of mitosis. Investigations into the genes that regulate cell size at cell division led to the identification of M phase-promoting factor (MPF) (Masui and Markert, 1971, Smith and Ecker, 1971). Subsequent studies revealed the components of MPF to be CDK1 and cyclin B (Lohka *et al.*, 1988). The CDK1-Cyclin B complex remains inactive until late G2 (Lindqvist *et al.*, 2007). Cyclin B binding is required for CDK1 activation, but it is not sufficient for complete activation of CDK1. After cyclin binding, the CDK-activating kinase (CAK) phosphorylates CDK-cyclin complex at conserved threonine residue within the T loop (Thr161, CDK1; Thr160, CDK2; Thr172 CDK4) (Draetta, 1993, Ji and T., 2013, Liu and Kipreos, 2013) (**Figure 1.2**).

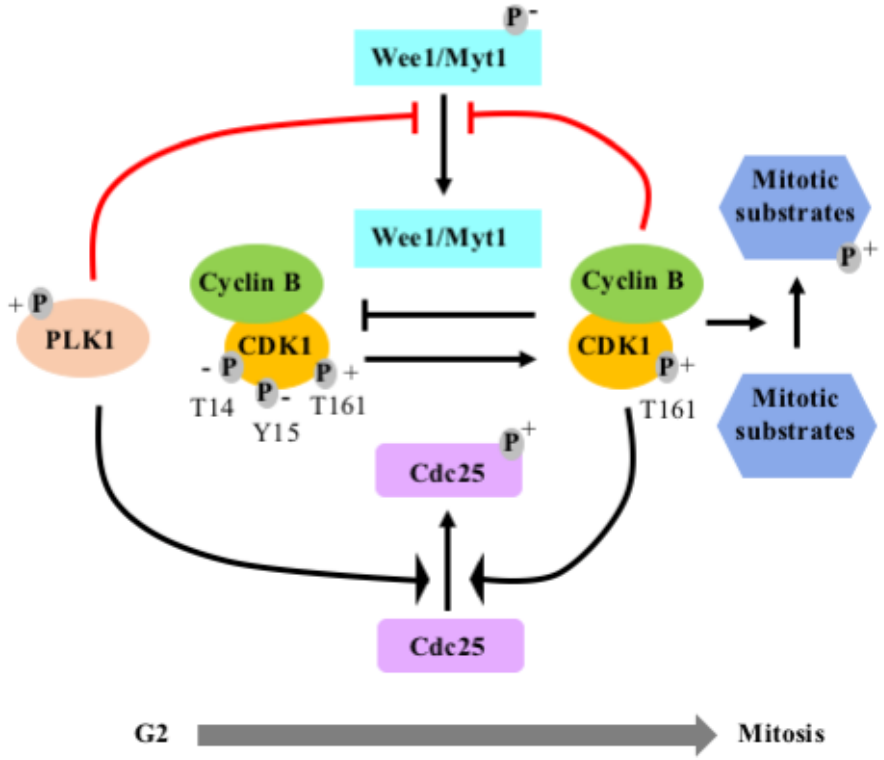

Figure 1.2 Activation of CDK1-Cyclin B via a feedback loop.
Schematic representation of Cyclin B-CDK1 activation at mitotic entry. Cyclin B binds with CDK1 and the complex is fully activated by CAK by phosphorylation at Thr161 (Kaldis, 1999). Inhibitory phosphorylation by Wee1/Myt1 on T14 (Thr14) and Y15 (Tyr15) keeps this complex inactive (Nurse and Thuriaux, 1980, Mueller et al., 1995). During the G2/M transition, Cdc25 phosphatase removes the inhibitory phosphorylation on T14 and Y15 to activate the CDK1-Cyclin B complex which then phosphorylates its mitotic substrates (Gautier et al., 1991). As a result, CDK1 activates Cdc25 and inhibits Wee1/Myt1 via phosphorylation thereby creating a feedback loop. PLK1 also promotes activation of CDK1-Cyclin B complex by activating Cdc25 and targeting Wee1/Myt1 for ubiquitin-mediated degradation (Kumagai and Dunphy, 1996, Watanabe et al., 2004, Inoue and Sagata, 2005).

These active complexes are kept inert by phosphorylation on two key residues on CDK1, Thr14 and Tyr15 that are located within the ATP binding domain (Gu *et al.*, 1992, Welburn *et al.*, 2007). Functional studies in *Schizosaccharomyces Pombe* (fission yeast) identified the Wee1 kinase playing a role in coordinating cell size with the cell cycle. This kinase was found to prevent cells of smaller size from entering mitosis. In humans, Wee1 only phosphorylates Tyr15 of CDK1 (Nurse and Thuriaux, 1980, Parker *et al.*, 1991, Parker and Piwnica-Worms, 1992, McGowan and Russell, 1993). Another kinase Myt1 was found to phosphorylate Thr14 and Tyr15 residues in *Xenopus leavis* cdc2 and this kinase is well conserved in humans. Both Wee1 and Myt1 are regulated by phosphorylation and localisation (Mueller *et al.*, 1995, Fattaey and Booher, 1997). At the G2/M transition, CDK1-Cyclin B initiates a negative feedback loop by phosphorylating Wee1 at Ser123 which then initiates a cascade of events for degradation of Wee1. Phosphorylation of Ser123 provides a docking site for PLK1 which further phosphorylates Wee1 at Ser53 resulting into its degradation by β-TrCP (reviewed in (Perry and Kornbluth, 2007)). Wee1 is also known to promote its activity via autophosphorylation of two tyrosine residues (Katayama *et al.*, 2005).

During mitotic entry, the Cdc25 phosphatase activates CDK1 by removing the inhibitory phosphorylation on Thr14 and Tyr15. Cdc25 is a dual specificity phosphatase that regulates both G1/S and G2/M transition. In higher eukaryotes, there are three Cdc25 genes, Cdc25A which predominantly regulates the G1/S transition and Cdc25 B and C which are involved in the G2/M transition (Gautier *et al.*, 1991, Hoffmann *et al.*, 1994, Jinno *et al.*, 1994, Blomberg and Hoffmann, 1999, Chen *et al.*, 2001). However, studies have shown that Cdc25A can activate CDK1-Cyclin B in the absence of Cdc25B and Cdc25C (Lindqvist *et al.*, 2005). During the G2/M transition, Cdc25 is phosphorylated at

Thr130 by PLK1 which releases it from the inhibitory binding to 14-3-3 proteins. However, complete activation of Cdc25 is only achieved upon phosphorylation of Ser214 of Cdc25 by CDK1-Cyclin B. This promotes protein-protein interaction (PPI) mediated dephosphorylation of Ser287. Together, CDK1-Cyclin B regulated positive and negative feedback loops ensure activation of activators and inhibition of inhibitors thereby amplifying activation of CDK1 leading to mitotic entry (**Figure 1.2**) (reviewed in (Perry and Kornbluth, 2007)).

1.1.3 Structure of CDK1-Cyclin B complex

The crystal structure of human CDK1 bound to Cks1 determined at 2.6 Å resolution (PDB 4YC6) shows the monomeric CDK1 to adopt a short α-helical structure with the c-helix displaced out of the active site (Brown *et al.*, 2015). The activation segment of CDK is incapable of adopting a conformation in its non-phosphorylated state. For substrate binding, the 'T-loop' needs to undergo conformational changes by binding to cyclin partner followed by active phosphorylation on Thr residue (Thr 161, CDK1; Thr 160, CDK2; Thr172. CDK4) (Draetta, 1993, Ji and T., 2013, Liu and Kipreos, 2013).

The crystal structure of the human CDK1 in complex with Csk2 and cyclin B was elucidated at 2.7 Å resolution (PDB 4YC3) (Brown *et al.*, 2015). The structure shows one molecule of each of the three protein partners forming a ternary complex. Cyclin B and Csk2 bind to different regions of CDK1, almost diametrically opposite. It further highlights the reorientation of C-helix of CDK1 upon binding to cyclin B (**Figure 1.3A**). The binding shows an opening at the interface associated with a twist between the two proteins. As a result, fewer interactions are made between CDK1 and cyclin B. Additionally, CDK1 forms a short β-hairpin with residue F153 and G154 that sits within

the hydrophobic groove of cyclin B creating a solvent filled cleft between CDK1 and cyclin B. The activation segment of $CDK1_{(146\text{-}173\ aa)}$ shows a disordered region that requires considerable rearrangement for peptide substrate recognition when bound to cyclin B (Petri *et al.*, 2007, Brown *et al.*, 2015).

CDK1 and CDK2 share 65% of the sequence identity (Brown *et al.*, 2015). However, the mechanism of their binding to respective cyclin partners varies, which governs their preference towards substrates. For example, the activation segment of CDK2 adopts a conformation that requires little rearrangement as a result of organised catalytic residues within the active site (Jeffrey *et al.*, 1995). Moreover, binding of CDK2 with cyclin A forms a large binding interface that is 30% greater than that of CDK1-Cyclin B (**Figure 1.3B**). In fact, the interaction interface of CDK2-CyclinA is also greater than that of CDK4-Cyclin D3 (**Figure 1.3C)**. Interestingly, binding of cyclin D3 to CDK4 is not sufficient to drive active conformation of CDK4 (Takaki *et al.*, 2009). The C-helix of CDK4 remains displaced from the active site with the activation segment making no contact with cyclin D3 subunit. Irrespective of phosphorylation and binding to cyclin D, CDK4 is unable to perform catalysis (Day *et al.*, 2009). Overall, by comparing the structure of different CDK-Cyclin complexes, a diverse response by CDK is observed upon cyclin binding.

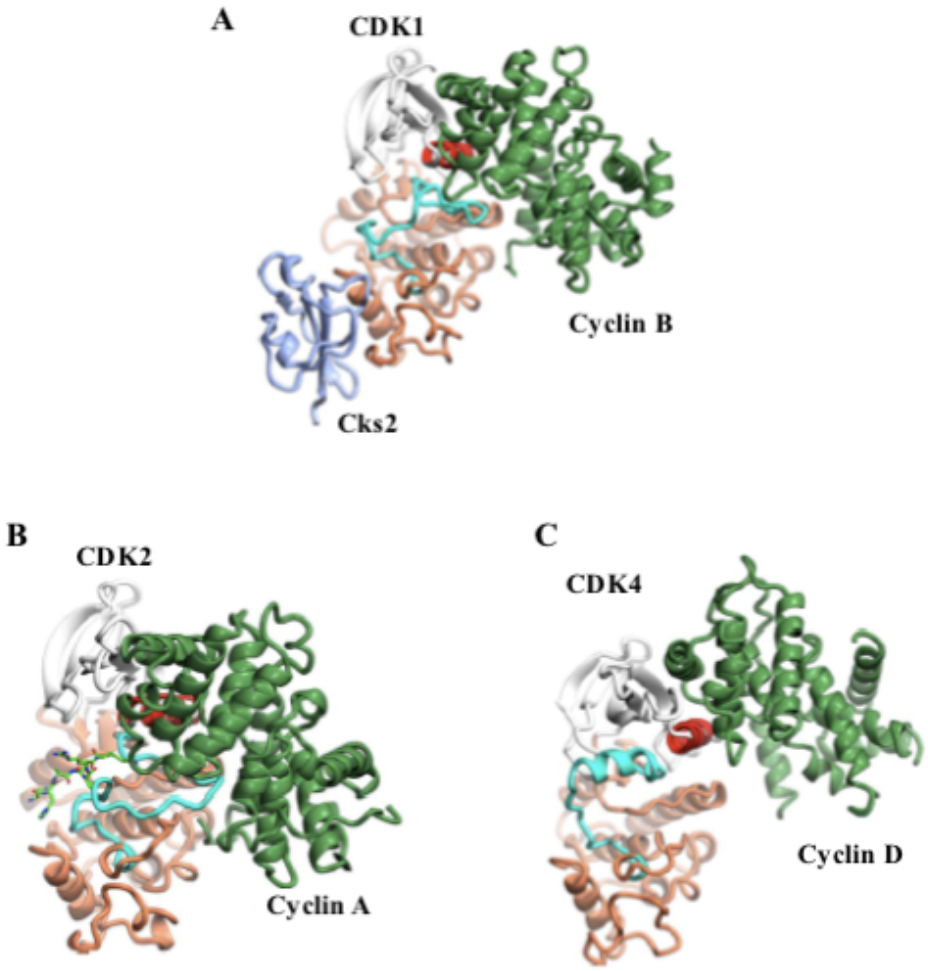

Figure 1.3 Comparison of the CDK1-Cyclin B-Cks2 structure with the CDK2-Cyclin A and CDK4-Cyclin D3 structure.
The complexes are shown in front view (A) CDK1-cyclin B-Cks1 (PDB 4YC3) (B) CDK2-cyclin A (PDB 1FIN) (C) CDK4-cyclin D3 (PDB 3G33). CDK N- and C-terminal lobes are coloured in white and coral respectively, with the activation segment coloured in cyan and the C-helix is coloured in red. Cyclin subunits are coloured green and the Cks subunit is coloured in ice blue (adapted from (Brown *et al*., 2015)).

1.1.4 The G2/M Checkpoint

The G2/M checkpoint is activated when cells experience DNA damage during the G2 phase. The CDK1-Cyclin B complex is a critical target of the G2/M checkpoint (reviewed in (Kastan and Bartek, 2004)). DNA damage induces the activation of the ATM/ATR pathway and the p53 pathway. ATM and ATR phosphorylate and activate their downstream activator kinases, Chk2 and Chk1 respectively. Chk kinases phosphorylate Ser216 of Cdc25 phosphatase and promote its binding to 14-3-3 proteins, thereby sequestering it outside the nucleus and inhibiting its activity (reviewed in (Vermeulen *et al.*, 2003)). As Cdc25 phosphatase is known to activate CDK1 at the G2/M boundary, by removing inhibitory phosphates on CDK1, inactivation of Cdc25 leads to accumulation of inactive CDK1 causing G2 blockade. Moreover, studies have shown that p53 promotes the binding of 14-3-3 proteins to CDK1-Cyclin B leading to its sequestration in the cytoplasm (Hermeking *et al.*, 1997, Chan *et al.*, 2000).

1.1.5 Mitotic Entry

Once the G2/M checkpoint is resolved, mitotic entry is initiated by activation of CDK1-Cyclin B complex via multiple feedback loops. CDK1-Cyclin B complexes are mostly cytoplasmic and upon activation, they localise to the nucleus and accumulate at the centrosomes. Cyclin B is known to shuttle between the nucleus and cytoplasm as a consequence of phosphorylation on serine residues in the cytoplasmic retention sequence (CRS) or the nuclear export signal (NES). PLK1 phosphorylates Ser133 and Ser147 residues of cyclin B and promotes its nuclear translocation. Phospho-mutants of these residues S133A and S147A resulted in cytoplasmic retention of cyclin B in prophase (Toyoshima-Morimoto *et al.*, 2001). In addition, recent studies found PLK1 mediated

active phosphorylation of Ser75 in Cdc25C leads to activation of the CDK1-Cyclin B complex (Gheghiani *et al.*, 2017). Once the threshold for active CDK1-Cyclin B is achieved, CDK1 phosphorylates Lamin proteins resulting in nuclear envelope breakdown. It also phosphorylates proteins that initiate substantial changes in chromatin and chromosomal structure essential for entry into mitosis (reviewed in (Foley and Kapoor, 2013). Overall, regulatory phosphorylation and localisation of serine/threonine protein kinases is crucial for cells to commit to mitosis in a tightly regulated manner.

1.2 The Kinetochore

Kinetochores are proteinaceous complexes made up of more than 100 different proteins which hierarchically assemble on the centromere during prophase (Gascoigne *et al.*, 2011). They are found on the outer surface of the centromere on each chromatid during mitosis. These large molecular machines serve as a platform to physically link the chromosome to microtubules (**Figure 1.4**).

Electron Microscopy studies of mammalian kinetochores have revealed that kinetochores are made up of two regions, the thin inner plate and thick outer plate (Rieder, 1982). The inner plate acts as a stabiliser through contacts with centromeric chromatin and the outer plate provides a surface for microtubule attachment. The constitutive centromere-associated network (CCAN) localises to the inner kinetochore. The components of CCAN then recruits the complexes forming the KMN (**K**NL1 complex, **M**is12 complex and **N**DC80 complex) network which localises to the outer kinetochore (Cheeseman and Desai, 2008, Gascoigne *et al.*, 2011).

Within the KMN network, the NDC80 complex has emerged as a crucial component of the kinetochore machinery. This complex is conserved from fungi to humans and is

known to play a key role in kinetochore-microtubule attachment (**Table 1.1**). It is also involved in the recruitment of the SAC (Spindle Assembly Checkpoint) proteins Mad1, Mad2 and Mps1 to unattached kinetochores and depletion of the NDC80 complex abrogates the SAC (reviewed in (Ciferri *et al.*, 2007)). The NDC80 complex is formed of four protein subunits, NDC80/Hec1, Nuclear filamentous 2 (Nuf2), Spindle pole component 24 and 25 (Spc24-Spc25) (**Figure 1.4**). These four proteins form a rod-like structure with globular heads at each end. The NDC80/Hec1 and Nuf2 form a sub-complex at one end which localises to the outer kinetochore whereas Spc24-Spc25 form a sub-complex at the other end localising to the inner kinetochore (Cheeseman and Desai, 2008).

Kinetochores are involved in two fundamental mechanisms, firstly they confirm the correct kinetochore-microtubule attachment and secondly they ensure synchronisation of complete kinetochore-microtubule attachment with progression of cell cycle (Santaguida and Musacchio, 2009). In budding yeast, histone-fold protein Cnn-1 (human homologue CENP-T) interacts with the Spc24-25 subunit by binding at the hydrophobic pocket in the globular domain of Spc24-25. This interaction is important for the attachment of the kinetochore to microtubules (Malvezzi *et al.*, 2013). Furthermore, structural studies using CENP-T from *Gallus Gallus* (chicken) reveals the α-helical region of CENP-T to associate closely with β-sheet of Spc25 (**Figure 6.5B**). Hydrophobic residues in Spc24-25 are critical for this interaction. In addition phosphorylation on the N-terminus of chicken CENP-T by CDK1 improves its binding affinity for Spc24-25 (Nishino *et al.*, 2013).

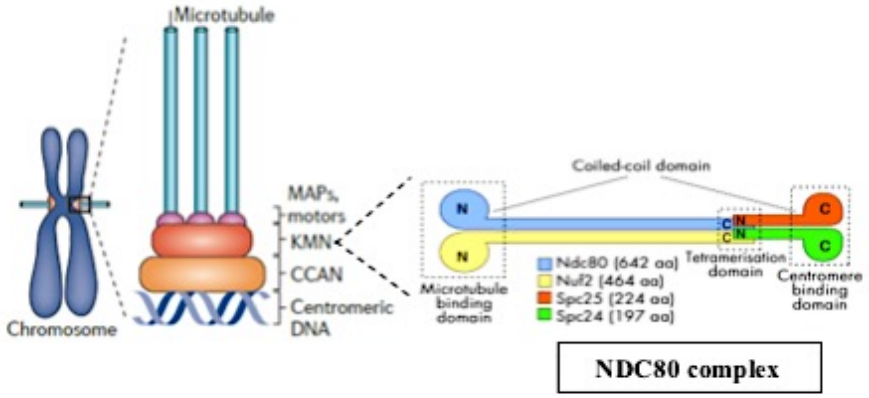

Figure 1.4 Structure of the Kinetochore.
Schematic representation of kinetochore organisation onto the centromere: The two main components of the kinetochore that make the inner plate and outer plate are constitutive centromere associated network (CCAN) and KMN network. The KMN network consists of the KNL1 complex, the Mis12 complex and the NDC80 complex. The structure of the NDC80 complex from the KMN is overall rod-like in shape: The N-terminal globular domain consists of NDC80 and Nuf2 complex poised at the outer kinetochore whereas the C-terminal is made up of Spc-24/25 and lies proximal to the chromosome (Santaguida and Musacchio, 2009, Lampert and Westermann, 2011).

Complex	*H. sapiens*	*S. cerevisiae*	*S.pombe*
CENP-T	CENP-T	Cnn-1	SBPC800/Cnp20
CENP-A nucleosome	CENP-A	Cse4	Cnp1
	CENP-B	-	Abp1, Cbh1, Cbh2
Knl1 complex	KNL1/Blinkin	Spc105	Spc7
	Zwint	YDR532c	Sos7
Mis 12 complex	MIS12	Mtw1	Mis12
	DSN1	Dsn1	Mis13
	NNF1	Nnf1	Nnf1
	NSL1	Nsl1	Mis14
Ndc80 complex	NDC80	Ndc80	Ndc80
	NUF2	Nuf2	Nuf2
	SPC24	Spc24	Spc24
	SPC25	Spc25	Spc25

Table 1.1 showing the conserved components of the inner kinetochore from yeast to humans (adapted from (Santaguida and Musacchio, 2009)).

1.3 Epstein Barr Virus (EBV)

Epstein Barr Virus is a human lymphotropic gamma-1 herpesvirus which infects over 90% of the worldwide population. It was first isolated in 1964 in B lymphocytes derived from an African Burkitt's Lymphoma (BL) (Epstein *et al.*, 1964) and was the first herpes virus to have its whole genome sequenced. EBV preferentially infects resting B cells as a persistent latent infection resulting in immortalisation of B-lymphocytes. To date it has been associated with numerous human cancers including Burkitt's lymphoma (BL), Hodgkin's lymphoma, nasopharyngeal carcinoma (NPC), gastric carcinoma, post-transplant lymphoproliferative disease (PTLD), AIDS-associated B-lymphoma and diffuse large B-cell lymphoma (DLBCL) (reviewed in (Young and Murray, 2003, Hong *et al.*, 2015, Young *et al.*, 2016). Like all other herpes viruses, EBV also has two phases in its life cycle: a dormant life phase also known as latent phase and an acute productive phase also known as the lytic phase. In latency, the virus maintains its genome persistently in infected cells whereas, during lytic phase, new viral particles are produced after the DNA has been replicated and packed in virions (reviewed in (Murray and Young, 2001).

There are two types of EBV, type 1 also known as type A (e.g. B95-8 strain) and type 2 also known as type B (e.g. AG876 strain). These two types are mainly classified based on variance in their DNA sequence of the EBNA2 latent gene (Adldinger *et al.*, 1985). Both types also differ in the sequence of other important latent genes, EBNA3A, EBNA3B, and EBNA3C (Sample *et al.*, 1990). These EBV latent genes are explained in detail in the following section. Type I is more prevalent in the West whereas 1 and 2 are equally found to be prevalent in Africa and Papua New Guinea. Recent studies suggest type 2 EBV to be dominant in Mexico (Tzellos and Farrell, 2012, Farrell, 2015).

Interestingly, studies have shown type 1 EBV to transform and immortalise B cell more efficiently than type 2, highlighting the role of EBNA2 in B cell transformation (Rickinson *et al.*, 1987).

Like all other herpesviruses, EBV has a naked double-stranded DNA core enclosed in a nucleocapsid. The size of the virion ranges between 120-260 nm. The nucleocapsid is further surrounded by a lipid layer composed of viral glycoprotein spikes namely gp350, gp150, gp42, gH, gB and gL. These glycoprotein spikes are used by the virus to attach and infect the host cell (Longnecker *et al.*, 2013, Pellet and Roizman, 2013). Although EBV preferentially infects B cells, it has the ability to infect epithelial cells mediated by the Ephrin receptor A2 (EphA2) on the epithelial cells (Zhang *et al.*, 2018). Recent studies also show EBV type 2 to exploit T cells by infecting them and establishing an additional latency reservoir (Coleman *et al.*, 2015, Coleman *et al.*, 2017, Zhang *et al.*, 2018).

1.3.1 EBV Genome

The complete sequence of the EBV genome was originally obtained by sequencing BamHI digested fragments of the B95-8 strain of EBV (Baer *et al.*, 1984). The BamHI fragments were given alphabetical letters (A-Z) based on the size of the fragment with 'A' being the largest fragment and 'Z' being the smallest. The various ORF were named based on their location and orientation of transcription within the BamHI digested fragment (Longnecker *et al.*, 2013).

The EBV genome is a linear, double-stranded DNA approximately 172 Kb in length which circularises upon infection and is detectable 20 hours post infection (reviewed in

(Kempkes and Robertson, 2015)). Circularisation of the genome occurs via fusion of the two-terminal repeat ends of the linear DNA. The EBV genome encodes approximately ninety genes. Out of these, only 11 coding genes in addition to several miRNAs are expressed when primary B cells are infected by EBV in culture generating lymphoblastoid cell lines (LCLs). These genes play a crucial role in EBV immortalisation (reviewed (Murray and Young, 2001, Young and Rickinson, 2004)). Expression of EBV latent genes is driven from several promoters: the LMP and the W, C, and Q promoters (**Figure 1.5**) (reviewed in (Young and Rickinson, 2004)). The transcription of the six EBV nuclear antigens (EBNA1, 2, 3A, 3B, 3C and -LP) is initiated from either Cp or Wp and transcription of latent membrane proteins, LMP1, 2A and 2B is initiated from LMP1 and LMP2 promoters, respectively. Following infection, Wp is activated by host cell factors resulting in transcription of EBNALP and EBNA2 expressing transcripts. Expression of EBNA2 switches promoter usage from Wp to the EBNA2-activated C promoter (Cp) leading to the expression of all the EBNAs. Wp becomes methylated within 36 hours of infection (Woisetschlaeger *et al.*, 1990). The Q promoter (Qp) drives expression of EBNA 1 in latent infections where EBNA2 is not expressed (see section 1.3.4) and leads to inactivation of Cp (reviewed in (Takacs *et al.*, 2010)). EBV does not encode its own RNA polymerase so relies on the cellular RNA polymerase II machinery (Bodescot and Perricaudet, 1986). The EBV genome also encodes several non-coding RNAs such as nonpolyadenylated EBV-encoded small RNAs (EBER) 1 & 2 (Lerner *et al.*, 1981) and multiple microRNAs (miRNA) that are derived from two independent transcripts, BamHI-A rightward transcript (BARTs) and BamHI rightward reading frame 1 (BHRF1) (reviewed in (Kempkes and Robertson, 2015)).

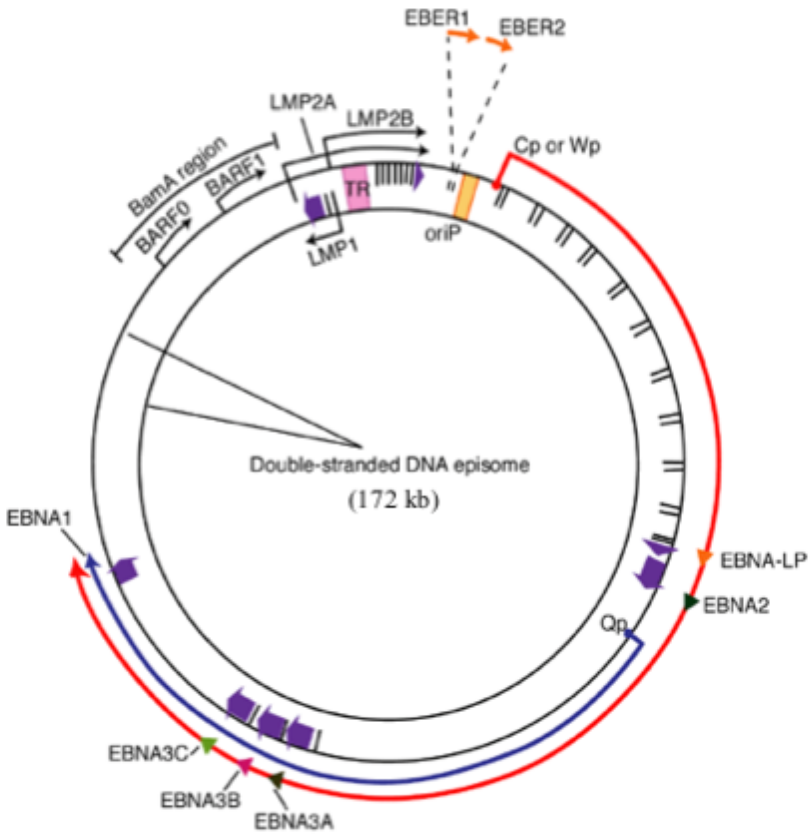

Figure 1.5 The EBV Genome.
The diagram shows transcription of latent genes on the double stranded viral genome of 172 kb. The purple blocks represent coding exons for latent proteins and the arrows indicate the direction in which they are transcribed. The blue line shows transcription of EBNA1 from promoter Q during latency I and II states of gene expression. The red line shows transcription of EBNAs from promoter C or W during latency III. The origin of plasmid replication is coloured orange (adapted from (Murray and Young, 2001)).

The EBV genome has a single origin of replication (OriP). Recent studies suggest OriP serves as a central hub in mediating several interactions with the viral genome. Chromatin conformation capture (3C) studies show OriP to act as transcriptional enhancer by physically interacting with the Cp and LMP1/2 promoters (Tempera *et al.*, 2011, Tempera and Lieberman, 2014). OriP is made up of two functional domains, the family of repeats (FR) and the Dyad symmetry (DS) element. Replication of EBV DNA during latency is mediated by binding of EBNA1 to the FR and DS elements followed by recruitment of the cellular DNA replication machinery (Yates *et al.*, 2000). DNA replication during lytic phase is directed by a distinct region of the viral genome, OriLyt (Hammerschmidt and Sugden, 1988, Schepers *et al.*, 1993).

1.3.2 EBV Infection

EBV is shed in saliva and usually spreads by salivary contacts e.g. kissing, sharing of food, sharing of cooking utensils, or parental food (Niederman *et al.*, 1976). EBV infection generally occurs during the early years of childhood and does not show any symptoms (De Matteo *et al.*, 2003). Primary infection when delayed until adolescence can lead to infectious mononucleosis (IM) (also known as glandular fever) in 30-50% of cases (reviewed in (Henke *et al.*, 1973, Klein *et al.*, 2010)).

Studies have reported infection of epithelial cells in the oropharynx to be less efficient than B-cells and to occur through a separate pathway which requires the gH and gL glycoproteins of EBV (Borza and Hutt-Fletcher, 2002, Shannon-Lowe and Rowe, 2011). Recently studies in human gastric adenocarcinoma cell line show EBV entry to be mediated by EphA2 (Chen *et al.*, 2018). The *in vitro* infection of epithelial cells does not activate the full-growth transforming programme of EBV and rarely achieves full lytic

replication. Interestingly, EBV infection of premalignant nasopharyngeal epithelial cells with inactive p16 support the establishment of EBV latency though the mechanism of latency establishment needs further elucidation (Tsang *et al.*, 2014). One of the malignancies associated with EBV infection of epithelial cells is Nasopharyngeal carcinoma (reviewed in (Young and Rickinson, 2004)).

EBV infects resting B-cells by binding of its viral envelope glycoprotein gp350 and gp42 to the CD21 (CR2) receptor on the surface of B-cells and the human leukocyte antigen (HLA) class II molecule acts as a co-receptor. Upon infection, the terminal repeats of EBV genome undergo circularisation and are maintained as an episome which is transcribed by the cellular transcription machinery to encode the series of EBV proteins needed to infect cells (Hurley and Thorley-Lawson, 1988).

EBV can persist in infected B cells in different latent states: Latency 0, Latency I, Latency II, and Latency III by expressing different latent genes (**Table 1.2**). Upon infection of epithelial cells, the infectious particles spread and infect the surrounding naïve B-cells. The virus establishes latent infection in B lymphocytes by using its growth program (Latency III), leading to uncontrolled cell proliferation. The proliferating blasts enter the germinal centre where they differentiate as memory B-cells during which the virus switches from growth program to default program expressing minimal latent proteins (Latency II) (reviewed in (Thorley-Lawson and Gross, 2004, Young and Rickinson, 2004)). EBV can persist life-long in the host by entering the pool of memory B-cells (Latency I/ Latency 0).

Latency Type	Genes Expressed	Diseases
Latency 0	None	-
Latency I	EBNA1 EBER1 EBER2	Burkitt's Lymphoma I, AIDS-related Diffuse large B cell lymphoma
Latency II	EBNA1 EBER1 EBER2 LMP1 LMP2A LMP2B	Hodgkin Lymphoma, Nasopharyngeal Carcinoma, T-cell Lymphoma
Latency III	EBNA1 EBER1 EBER2 LMP1 LMP2A LMP2B EBNA2 EBNA3A EBNA3B EBNA3C EBNA LP	Post-transplant lymphoproliferative disorder, AIDS-related diffuse large B cell lymphoma IB

Table 1.2 showing the proteins expressed during different Latencies by EBV and the associated malignancies.

These memory B-cells can exit the cell cycle and enter the peripheral circulation and differentiate into plasma cells in response to signals from T-cells. The infected plasma cells are capable of producing virions as they undergo cell division as a part of the normal mechanism leading to replication of viral DNA, producing infectious virus (**Figure 1.6**) (reviewed in (Young *et al.*, 2016)).

After infection of B-cells, the virus upregulates the expression of B-cell activation markers including CD23, CD30, CD39 and CD70 as well as cell adhesion molecules such as CD11a, CD58 and CD54 which are normally expressed at low levels by resting B-cells and are activated by antigenic stimuli. This indicates that EBV induces immortalisation of B cells though constitutive activation of the same cellular pathways that drive physiological B-cell proliferation (reviewed in (Young and Rickinson, 2004)).

1.3.3 EBV Latent Cycle

EBV primary infection triggers an inflammatory response like any other infectious agent. EBV-mediated transformation of B cells initiates $CD8^+$ and $CD4^+$ T cells immune response. These T cells are reactive to EBV latent and lytic antigens, thereby inhibiting the growth of infected cells (Landais *et al.*, 2005). The 'growth latency program' (Latency III) is usually observed in EBV infected B cells that transform into proliferating blasts and in B cell tumours that arise in AIDS patients or post-transplant patients and in *in vitro* infected LCLs as the T-cell response is absent. In Latency II, the expression pattern of latent genes is restricted by the virus in order to access B cell differentiation pathways and is detected in undifferentiated nasopharyngeal carcinoma, Hodgkin's disease and T-cell lymphoma.

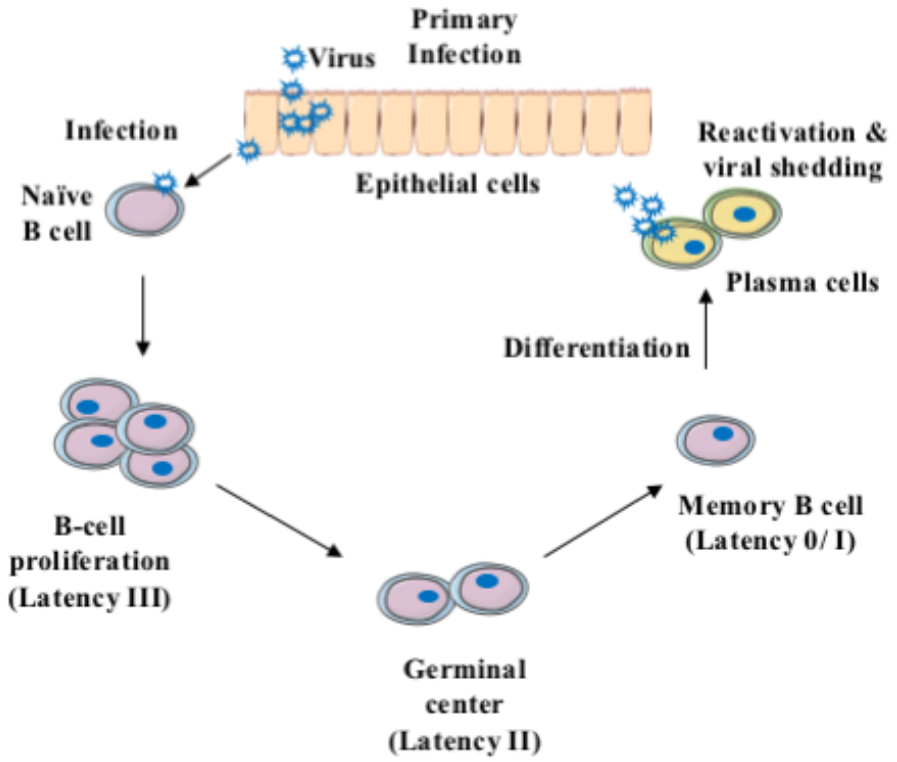

Figure 1.6 EBV infection.
EBV infects epithelial cells in the oropharynx. The virus then infects B cells that are trafficking through the oropharynx. Infection of naïve B cells transforms them into proliferating blasts expressing all the latent genes. These blasts enter germinal center where the virus switches from growth program to default program by expressing only EBNA1 and latent membrane proteins. These cells can enter pool of memory B cells where the virus further switches off the expression of viral proteins and do not stimulate any immune response. The memory B cells exit the cell cycle and differentiate into plasma cells through periodic activation by antigen. The plasma cells can reactivate lytic replication of the virus by switching on the lytic genes leading to subsequent production and release of virions into saliva.

Latency I is an immune invasion strategy by the virus as the infected cells are less antigenic and are detected in Burkitt's lymphoma and AIDS-related DLBCL where minimal EBV genes are expressed to allow maintenance of the viral genome. In Latency 0 none of the EBV latent proteins are expressed indicating that the infected cells have the ability to shut off latent gene expression and switch it back on when the virus needs to replicate (reviewed in(Young and Murray, 2003, Young and Rickinson, 2004)).

1.3.4 EBV Latent Proteins

Some of the EBV latent proteins are crucial for immortalisation of infected B-cells. They play a role in hijacking various cellular pathways by mimicking cellular receptors, driving cell growth, remodelling of chromatin, transformation and immune evasion thereby allowing the virus to establish a persistent infection. The role of each of these latent proteins is discussed in the following paragraphs:

1.3.4.1 **EBNA1**

EBNA1 is expressed in all virus-related tumours. EBNA1 is ~76 kDa in size and contains two Glycine-Arginine rich regions: a variable Glycine-Alanine repeat, and a DNA binding and dimerisation domain. EBNA1 plays a key role in virus transcription, DNA replication, episome maintenance and host-cell survival (exemplified in (Frappier, 2012)). During Latency I, EBNA1 is transcribed from the Q promoter (Qp). It then binds to the Origin of replication (OriP) throughout the cell cycle and is known to recruit the cellular origin recognition complex (ORC) to the DS element of OriP for initiation of EBV DNA replication (Hsieh *et al.*, 1993, Schepers *et al.*, 2001). The viral episome is replicated once in each cell cycle along with the host DNA.

Binding of EBNA1 to the FR element of OriP is requisite for it to act as a transcriptional activator (Lupton and Levine, 1985, Reisman and Sugden, 1986). EBNA1 induces the expression of other EBV latent genes by trans-activating the Cp and LMP1 promoter. The transcriptional activation of genes by EBNA1 is mapped to the 65-83 amino acid residues in the N-terminal of EBNA1. Deletion of this region impaired the ability of EBNA1 to induce the expression of EBNA genes from Cp which in turn reduced the ability of the virus to transform cells (exemplified in (Frappier, 2012)). However, this mutation did not affect the replication of plasmid. Moreover, transcriptional activation by EBNA1 requires the recruitment of nucleosome assembly proteins and Brd4 to the FR element (Lin *et al.*, 2008). EBNA1 can negatively regulate its own expression by binding to two sites downstream of Qp (Nonkwelo *et al.*, 1996), once the binding of EBNA1 to DS and FR elements has reached saturation. This feedback mechanism allows cells to maintain the expression of viral latent proteins (Jones *et al.*, 1989, Ambinder *et al.*, 1990).

Interaction of EBNA1 with CK2 (Casein kinase) triggers degradation of PML (Promyelocytic leukaemia) nuclear bodies (Holowaty *et al.*, 2003, Sivachandran *et al.*, 2010). EBNA1 also interacts with USP7 (Ubiquitin-specific protease) which negatively regulates the replication (Holowaty *et al.*, 2003, Sivachandran *et al.*, 2010). USP7 is known to regulate the expression of p53 and Mdm2 by removing the polyubiquitin chains on them thereby preventing their degradation (Li *et al.*, 2002). However, EBNA1 outcompetes p53 and Mdm2 due to its higher affinity binding to USP7 thereby reducing the accumulation of p53 in response to DNA damage (Saridakis *et al.*, 2005, Sivachandran *et al.*, 2008). The crystal structure of the EBNA1-USP7 complex showed that USP7 binds to the region just before DNA binding domain (amino acid 442-448) of EBNA1 (Saridakis *et al.*, 2005). Recent studies in transgenic mice showed that inhibition

of Mdm2 led to the death of EBNA1 driven tumour cells due to drastic downregulation of EBNA1 and E2F1 in these cells (AlQarni *et al.*, 2018). This indicates a role of EBNA1 in promoting cell survival of EBV-infected cells.

EBNA1 has also been reported to modulate several signalling pathways such as the JAK/STAT1, TGF-β and NF-κB pathways. It induces the phosphorylation of STAT1 leading to nuclear localisation of STAT1, thereby sensitising carcinoma cells to IFNγ treatment (Wood *et al.*, 2007). EBNA1 was also reported to repress the TGF-β signalling pathway by decreasing the SMAD2 protein half-life by 50% as compared to control cells thereby affecting TGF-β induced transcription (Wood *et al.*, 2007, Flavell *et al.*, 2008). In addition, studies using NF-κB reporter plasmids demonstrated that EBNA1 inhibits the canonical NF-κB pathway in carcinoma cell lines by reducing the phosphorylation of p65 kinase and IKKα/β (Valentine *et al.*, 2010). EBNA1 expression also increases the transcription of EBV non-coding RNAs (EBER) by inducing the expression of ATF-2 (pol II). It regulates the expression of several cellular miRNAs as well including let-7, miR-200a and miR-200b (Ellis-Connell *et al.*, 2010, Hsu *et al.*, 2014, Wang *et al.*, 2014) suggesting a role of EBNA1 in transcription activation.

1.3.4.2 **EBNA-Leader Protein (EBNA-LP)**

EBNA-LP is transcribed from either the W or C promoter across the BamHI W repeat region. EBNA-LP varies in size depending on the number of BamHI W repeats in a particular EBV isolate (exemplified in (Murray and Young, 2001)). Previous studies have shown EBNA-LP to cooperate with EBNA2 in activation of various promoters (Kang and Kieff, 2015, Kempkes and Ling, 2015). The reporter assays in EBV-negative B cells

show EBNA-LP along with EBNA2 activates the expression of Cp or LMP promoter by 10-30 fold as compared to EBNA2 alone (Harada and Kieff, 1997) suggesting a role of EBNA-LP as a transcription activator. Cell cycle studies in primary B cells show that EBNA-LP along with EBNA2 promotes G0 to G1 transition by stimulating the transcription of cyclin D (Sinclair *et al.*, 1994). However, recent studies report EBNA-LP not only co-operates with EBNA2 but also facilitates the recruitment of transcription factors to the viral genome (Szymula *et al.*, 2018). Expression of EBNA-LP is also essential for outgrowth of lymphoblastoid cell lines (LCLs) (Allan *et al.*, 1992).

EBNA-LP is a phosphoprotein which is predominantly phosphorylated at serine residues. The protein is expressed throughout the cell cycle but the phosphorylation of this protein changes during different phases of the cell cycle. During G1/S the protein is hypophosphorylated whereas in G2/M it is hyperphosphorylated by CDK1 on two potential serine residues (Ser33 and Ser62) which contains the CDK1 consensus site (Kitay and Rowe, 1996). Additionally, phosphorylation of EBNA-LP at Ser35, 107 and 167 has been shown to be crucial for EBNA-LP mediated co-activation of genes with Ser35 being the major site (Peng *et al.*, 2000, McCann *et al.*, 2001, Yokoyama *et al.*, 2001).

1.3.4.3 **EBNA2**

EBNA2 functions as a transcriptional regulator of both viral and cellular genes. EBNA2 was isolated from EBV strain B95-8 with an apparent molecular weight of ~84 kDa (Baer *et al.*, 1984). The key role of EBNA2 during infection was determined by studies using EBV strain P3HR-1 which has a natural deletion for EBNA2 and EBNA-LP. The isolated virus from Burkitt's lymphoma failed to transform B cells *in vitro* (Cohen *et al.*, 1989).

Later, studies in EBV-immortalised LCLs (EREB 2.5) that expresses a conditionally-active estrogen receptor (ER)-EBNA2 fusion protein showed the cells to maintain their growth only in the presence of active EBNA2 protein (Kempkes *et al.*, 1995). Therefore, suggesting the role of EBNA2 in growth maintenance of infected cells.

Although EBNA2 acts as a transcription factor, it cannot bind to DNA directly, instead, it utilises sequence-specific DNA binding factors to mediate transcriptional regulation. It associates with RBP-Jκ and PU.1 to activate the transcription of LMP2A, LMP2B and LMP1 respectively by binding to promoter-proximal elements (Wang *et al.*, 1990, Grossman *et al.*, 1994, Henkel *et al.*, 1994, Laux *et al.*, 1994, Robertson *et al.*, 1996). RBP-Jκ generally represses transcription by recruiting co-repressor complexes to DNA. This co-repressor complex constitutes of SMRT/N-CoR, CIR, SKIP, Sin3A, SAP30 and HDAC1 which interferes with histone acetylation (an active chromatin mark) (reviewed in (Lai, 2002)). However, binding of EBNA2 to RBP-Jκ displaces the repressive complex resulting into active transcription (Hsieh and Hayward, 1995). Studies show that EBNA2 binds to RBP-Jκ via RAM (RBP-Jκ-associated molecule) motif 'WϕP' found in the Notch proteins. Binding of EBNA2 is followed by recruitment of co-activators and general transcription factors (TFIIB, TAF40) as well as histone acetylases proteins (CBP/P300) at the binding site (Grossman *et al.*, 1994, Henkel *et al.*, 1994, Waltzer *et al.*, 1994). Genome-wide ChIP-seq analysis showing binding of EBNA2 to the cellular genome revealed EBNA2 to bind at promoter proximal and distal sites. EBNA2 and RBP-Jκ have been shown to often co-occupy cellular enhancer (region with high levels of H3K27ac) and super-enhancer (region with extraordinarily high and broad H3K27ac signals) regions with 72% overlap, suggesting RBP-Jκ to be the major DNA binding

adaptor EBNA2 for DNA binding (Zhao *et al.*, 2011b). In addition to RBP-Jκ, recent studies have reported the binding of EBNA2 to another adaptor, EBF1 in LCLs. This adaptor allows the binding of EBNA2 to sites independent of RBP-Jκ and was found to be critical for EBNA2 mediated activation of LMP1 (**Figure 1.7A**) (Glaser *et al.*, 2017). Further investigation in regulation of LMP1 expression reported EBNA2 mediated activation of LMP1 promoter may involve the ATP-dependent chromatin remodelling complex SWI/SNF. This is because microccocal nuclease digestion of LMP1 showed nucleosome remodelling at the LMP1 promoter (Johansson, 2007).

Previous studies have revealed numerous cellular genes to be transcriptionally activated by EBNA2 including *CD21*, *CD23*, *CCR7*, *Hes-1*, *BATF*, *IRF4*, *PAX5*, *SP1, Bcl3*, *CCL3*, *CCL4*, *CXCR7*, *MFN1*, *FcRH5*, *MYC*, *RUNX3* and the p55α subunit of *PIK3R1*. By activation of these cellular genes, EBNA2 promotes the growth and proliferation of infected cells. Studies carried out to understand the mechanism of regulation of *MYC* show increased looping of the *MYC* enhancer (+1.8/1.9 Mb) to the promoter induced by EBNA2 leading to upregulation of MYC expression and promoting proliferation of infected cells. This looping was found to be dependent on the SWI/SNF ATPase BRG1 (chromatin remodeller) (**Figure 1.7B**) (Zhao *et al.*, 2011b, Wood *et al.*, 2016). More recently, EBNA2 has been shown to activate transcription of RUNX3 and RUNX1 through their distal super enhancer at -97 kb and -139 to -250 kb respectively. RUNX family proteins are transcription factors that play a key role in B lymphogenesis therefore modulation of RUNX by EBNA2 allows the virus to manipulate the B cell growth (Gunnell *et al.*, 2016). Previous studies in LCLs showed EBNA2 to activate the p55α regulatory subunit of PI3K kinase and RNAi of EBNA2 in these cells led to apoptosis

showing EBNA2-mediated upregulation of the p55α was important for cell survival (Spender *et al.*, 2006). These data suggest the critical role of EBNA2 in cell transformation, viability and proliferation of infected cells.

Interestingly, most of these genes were found to be targeted by EBNA3 as well, with approximately 25% of the mapped sites shared between the two (McClellan *et al.*, 2013, Portal *et al.*, 2013). How EBNA2 and EBNA3 regulate these genes will be discussed briefly in the following paragraphs.

1.3.4.4 **EBNA3 Family of Proteins**

The EBNA3A, 3B and 3C genes probably arose by a series of gene duplication events arranged in tandem sequence in the EBV genome (White *et al.*, 2010). All three genes share a similar structure with short 5' coding exon and long 3' coding exon. Each of these proteins have a proline-rich region as well as a 'homology domain' (20-30% identity) located near the N-terminus (reviewed in (Styles *et al.*, 2018)). Moreover, immunostaining showed all the EBNA3 proteins to localise in the nucleus as each of these large proteins have multiple nuclear localisation signals ((Le Roux *et al.*, 1993, Krauer *et al.*, 2004a, Burgess *et al.*, 2006). Initial studies using recombinant virus suggested EBNA3A and EBNA3C to be essential for transformation of B cells whereas EBNA3B was dispensable (Tomkinson *et al.*, 1993). However, more recently, EBNA3A-deficient LCLs were established under appropriate conditions but with reduced efficiency (Hertle *et al.*, 2009).

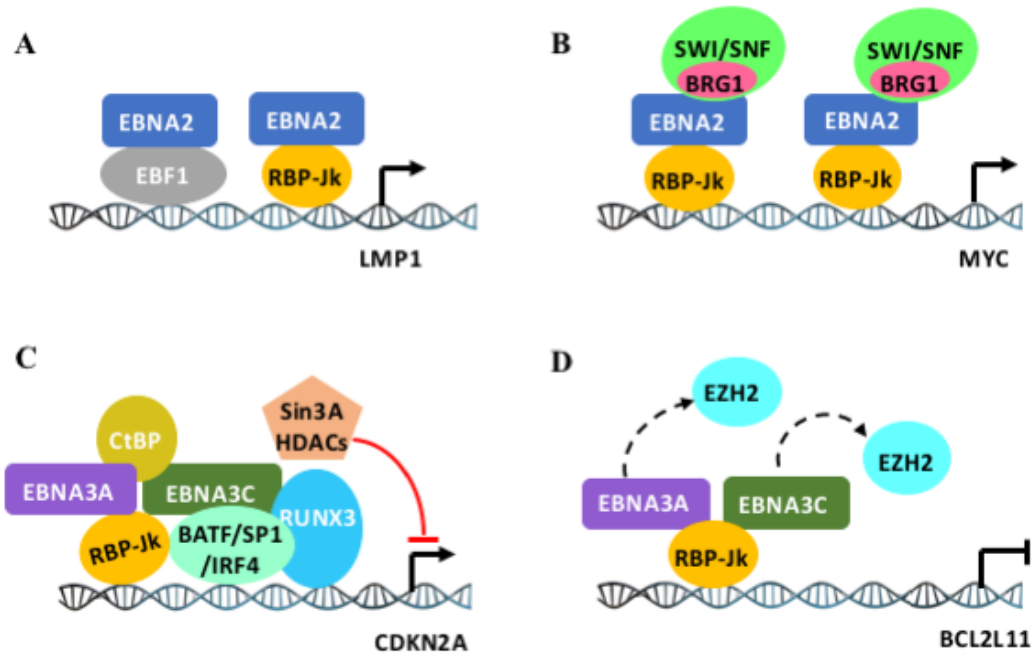

Figure 1.7 Working models for transcription regulation by EBNA2 and EBNA3s.
(A) EBNA2 regulates the transcription of EBV latent membrane protein (LMP1) by associating with the DNA adaptors RBP-Jκ and EBF1. (B) EBNA2 binds upstream enhancers via RBP-Jκ and activates *MYC* by enhancer-promoter looping mediated through association with the SWI/SNF chromatin remodeller, BRG1. (C) EBNA3C in cooperation with EBNA3A repress *CDKN2A* locus through BATF/SP1/IRF4/RUNX/CtBP transcription factors and further recruits Sin3A repressor complex to the promoter. (D) EBNA3C and EBNA3A repress *BCL2L11* by inactivating long-range regulatory hub by recruitment of EZH2 although no direct interaction has been shown between EBNA3 and the PRC component EZH2 (adapted from (Pei *et al.*, 2017)).

The EBNA3 family of proteins function as transcriptional regulators by activating and repressing host cellular genes. Like EBNA2, EBNA3 proteins cannot bind to DNA directly and they were shown to bind to RBP-Jκ for transcriptional regulation (Robertson *et al.*, 1995, Robertson *et al.*, 1996). The EBNA3 proteins share a highly conserved N-terminal homology domain with a 'TFGC' motif which allows them to bind to RBP-Jκ (Robertson *et al.*, 1995, Waltzer *et al.*, 1995, Robertson *et al.*, 1996). Mutation of these residues in the homology domain to 'AAAA' prevented the binding of EBNA3C to RBP-Jκ. In addition, Calderwood and colleagues identified RAM-like motif 'WTP' in EBNA3C. This motif is absent in EBNA3A and EBNA3B. Mutating the 'WTP' motif in EBNA3C alone was not sufficient to inhibit growth in LCLs or to repress EBNA2-mediated transcription activation. However, mutation of 'TFGC' along with 'WTP' showed effective loss of EBNA3C with RBP-Jκ (Calderwood *et al.*, 2011). An initial study of transcription regulation by EBNA3 proteins was investigated by transient reporter assays which showed that EBNA3s repressed EBNA2 mediated activation of viral promoters (LMP2A and Cp). Two mechanisms have been proposed for regulation of EBNA2 mediated activation by EBNA3s: The first model proposes that EBNA2 transactivates genes when bound to RBP-Jκ which is counteracted by competitive binding by EBNA3s causing destabilisation of RBP-Jκ binding to DNA. The second model suggests recruitment of repressive transcription factors by EBNA3s to RBP-Jκ binding site thereby exhibiting strong repressor activity (reviewed in (Allday *et al.*, 2015)). Consistent with the repressive activity, EBNA3A and EBNA3C have been shown to interact with repressive transcription factors such as histone deacetylases (HDACs), Sin3A, CtBP and NCoR (Radkov *et al.*, 1999, Touitou *et al.*, 2001, Hickabottom *et al.*, 2002, Knight *et al.*, 2003). ChIP-seq studies show 25% overlap in the regulatory elements

bound by EBNA3 and EBNA2 in the human genome suggesting co-regulation of cellular genes by these proteins (Hertle *et al.*, 2009). Interestingly, most of the RBP-Jκ binding sites bound by EBNA3 were also found to be bound by EBNA2 (McClellan *et al.*, 2013, Jiang *et al.*, 2014). This suggests that EBNA3s might cooperate or antagonise the regulation of genes expression by EBNA2 (Le Roux *et al.*, 1994, Robertson and Kieff, 1995, Robertson *et al.*, 1995, Johannsen *et al.*, 1996, Radkov *et al.*, 1997).

EBNA3C is essential for the growth maintenance of LCLs as inactivation of EBNA3C in LCL 3CHT (conditionally active EBNA3C) cell line stopped the cells from growing. As EBNA3 regulates cellular gene expression dominantly by binding to RBP-Jκ, the role of this interaction in cell proliferation was studied. LCL 3CHT exogenously expressing EBNA3C 'TFGC' mutant failed to sustain the proliferation due to the abrogation of EBNA3C interaction with RBP-Jκ. The interaction of EBNA3A and EBNA3C with RBP-Jκ was shown to be required for regulation of EBNA2 mediated activation as well as for maintaining proliferation of LCLs (Maruo *et al.*, 2005, Lee *et al.*, 2009, Maruo *et al.*, 2009).

Studies examining host cell gene repression by EBNA3s found EBNA3A and EBNA3C but not EBNA3B to bind to a highly conserved family of co-repressor of transcription, CtBP (C-terminal binding protein) (Touitou *et al.*, 2001, Hickabottom *et al.*, 2002, Chinnadurai, 2007). EBNA3A and EBNA3C interact with CtBP through a consensus binding motif located in the C-terminal regions, ALDLA (aa 857-861), VLDLS (aa 886-890) and PLDLS (aa 728-732) respectively (Touitou *et al.*, 2001, Hickabottom *et al.*, 2002). Interaction of EBNA3s with CtBP is important for EBV-mediated transformation of cells by epigenetic repression of CtBP associated proteins ($p16^{INK4a}$, $p18^{INK4c}$, and

p15^{INK4b}) as mutation in the binding motifs delayed the outgrowth of immortalized cells (Touitou *et al.*, 2001, Hickabottom *et al.*, 2002, Skalska *et al.*, 2010).

Microarray analysis using stable cell lines generated by infection of EBV-negative B cells with recombinant EBV bacmids have further highlighted the role of EBNA3s in the regulation of cellular genes. Gene regulation using these stable cell lines generated in BL and LCL cell background identified a quarter of genes regulated by EBNA3s in LCLs were also regulated in BL31 cell line (Chen *et al.*, 2005, Zhao *et al.*, 2006, Hertle *et al.*, 2009, Skalska *et al.*, 2010, White *et al.*, 2010, McClellan *et al.*, 2012). Together, the gene expression studies reveal EBNA3 proteins to repress several cellular genes including *p16*^{INK4A}, *BCL2L11, CXCL9, CXCL10, BUBR1, ADAM28, ADAMDEC1* (Maruo *et al.*, 2006, Anderton *et al.*, 2008, Gruhne *et al.*, 2009, Hertle *et al.*, 2009, McClellan *et al.*, 2012, McClellan *et al.*, 2013, Skalska *et al.*, 2013, Wood *et al.*, 2016).

EBNA3A in cooperation with EBNA3C have been reported to recruit polycomb repressor complex (PRC) 2 at the site of binding in order to repress certain cellular genes for example p*16*^{INK4A}, p18^{INK4c}, and p15^{INK4b} (CDK inhibitors) encoded by *CDKN2A* and *CDKN2B* locus and the pro-apoptotic *BCL2L11* (BIM) gene (**Figure 1.7C & D**). This repression correlates with deposition of repressive H3K27me3 epigenetic mark (Anderton *et al.*, 2008, Skalska *et al.*, 2010, Maruo *et al.*, 2011, McClellan *et al.*, 2013, Styles *et al.*, 2018). Studies using CtBP-mutant virus showed the repression of *BCL2L11* by EBN3A and EBNA3C to be dependent on interaction of EBNA3A and EBNA3C with CtBP however, the mechanism of repression has not been demonstrated (Paschos *et al.*, 2012). More recently, the repression of *BCL2L11* by EBNA3A and EBNA3C in B cells

was shown as a result of inactivation of long-range regulatory hub by recruitment of the PRC2 methyltransferase EZH2 (Wood *et al.*, 2016).

Interestingly, EBNA3A and EBNA3C are also known to repress *ADAM28* and *ADAMDEC*1 (members of a disintegrin and metalloprotease family) by binding to an intergenic site. Repression of this locus occurs via enhancer looping to the TSS thereby providing the first evidence of EBNA3C association with cellular-gene control regions (McClellan *et al.*, 2013). Studies using EBNA3C conditional LCLs (LLC 3CHT) report the repression of *ADAM28-ADAMDEC1* locus was dependent on the ability of EBNA3C to bind to RBP-Jκ (Kalchschmidt *et al.*, 2016b). In summary, studies by various groups show EBNA3 proteins play a key role in EBV induced transcriptional regulation, transformation and apoptosis resistance.

1.3.4.5 **EBNA3s Hijacks the Cell Cycle Machinery**

The first evidence of the ability of EBNA3 proteins to regulate the host cell cycle machinery came from studies in an EBV-positive Burkitt's lymphoma (Raji) cell line carrying a deletion of the EBNA3C gene. These cells could override G1 arrest upon ectopic expression of EBNA3C (Allday and Farrell, 1994). Subsequently, EBNA3C in cooperation with Ras was shown to catalyse the phosphorylation of retinoblastoma (Rb) as well as degrade p53 by binding and stabilising the ubiquitin ligase MDM2 (Parker *et al.*, 1996, Saha *et al.*, 2009). This implies a role of EBNA3C in regulating G1 checkpoint by modulating the Rb/p53 axis. In serum-starved NIH 3T3 cells, expression of EBNA3C was shown to override the G1/S checkpoint (Parker *et al.*, 2000). Moreover, as mentioned earlier EBNA3C in cooperation with EBNA3A represses the CDK4/CDK6 inhibitor, $p16^{INK4A}$, via interaction with CtBP thereby promoting cell proliferation (Skalska *et al.*,

2010, Maruo *et al.*, 2011). Consistent with the previous reports on G1 checkpoint regulation by EBNA3C, studies in HEK 293T (human embryonic kidney) cells reported EBNA3C to block $p27^{KIP1}$ mediated repression of CDK2-Cyclin A complex by degrading $p27^{KIP1}$ (Knight *et al.*, 2005). Alongside the repression of $p27^{KIP1}$, EBNA3A and EBNA3C have been shown to repress $p57^{KIP2}$ and $p21^{WAF1/CIP1}$ (Banerjee *et al.*, 2014, Bazot *et al.*, 2015) thereby promoting cell cycle progression.

Investigations into G2/M checkpoint regulation by EBV found LCLs expressing EBNA3s to disrupt the G2/M checkpoint induced by treatment with the histone deacetylase inhibitor azelaic bishydroxamine (ABHA) (Krauer *et al.*, 2004b). The same group also reported EBNA3s to reduce the accumulation of inactive CDK1 during G2/M arrest. Moreover, EBNA3C was also able to suppress the G2/M arrest induced by microtubule destabilising drug nocodazole. This was due to the downregulation of CHK2 (effector of ATM/ATR signalling) by EBNA3C resulting into repression of ATM/ATR signalling (Parker *et al.*, 2000, Choudhuri *et al.*, 2007a, Choudhuri *et al.*, 2007b). Interaction of EBNA3C with CHK2 promotes phosphorylation of Cdc25c at Ser216 leading to its sequestration in the cytoplasm. In cytoplasm, Cdc25c phosphatase activates the CDK1-Cyclin B complex and bypasses the G2/M block. Additionally, recent studies show repression of the Wee1 kinase, an inhibitor of CDK1, via enhancer-promoter looping by EBNA3C possibly promoting G2/M transition during outgrowth of EBV-infected cells (McClellan *et al.*, 2013). Together, these findings suggest EBNA3 proteins, especially EBNA3C, to play a role in EBV-mediated cell-cycle disruption of G1/S, G2/M and mitotic checkpoints (Parker *et al.*, 1996, Parker *et al.*, 2000, Choudhuri *et al.*, 2007b).

1.3.4.6 **LMP1 and LMP2**

LMP1 is an essential EBV latent membrane protein required for the immortalisation of B cells. LMP1 expression is detected in several malignancies including HL, LCLs, and undifferentiated NPC (UNPC). It is also expressed during the EBV lytic cycle (Kang and Kieff, 2015). LMP1 protein consists of short cytoplasmic N-terminus, six transmembrane domains and a C-terminal signalling domain. The transmembrane domain initiates signal transduction by forming homo-oligomers in the membrane (Gires *et al.*, 1997). Studies by several groups have reported LMP1 to regulate the expression of genes from at least four signalling pathways; NF-κB, JNK/AP1, p38/MAPK and JAK/STAT (Laherty *et al.*, 1992, Dawson *et al.*, 2003, Liu *et al.*, 2003, Stewart *et al.*, 2004, Zhao *et al.*, 2014). This is mediated by two activation regions, CTAR1 and CTAR2 in the cytoplasmic C-terminal of LMP1. For inducing the NF-κB and p38/MAPK signalling pathway, both CTAR1 and CTAR2 are required whereas CTAR2 alone is sufficient for activation of the JNK/AP1 pathway (reviewed in (Young *et al.*, 2016)). Recruitment of cellular signalling molecules by LMP1 allows it to mimic signals of the CD40 receptor in EBV-infected B-cells (**Figure 1.8A**). Studies using primary B-cells infected with LMP1-deficient EBV found these cells to be unable to induce lymphomas in immunodeficient mice indicating a role of LMP1 in driving B-cell proliferation (Dirmeier *et al.*, 2003). In addition, LMP1 promotes the survival of infected cells by phosphorylating Ser473 residue of Akt thereby activating its downstream signalling pathway (Dawson *et al.*, 2003).

LMP1 is also expressed during the lytic cycle (lytic LMP1) as a truncated variant. The lytic variant does not transduce signals or transforms B cells but it inhibits the activity of

full-length LMP1 (Hudson *et al.*, 1985, Erickson and Martin, 1997, Erickson and Martin, 2000).

LMP2 is expressed only when the genome is circularised upon infection. Out of several transcript variants, two predominant transcripts, LMP2A and LMP2B, are well studied and are found to be controlled by two different promoters (Laux *et al.*, 1988, Laux *et al.*, 1989, Sample *et al.*, 1989). LMP2 expression is associated with several malignancies related to Latency II and Latency III of EBV infection. Interestingly, LMP2A expression is detectable in EBV associated malignancies independent of EBNA2 expression. Studies identified constitutive activation of Notch, functional homologue of EBNA2, by LMP2A as an alternative mechanism to control its own expression. This auto-regulation is dependent on the presence of RBP-Jκ binding site in the LMP2 promoter (Anderson and Longnecker, 2008).

LMP2 proteins consist of 12 transmembrane domains but LMP2B lacks the cytoplasmic signalling domain. LMP2A has tyrosine residues in the N-terminal that form an immunoreceptor tyrosine-based activation motif (ITAM) which upon phosphorylation mimics the B-cell receptor (BCR). LMP2A recruits tyrosine kinases Lyn & Syk from the BCR complex thereby activating the downstream signalling pathways such as Ras, PI3K-Akt, Bcl-xL pathways (**Figure 1.8B**) (Portis and Longnecker, 2004, Pan *et al.*, 2008).

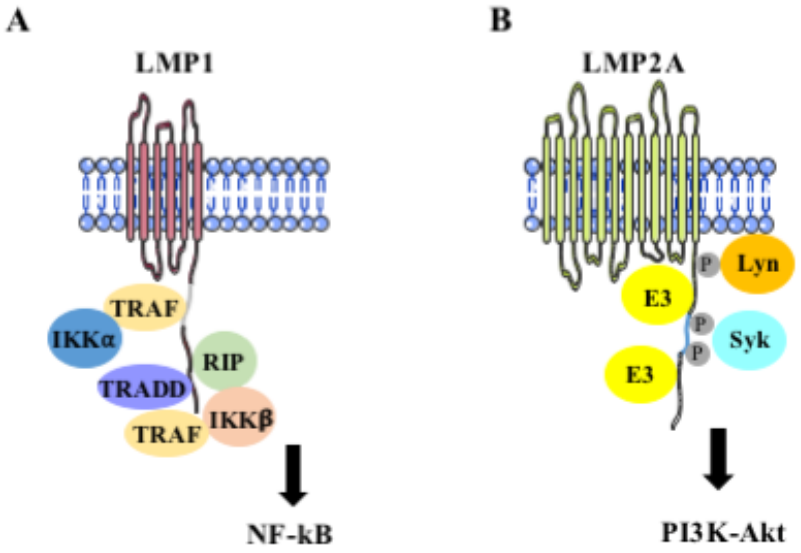

Figure 1.8 Role of LMP1 & LMP2A in BCR signalling.
(A) LMP1 mimics the CD40 receptor. LMP1 induces canonical and non-canonical NF-κB signalling mediated through association of the C-terminal cytoplasmic domain of LMP1 with TNF receptor associated factors (TRAF), TNFR1-associated death domain (TRADD) and receptor interacting protein (RIP). (B) LMP2A mimics the BCR by associating with Lyn and Syk tyrosine kinases. Phosphorylation of LMP2A by Lyn leads to the recruitment of Syk to immunoreceptor tyrosine based activation motif (ITAM). The PI3K-Akt pathway is then activated through active Syk downstream signalling. LMP2A can also block BCR by ubiquitination of Lyn and Syk through association with E3 ubiquitin ligases (adapted from (Gordon and Longnecker, 2012)).

This enables the infected cells to survive. Studies have also reported negative regulation of BCR by LMP2A through recruitment of E3 ubiquitin ligase which leads to degradation of BCR signalling molecules (reviewed in (Murray and Young, 2001)). Intracellular calcium mobilisation is inhibited by LMP2A expression in EBV-negative BJAB cells as a result of a LMP2A-mediated block of the BCR (Miller *et al.*, 1993). LMP2A expression has been shown to activate Erk resulting in increased invasiveness of the cells (Chen *et al.*, 2002). LMP2A helps the virus to maintain latency by regulating the expression of immediate early lytic viral gene, BZLF1 and late lytic viral gene gp350/220 in BL cells. LMP2B, on the other hand, contradicts the role of LMP2A by inhibiting the phosphorylation of LMP2A resulting into restoration of calcium mobilisation as well as the phosphorylation of Lyn kinase (Rovedo and Longnecker, 2007).

1.3.5 EBV-associated Diseases

1.3.5.1 **Infectious Mononucleosis (IM)**

Infectious mononucleosis, also known as glandular fever, is caused by primary EBV infection mostly in adolescents and young adults (Krabbe *et al.*, 1981). It is also known as kissing disease because it is primarily transmitted through kissing in young adults (Balfour *et al.*, 2013). IM was identified as an EBV-associated disease in 1968 (Henle *et al.*, 1968) but has been reported to be caused by another virus, cytomegalovirus (CMV). The typical symptoms of IM infection include sore throat, general fatigue, mild transient fever for several weeks and swollen lymph nodes (Hickey and Strasburger, 1997). IM is usually self-limiting but can be prolonged in certain cases for 6 months or more and has been a significant economic burden (reviewed in (Cohen *et al.*, 2013)).

1.3.5.2 **Burkitt's Lymphoma (BL)**

Burkitt's lymphoma (BL) discovered as a prevalent childhood cancer in equatorial Africa can be classified into three types: endemic BL, sporadic BL and immunodeficiency-related BL (Burkitt and O'Conor, 1961, Schmitz *et al.*, 2014). Endemic BL is frequent in equatorial Africa and Papa New Guinea areas where malaria is holoendemic. Sporadic BL, however, occurs worldwide at a lower frequency (reviewed in (Young and Rickinson, 2004)). EBV association with these different types of BL varies with over 98% of endemic BL (EBV positive), 15% of sporadic and between 30-40% of immunodeficiency-related BL (Magrath *et al.*, 1992). Patients with endemic BL are usually present with a large tumour of the jaw, abdomen or less frequently of the liver or intestine (Burkitt, 1958, Burkitt and O'Conor, 1961).

Regardless of the EBV status, BL is characterised by a chromosomal translocation of *MYC* from chromosome 8 to the Ig heavy, lambda or kappa light chain on chromosome 14, 22 and 2 respectively. Although the translocation to 8:14 is most commonly reported (85% BL cases), this results in high constitutive expression of *MY*C thereby promoting cell cycle progression (Zech *et al.*, 1976, Cesarman *et al.*, 1987, Magrath, 1990, Bhatia *et al.*, 1996). Studies by several groups showed dysregulation of the proto-oncogene *MYC* in numerous B cell lymphomas. Dysregulation of *MYC* includes gene translocation and gene amplification (reviewed in (Nguyen *et al.*, 2017)). Recent studies on the role of EBV in BL identified the virus to induce expression of *MYC* and silence the pro-apoptotic *BCL2L11* by reconfiguration of DNA loops to drive cell proliferation (Wood *et al.*, 2016).

In BL tumours, EBV displays the latency I pattern of gene expression with only EBNA1 and non-coding RNAs such as EBERs and miRNAs expressed (Rowe *et al.*, 1986). In

1969, the role of malaria in BL development was identified although the mechanism of pathogenesis remains unclear (Burkitt, 1969). Studies reported malarial infection to affect the B-cell memory compartment through the cysteine-rich inter-domain region 1α (CIDR1α) encoded by *Plasmodium falciparum*. CIDR1α induces lytic cycle activation by increasing the expression of EBV lytic promoter BZLF1 (Rochford *et al.*, 2005). Moreover, recurrent malarial infection in children has shown high viral load as a result of reduced EBV-specific T cell response to EBV lytic and latent antigens (Moormann *et al.*, 2007).

1.3.5.3 **Hodgkin's Lymphoma (HL)**

Hodgkin's lymphoma is one of the most prevalent lymphomas in western countries (reviewed in (Murray and Bell, 2015)). It is characterised by the presence of malignant HRS (Hodgkin/Reed-Sternberg) cells. These are large multinucleated cells usually originating from pre-apoptotic germinal centre B-cells (Kuppers, 2009). HL is subdivided into two types: classical (cHL) which accounts for 95% of cases and nodular-lymphocyte accounting for 5% of the HL cases. Classical HL is further classified into three types based on appearance: mixed cellularity, nodular sclerosing and lymphocyte-depleted (reviewed in (Young and Rickinson, 2004)).

EBV is associated with approximately 40% of cases of classic Hodgkin's lymphoma worldwide (Kapatai and Murray, 2007). The association of EBV with HL was first established in 1989 as monoclonal EBV was detected in the HRS cells in HL (Weiss *et al.*, 1989). This suggests that HL results from expansion of one infected cell similar to BL (Gulley *et al.*, 1994). In HL tumours, EBV displays the latency II pattern of gene expression with the expression of EBNA1, LMPs and non-coding RNAs EBERs and

miRNAs. HRS cells lack a functional B-cell receptor (BCR) as a result of mutations in the immunoglobulin gene. However, studies show EBV to promote survival of these cells as the EBV latent membrane protein (LMP1 & LMP2) proteins mimic the CD40 and BCR signalling respectively resulting in strong activation of NF-κB pathway (reviewed in (Young and Rickinson, 2004)).

1.3.5.4 **Lymphoproliferative Disease in Immunodeficiency**

Post-transplant lymphoproliferative disease (PTLDs) develops in patients suffering from congenital or acquired immunodeficiency as well as post-transplant patients who are taking immunosuppressive drugs (Penn, 2000). These lymphomas are mostly of B-cell origin and they arise as polyclonal or monoclonal lesions within the 1st year of transplant. These tumours are generally present in extranodal locations such as the gastrointestinal tract or in the allograft organ itself (reviewed in (Murray and Young, 2001)). PTLD can be classified into early lesions, monomorphic PTLD, and polymorphic PTLD based on the morphology of lesions (Ok *et al.*, 2015). Early lesions are more IM like whereas polymorphic PTLD includes lesions from plasma cells and B-cells from different maturation stages. Monomorphic PTLD includes Burkitt's lymphoma, diffuse large B-cell lymphoma and classic Hodgkin lymphoma (Carbone *et al.*, 2008, Ok *et al.*, 2015).

Most of the PTLD cases are EBV positive with cells showing the EBV latency III pattern of gene expression. The infected B cells proliferate due to low amount of EBV-specific cytotoxic cells which are unable to fight the infection (Holmes and Sokol, 2002). Similar to other EBV lymphomas, monomorphic PTLD cells have monoclonal EBV genomes suggesting that the infection occurs earlier than the expansion of malignant cells (Carbone *et al.*, 2008).

1.3.5.5 **Nasopharyngeal Carcinoma (NPC)**

Nasopharyngeal carcinoma is a head and neck tumour originating from the nasopharynx and is particularly common in China and South-east Asia (Yu *et al.*, 1981). Apart from genetic predisposition, environmental factors such as dietary components (e.g. salted fish) are etiologic factors for high incidence rates in Chinese individuals. This is because the preserved food is reported to contain carcinogenic nitrosamines (Yu *et al.*, 1981, Ward *et al.*, 2000). NPC is classified into three subtypes: keratinizing squamous cell carcinoma (type I), non-keratinizing squamous cell carcinoma (type II) and undifferentiated non-keratinizing squamous cell carcinoma (type III) (reviewed in (Young and Dawson, 2014)).

EBV genomes were first detected in malignant epithelial cells of patients with NPC in 1966 (Old *et al.*, 1966). Southern-blot hybridisation of DNA from NPC cells show these cells to carry monoclonal EBV genome indicating clonal expansion of malignant cells (Raab-Traub *et al.*, 1987). EBV displays latency II pattern of gene expression in NPC cells, however, these cells are mainly characterised by abundant transcription of BARF1 (Chen *et al.*, 1992, Brink *et al.*, 1998, Decaussin *et al.*, 2000). EBV related undifferentiated NPC shows the most consistent worldwide association (reviewed in (Young and Rickinson, 2004)).

1.4 Response Gene to Complement-32 (RGC-32/RGCC)

The West laboratory identified the expression of RGC-32 protein to be upregulated in EBV-infected cells expressing the full panel of latent genes (Latency III) (Schlick *et al.*, 2011). Response gene to complement-32 (RGC-32) was first discovered in rat oligodendrocytes by differential display in 1998 (Badea *et al.*, 1998). Badea *et al.*

performed a screen to identify novel genes whose expression was altered upon sub-lytic complement treatment by C5b-9 which induces cell cycle activation (Badea *et al.*, 1998). The genes that responded to sub-lytic complement were designated as Response gene to complement (RGC) and numbered from 1-32. Most of these genes were found to encode for known proteins involved in DNA repair, genomic stability, ATP binding, T cell adhesion. However, RGC-32 mRNA encoded an unknown protein of 137 amino acids in rat. The human RGC-32 protein has 92% sequence similarity with rat and mouse RGC-32 (Badea *et al.*, 1998). Human RGC-32 gene is located on chromosome 13 and encodes a 117 amino acid protein. RGC-32 was also known as C13ORF15 and has been recently designated as RGCC. RGC-32 runs with a molecular weight of 14 kDa on SDS PAGE and does not have significant sequence homology to other human proteins.

Human RGC-32 has two splice variants, a shorter form which lacks the end of exon 1 and start of exon 2 (117 aa) and a longer form which encodes for 20 more amino acids in the N-terminus (NM_014059) (Badea *et al.*, 2002). RGC-32 protein is expressed in most tissues including kidney, heart, brain, lung, skin, spleen and thymus but not in the testes and liver (Badea *et al.*, 1998, Badea *et al.*, 2002). RGC-32 mRNA and protein levels were found to be upregulated in several tumours e.g. breast, colon, lung, stomach, ovarian, prostate (Kang *et al.*, 2003, Donninger *et al.*, 2004, Fosbrink *et al.*, 2005) and downregulated in multiple myeloma, astrocytomas and glioblastoma (Zhan *et al.*, 2006, Saigusa *et al.*, 2007). These data suggest a dual role of RGC-32 in tumorigenesis dependent on the tissue type. The protein is localised in the cytoplasm and found to translocate to the nucleus in smooth muscle cells when exposed to sublytic complement (C5b-9) (Badea *et al.*, 2002). A study by another group showed RGC-32 to translocate

from the cytoplasm to nucleus at the start of mitosis and was concentrated on the centrosomes and spindle poles during mitosis (Saigusa *et al.*, 2007).

The C5b-9 complex regulates cell cycle by increasing the activity of CDK1, CDK2 and CDK4 (Rus *et al.*, 1996, Niculescu *et al.*, 1999, Badea *et al.*, 2002). Overexpression of RGC-32 was shown to promote cell cycle progression as a result of increased DNA synthesis in response to complement activation. Interestingly, overexpression of RGC-32 in serum-starved aortic smooth muscle cells also led to cell cycle progression into S and M phase of G1 arrested cells. A significant shift of cells from S to G2/M was observed upon exposing these cells to complement activation (Badea *et al.*, 2002). However, T-cells from mice carrying a homozygous deletion of RGC-32 showed cell-cycle increased T cell activation (Tegla *et al.*, 2015). These mice appeared to develop normally but another study found RGC-32 knock-out mice to be smaller than wild-type littermates as a result of impaired placental angiogenesis (Cui *et al.*, 2013). These findings suggest RGC-32 to either stimulate growth or suppress it based on cell type and physiological conditions.

Studies in aortic smooth muscle cells showed increased CDK1 activity during RGC-32-mediated S phase entry thereby identifying a new role of CDK1 apart from transition into mitosis (Badea *et al.*, 2002). RGC-32 was found to bind to CDK1 by Glutathione S-transferase pull-down assays *in vitro* and by co-immunoprecipitation *in vivo*. This binding was shown to be specific as RGC-32 was unable to bind CDK2 and CDK4 in these assays. *In vitro* kinase assays showed RGC-32 to increase CDK1 activity (Badea *et al.*, 2002). The same group also showed that RGC-32 was unable to activate CDK1 in the presence of the CDK1 inhibitor $p27^{KIP1}$. As CDK1 is a major target for the G2/M checkpoint and

its activity is required for mitosis, RGC-32-mediated activation of CDK1 may increase cell cycle progression into mitosis. Human RGC-32 has a CDK1 phosphorylation consensus motif, TPQK $_{(91\text{-}94\ aa)}$, and it is shown to be phosphorylated by CDK1-Cyclin B1 *in vitro* at Thr91 residue. Mutation of the Thr91 residue of RGC-32 to Alanine not only prevented the phosphorylation of RGC-32 by CDK1 but also abolished the ability of RGC-32 to induce CDK1 activity (Badea *et al.*, 2002).

Contradictory to the previous findings, studies by another group in glioma cell lines implicated RGC-32 as a tumour suppressor gene. RGC-32 expression is silenced in glioma cell lines and restoration of RGC-32 expression resulted in suppressed growth of these cells (Saigusa *et al.*, 2007). Also, overexpression of RGC-32 protein delayed mitotic progression in HeLa cells. RGC-32 mRNA levels were increased by exogenous expression of p53 in primary astrocytomas with p53 mutations implicating p53 as a transcriptional regulator of RGC-32. This was confirmed by transfecting U-373MG cells which increased RGC-32 mRNA expression (Saigusa *et al.*, 2007). The same group reported RGC-32 to interact with Polo-like Kinase 1 (PLK1), and not with CDK1-Cyclin B. RGC-32 interacted with PLK1 via the Polo-box domain (PBD) in HEK 293T cells and was phosphorylated by PLK1 *in vitro*.

Other studies have described a role for RGC-32 in muscle cell differentiation. RGC-32 expression was induced 50-fold in neural crest cells upon treatment with transforming growth factor (TGF)-β (Li *et al.*, 2007). TGF-β plays a crucial role in promoting Th17-mediated immune response in multiple sclerosis. Consistent with the previous finding, studies in RGC-32 knockout mice show that RGC-32 was upregulated in proinflammatory Th17 cells and was required for its differentiation both *in vitro* and *in*

vivo (Rus *et al.*, 2017), therefore implicating TGF-β as another regulator of RGC-32 expression.

Data from our laboratory confirmed the expression of the short form of RGC-32 (117 amino acid) in B cell lines. Studies from our group also supported the role of RGC-32 in proliferation of EBV infected cells as stable overexpression of RGC-32 alone was sufficient to disrupt the G2/M checkpoint in B cell lines. This indicates a potential role of RGC-32 in EBV transformation mechanism (Schlick *et al.*, 2011).

Moreover, our laboratory identified RGC-32 to be differentially regulated in Latency I and Latency III cell lines. The high levels of RGC-32 protein did not correlate with RGC-32 mRNA levels and vice versa (Schlick *et al.*, 2011). Further investigation into the regulation of RGC-32 identified Pumilio-mediated translational repression at post-initiation stage (Brocard *et al.*, 2018). Pumilio proteins act as RNA-binding proteins (RBP) which in co-operation with other RBP repress translation and/or promote mRNA degradation (Quenault *et al.*, 2011). These proteins are shown to regulate the expression of several genes from the cell-cycle machinery. Interestingly, Pumilio represses the translation of the speedy/RINGO family of atypical CDK1 activators by binding to their 3'UTR (Padmanabhan and Richter, 2006) suggesting a common mechanism of regulation of CDK activators. Although RGC-32 has no homology to any other human proteins, it may be functionally similar to the Speedy/RINGO proteins. Altogether, a new mechanism of regulation of RGC-32 expression has been identified that is likely to be relevant in numerous tumour contexts.

1.5 B-cell Receptor (BCR) Signalling

BCR signalling plays an important role in the growth and survival of normal B-cells and can induce apoptosis in malignant B-cells. Each B-cell has a distinct BCR consisting of a pair of heavy (IgH) and light (IgL) chain immunoglobulins. BCR anchors to the plasma membrane through non-covalently associated transmembrane molecules, Igα (CD79A) and Igβ (CD79B) (Niiro and Clark, 2002). Activation of BCR is dependent on change in the phosphorylation status of signalling molecules (Niiro and Clark, 2002). Lyn, a src-family protein tyrosine kinase (src-PTK) is abundantly expressed in B-cells. Lyn is known to initiate downstream pathways in BCR signalling. It acts as a positive and negative regulator of BCR by phosphorylating tyrosine kinases such as SYK and BTK and phosphorylation of the ITIMS (immunoreceptor tyrosine-based inhibition motif) of inhibitory receptors such as CD22 and FcϒRIIB. This leads to the recruitment of phosphatases SHP-1 and SHIP-1 respectively (DeFranco *et al.*, 1998, Niiro and Clark, 2003, Monroe, 2006). Lyn, Syk and Btk play a key role in the initiation of BCR signalling as deletion of these protein tyrosine kinases prevents signalling (Niiro and Clark, 2002).

Stimulation of the BCR activates several downstream pathways such as PLCϒ, PI3K, AKT, NF-κB, MAPK-Erk and RAS (**Figure 1.9**). Phosphorylation of SYK and Btk leads to the recruitment of non-enzymatic linker signalling proteins such as BLNK, BAM32, BCAP and GRB2. These proteins link SYK and Btk to the PLCϒ and MAPK-ERK signalling pathways. Survival and proliferation pathways are induced downstream of these linker proteins (Niiro and Clark, 2002, Niiro and Clark, 2003, Monroe, 2006).

In malignant and self-reactive B cells, BCR-mediated apoptotic cell death is induced. Activation of the PLCϒ pathway has been reported to induce apoptosis by increasing Ca^{2+}

levels which leads to the activation of caspase 2, NFAT-c2 or MAPK p38 and JNK via inducing the activity of a protein phosphatase calcineurin (Graves *et al.*, 1996, Campbell, 1999, Chen *et al.*, 1999, Kondo *et al.*, 2003). Additionally, BCR-induced downregulation of the PI3K pathway is known to trigger apoptosis by increasing the activation of $p27^{KipI}$ and depressing the activity of MYC (Carey and Scott, 2001). Alternatively, BCR complex associates with lipid rafts to regulate the induction of apoptosis. In immature B cells, antigen binding activates cell death as lipid rafts do not associate with BCR (Pierce, 2002). On the other hand, BCR stimulates survival and proliferation of B cells by inducing the PI3K-Akt, MAPK-ERK and NF-κB pathways.

Activation of the Akt and NF-κB pathways promote cell proliferation by inducing the expression of cyclin D. NF-κB pathway promotes cell survival by repressing the expression of pro-apoptotic proteins such as Bim, Bik, Bad, Bax and Bam (Niiro and Clark, 2002). ERK has also been implicated in B cell survival as activation of ERK leads increased expression of transcription factors such as CREB (cAMP response element-binding protein) and Elk1 (ETS domain-containing protein), crucial regulators of cell proliferation (Koncz *et al.*, 2002). PI3K-Akt mediated positive regulation is discussed in detail in the following section.

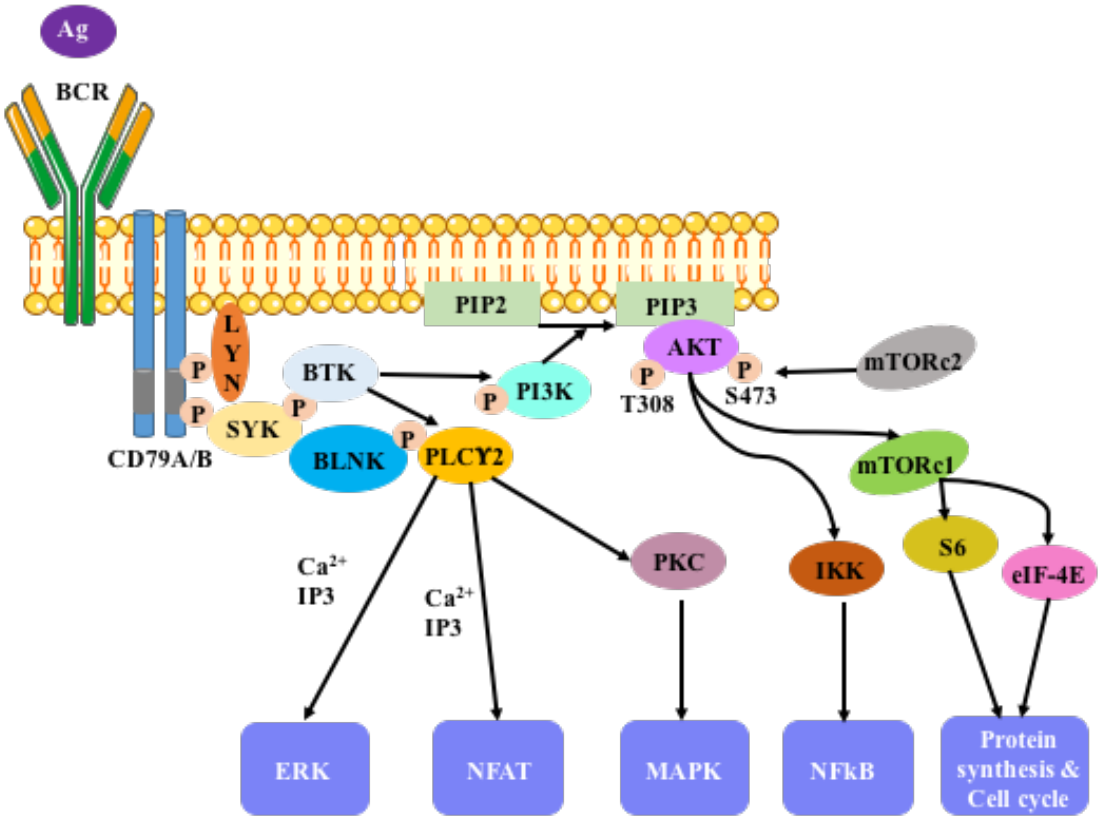

Figure 1.9 The BCR signalling pathway.
B-cell receptor (BCR) consists of a pair of heavy (IgH) and light (IgL) chain immunoglobulin which associates with a CD79 A/B heterodimer. Antigen binding to BCR induces phosphorylation of tyrosine kinases, LYN and SYK, initiating a cascade of downstream signalling pathways. Pathways such as PLCγ2, PI3K, Akt, NF-κB, MAPK-ERK, Ras, protein synthesis and cell cycle progression are stimulated via phosphorylation of signalling molecules. Together, these events result in increased proliferation and survival of B cells (adapted from (Chavez *et al.*, 2013)).

1.5.1 PI3K-Akt Signalling Pathway

The PI3K pathway is activated upon binding of extracellular factors such as cytokines, growth factors or virus to cell surface receptors such as G protein coupled receptor (GPCRs), B cell receptor (BCR) or integrins that have tyrosine kinase activity. PI3K is divided into three subclasses based on structure, regulation and substrate specificity (Engelman, 2009). Activation of PI3K leads to its translocation from the cytoplasm to the plasma membrane where the regulatory subunit p85 relieves its inhibitory activity on the catalytic domain p110 (Cuevas et al., 2001). The active catalytic domain phosphorylates membrane-bound phosphatidylinositol 4,5-biphosphate (PIP2) to generate phosphatidylinositol 3,4,5-triphosphate (PIP3). This allows the recruitment of phosphoinositide-dependent protein kinase 1 (PDK1) and the serine/threonine kinase Akt to PIP3 at the plasma membrane (James et al., 1996).

Regulation of Akt activity is dependent on two regulatory phosphorylation sites, Thr308 in the activation loop within the kinase domain and Ser473 in the C-terminal regulatory domain (reviewed in (Song *et al.*, 2005)). Akt is activated by class I PI3K and this class of PI3Ks is extensively exploited by viruses (Chen *et al.*, 2012). PIP3 does not phosphorylate Akt directly but alters its conformation to allow phosphorylation by PDK1 (Stokoe *et al.*, 1997). The Thr308 residue of Akt is phosphorylated by PDK1 which partially activates the kinase. Full activation of Akt requires both the residues to be phosphorylated. Phosphorylation at S473 is carried out by mTORC2 (mammalian target of rapamycin) (**Figure 1.8**) (reviewed in (Liu and Cohen, 2015)).

Activation of Akt induces phosphorylation of several downstream targets that regulate cell survival. Akt mediated inactivation of pro-apoptotic proteins such as BAD, Bim and

caspase 9 inhibits apoptosis. Moreover, Akt increases the expression of anti-apoptotic proteins such as Bcl-xL, Bcl-2, Mcl-1 thereby promoting cell survival (exemplified in (Liu and Cohen, 2015)). Active Akt also regulates the cell cycle by inactivating the CDK inhibitor $p21^{CIPI}$ and $p27^{KIPI}$ by phosphorylation (Rossig *et al.*, 2001, Fujita *et al.*, 2002). The PI3K-Akt signalling pathway is negatively regulated by several phosphoinositide phosphatases which dephosphorylate PIP3. For example, INN4B dephosphorylate PIP3 generating PIP2 which in turn dephosphorylate Akt (exemplified in (Liu and Cohen, 2015)).

1.5.2 BCR Signalling in Malignancies

The BCR receptor is known to play a role in leukaemia with increasing evidence of the receptor being exploited by malignant cells. Most lymphomas maintain BCR expression in order to promote proliferation and survival of malignant B-cells. B-cell lymphomas typically retain IgM expression as IgM-BCR signalling promotes the survival and proliferation of B-cells. This is observed in several malignancies including follicular lymphoma, Burkitt's lymphoma, DLBCL, B-CLL. Constitutive activation of BCR stimulates the activation of downstream signalling pathways (reviewed in (Young and Staudt, 2013)).

In B-CLL (Chronic lymphocytic leukaemia), increasing number of antigens bound by the BCR have been identified (reviewed in (Niemann and Wiestner, 2013)). BCR of CLL cells recognise an epitope which is a part of CLL BCR itself resulting into auto-stimulation of single cells (Duhren-von Minden *et al.*, 2012). Studies in Burkitt's lymphoma cell lines showed knockdown of CD79A and SYK to cause cell death (Schmitz *et al.*, 2012) suggesting a critical role of BCR signalling for the survival of these

cells. In addition, the PI3K-Akt pathway is found to be altered in many human cancers making it an important target for drug development for treating different malignancies as well as virus infections (reviewed in (Liu and Cohen, 2015)). Interestingly, Burkitt's and Hodgkin's lymphoma show activation of the PI3K-pathway and activated PI3K-Akt signalling has been crucial for survival of BL cells. Studies in Burkitt's lymphoma cell lines showed cell death when treated with either PI3K inhibitor (BKM120) or rapamycin, a universal inhibitor of mTORC1 (Schmitz *et al.*, 2012). Similarly, reduced phosphorylation of S6 and 4E-BP1 in BL cells leading to G1 arrest was observed upon treatment with a dual inhibitor of PI3K-mTOR thereby confirming the significance of PI3K-Akt signalling in survival of BL cells (Spender and Inman, 2012). On the other hand, GCB DLBCL depends on intrinsic activation of PI3K independent of BCR signalling (So and Fruman, 2012). Overall, these studies show manipulation of BCR mediated survival pathways in various lymphomas.

1.6 Aim of the Thesis

EBV deregulates several growth and survival pathways and the cell cycle by overriding the G1/S, G2/M and Mitotic checkpoint. ChIP-seq studies in Mutu III cells by our laboratory identified B cell receptor (BCR) signalling to be significantly enriched for promoter-proximally-EBNA-bound genes or genes closest to the top most significantly-bound EBNA2 sites. Therefore, the aim of this thesis was to understand how deregulation of these pathways by EBV latent proteins promotes growth and survival of infected B cells. To address this, I investigated EBV-mediated cell cycle regulation by studying the role of a novel CDK1 activator, RGC-32, which is translationally up-regulated in EBV-infected Latency III cells. Additionally, I studied the regulation of BCR signalling genes by EBNA2 and EBNA3s and its effects on downstream signalling. My objectives included:

(1) Investigating the role of RGC-32 in the transformation of EBV-infected B cells by characterising the molecular mechanism of interaction of RGC-32 with CDK1-Cyclin B. I also investigated the interaction of RGC-32 with the kinetochore subunit Spc24-25.

(2) To understand the role of RGC-32 in the G2/M transition and mitosis by analysing the effect of RGC-32 on CDK1 activity *in vivo*.

(3) Identifying new target genes and confirming the previously reported genes from BCR signalling that are regulated by EBNA2 and EBNA3 using gene expression analysis. Additionally, examining the impact of EBNAs on positive as well as negative regulation of BCR signalling by studying the phosphorylation of several downstream pathways.

2 Materials and Methods

2.1 Cell Culture Reagents

Dulbecco Modified Eagles medium (DMEM): with 4.5 g/L glucose, 110 mg/L sodium pyruvate, non-essential amino acids and with L-Glutamine.

RPMI 1640 medium (RPMI): Without L-Glutamine (Invitrogen).

Fetal Bovine Serum (FBS): pre-screened for Mycoplasma and viruses, performance tested. Heat-inactivated at 56^{o}C for 1hr and stored at -20^{o}C in 50 ml aliquots (Fisher Scientific Gibco, Cat. No. 11550356 Batch No. 08F7674K).

100X Penicillin-Streptomycin-Glutamine (PSG): containing 10,000 units/ml penicillin G sodium, 10 mg/ml streptomycin sulfate, 29.2 mg/ml L-glutamine and 10 mM sodium citrate in 0.14% NaCl. It was stored in 5 ml aliquots at -20^{o}C.

Dulbecco's Phosphate Buffered Saline (PBS): without Calcium Chloride and Magnesium Chloride.

Trypsin: Trypsin-EDTA (1X) in Hank's Balanced Salt Solution (HBSS), without calcium and magnesium.

Wash Buffer (mitotic entry): PBS containing 3% FBS.

2.2 Molecular Biology Reagents

Luria broth (LB): 10 g tryptone (Oxoid), 5 g yeast extract (Oxoid) and 10 g NaCl in 1 L of dH_2O.

LB Agar: 5 g agar in 400 ml L broth.

1X SeeBlue® Plus 2 Prestained Standard: Prestained coloured marker for SDS-PAGE containing 10 proteins (Invitrogen, Cat. No. LC5925).

SDS-PAGE running buffer: 20x NuPAGE® MOPS or MES SDS running buffer (Invitrogen, Cat. No. NP0001 and NP0002).

1X GSB (gel sample buffer): 50 mM Tris, 4% SDS, 5% 2-Mercaptoethanol (Sigma), 10% glycerol, 1 mM EDTA and 0.01% Bromophenol Blue.

Washing Buffer (PBS-T): 100 PBS tablets (Fisher, Cat. No. 18912014) and 10 ml Tween 20 (Fisher, Cat. No. P9416) in 10 L dH2O.

Transfer Buffer: 1 L methanol (Fisher), 75 g glycine (Fisher), 15 g tris (hydroxymethyl)-methylamine (Fisher) in 4 L dH_2O.

ECL solution I: 40 µl of 25 mM luminal, 17.6 µl coomaric acid, 400 µl Tris pH 8.5 made up to 4 ml by dH_2O.

ECL solution II: 2.6 µl 30% H_2O_2, 400 µl Tris pH 8.5 made up to 4 ml by dH_2O.

10X TBE: 108 g Tris, 55 g Boric Acid and 9.3 g EDTA dissolved in 1 L of H_2O.

GFP-Trap lysis buffer: 10 mM Tris-HCl pH 7.5, 150 mM NaCl, 0.5 mM EDTA, 0.5% Nonidet P-40 (Sigma), 2.5 mM $MgCl_2$, 1 mg/ml DNase, 1 mM PMSF and PIC.

FLAG IP lysis buffer: 10 mM Tris-HCl pH 7.5, 150 mM NaCl, 0.5 mM EDTA, 0.5% Nonidet P-40 (Sigma), 1 mM PMSF and PIC.

IP dilution buffer: 10 mM Tris-HCl pH 7.5, 150 mM NaCl, 0.5 mM EDTA.

MST optimised buffer: 50 mM Tris-HCl pH 7.4, 150 mM NaCl, 10 mM $MgCl_2$, 0.05% Tween-20.

Protein purification buffers

Recombinant Protein	Lysis Buffer	Wash Buffer	
		High Salt	Low Salt
GST-RGC-32, Untagged-RGC-32 and GST-FLAG-RGC-32	20 mM HEPES pH7.5, 500 mM NaCl, 5 mM EDTA	20 mM HEPES pH7.5 and 1 M NaCl	20 mM HEPES pH7.5 and 500 mM NaCl
GST-Chicken Spc-24(125-195 aa)-25(132-234 aa) and GST-Human Spc24(121-197 aa)-25(123-224 aa)	20 mM Tris-HCL pH7.5, 200 mM NaCl, 5 mM EDTA, 0.4% NP-40	20 mM Tris-HCL pH7.5, 1 M NaCl	20 mM Tris-HCL pH7.5, 200 mM NaCl

Storage buffers

Protein	Assay	Storage Buffer
Untagged-RGC-32	Crystallisation	20 mM HEPES pH 7.4, 500 mM NaCl, 0.5 mM TCEP
GST-RGC-32	Interaction studies (SPR, MST)	20 mM HEPES pH 7.4, 300 mM NaCl, 10 mM MgCl2, 0.01% Tween 20 and 0.5 mM TCEP
Untagged-RGC-32	Interaction studies (SPR, MST) and ADP-Glo Kinase Assay	20 mM HEPES pH 7.4, 300 mM NaCl, 10 mM MgCl2, 0.01% Tween 20 and 0.5 mM TCEP
FLAG-RGC-32	Interaction studies (HTRF)	20 mM HEPES pH 7.4, 300 mM NaCl, 10 mM MgCl2,

Protein	**Assay**	**Storage Buffer**
		0.01% Tween 20 and 0.5 mM TCEP
Chicken Spc-24(125-195 aa)-25(132-234 aa) and Human Spc24(121-197 aa)-25(123-224 aa)	Interaction studies (MST)	20 mM Tris-HCL pH7.5, 200 mM NaCl, 0.5 mM TCEP

2.3 Cell Culture

2.3.1 Transformed cell lines

The list of cell lines used for biochemical and cell biology studies is attached in Appendix 7.9.

2.3.2 Stable cell lines

A. BL31 cell lines

The EBV-negative Burkitt's lymphoma (BL31) cell line was infected with wild-type recombinant EBV bacmids or EBNA 3A, 3B and 3C knock-out and revertant bacmids. The knock-out cell lines carried an internal deletion for EBNA3A and EBNA3B and for EBNA3C only exon 2 was deleted. BL31 and these BL31 cell lines were kindly provided by Prof M. Allday (Anderton *et al.*, 2008). Cells were cultured in RPMI medium (Invitrogen) supplemented with 10% fetal bovine serum (FBS), 1% penicillin-streptomycin, glutamine (PSG), 1 mM sodium pyruvate (Sigma) and 50 µM α-thioglycerol (Sigma). 100 µg/ml Hygromycin B (Invitrogen) was added to the media to select for resistant cells containing recombinant EBV.

B. LCL EBNA3A and EBNA3B cell lines

LCLs established by infecting primary B cells with either wild-type EBV (LCL3A wt) or mutant virus lacking the coding sequence for EBNA3A (LCL 3A mutB) were kindly provided by Prof Kempkes. These stable cell lines were maintained by supplementing the cell culture medium with 100 µg/ml Hygromycin B (Invitrogen) (Hertle *et al.*, 2009). LCL EBNA3B KO, wt BAC and EBNA3B revertant cell lines were established by

infecting peripheral blood leukocytes (PBLs) from donor 2 (D2). These cell lines were kindly provided by Prof M. Allday (White *et al.*, 2010) .

C. EREB 2.5 cell line

The EBV-immortalised LCL that expresses a conditionally-active estrogen receptor (ER)-EBNA2 fusion protein was kindly provided by Prof B. Kempkes (Kempkes *et al.*, 1995). These cells were cultured in the presence of β-estradiol (Sigma, Cat. No. E8875). For inactivation and reactivation of EBNA2, cells were maintained in the absence of β-estradiol for 4 days and 1 μM β-estradiol was re-added for either 8 hr or 17 hr prior to cell harvest.

D. LCL 3CHT cell line

This LCL is infected with recombinant EBV expressing EBNA3C fused to a 4-hydroxytamoxifen (HT)-sensitive murine oestrogen receptor (LCL 3CHT) was kindly provided by Prof M. Allday (Skalska *et al.*, 2013). For 4-hydroxytamoxifen (Sigma, UK) withdrawal and add back experiments, cells were maintained in the presence of 400 nM of 4-hydroxytamoxifen for 25 days, HT was then washed off and cells were cultured in media without HT for 21 days. HT was re-added as required and cells were cultured for a further 10 days.

E. HeLa cdk1as and U2OS cdk1as cell lines

Human cervical epithelial cancer cells (HeLa) and Human osteosarcoma cells (U2OS) expressing analogue sensitive (as) CDK1 were generated by disrupting the endogenous CDK1 and expressing *Xenopus laevis* cdk1as from a stably maintained plasmid was kindly provided by Dr Helfrid Hochegger (Ruppert *et al.*, 2018). CDK1AS is sensitive to

the inhibition by the bulky ATP analogue 1NM-PP1 which leads to arrest cells in G2. The cell line was maintained in DMEM medium (Invitrogen) supplemented with 10% fetal bovine serum (FBS), 1% penicillin-streptomycin, glutamine (PSG).

2.3.3 Transient Transfection

A. Electroporation

DG75 cells were diluted 1:3 24 hours before electroporation. Cells were pelleted at 1300 rpm in a Sorvall Legend RT centrifuge with swing bucket rotor (Thermofisher) and the supernatant was kept as conditioned media. The DNA was mixed in Eppendorf tubes in a total volume of 50 µl and incubated on ice for 10 minutes. The cells were resuspended in serum-free media, counted, re-pelleted and resuspended at $2x10^7$ cells/ml in serum-free media. 0.5 ml of cells were added to each Eppendorf tube, mixed with the DNA and moved to electroporation cuvettes (0.4 cm gap, VWR). Samples were cooled on ice for 10 minutes and then electroporated at 230 V and 950 µF using a BioRad Gene Pulser II. Following incubation at 37°C with 5% CO_2 for 30 minutes, the cells were transferred into 25 cm^3 flasks containing 10 ml warm conditioned media and incubated at 37°C for 48 hours.

B. Lipofectamine® 2000

HeLa or HeLa cdk1as cells were seeded in 35 mm glass bottom microwell (14 mm, No. 1.5 coverglass) dishes (MatTek Corporation, Cat. No. P35G-1.5-14-C) at $3.5x10^5$ in 2 ml of supplemented media 24 hr prior to transfection. 2.5 µl of Lipofectamine® reagent (Invitrogen, Cat. No. 11668027) was diluted in 100 µl of serum-free media. 1 µg of DNA was diluted in 100 µl of serum-free media in a different tube. The diluted DNA was added

to the diluted transfection reagent and incubated at room temperature for 10 minutes. The transfection reagent: DNA complex was added to the cells in a drop-wise manner and plates were swirled briefly to ensure even distribution over the plate. The media with transfection complex was changed 8 hours post-transfection and the cells were incubated in supplemented media at 37^{o}C for 24 hours.

C. Calcium Chloride ($CaCl_2$) transfection

HEK 293 cells were seeded into 10 cm^3 culture dishes at 0.75x10^6 cells in 10 ml media. Cells were transfected the next day using the calcium phosphate precipitation method. 5 µg of plasmid DNA was added to 61 µl of 2M $CaCl_2$ to a final volume of 500 µl. This solution was added dropwise to 500 µl of 2X HEPES-Buffered Saline Solution (HBSS) (12 mM dextrose, 50 mM HEPES, 10 mM KCl, 280 mM NaCl, 1.5 mM disodium hydrogen phosphate dihydrate (Na_2HPO_4.2H2O)) while bubbling gently using a 1 ml pipette and electronic pipette to mix. The 1 ml solution was then immediately added dropwise to the cells and swirled to mix. The next day the precipitate-containing medium was removed, the cells were washed with PBS and complete media was added. Cells were harvested 48 hours following the transfection.

2.3.4 Generation of the U2OS cdk1as eGFP-RGC32 stable cell line

3x10^5 U2OS cdk1as cells were plated in a 6 cm dish in 2 ml of media 24 hour prior to transfection. Cells were transiently transfected using Lipofectamine® 2000 reagent as follows;

Tube 1	1.5 µg ROSA26_eGFP-RGC-32 + 0.5 µg guide RNA oligos (gRNA) for *ROSA26* locus + 100 µl Serum Free Media
Tube 2	2.5 µl of Lipofectamine® Reagent + 100 µl Serum Free Media

The gRNA (gRNA Forward: CACCGGACCTGCTACAGGCACTCGT; gRNA Reverse: AAACACGAGTGCCTGTAGCAGGTCC) has a complementary sequence to the target region and a 'PAM' (Protospacer adjacent motif) sequence recognised by the Cas9 nuclease which targets homologous recombination at the region of interest in *ROSA26* locus. Diluted DNA/gRNA mix was added to the diluted reagent and incubated at room temperature for 10 minutes. The transfection reagent: DNA complex was added to the cells in a drop-wise manner and plates were swirled briefly to ensure even distribution over the plate. Cells were trypsinised 48 hours post transfection and diluted in complete DMEM media with Zeocin (200 µg/ml, Invitrogen, Cat. No. R25001) to obtain single cells per well in 96-well plates. After 3 weeks, zeocin-resistant single cell colonies were screened for the integration of eGFP-RGC-32 at the *ROSA26* locus using specific primers (Appendix 7.6). Colonies that tested positive for integration were further grown to test the inducible expression of eGFP-RGC-32 upon addition of Doxycycline (1 µg/ml).

2.3.5 Generation of the IB4 stable cell line (Neon Transfection Kit)

IB4 cells were split 1:3 one day prior to transfection. $5x10^6$ cells were washed in PBS once and resuspended in 100 µl of Buffer T (Neon Transfection Kit, Invitrogen). 5 µg of pRTS-1 or pRTS-1 RGC-32 was added to the cells to a final volume of 120 µl. Cells were

transfected using a 100 µl Neon tip at 1300 V, 30 msec, and 1 pulse. Transfected cells were then transferred to a flask containing pre-warmed media (without antibiotics) followed by recovery for 48 hours. Initially, 100 µg/ml Hygromycin B (Invitrogen) was added to cells to select the transfected cells and was then increased to 300 µg/ml Hygromycin B after one week. Within the next 4 weeks, hygromycin-resistant cell grew out which stably contained the inducible plasmids, pRTS-1 or pRTS-1 RGC-32.

2.3.6 Constitutive RGC-32 silencing in the IB4 cell line

IB4 pRTS-1 and IB4 pRTS-1 RGC-32 cells were treated with 1 µg/ml Doxycycline (Sigma) for 24 hrs to induce the expression of RGC-32. $1x10^5$ IB4 pRTS-1 and IB4 pRTS-1 RGC-32 cells were transduced with either Mission lentiviral transduction particles (Sigma) containing shRNA sequences against human RGC-32 (shRNA 5: TRCN0000153026, shRNA 6: TRCN0000156253) or Mission lentiviral Non-Mammalian shRNA control transduction particles (SHC002V) by spinoculation for 2 hrs at 1,200 g at 32^{o}C at MOI 5. After transduction, cells were maintained in 1 µg/ml Doxycycline and 300 µg/ml Hygromycin B for 4 days followed by the selection of transfected cells by addition of 0.5 µg/ml of Puromycin (Sigma) up to 5 days. The percentage of GFP-positive cells was counted using FACS (BD Accuri C6).

2.3.7 siRNA Transfection

siRNA was transfected by reverse transfection. For this technique, trypsinised cells at the concentration of 1 $x10^5$ cells/ml were used. U2OS cdk1as eGFP-RGC-32 cells were transfected using Lipofectamine^{TM} RNAiMAX reagent (Invitrogen, Cat. No. 13778030) as follows;

Tube 1	20 nM of siRNA + 250 µl Serum Free Media
Tube 2	5 µl of LipofectamineTM RNAiMAX reagent + 250 µl Serum Free Media

This mixture was incubated at room temperature for 10 minutes and then mixed with 2 ml of the cell culture. The cells-siRNA mix was then plated into 6-well dish. Cells were then grown at 37^{o}C for 48 hr before the lysates were collected for immunoblotting using appropriate antibodies (Appendix 7.1 & 7.2). The sequences of siRNA oligos used in this study are listed in Appendix 7.7.

2.4 Molecular Biology

2.4.1 Miniprep

Several colonies were picked with a sterile tip and each colony was grown separately in 5 ml of LB containing appropriate antibiotics. The transformed bacteria were incubated at 37^{o}C overnight in a shaking incubator at 225 rpm. The culture was then transferred to a 15 ml tube and cells were harvested by centrifugation at 4000 rpm for 5 minutes using Heraeus MegaFuge 8R centrifuge (Thermofisher). Plasmid DNA was extracted using a Qiagen Spin Miniprep kit (Qiagen, Cat. No. 27104) following the manufacturer's instructions.

2.4.2 Maxiprep

Several colonies were picked with a sterile loop and each colony was grown in 2 ml of LB containing appropriate antibiotics. The transformed bacteria were incubated at 37^{o}C in a shaking incubator at 225 rpm for 3-4 hr. An overnight culture was set up by adding 500 µl of the day culture to 100 ml of LB containing appropriate antibodies and was incubated at 37^{o}C overnight in a shaking incubator at 225 rpm. The cells were harvested by centrifugation at 6000 g for 15 minutes at 4^{o}C using Heraeus MegaFuge 8R centrifuge (Thermofisher). Plasmid DNA was extracted using a Qiagen Plasmid Maxi Kit (Qiagen, Cat. No. 12162) according to the manufacturer's instructions.

2.4.3 Restriction Enzyme Digestion

Restriction enzyme digestion reactions were set up as below:

Experimental Reaction	Volume (µl)
Restriction Enzyme (20,000 units/ml)	2
DNA template (6 µg)	x
10X NEBuffer	2
Final volume	20

The samples were incubated at 37^{o}C for 1 hr 30 minutes. The linearised DNA fragments were separated on a 1% agarose gel in TBE and the DNA was purified by gel extraction as required.

2.4.4 DNA gel purification

The DNA of interest was cut out of the agarose gel using a razor blade. DNA was purified using the QIAquick Gel Extraction Kit (Qiagen, Cat. No. 28704) following the manufacturer's instructions. The DNA was eluted in 50 µl of nuclease-free water.

2.4.5 Alkaline phosphatase treatment of DNA

To prevent single cut linearised vector from re-ligating, the samples were treated with alkaline phosphatase (Roche, Cat. No. 10713023001) to remove the 5' phosphate group

from the cut ends. Reactions were set up as below; the samples were incubated at 37^{o}C for 30 minutes.

Experimental Reaction	Volume (µl)
Alkaline phosphatase (1unit/µl)	4
DNA template (digested)	x
10X Alkaline dephosphatase buffer	4
Final volume	40

2.4.6 Ligation

The gene of interest was cloned into the destination vector at the multiple cloning site. To achieve ligation, approximately 100 ng of the vector was mixed with the insert in molar ratios 1:1, 1:3, 1:6, 1:9 in the presence of 2 µl of 10 X T4 DNA Ligase buffer and 1.5 µl of T4 Ligase and filtered sterilised water in a final volume of 20 µl. The samples were incubated overnight on ice on the bench. These samples were then used for transformation of *E.coli* DH5α.

2.4.7 Genomic DNA extraction from mammalian cells

Cells were grown in 35cm dish until ~70% confluent to extract genomic DNA. Cells were first washed once with PBS followed by cell lysis and DNA extraction using the Wizard® SV Genomic DNA Purification System (Promega, Cat. No. A2360).

2.4.8 Gibson Assembly

The insert DNA, eGFP-RGC-32 was amplified from pEGFP-C3-RGC-32 using ROSA26_eGFP-RGC-32 primers by PCR (Appendix 7.6). Both vector (pROSA26 MCS) and amplified insert (eGFP-RGC-32) were digested with AgeI restriction enzyme. 70 ng of vector and 3-fold excess of insert DNA was used to set up the reaction as shown below:

Experimental Reaction	Volume (µl)
DNA fragments (70 ng)	x
Gibson Assembly Master Mix (2x)	10
dH_2O	10-x
Final volume	20

The reaction mixture was incubated at 50^{o}C for 15 minutes. Samples were either stored in -20^{o}C or transformed into competent *E.coli* cells (DH5α) with 2 µl of reaction mix.

2.4.9 SLIC cloning

RGC-32 in fusion with N-terminal FLAG-tag was cloned into pGEX-6P3 using sequence and ligation independent cloning. First, FLAG-RGC-32 was amplified using Phusion polymerase from a plasmid (pFLAG-RGC-32) previously generated in the laboratory with pGEX6P3_FLAG RGC-32 PCR primers (Appendix 7.6). The amplified insert and BamHI digested pGEX6P3 were ligated as below:

Reaction	Volume (µl)
Vector (40 ng)	x
Insert (80 ng)	y
T4 DNA polymerase	0.25
Buffer (2.1 NEB)	1
dH_2O	Up to 10

The reaction was incubated at room temperature for 10 minutes for the T4 DNA polymerase to resect the cut ends and ligate the insert to single-stranded vector. Subsequently, the reaction mix was incubated on ice for 10 minutes to fill the single-strand DNA gap through DNA repair. Thereafter, the final mix containing the ligated vector was transformed into competent DH5α cells.

2.4.10 Transformation of bacterial cells

100 ng of plasmid DNA or ligated DNA was mixed with 100 µl of competent *E.coli* DH5α cells or 75 µl of BL21 (DE3) Rosetta2 pLysS cells and incubated on ice for 10 minutes. The cells were then heat shocked at 42^{o}C for 45 seconds and incubated on ice for another 5 minutes. 900 µl of LB was added to cells and transformed bacteria were incubated at 37^{o}C for 45 minutes in a shaking incubator at 225 rpm. The transformed

cells were pipetted onto agar plates (20 µl, 70 µl, 100 µl) containing appropriate antibiotics and spread using a sterile spreader. Colonies were grown overnight at 37^{o}C.

2.4.11 Glycerol stock

DH5α or BL21 (DE3) Rosetta2 pLysS competent cells were transformed with plasmid DNA and streaked onto agar plates containing appropriate antibiotics. One colony was picked and inoculated into 10 ml of LB containing appropriate antibiotics in a centrifuge tube. The tube was placed in a shaking incubator at 37^{o}C with 225 rpm overnight. The 15% glycerol stock was prepared by adding 150 µl of glycerol to 850 µl of culture and transferring to cryogenic vial. Vials were then stored at -80^{o}C.

2.4.12 RNA Extraction

RNA was extracted from cells using Tri Reagent (Sigma) using 1ml per 1x10^{7} cells according to the manufacturer's instructions. 1-2 µg of extracted RNA was further purified using the RNeasy Mini Kit (Qiagen, Cat. No. 74104) according to the manufacturer's instructions and stored at -80^{o}C.

2.4.13 cDNA Synthesis

cDNA synthesis from RNA was carried out using the ImProm-II™ Reverse Transcription System Kit (Promega, Cat. No. A3800). Based on the manufacturer's instructions, 1 µg of each RNA was mixed with 1 µl Random Primer and water added to a final volume of 5 µl. The samples were incubated at 70^{o}C for 5 minutes and then placed on ice for another 5 minutes. The reaction for cDNA synthesis was set up as below;

Experimental Reaction	Volume (µl)
5X ImProm™ Reaction Buffer	4
$MgCl_2$	4
dNTP Mix	1
Recombinant Rnasin® Ribonuclease inhibitor	0.5
Reverse transcriptase	1
Nuclease-free H_2O	x
Final volume	15

15 µl of the above master mix was added to the RNA and primer mix and the samples were then incubated for 5 minutes at 25^{o}C, 60 minutes at 42^{o}C and 15 minutes at 70^{o}C and finally stored at -80^{o}C.

2.4.14 Real-time Polymerase Chain Reaction

GoTaq qPCR SYBR® Green (Promega, Cat. No. A6001) was used for the standard quantification assay. According to the manufacturer's instructions, 3 µl of diluted (1:10) cDNA was added to 12 µl of PCR cocktail containing 7.5 µl 2X GoTaq qPCR SYBR® Green Master Mix, 0.15 µM forward and 0.15 µM reverse primers and the total volume was made up to 15 µl by nuclease-free water. Power SYBR® Green Cells-to-CT™ Kit (Applied Biosystems) was used for real time PCR reactions from RGC-32 knockdown rescue experiment. According to manufacturer's instructions, 4 µl of cDNA was added to 16 µl of PCR cocktail (containing 10 µl Power SYBR® Green PCR master mix, 300

nM forward primer, 300 nM reverse primer and the total volume was made up to 16 µl by nuclease free water). A thermal cycler 7500 Real Time PCR system from Applied Biosystems was used for PCR using the following cycling conditions;

System	Initial Denaturation	Denaturation	Anneal	Dissociation Curve		
	1 cycle	40 cycles		1 cycle		
Temp. (°C)	95	95	60	95	60	95
Time (mm:ss)	10:00	00:15	01:00	00:15	01:00	00:15

For standard quantification, cDNA from an appropriate cell line was used to generate a standard curve for each primer set. A 1:5, 1:25, 1:125, 1:625 and 1:3125 dilution of cDNA corresponded to 50, 10, 2, 0.4 and 0.08 ng of input RNA. These standard curves were used to convert the crossing threshold (Ct) values obtained for all samples into arbitrary RNA quantity values. This allows normalisation to a control transcript (GAPDH) between different cell lines.

2.4.15 Gene Expression Analysis using TaqMan array cards

TaqMan array cards preloaded with genes expression assays for BCR signalling genes and genes close to significant EBNA2 or EBNA3 peak in addition to four control (GAPDH, GUSB, RPLP0, and HPRT1) genes was designed by Dr Michael McClellan. Control genes were used to measure gene expression using the comparative Ct method of relative quantification. cDNA was synthesised from 1 µg of RNA of BL31 cell lines, LCL

stable cell lines and EREB 2.5 cells using the ImProm IITM Reverse Transcriptase System Kit (Promega). 50 µl of TaqMan Universal PCR Master Mix (2x) with UNG was added to 200 ng of cDNA and nuclease-free water was added to a final volume of 100 µl. The samples were centrifuged briefly to remove all the air bubbles. The TaqMan array card was placed on the bench with the foil side down and was allowed to reach room temperature before loading the samples. 100 µl of cDNA sample with master mix was loaded into each fill reservoir in such a way that the sample sweeps in and around the fill reservoir towards the vent port. The array card was centrifuged twice at 1,200 rpm for 1 minute. The card was sealed, and the ports and the A1 corner were cut off using scissors. It was then loaded into Applied Biosystems 7900HT TaqMan Array Microfluidic Card Thermal Cycling block in such a way that the A1 corner is placed onto the adapter, and wells with controls and samples were selected using the software from the manufacturer. The following program was used;

System	**UNG incubation**	**Polymerase activation**	**PCR**	
			Cycles (40 cycles)	
	Hold	**Hold**	**Denature**	**Anneal/ extend**
Temp. (^{o}C)	50	95	95	60
Time (mm:ss)	02:00	10:00	00:15	01:00

The data was analysed with the cloud suite software Symphoni (Life Technologies) using the Relative Quantification Module.

2.5 Microscopy

2.5.1 Time-lapse Microscopy

For time-lapse microscopy, $3.5x10^5$ cells were plated in 35 mm glass bottom microwell (14mm, No. 1.5 coverglass) dishes (MatTek Corporation) and images were captured 24 hours after DNA transfection in a heated chamber (37^oC) using the Olympus IX73 microscope. *Z*-stacks were collected at 1 μm intervals every 1-5 minutes. All the images presented were processed in Omero software.

2.5.2 Mitotic entry

U2OS cdk1as eGFP-RGC-32 cells were plated in an 8-well chambered slide at $1.9x10^4$ cells per well. The following day cells were treated with 1 μg/ml doxycycline (Sigma, Cat. No. D9891) 48 hrs to induce the expression of GFP-RGC-32. Cells were arrested in G2 phase using 2 μM of CDK1 inhibitor 1NM-PP1 20 hour along with 2 μM of SiRDNA (Nuclear stain, Spirochrome, Cat. No. CY-SC007) prior to time-lapse imaging. In order to release the cells from G2 arrest, 1NM-PP1 was washed off using 3% FBS in PBS (1X) for 5 times and live-cell media containing 25 μM MG132 (Selleckchem, Cat. No. S2619) was added in the presence or absence of doxycycline. Different concentrations of the CDK1 inhibitor 1NM-PP1 were also added to the cells for partial inhibition of CDK1 activity. Time-lapse imaging was performed for 4 hours with images taken every 15 minutes using a 20x lens using the Olympus IX73 microscope.

Mitotic entry with Wee1 inhibitor, MK-1775 (Selleckchem, Cat. No. S1525) was performed by adding Wee1 inhibitor (500 nM) to the cells 30 minutes prior to wash off and cells were analysed as above.

2.5.3 High Content Image Analysis

Fixed cell images were collected for each condition with the Olympus ScanR microscope using a 20x lens. Each image was first processed (ScanR software) to identify the nuclei in each well by using the Hoechst channel followed by background correction for each channel. Cells were gated based on the presence or absence of nuclear envelope as in G2 or in Mitosis population and the mean intensity of each channel (Cy5, TxRed) for the gated population was calculated. ScanR derived data was used to generate box plots and histograms in PyCharm.

2.6 Biochemical Methods

2.6.1 SDS-PAGE

10-15 µl of whole cell lysate was resolved using 4-12% Bis Tris gel or Tris Glycine gels (Invitrogen). Gels were run at 200 V for 50 minutes in MOPS buffer or 35 minutes in MES buffer. 5 µl of marker (1X See Blue® Plus 2 pre-stained standard, Invitrogen) was used to determine the molecular weights of proteins.

2.6.2 Western Blotting

After the separation of the proteins by SDS-PAGE, the proteins were transferred to Protran nitrocellulose membrane 0.45 µm (GE Healthcare, Cat. no. 15239824) by western blotting at 85 V for 90 minutes with cooling in transfer buffer using a transblot apparatus (Biorad). The blot was stained with Ponceau stain (Sigma, Cat. No. P7170-1L) for 1 minute in order to check if the transfer was successful. Subsequently, the stain was washed off with PBS-Tween and the blot then blocked with 5% milk in PBS-Tween for 1 hour. The blot was incubated with appropriate primary antibody diluted in 10 ml PBS-Tween containing 5% milk, overnight at 4^{o}C on a rocker. Next day, the blot was washed three times for 10 minutes each with PBS-Tween. The blot was then incubated for 1hr with horseradish peroxidise-conjugated secondary antibody diluted in 10 ml PBS-Tween containing 5% milk at room temperature (RT). The blot was given a quick rinse in PBS-Tween and then washed in PBS-Tween for 3 times for 10 minutes each. Each membrane was then briefly incubated with a total volume of 4 ml enzymatic chemiluminescence (ECL) solution (1:1 mixture of solution I and solution II). The membrane was exposed directly to the Odyssey Fc Imager (LiCor) for both Chemiluminescence and the 700 nm channel to visualise the markers.

2.6.3 Bradford Assay

10 µl diluted or undiluted protein samples were added with 200 µl 1:5 dye reagent (BIO-RAD) and absorbance at 600 nm was measured using the GloMax-Multiplate reader system (Promega, Cat. No. GM3000). The standard curve consisted of BSA diluted in water to give a final concentration of 25 µg/ml, 125 µg/ml, 250 µg/ml, 500 µg/ml, 750 µg/ml, 1000 µg/ml, 1500 µg/ml, and 2000 µg/ml.

2.6.4 GFP-Trap Immunoprecipitation Assay

$2x10^6$ cells expressing GFP-tagged RGC-32 were harvested 48 hr post-transfection. The cell pellet was washed with 1 ml for three times of ice-cold PBS and centrifuged at 500 *g* for 3 minutes at 4°C. The cells were resuspended in 500 µl ice-cold GFP-trap lysis buffer (10 mM Tris-HCl pH 7.5, 150 mM NaCl, 0.5 mM EDTA, 0.5% Nonidet P-40 (Sigma), 2.5 mM $MgCl_2$, 1 mg/ml DNase, 1 mM PMSF and PIC) and placed on ice for 30 minutes with extensive pipetting every 10 minutes. The cell lysate was centrifuged at 13,000 rpm for 15 minutes at 4°C and the lysate was transferred to a tube with 300 µl of IP dilution buffer (10 mM Tris-HCl pH 7.5, 150 mM NaCl, 0.5 mM EDTA). GFP-Trap_M beads (Chromotek, Cat. No. gtm-20) were washed three times with 500 µl IP dilution buffer followed by magnetic separation of beads until the supernatant was clear. The lysate was incubated with the equilibrated GFP-trap M beads, with rotation at 4°C for 1 hr. Beads were separated magnetically and washed three times with 500 µl IP dilution buffer. The GFP-trap M beads were resuspended in 50 µl 2X gel sample buffer (GSB) and heated at 95°C for 10 minutes and centrifuged. The protein samples were analysed by western blotting for CDK1, PLK1, Spc24 and Spc25 using appropriate antibodies (Appendix 7.1 & 7.2).

2.6.5 FLAG Immunoprecipitation Assay

$2x10^6$ cells expressing FLAG-tagged RGC-32 were harvested 48 hours post- transfection. For crosslinking, 1% of Formaldehyde (Sigma) in PBS was added to cells and the cells were incubated at room temperature for 10 minutes on a roller. The reaction was terminated by adding 2 M Glycine followed by incubation at room temperature for 5 minutes. Cell pellets -/+ formaldehyde treatment were washed three times with 1 ml of ice-cold PBS and centrifuged at 500 g three times at 4^{o}C. The cells were resuspended in 300 µl ice-cold FLAG IP lysis buffer (10 mM Tris-HCl pH 7.5, 150 mM NaCl, 0.5 mM EDTA, 0.5% Nonidet P-40 (Sigma), 1 mM PMSF and PIC) and placed on ice for 45 minutes with regular extensive pipetting. The cell lysate was centrifuged at 13,000 rpm for 15 minutes at 4^{o}C and the lysate was transferred to a tube with 200 µl of IP dilution buffer (10 mM Tris-HCl pH 7.5, 150 mM NaCl, 0.5 mM EDTA). A Bradford assay was performed in order to ascertain equal loading of input sample for each condition. Anti-FLAG M2 beads (Sigma, Cat. No. M8823) were washed 500 µl three times with IP dilution buffer followed by magnetic separation of beads until supernatant is clear. Lysate was incubated with equilibrated Anti-FLAG M beads, rotating at 4^{o}C, overnight. Beads were separated magnetically and washed once with 500 µl high salt wash buffer (10 mM Tris-HCl pH 7.5, 500 mM NaCl, 0.5 mM EDTA, 0.5% Triton-X100), twice with low salt wash buffer (10 mM Tris-HCl pH 7.5, 150 mM NaCl, 0.5 mM EDTA, 0.5% Triton-X100) and 500 µl once with IP dilution buffer. The Anti-FLAG M beads were resuspended in 25 µl 2X gel sample buffer (GSB), heated at 95^{o}C for 10 minutes and centrifuged. The protein samples were analysed by western blotting for CDK1 and RGC-32 using appropriate antibodies (Appendix 7.1 & 7.2).

2.6.6 Protein expression

Plasmids containing the desired protein construct (Appendix 7.9) were transformed into *E.coli* BL21 (DE3) Rosetta2 pLysS cells. A single colony was used to inoculate 50 ml of LB containing appropriate antibiotics, which was placed at 37^{o}C in a shaking incubator overnight. The next day the overnight culture was used to inoculate a day culture for protein expression at 37^{o}C until the cells reached the optical density (OD) of 0.8 as measured at 600 nm. Protein expression was induced with 0.8 mM IPTG and the cultures were grown further at 18^{o}C overnight in a shaking incubator at 225 rpm. The cells were harvested by centrifugation at 5,000 rpm for 20 minutes at 4^{o}C. Cell pellets were either stored at -80^{o}C until required or used directly for purification.

2.6.7 Protein purification

Cell pellets were resuspended in 100 ml lysis buffer with PMSF, Lysozyme (0.25 mg/ml) and Protease Inhibitor Cocktail EDTA-free (Roche, 11836170001). Cell lysis was performed by sonication using the 3 mm probe at 35% amplitude for 10 minutes with 5 seconds on and 5 seconds off pulse to break open the cells. The cell lysate was centrifuged at 15,000 rpm for 45 minutes at 4^{o}C and the supernatant obtained was used for further purification. 1 ml of Glutathione Sepharose 4B beads slurry (GE Healthcare, Cat. No. GE17-0756-01) pre-equilibrated with lysis buffer for every 1 L of culture. The pre-equilibrated beads were incubated with the cell-free extract on a rotor for 2 hr at 4^{o}C. The beads were then washed twice with 25 ml high salt wash buffer and three times with 25 ml low salt wash buffer.

For GST-RGC-32, the protein was eluted with 10 ml of elution buffer (20 mM HEPES pH7.5, 500 mM NaCl and 20 mM L-Glutathione) and injected onto a desalting column pre-equilibrated in 20 mM HEPES pH7.5, 500 mM NaCl. For Untagged-RGC-32, FLAG-RGC-32, Untagged-Chicken Spc24-25 and Human Spc24-25, the GST-tag was cleaved on the beads to which the proteins were bound by incubating the beads with PreScission buffer (400 µl of 2 mg/ml PreScission protease in low salt wash buffer + 1 mM DTT) at 4^{o}C overnight. Both GST-RGC-32 and cleaved proteins were further purified using a gel filtration column S200 16/600 (GE Healthcare) and S75 16/600 (GE Healthcare) respectively.

2.6.8 Surface Plasmon Resonance Analysis

Immobilisation of bait proteins (GST-RGC-32 or GST-CDK1 and GST-CDK1-Cyclin B) was performed by injecting 30 µg/ml of bait protein onto Anti-GST CM5 sensor chip to give a surface density of 6000-25000 RU. Ligand proteins (CDK1, CDK1-Cyclin B, Cyclin H or RGC-32 and Cks1) were injected for 60 seconds at a flow rate of 30 µl/minute for each sensorgram. The sample was injected in a 5-fold dilution starting at 5000 nM and the contact time was 500 seconds for RGC-32 as bait and 4000 seconds for CDK1/ CDK1-Cyclin B as bait. All the reactions were performed in 20 mM Hepes pH7.4, 100 mM NaCl, 10 mM MgCl2, 0.01% Tween 20.

2.6.9 Labelling of protein

Fluorescent dye NT-647 NHS (Nanotemper Technologies, Cat. No. L001) was used to label untagged-RGC-32 (20 µM) protein. First, the solid dye was dissolved in 100% DMSO to a final concentration of 435 µM. The concentration of dye was adjusted to 60

µM using the labelling buffer (Nanotemper Technologies). Protein and dye were mixed in 1:3 ratio to a final volume of 200 µl and incubated at room temperature for 30 minutes in dark. The mixture was then passed through the gravity column (Nanotemper Technologies) to remove the unreacted free dye from the protein. The purity of the labelled-protein was determined by measuring the 260 nM: 650 nM ratio using a spectrophotometer.

2.6.10 MicroScale Thermophoresis (MST)

MST was performed by titrating pCDK1-Cyclin $B_{(165\text{-}433 \text{ amino acids})}$, pCDK2-Cyclin $A_{(174\text{-}432 \text{ amino acids})}$ and Chicken Spc24-25 against fluorescently labelled RGC-32. Binding of RGC-32 to different ligands was determined using a Monolith N11.5 machine (Nanotemper Technologies) with standard treated capillaries (Nano temper technologies, Cat. No. M0-K002). First, a pre-test check was performed to determine the homogeneity and optimal working concentration of fluorescently-labelled RGC-32. Once an optimal concentration was determined, the RGC-32 protein was diluted using MST optimised buffer (50 mM Tris-HCl pH 7.4, 150 mM NaCl, 10 mM $MgCl_2$, 0.05 % Tween-20) to make a stock of 100 nM. Ligand proteins were serially diluted to give 16 reaction concentrations using MST optimised buffer in 16 serial steps in a volume of 10 µl in PCR tubes. After this, 10 µl of fluorescently-labelled RGC-32 was added to each tube to give a final concentration of 50 nM. Capillary tubes were filled by dipping the capillaries in each tube and then placed onto the capillary tray. Monolith binding affinity program was run to determine the affinity of binding. All the experiments were carried out at 25^{o}C.

2.6.11 Crystallisation of RGC-32

Purified RGC-32 protein at 8 mg/ml was used to set up crystal trials. An Art Robins Phoenix robot was used to load 400 nl of purified protein onto each of the 96 sitting drop crystallisation well. PACT *premier* HT-96 and JCSG *plus* HT-96-well deep blocks were used for the screening crystallisation conditions as they cover a broad range of PEG and salt conditions. The plates were stored at 20^{o}C.

2.6.12 RGC-32-CDK1-Cyclin B model generation

A 3-D model for the complex was generated using an online Z-Dock server. The RGC-32 model was initially generated using the Raptor 3-D prediction program. The RGC-32 model was used as an input ligand while the CDK1-Cyclin B structure (PDB 4YC3) was used as a receptor (Brown *et al.*, 2015). The Z-dock program generates a structure model of the complex based on all possible combinations in the translational as well as rotational space between the ligand and the receptor proteins. It screens each model using an energy-based function and generates five models. Each model generated will have different energy content. For the interaction to be favourable, the energy for the complex should be less than the energy of the individual molecules. The complex with the least energy content (model 1) was used for our analysis.

2.6.13 Immunostaining

Cells were treated with 2 μM of 1NM-PP1 (EMD MILLIPORE, Cat. No. 529581) for 20 hrs before washing them into mitosis. For fixing, the media was aspirated at each time point and cells were washed with warm PBS. The cells were then fixed with 4% freshly made paraformaldehyde (Electron Microscopy Sciences, Cat. No. 15714) for 15 min at

room temperature. The fixed cells were next washed with PBS three times. Cells were permeabilised using PBS-0.1% Triton X-100 (Fisher) for 15 minutes at room temperature. After this, the cells were blocked for 60 minutes at room temperature in 3% BSA-PBS-0.1% Triton-X 100. Primary antibody (Appendix 7.3) made up in 3% BSA-PBS was added to the cells overnight at 4^{o}C on a rocker. Cells were then washed three times with PBS and incubated in secondary antibodies (Appendix 7.4) diluted in 3% BSA-PBS for 2 hr at room temperature in dark. The cells were washed three times with PBS followed by addition of Hoechst 33342 (Life Technologies) in PBS (1:1000) to stain the nucleus. Stained cells were stored at 4^{o}C in dark.

2.6.14 Propidium Iodide (PI) Staining

For propidium iodide staining, 2x10^{4} cells were pelleted at 1300 rpm for 5 minutes at 4^{o}C. Cells were washed once with cold PBS (1X) and pelleted again. Cells were fixed by resuspending in 70% ethanol (cold) at -20^{o}C for 1 hr. Cells were washed twice with cold PBS (1X) and pelleted again. Cell pellets were resuspended in 500 µl of PI stain containing 50 µg/ml RnaseA (Sigma), incubated for 30 minutes at RT and strained using 40 µM strainer. Fixed cells were analysed for 10,000 events using BD Accuri C6 flow cytometer. Percentage of cells in G2 was determined by gating the cells for cell count versus FL2-A.

2.6.15 FACS Analysis

Flow cytometry was used to analyse GFP-positive population or cell cycle distribution. 2x10^{4} cells were pelleted at 1300 rpm for 5 minutes at 4^{o}C. Cells were washed once with cold PBS (1X) and pelleted again. Cell pellets were resuspended in 500 µl of 0.5%

Formaldehyde in PBS (1X) and strained using 40 μM strainer. Fixed cells were either stored at 4^{o}C (short-term) or directly analysed for 10,000 events using BD Accuri C6 flow cytometer. Percentage of GFP-positive cells was determined by gating the cells for cell count versus FL1-A.

3 Characterisation of RGC-32 interaction with CDK1 and the kinetochore subunits Spc24-25

3.1 Introduction

RGC-32 was first reported as a cell cycle regulator in aortic smooth muscle cells by Badea *et al*. (Badea *et al.*, 2002). The human RGC-32 protein consists of 117 amino acid residues. We carried out secondary structure prediction analysis using JPRED (Drozdetskiy *et al.*, 2015) which predicted that most of the RGC-32 protein is intrinsically disordered, but there are three predicted short α-helices, α-1, α-2 and α-3 (**Figure 3.1A**). A three-dimensional structure prediction analysis using PHYRE2.0 was carried out (Kelley *et al.*, 2015) but the overall confidence level of the tertiary structure prediction was low (**Figure 3.1B**). However, the secondary structure analysis by PHYRE2.0 also predicted three main α-helices in RGC-32 sequence, which is in agreement with the JPRED prediction. The PHYRE2.0 predication also showed that about 54% of RGC-32 sequence is disordered (**Figure 3.1C**), indicating that RGC-32 is an intrinsically disordered protein. This may explain the low confidence level in its tertiary structure prediction. RGC-32 was further confirmed to be highly disordered protein using a disorder prediction software, RONN (Yang *et al.*, 2005) (**Figure 3.2**).

Previous pull-down studies showed that RGC-32 interacted with CDK1 both *in vitro* and *in vivo*. This interaction, however, was not observed with CDK2 and CDK4. They further showed that the kinase activity of CDK1 was enhanced by RGC-32 in a dose-dependent manner *in vitro* (Badea *et al.*, 2002).

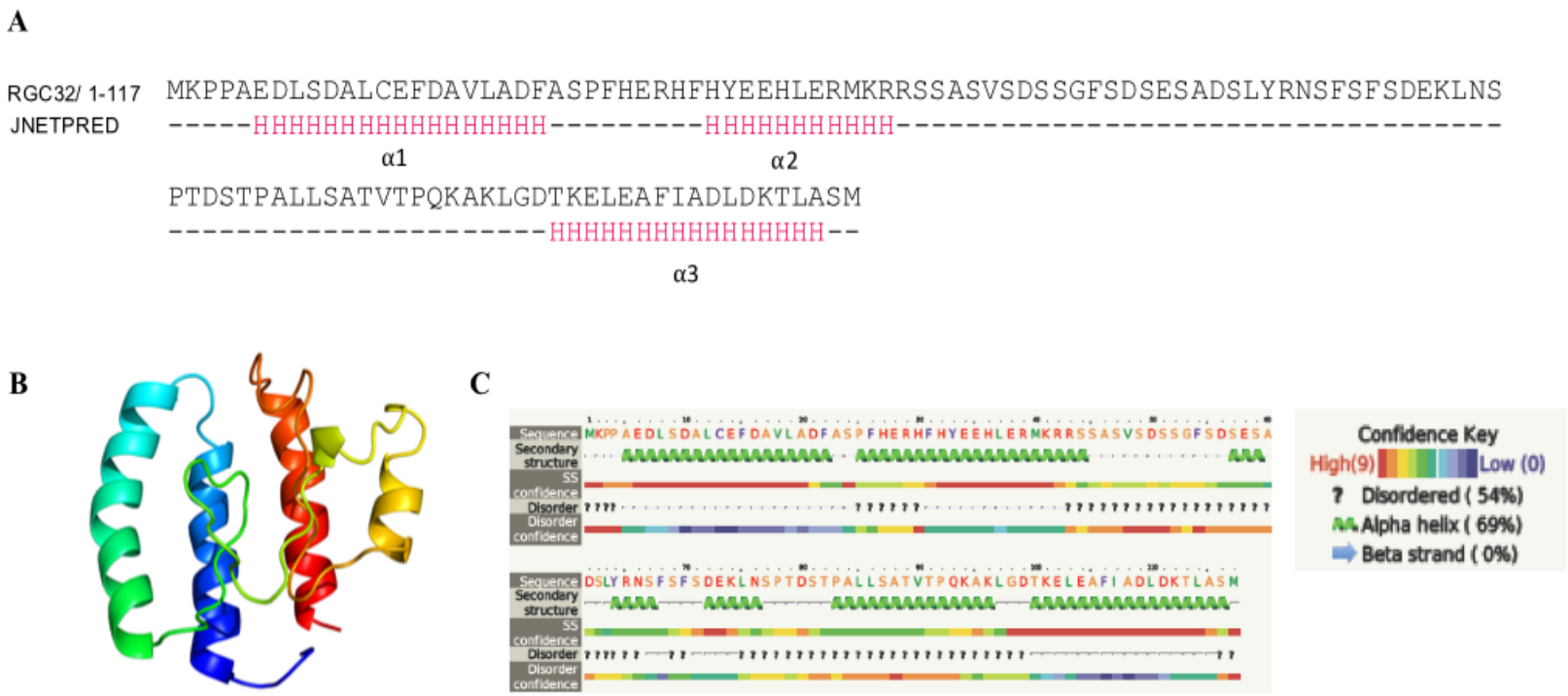

Figure 3.1 Secondary and tertiary structure prediction analysis of RGC-32.

(A) RGC-32 secondary structure prediction using JPRED shows the presence of three α-helices (α1, α2 and α3) with a long coiled-coil region between α2 and α3 (Drozdetskiy *et al.*, 2015). (B) Tertiary prediction analysis of RGC-32 using PHYRE2.0 showing three major helices. (C) Secondary structure analysis of RGC-32 from PHYRE2.0 showing the three main α-helices as predicted by JPRED. This analysis also shows that 54 % of the protein is disordered (Kelley *et al.*, 2015).

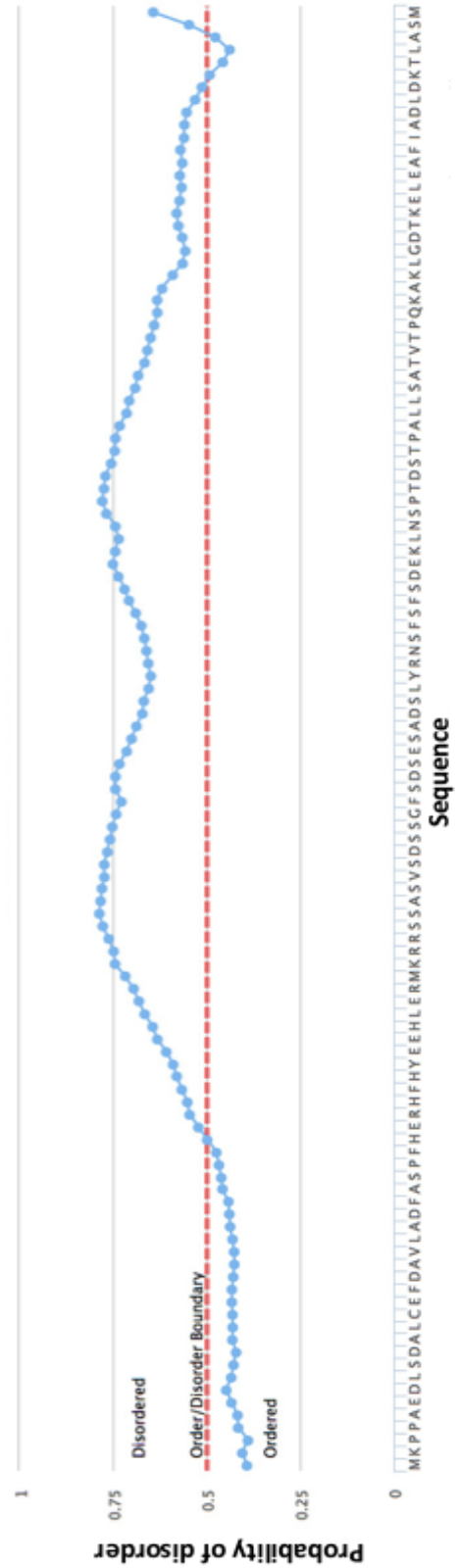

Figure 3.2 Prediction of disordered regions of RGC-32 by RONN analysis.
Plot from RONN disorder prediction software showing that the majority of the RGC-32 sequence has a high likelihood of disorder (Yang *et al.*, 2005).

Interestingly, another group reported that RGC-32 binds to PLK1, another key mitotic kinase, *in vitro* but not to the CDK1-Cyclin B1 complex (Saigusa *et al.*, 2007). To address these contradicting reports, Dr Lina Chen in our laboratory carried out pull-down assays and confirmed that RGC-32 binds to both mitotic kinases, CDK1 and PLK1, in B cell lysates. This chapter aimed to determine whether the interaction between RGC-32 and CDK1 was direct, to characterise the interaction and to examine potential new binding partners in order to gain more insight into the function of RGC-32 at the molecular level.

3.2 Production of recombinant RGC-32

To study RGC-32 interactions, N-terminal GST-tagged RGC-32 was expressed and purified from 3 L of *E.coli* BL21 (DE3) Rosetta pLysS cells using Glutathione-affinity purification. The GST-tag was removed by 3C PreScission Protease cleavage on beads at 4^{o}C overnight. Untagged RGC-32 protein was concentrated and further purified by S75 16/600 size exclusion chromatography (SEC). The elution profile obtained using SEC showed that RGC-32 ran as a higher molecular weight species than its predicted molecular weight (~13 kDa) (**Figure 3.3A**). Upon calculating the molecular weight based on elution volume, it was found that RGC-32 possibly forms a dimer or trimer. However, this might also be due to the fact that RGC-32 is mostly unstructured and therefore runs as an elongated protein. Analysis of fractions from SEC by SDS-PAGE demonstrated that RGC-32 was highly pure and present in fractions B2-B7 (**Figure 3.3B**).

After initial purification of RGC-32, we attempted to crystalise RGC-32 to determine its three-dimensional structure. For crystallisation, fractions B3-B10 of purified RGC-32

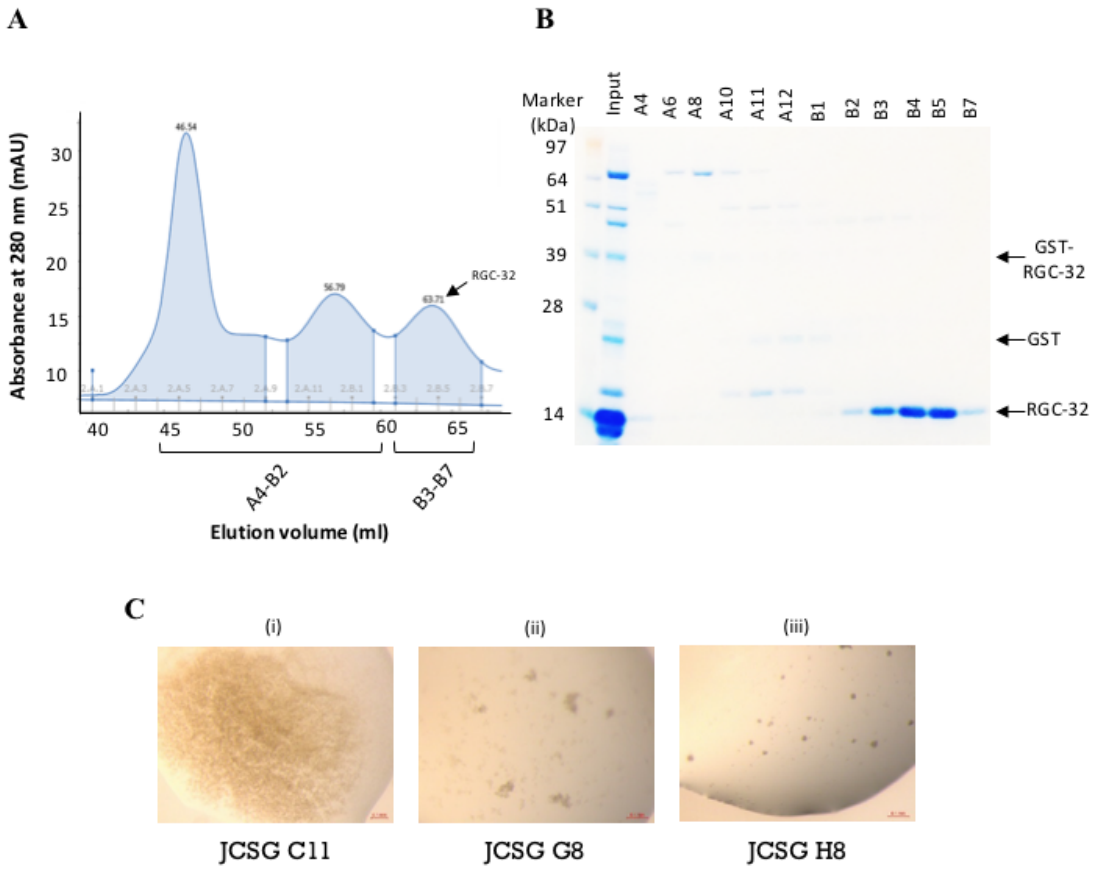

Figure 3.3 Purification of RGC-32 and crystallisation.
(A) Elution profile of RGC-32 from S75 16/600 size exclusion chromatography (SEC) eluted in 20 mM Hepes pH 7.4, 500 mM NaCl, 0.5 mM TCEP. (B) Coomassie stained gel showing samples from SEC. (C) Images of wells showing crystalline precipitant of RGC-32 in (i) 2 M ammonium sulfate, 0.1% Na acetate pH 4.6 (ii) 0.15 M DL-Malic acid, 20% w/v PEG 3350 and (iii) 0.2 M NaCl, 0.1 M Bis-tris pH 5.5, 25% w/v PEG 3350 conditions from JCSG *plus* screen used for crystal trials.

protein were concentrated to 7.9 mg/ml in a final volume of 100 μl. Crystal trials were set up by Phoenix robot using the sitting drop method (400 nl) with the PACT *premier* HT-96 and JCSG *plus* HT-96 screens (Molecular Dimensions). Plates were incubated at 20^{o}C for four weeks. Many crystalline precipitations were observed in JCSG plate but unfortunately, they were not big enough for structural studies (**Figure 3.3C**). These conditions need further optimisation in order to produce a good quality crystal for structure elucidation but given the disordered nature of RGC-32 we reasoned that it was unlikely to crystallise it in the absence of a binding partner that may promote its folding.

3.3 Can RGC-32 bind directly to the mitotic kinase CDK1?

Studies by other groups and experiments carried out in our laboratory demonstrated the ability of RGC-32 to bind to CDK1. However, all these studies were performed using whole cell lysates, which leaves a possibility that this interaction may be mediated by another protein. Interestingly, RGC-32 did not pull-down cyclin B1 in the studies in our laboratory using GST-RGC-32 incubated with B cell lysates (Dr Lina Chen). Therefore, to investigate whether RGC-32 binds directly to CDK1, but perhaps not to CDK1-Cyclin B complex, surface plasmon resonance (SPR) experiments were carried out by Prof. Jane Endicott (Newcastle University). This technique detects the changes in the refractive index due to a change in mass at the surface to which a bait protein is coupled. To carry out these experiments, recombinant untagged RGC-32 protein was expressed and purified from *E.coli* as described earlier. CDK1, CDK1-Cyclin B both GST-tagged and un-tagged and Cyclin H proteins were purified by the Endicott lab (Newcastle University), however, the evidence of the purified proteins and their activity was not available to us and these experiments would have been better controlled if they were presented.

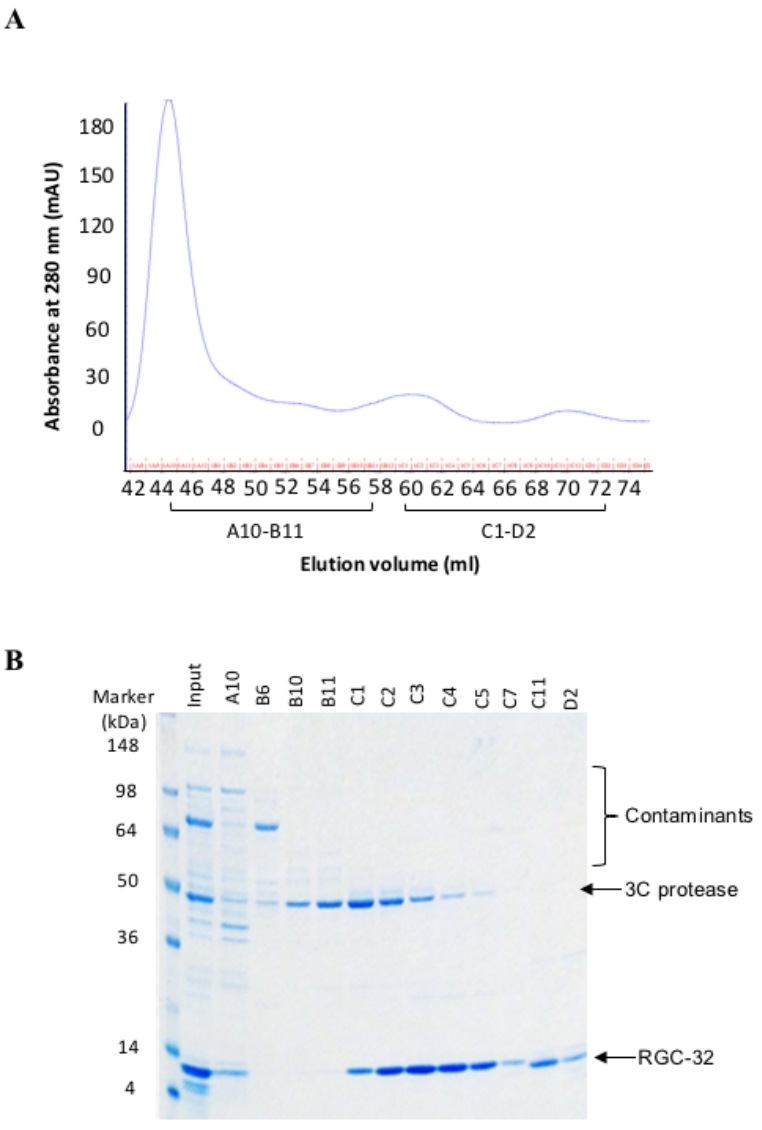

Figure 3.4 Purification of RGC-32 for interaction studies.
(A) Elution profile of GST-cleaved RGC-32 from S75 16/600 size exclusion column pre-equilibrated in 20 mM Hepes pH 7.4, 300 mM NaCl, 10 mM MgCl2, 0.01% Tween 20, 0.5 mM TCEP. (B) Coomassie stained gel shows samples from gel filtration separated on 10-20% NuPAGE Novex Tris-Glycine gel (Invitrogen).

Figure 3.4A shows the elution profile of untagged RGC-32 from SEC. When elution fractions were analysed by SDS PAGE, an additional protein running ~48 kDa was also observed partially overlapping the RGC-32 peak. This could be 3C PreScission Protease that has a molecular weight of 46 kDa because of excessive amount added to the protein during GST-tag cleavage (**Figure 3.4B**). Due to the presence of contamination in the initial fractions of GST-RGC-32, only fractions C4-C7 were concentrated and used for interaction studies. For SPR studies, 10 μM of anti-GST antibody was immobilised on a sensor chip (Biacore) and binding of untagged RGC-32 to GST-CDK1 and GST-CDK1-Cyclin B (bait) was studied by coupling the bait proteins to GST antibody on the sensor chip. Binding of Cks1 was used as a positive control since it is a known binding partner of CDK1 (Hayles *et al.*, 1986). Previous structural studies have shown that Cks1 binds to both CDK1 and CDK1-Cyclin B complex (Patra and Dunphy, 1998) making it a good positive control for both. Cks1 and untagged RGC-32 were flowed over the chip at a range of concentrations. The highest concentration of Cks1 and RGC-32 used was 4000 nM followed by 4-fold dilutions (15.6 nM to 4000 nM). As shown in **Figure 3.5 (A & B)**, Cks1 binds to GST-CDK1 and GST-CDK1-Cyclin B with fast association and dissociation rate. The K_D determined for Cks1 binding with both CDK1 and CDK1-Cyclin B was 12.1 nM and 11.3 nM respectively. The binding affinity of Cks1 to CDK1 was found to be similar to the previously reported binding affinity of Cks1 to CDK2 (77 nM) (Bourne *et al.*, 1996). For RGC-32, although concentration-dependent binding was observed for both CDK1 and the CDK1-Cyclin B complex, the binding did not reach saturation and dissociation was very slow. This meant the dissociation constant determined could be inaccurate. The K_D for binding of RGC-32 to CDK1 and CDK1-

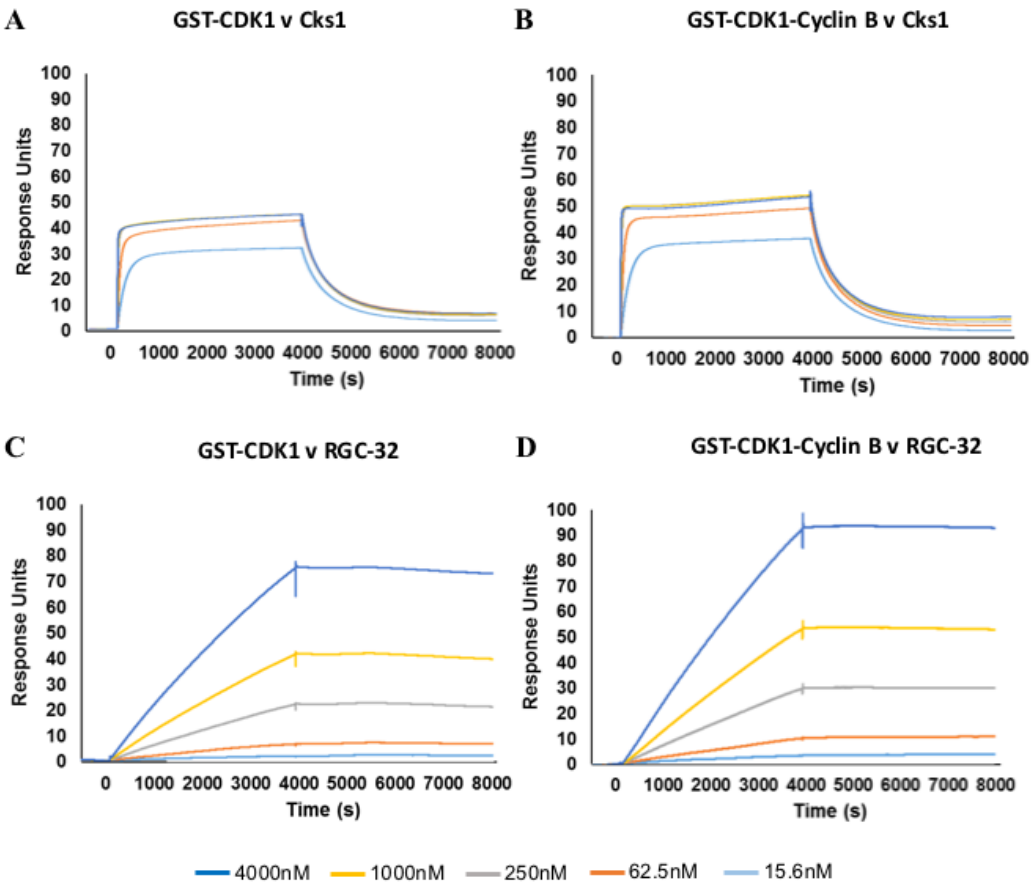

Figure 3.5 Surface Plasmon resonance analysis of CDK1 and CDK1-Cyclin B binding to Cks1 and RGC-32.

Representative graphs showing the interaction curves obtained with increasing concentration of analyte, (A & B) Cks1 and (C & D) RGC-32. Results shown are representative of two independent experiments. Untagged RGC-32 was purified by me and SPR studies were performed by Prof. Jane Endicott group (Newcastle University).

Cyclin B was estimated to be ~400 nM and ~80 nM respectively (**Figure 3.5C & D**). Therefore, it seems that the presence of cyclin B enhances the interaction of RGC-32 with CDK1. To further validate the binding observed was not a result of surface dependent changes to the protein (bait) due to immobilisation on the sensor chip, SPR studies were repeated by swapping the bait and analyte. Recombinant GST-RGC-32 was expressed and purified from *E.coli* using Glutathione beads as described earlier. Beads were washed with high salt wash buffer followed by low salt to remove non-specifically bound proteins. Bound GST-RGC-32 was eluted from the beads with elution buffer (20 mM HEPES pH7.5, 500 mM NaCl and 20 mM L-Glutathione) followed by removal of L-Glutathione using a desalting column. GST-RGC-32 was eluted, concentrated and injected onto an S200 16/600 SEC column. **Figure 3.6A** shows the elution profile of GST-RGC-32. Fractions were analysed by SDS-PAGE and fractions C8-D3 were concentrated and used as bait for interaction studies (**Figure 3.6B**). Purified CDK1, CDK1-Cyclin B and cyclin H (analyte) were flowed over the chip in separate reactions using increasing concentrations (40 nM to 5000 nM). Cyclin H was included as a negative control for the experiment. As observed in **Figure 3.7**, the binding of CDK1 to GST-RGC-32 increased with increasing concentration of the injected protein. The association and dissociation were again found to be slow for this interaction (**Figure 3.7A**). On the other hand, CDK1-Cyclin B and Cyclin H showed no evidence of interaction even at the highest concentration (**Figure 3.7B & C**). This contradicts with our previous observation of interaction between RGC-32 and CDK1 to be enhanced in the presence of cyclin B. However, we did not have a positive control (e.g. GST-Cks1) for binding of CDK1-Cyclin B due to which we could not prove that the complex was functional or shows clear

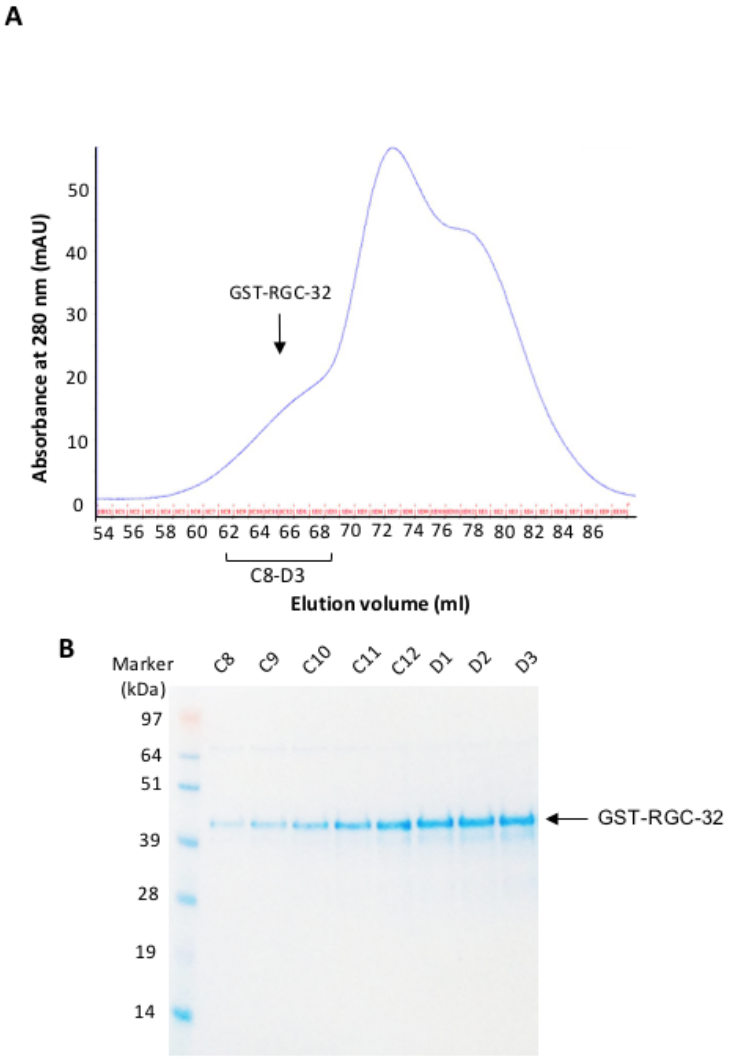

Figure 3.6 Purification of GST-RGC-32 for interaction studies.
(A) Elution profile of GST-RGC-32 from S200 16/600 size exclusion chromatography (SEC) eluted in 20 mM Hepes pH 7.4, 300 mM NaCl, 10 mM MgCl2, 0.01% Tween 20, 0.5 mM TCEP. (B) Coomassie stained gel showing purified GST-RGC-32 in fractions C8-D3 from the SEC.

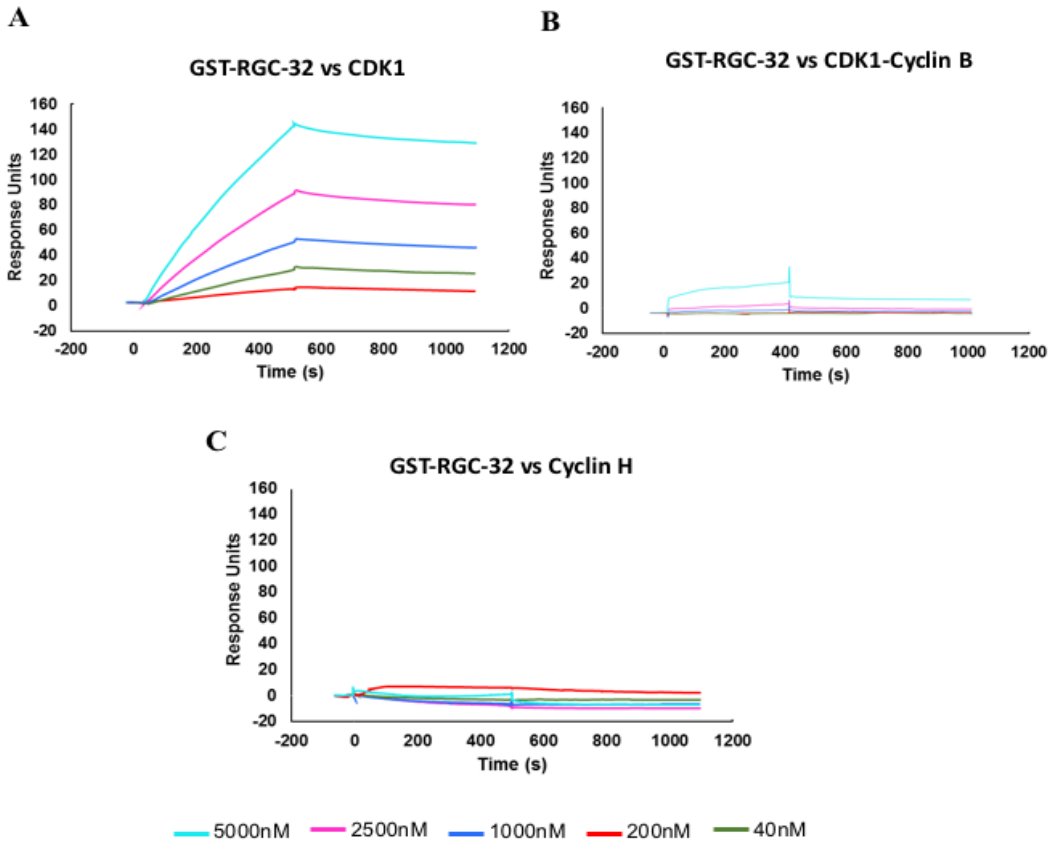

Figure 3.7 Surface Plasmon resonance analysis of RGC-32 binding to CDK1, CDK1-Cyclin B and Cyclin H.
Representative graphs showing the interaction curves obtained with increasing concentration of analyte, (A) CDK1 (B) CDK1-Cyclin B and (C) Cyclin H. Results shown are representative of two independent experiments. GST-RGC-32 was purified by me and SPR studies were performed by Prof. Jane Endicott group (Newcastle University).

binding to a bait in SPR. Therefore, we could not make any secure conclusions about the ability of RGC-32 to bind to CDK1-Cyclin B from these SPR studies. Since SPR did not allow us to properly study the interaction between RGC-32 and CDK1 or CDK1-Cyclin B, we used an alternative technique, MicroScale Thermophoresis (MST). In MST, one of the molecules under study is fluorescently labelled and its rate of movement across a temperature gradient is measured in the presence of different concentrations of an unlabelled partner protein. The rate of movement depends on several factors such as size, charge and confirmation of the molecule. Purified CDK1 and CDK1-Cyclin B complex were provided to us by Prof. Jane Endicott for use in MST (Newcastle University). Untagged RGC-32 was purified as described earlier (**Figure 3.8A**) and covalently labelled with the fluorescent dye NT-647 NHS. Both CDK1 and CDK1-Cyclin B were titrated to achieve a gradient starting with the highest concentration (38.1 μM to 0.00116 μM) and (8.49 μM to 0.000259 μM) respectively. Each dilution series was incubated with 50 nM of labelled RGC-32. **Figure 3.8** shows the binding curves for RGC-32 obtained using CDK1 and CDK1-Cyclin B respectively. The K_D determined for CDK1 was 7.4 ± 4.7 μM and for CDK1-Cyclin B was 5.9 ± 7.3 nM. These values confirm the initial SPR results that RGC-32 binds to the CDK1-Cyclin B complex with higher affinity than CDK1 alone. In order to confirm that the interaction between RGC-32 and CDK1-Cyclin B complex was specific, we examined the binding of RGC-32 to CDK2-Cyclin A complex using MST. The purified CDK2-Cyclin A complex was titrated (4.25 μM to 0.00104 μM) against fluorescently labelled RGC-32 (50 nM) (**Figure 3.9A**). No significant change in fluorescence was observed in the thermophoretic signal of RGC-32 even at high concentrations of CDK2-Cyclin A complex (**Figure 3.9B**). Therefore, these

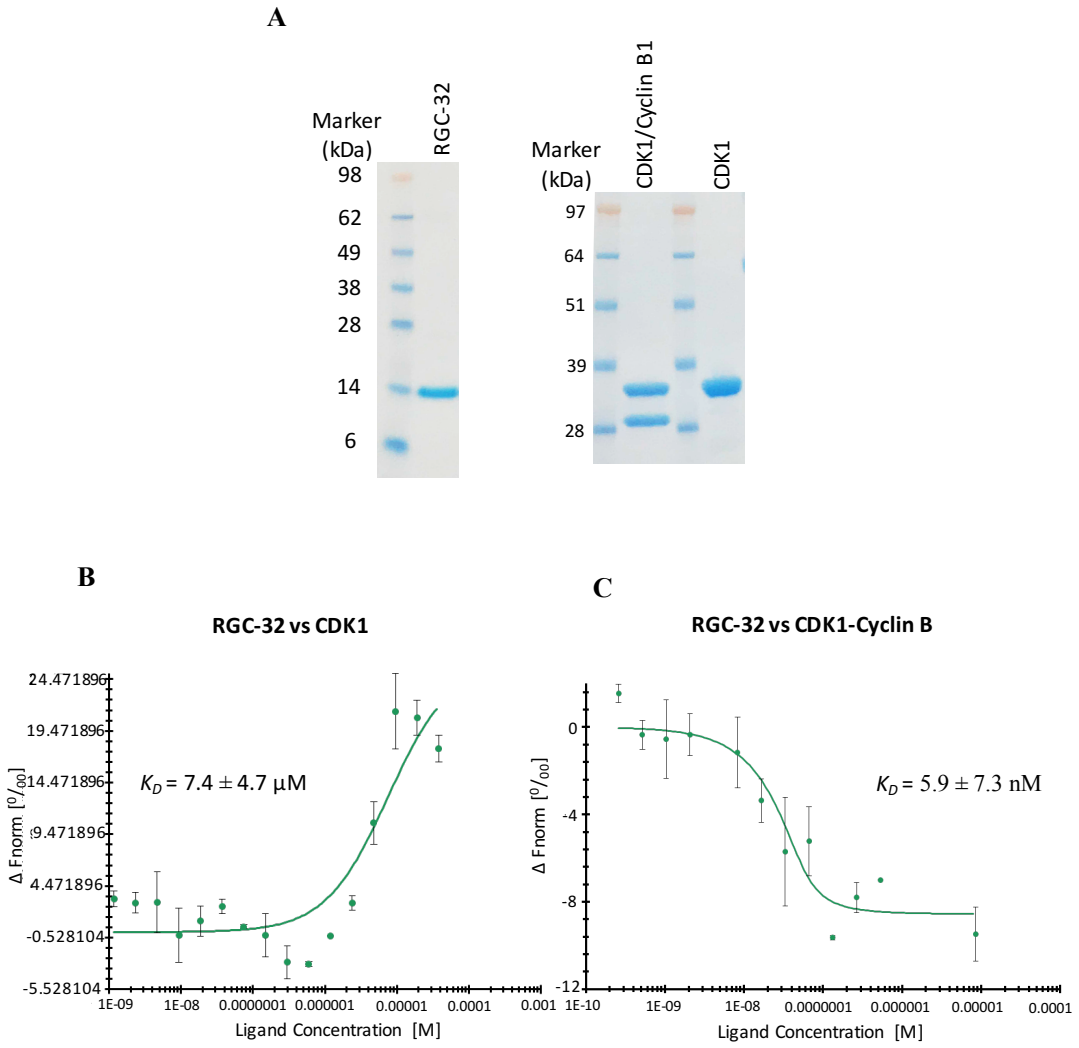

Figure 3.8 Microscale thermophoresis analysis of CDK1 and pCDK1-Cyclin B binding to RGC-32.

(A) Coomassie stained gel showing the purified RGC-32, CDK1 and pCDK1-Cyclin B complex used for analysis. Graphs showing the change in thermophoretic signal upon binding of CDK1 (B) and pCDK1-Cyclin B (C) to 50 nM of fluorescently labelled (NT647NHS) RGC-32. Results show the mean of three independent experiments ± standard deviation.

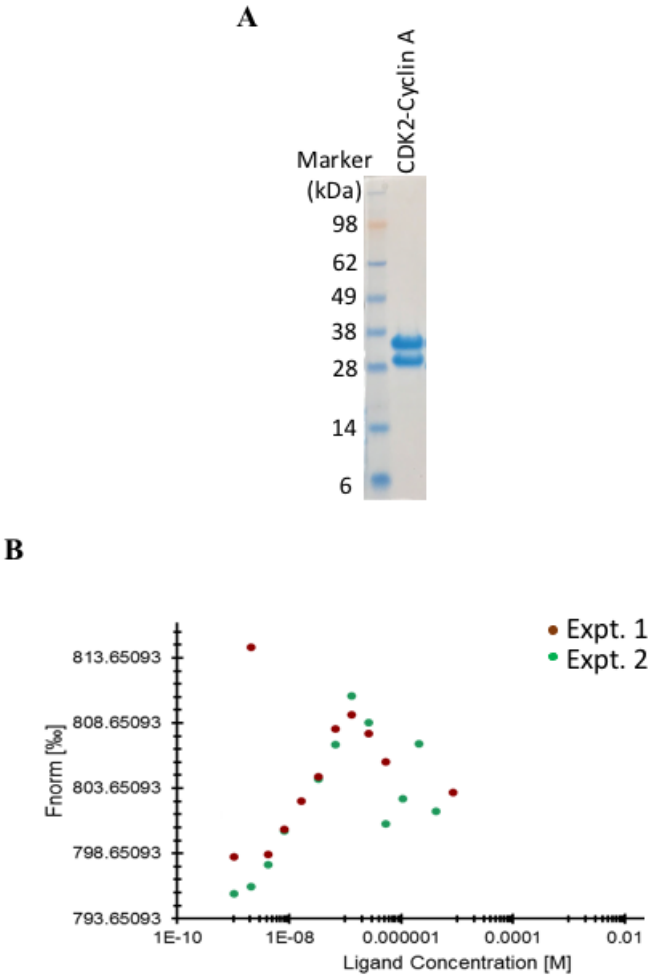

Figure 3.9 Microscale thermophoresis analysis of pCDK2-Cyclin A binding to RGC-32.

(A) Coomassie stained gel showing the purified pCDK2-Cyclin A used for analysis. (B) Graph showing no change in thermophoretic signal upon binding of pCDK2-Cyclin A to 50 nM of fluorescently labelled (NT647NHS) RGC-32. Therefore, the data is represented as Fnorm [$^{0}/_{00}$].

data confirms previous studies that RGC-32 does not interact with CDK2-Cyclin A but has specificity towards CDK1 (Badea *et al.*, 2002). Overall, both SPR and MST studies provided us with evidence that RGC-32 can directly bind to CDK1. However, SPR could not accurately determine the K_{Ds} of the interaction and surprisingly, MST gave us a 1000-fold difference in K_D values. Therefore, the interaction of RGC-32 with CDK1 +/- Cyclin B needed further characterization using an established Homogenous Time-Resolved Fluorescence (HTRF) assay set up by the Endicott-Noble laboratory. This technique exploits Fluorescence Resonance Energy Transfer (FRET) signal with time-resolved measurement of fluorescence. In this technique, fluorescent antibodies are used against the tag of each protein thereby making a 'sandwich' assay. The interaction between the two proteins is then measured by fluorescence as a result of energy transfer between both the proteins upon excitation. The time-resolved measurement of fluorescence allows elimination of transient background signal. In order to perform this assay, we expressed and purified good quality FLAG tagged-RGC-32 by cloning into a GST expression vector (pGEX6P3, **Appendix 7.8**). However, due to time constraints and delays with our collaborators, these experiments were never completed.

3.4 Expression and purification of chicken Spc24-25 and human Spc24-25 kinetochore subunits

During the course of this study, a tertiary structure prediction program identified similarity between the 3rd α-helix of RGC-32 and a receptor motif in the N-terminus of a histone-fold protein CNN-1 from budding yeast. These regions showed 37% sequence identity using HHpred but some key interacting residues were conserved (**Figure 3.10**). CNN-1 acts as a centromere receptor for the binding of the NDC80 complex which is a crucial microtubule binding component of the kinetochore and is known to be

evolutionarily conserved across species (Schleiffer *et al.*, 2012). The CNN-1 receptor motif binds to the Spc24-25 heterodimer of NDC80 complex as a 'molecular hook' which securely tethers the NDC80 complex to the inner kinetochore. This interaction was found to be crucial for connecting the microtubules to the centromere thereby allowing proper segregation of chromosomes. The interaction between CNN-1 and Spc24-25 requires three hydrophobic residues F69, L70, and L73 in CNN-1 which binds in the hydrophobic pocket of the Spc24-25 globular domain (Malvezzi *et al.*, 2013). Interestingly, out of these three hydrophobic residues, two were conserved and one was found to be similar at the corresponding positions in the 3rd α-helical region of RGC-32 (F106, I107 and L110). Preliminary studies were performed by Dr Lina Chen in our laboratory to investigate whether RGC-32 binds to Spc24. She found that RGC-32 was able to pull-down Spc24 from B cell lysates indicating the ability of RGC-32 to interact with Spc24 subunit of kinetochore (unpublished data).

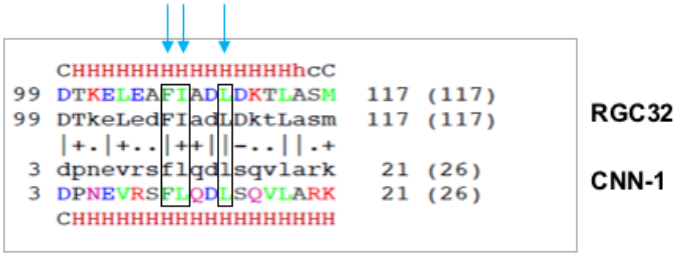

Figure 3.10 Sequence alignment of RGC-32 and CNN-1.
The sequence alignment showed 37% identity using HHpred. RGC-32 has two conserved and one similar hydrophobic residue to CNN-1 which is required for Spc24-25 interactions. The residues are marked with blue arrows (Malvezzi *et al*., 2013).

Therefore, based on this preliminary result, we set out to characterise the interaction of RGC-32 with the kinetochore proteins Spc24 and Spc25. Dr Chris Prodromou (University of Sussex) kindly provided us with the recombinant constructs for both chicken and human Spc24-25. Since the sequence of Spc24 and Spc25 globular domains is highly conserved between chicken and human with a sequence identity of ~60% (**Figure 3.11**), we decided to pursue the experiments using Spc24-25 heterodimers from both the species to increase the likelihood of being able to purify recombinant proteins for our studies. Structurally, chicken and human Spc24-Spc25 are highly conserved (Malvezzi *et al.*, 2013, Nishino *et al.*, 2013). Chicken $Spc24_{(125\text{-}195\ aa)}$ and human $Spc24_{(121\text{-}197\ aa)}$ were cloned separately into a His_6-tag expression vector (p2E) and chicken $Spc25_{(132\text{-}234\ aa)}$ and human $Spc25_{(123\text{-}224\ aa)}$ were cloned separately into a 2X-Strep-His_6-tag expression vector (pET28b) by the Prodromou laboratory (University of Sussex). The regions cloned for recombinant protein purification consisted of the globular domains of Spc24-25 as these regions have been previously expressed from chicken and human for interaction studies with CENP-T proteins (homolog of CNN-1) (Nishino *et al.*, 2013) (**Figure 3.12A**). Purification of these four recombinant proteins was carried out by the Prodromou laboratory (University of Sussex) but the proteins were insoluble, with most protein found in the pellet. Therefore, in order to improve solubility, I sub-cloned the globular domains into an N-terminal GST-tag expression vector (p3E). This is because GST-tagged proteins often have improved solubility and stability (Zhou and Wagner, 2010). A solubility test was carried out by expressing recombinant GST-tagged

Figure 3.11 Sequence alignment of Spc24 and Spc25 globular domains.
Sequence alignment of (A) Spc24 and (B) Spc25 globular domains from human and chicken showing ~60% identity using Clustal Omega.

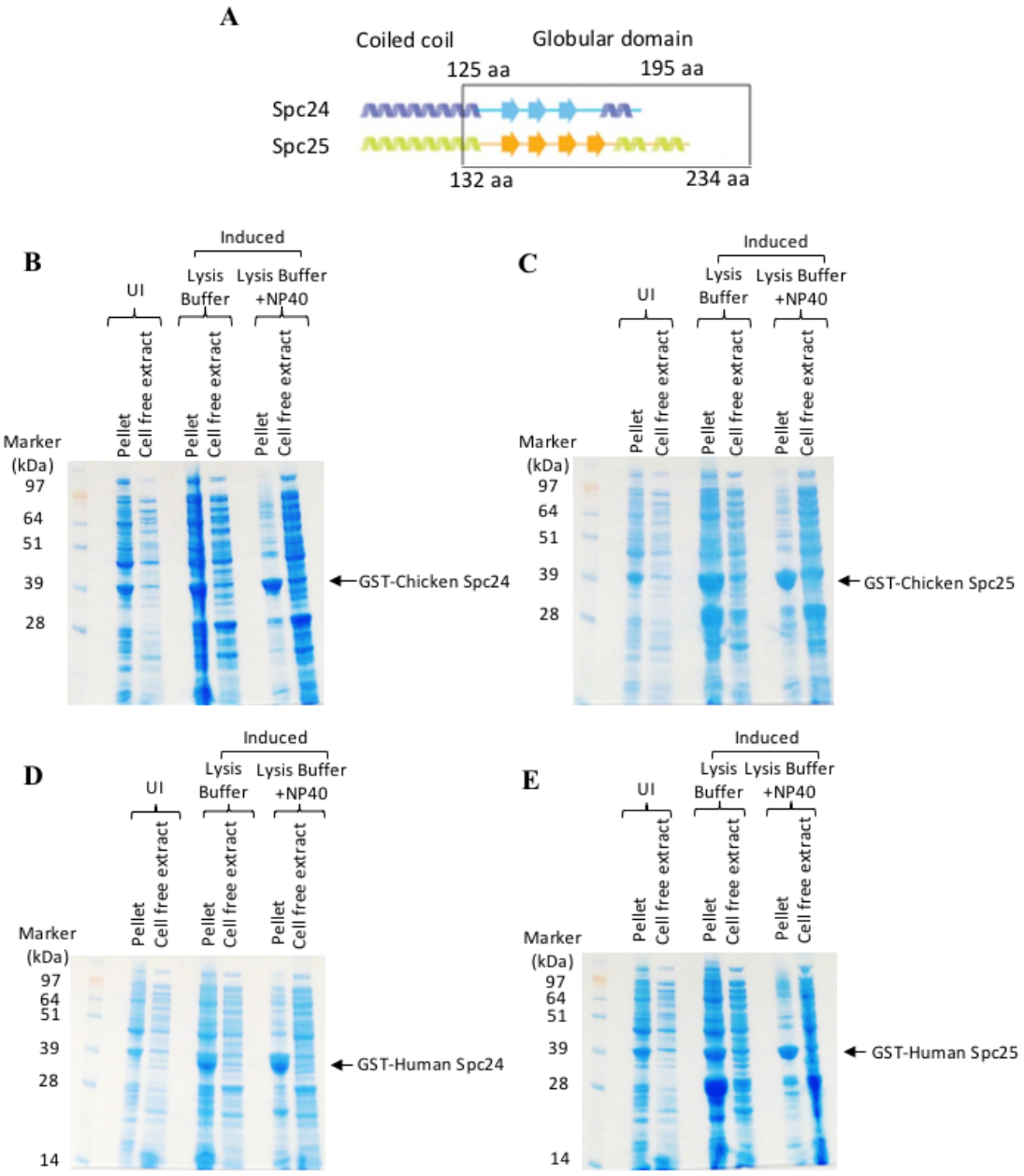

Figure 3.12 Testing the solubility of recombinant Chicken Spc24-25 and Human Spc24-25 globular domains.

(A) Schematic diagram of Chicken Spc24 and Spc25. The globular domains used for interaction studies are boxed. (B-E) Coomassie stained gel showing solubility of GST-Chicken Spc24, GST-Chicken Spc25, GST-Human Spc24 and GST-Human Spc25 proteins respectively with and without detergent in the lysis buffer. Uninduced samples are denoted as UI.

chicken (Spc24 & Spc25) and human (Spc24 & Spc25) proteins in *E.coli*. The cell pellets were lysed in buffer with and without detergent (NP-40). Both insoluble and soluble fractions of uninduced and induced (0.8 mM IPTG) samples were analysed by SDS-PAGE (**Figure 3.12B-E**). The presence of the GST tag led to the improved expression of the proteins overall. The solubility of chicken Scp24 and Spc25 was increased when detergent was present in the lysis buffer (**Figure 3.12 B and C**), but both human proteins were poorly soluble even in the presence of detergent (**Figure 3.12 D and E**). As Spc24 and Spc25 subunits are known to form heterodimers within the NDC80 complex (**Figure 1.4**), we tested whether co-expression of these proteins could further improve their overall solubility. Following protein expression, cells were lysed in buffer with and without detergent (NP-40) and insoluble and soluble fractions were analysed by SDS-PAGE. We observed improved solubility when they were co-expressed particularly in the presence of detergent (**Figure 3.13**). In fact, co-expression improved the solubility of Spc25 even in the absence of detergent. We next purified the chicken Spc24-25 heterodimer on a larger scale (2 liters) to obtain recombinant proteins for interaction studies. The cells were lysed in lysis buffer and Glutathione-affinity purification was performed. Following binding, beads were extensively washed with high salt and low salt wash buffers to remove the non-specifically bound proteins and the GST-tag was cleaved on beads with 3C Prescission protease. The cleaved chicken Spc24-25 protein was concentrated and applied to a S75 16/600 SEC in order to remove any contaminants. **Figure 3.14A** shows the elution profile of the chicken Spc24-25 heterodimer from SEC. Fractions obtained from all peaks were analysed by SDS PAGE. Both Spc24 and Spc25 eluted in the same fractions indicating their association as a dimer (**Figure 3.14B**).

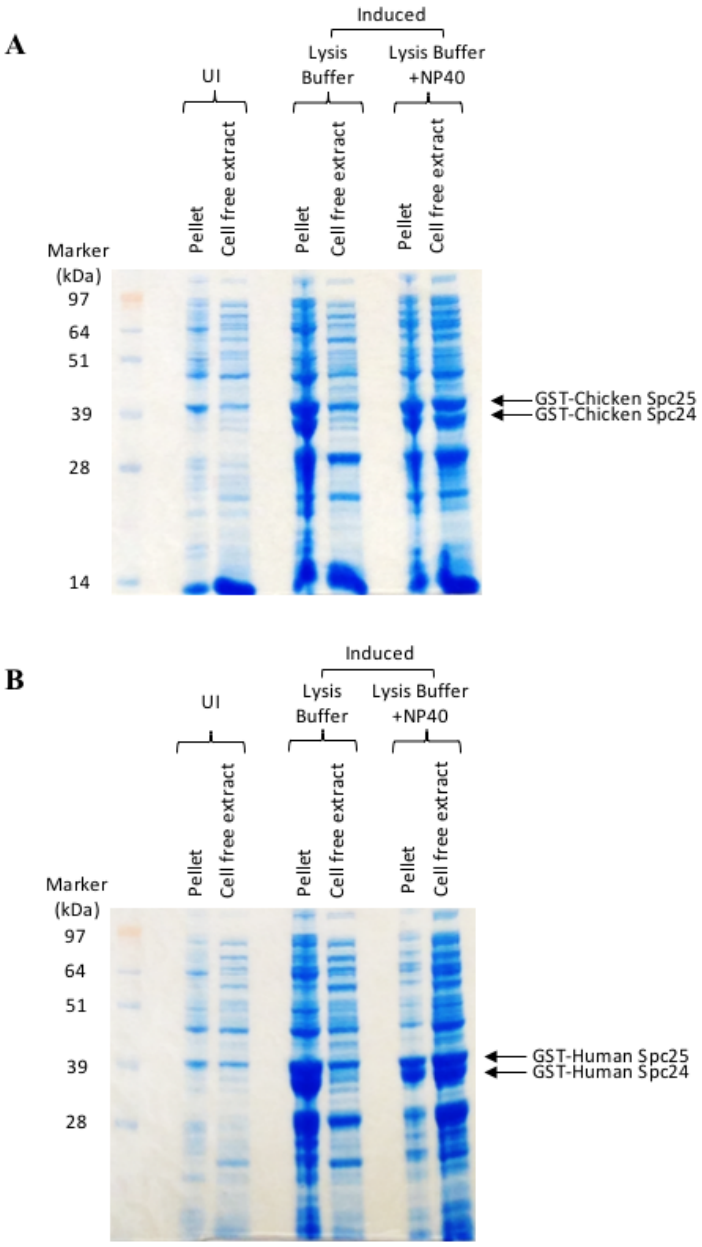

Figure 3.13 Co-expression of recombinant Chicken Spc24-25 and Human Spc24-25 globular domains.
(A) & (B) Coomassie stained gels showing solubility of co-expressed Chicken Spc24-25 and Human Spc24-25 proteins respectively with and without detergent in the lysis buffer. Uninduced sample is denoted as UI.

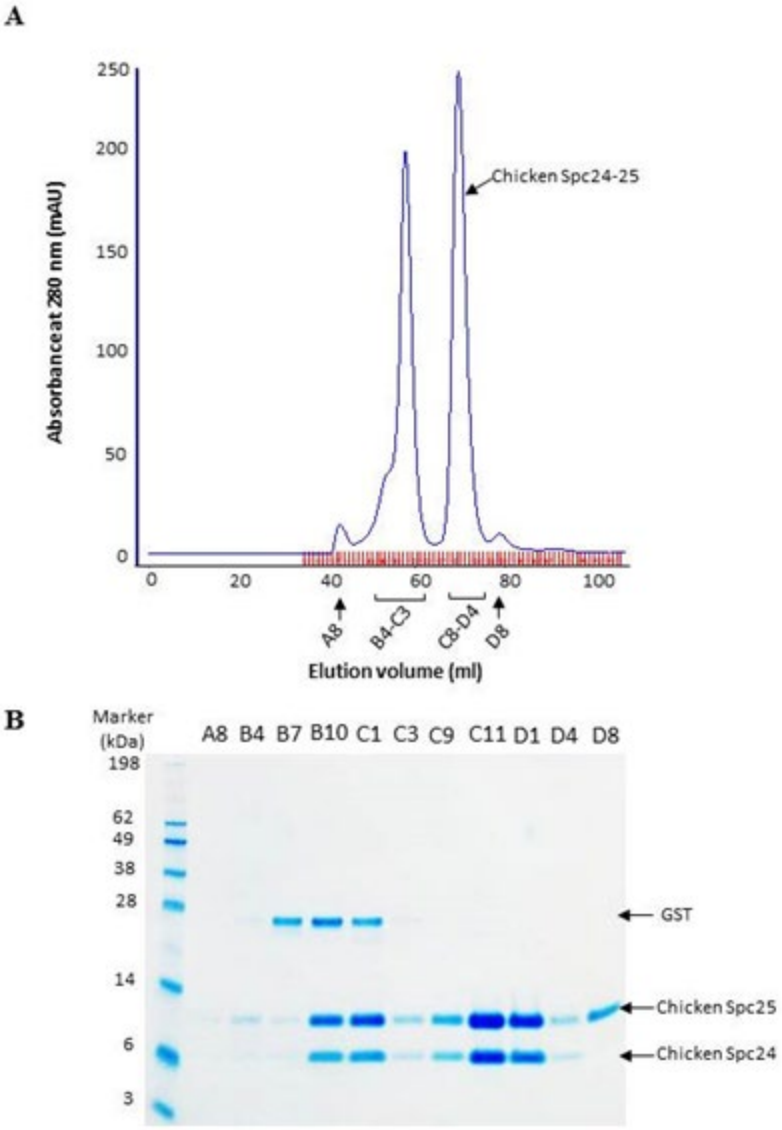

Figure 3.14 Large scale purification of recombinant Chicken Spc24-25 globular domains. (A) Elution profile of GST-cleaved Chicken Spc24-25 from S75 16/600 size exclusion column pre-equilibrated in 50 mM Tris-HCL pH7.5, 150 mM NaCl, 0.5mM TCEP showing two distinct peaks. (B) Coomassie stained gel showing samples from the size exclusion column. Both Spc24 and Spc25 subunits eluted together as a complex.

The first large peak contained free GST protein in addition to Spc24-25 whereas the second larger peak contained pure Spc24-25 protein. Therefore, fractions C8 to D4 containing only Spc24 and Spc25 from the second peak were concentrated and stored at -80^{o}C for interaction studies. Next, the recombinant human Spc24-25 heterodimer was purified on a larger scale following the same protocol (**Figure 3.15A**). Fractions from both major peaks were analysed by SDS-PAGE. Again, most of the fractions from the first large peak had GST protein as a contaminant whereas the 2nd smaller peak did not have any Spc24 protein and contained only Spc25. Therefore, these proteins were not used for interaction studies (**Figure 3.15B**).

3.5 Can RGC-32 interact directly with Spc24-25?

To test whether RGC-32 interacted with the Spc24-25 heterodimers, MST studies were performed using the purified chicken Spc24-25 and untagged RGC-32 (**Figure 3.16A**). The chicken Spc24-25 heterodimer (ligand) was titrated (50 μM to 0.0061 μM) against a constant amount of fluorescently labelled RGC-32 (50 nM). A change in thermophoretic signal of RGC-32 was observed with increasing concentration of ligand indicating an interaction between RGC-32 and the Spc24-25 heterodimer. The K_D of the interaction was determined to be 152 ± 41 nM suggesting that the interaction between these proteins to be of high affinity (**Figure 3.16B**). As we were unable to perform MST studies using human Spc24-25 and the interaction studies that were carried out using purified proteins used only the globular domains of chicken Spc24-25, we investigated whether RGC-32 was able to bind to the human Spc24-25 dimer *in vivo*. EBV-negative Burkitt's lymphoma (DG75) cells were transiently transfected with a mammalian expression plasmid expressing GFP-RGC-32 (pEGFP-C3-RGC-32) or the empty vector (pEGFP-C3). The

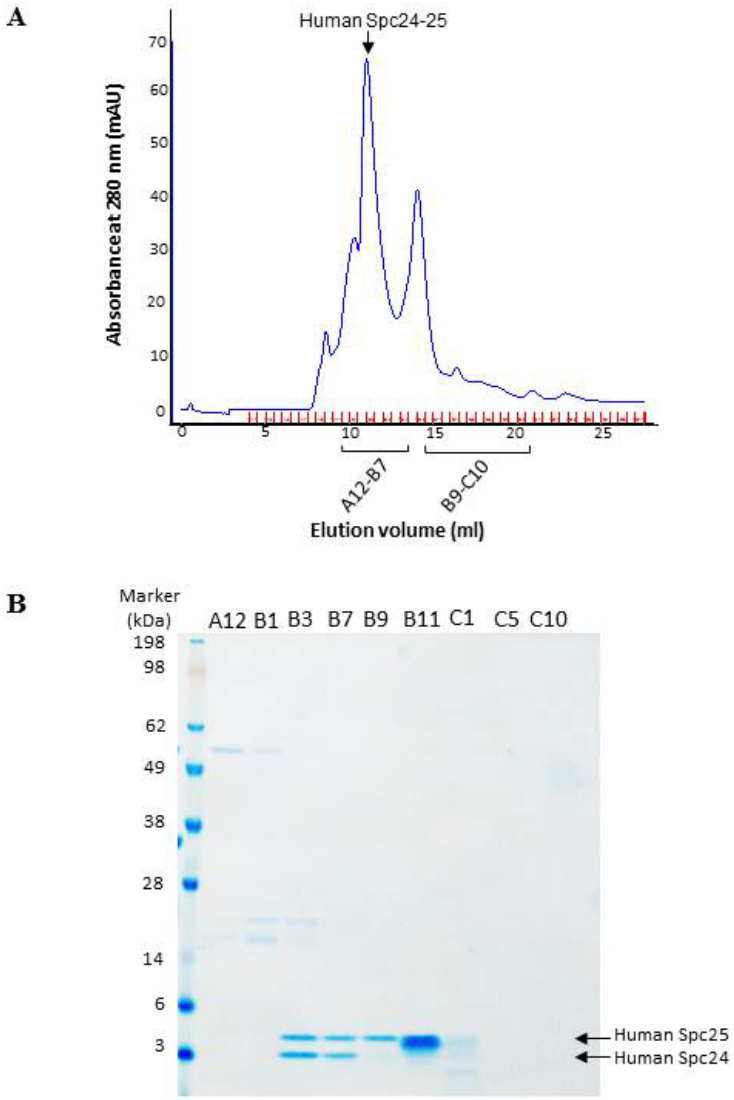

Figure 3.15 Large scale purification of recombinant Human Spc24-25 globular domains. (A) Elution profile of GST-cleaved Human Spc24-25 from S75 10/300 size exclusion column pre-equilibrated in 50 mM Tris-HCL pH7.5, 150 mM NaCl, 0.5mM TCEP. (B) Coomassie stained gel showing samples from the size exclusion column. Fractions B3-B7 show purified human Spc24-25, but only fraction B7 has no higher molecular weight contaminants.

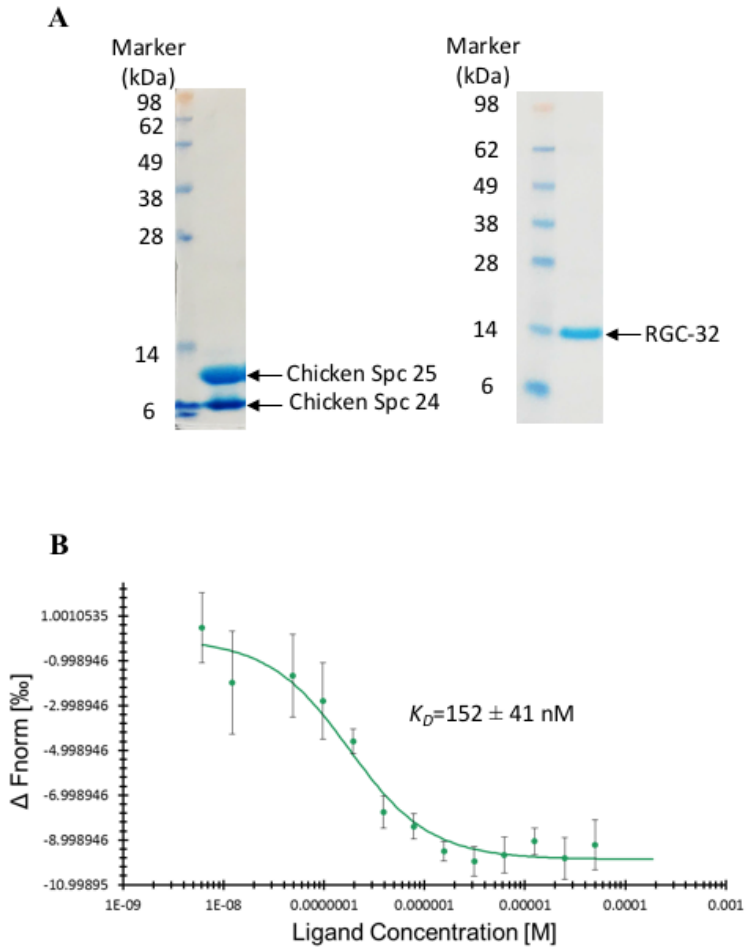

Figure 3.16 Microscale Thermophoresis analysis of Chicken Spc24-25 globular domain binding to RGC-32

(A) Coomassie stained gel showing purified Chicken Spc24-25 and RGC-32 proteins used for analysis. (B) Graph showing the change in thermophoretic signal upon binding of Chicken Spc24-25 to 50 nM of fluorescently labelled (NT647NHS) RGC-32. Results shown are the mean of three independent experiments ± standard deviation.

transfection efficiency was monitored by flow cytometry 48 hour post-transfection and was found to be approximately 16% for GFP control and 4% for GFP-RGC-32 (**Figure 3.17A**). The low transfection efficiency for eGFP-RGC-32 could be due to cell death as a result of RGC-32 expression. The cell lysate was incubated with GFP-trap M beads (Chromotek) to precipitate RGC-32 and any associated proteins. Immunocomplexes were analysed by western blotting. PLK1 was used as a positive control in this study as it has been shown to bind to RGC-32 previously (Saigusa *et al.*, 2007). Overexpression of eGFP-RGC-32 was also verified by western blot (**Figure 3.17B**). Immunoblots detected precipitation of PLK1 by RGC-32 as expected and GFP-RGC-32 also precipitated Spc25 (**Figure 3.17C**). However, Spc24 was precipitated to the same extent by GFP-RGC-32 and GFP control beads indicating no detectable specific interaction (**Figure 3.17C**). As the transfection efficiency was low in B cells, we decided to use another cell line that can be more easily transfected. We first performed western blotting to test the expression of endogenous RGC-32 in adherent cell lines from different backgrounds- HEK 293, HeLa and U2OS and found that the protein was not expressed in any of these cell lines (**Figure 3.18A**). We chose to use HEK 293 cells and these cells were transiently transfected with empty pEGFP-C3 and pEGFP-C3-RGC-32 plasmids. Immunoprecipitation was carried out using GFP-trap M beads. CDK1 was used as a positive control for an RGC-32 interacting protein in these experiments (Badea *et al.*, 2002, Schlick *et al.*, 2011). Immunoblots showed that eGFP-RGC-32 efficiently pulled down CDK1, Spc24 and Spc25 (**Figure 3.18B**). This confirmed that the human Spc24-25 dimer interacts with RGC-32. However, due to the absence of a negative control for RGC-32 binding in immunoprecipitation studies, an extended investigation with mutating the three residues

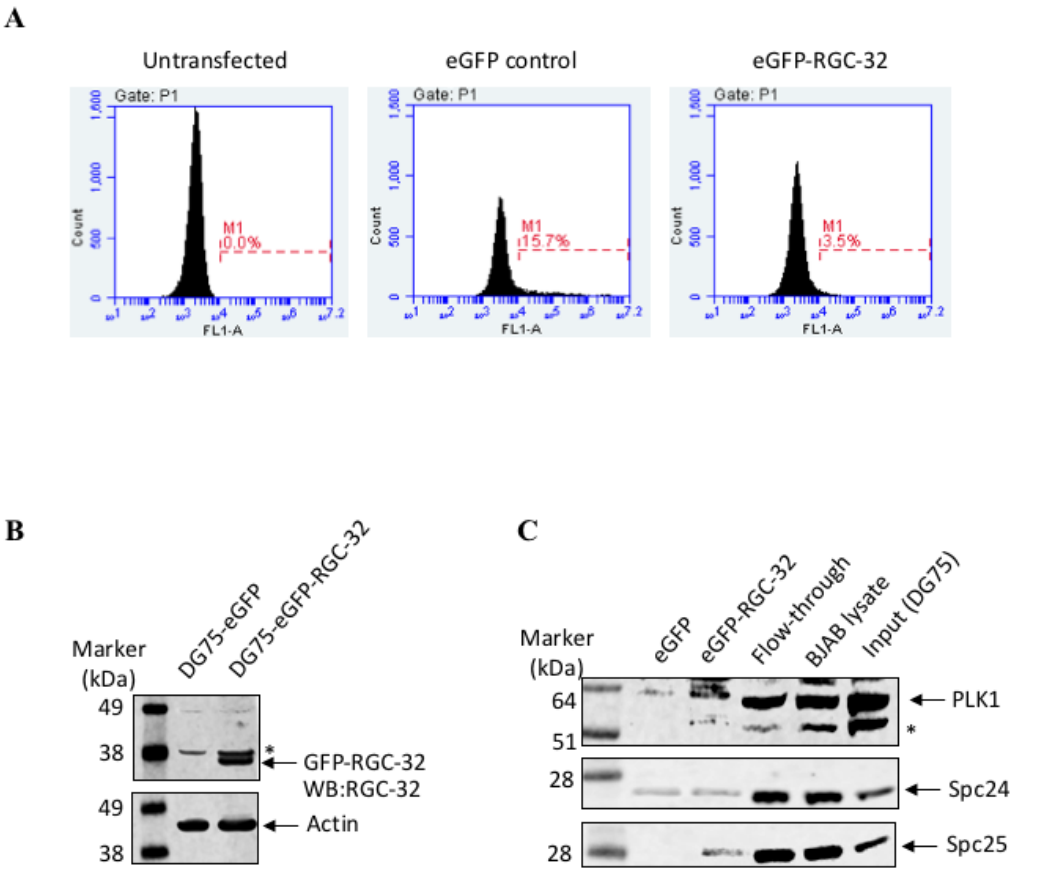

Figure 3.17 The interaction of RGC-32 with Spc24 and Spc25 by immunoprecipitation studies in EBV-negative B cells (DG75).
(A) Flow cytometry analysis of GFP positive cells used to determine transfection efficiency. (B) Western blot analysis showing overexpression of RGC-32 in DG75 cells using antibodies specific to RGC-32 (C) Western blot analysis of the interaction of RGC-32 with PLK1, Spc24 and Spc25 using specific antibodies (See Appendix 7.1 & 7.2). Actin was used as a loading control. In blot (C) Input (DG75) and BJAB lysate were used as a control for PLK1, Spc24 and Spc24 expression. * Non-specific bands.

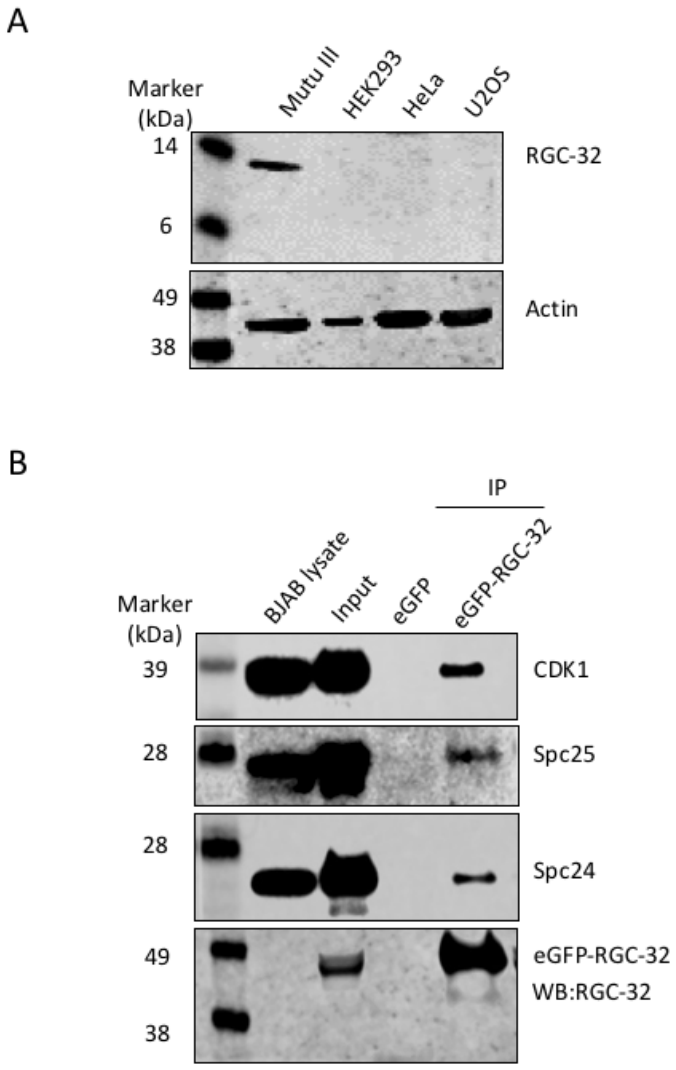

Figure 3.18 The interaction of RGC-32 with Spc24 and Spc25 by immunoprecipitation studies in Human embryonic kidney cells (HEK 293).
(A) Western blot analysis for RGC-32 protein expression in EBV-infected Latency III B-cell (Mutu III) and a panel of adherent cell lines. (B) Western blot analysis for interaction of RGC-32 with CDK1, Spc24 and Spc25 in HEK 293 using specific antibodies (See Appendix 7.1 and 7.2). Actin was used as a loading control. BJAB lysate was used as a control for CDK1, Spc24 and Spc25 expression.

in 3rd α-helical region of RGC-32 would be required prior to publication. Therefore, taken together our MST studies and preliminary *in vivo* interaction studies indicate that RGC-32 can associate with Spc24-25.

3.6 Discussion

This chapter focused on the interaction of RGC-32 with different proteins involved in cell cycle regulation. Secondary structure prediction for RGC-32 by JPRED showed that RGC-32 is mostly unstructured apart from three predicted α-helices. The presence of a long coiled-coil region between the α-2 and α-3 helices suggests the protein could be intrinsically disordered. When RGC-32 was purified for structural studies, the elution profile from SEC suggested RGC-32 to run as a higher molecular weight species (**Figure 3.3B**). It could be possible that RGC-32 forms a dimer or trimer *in vitro*. This unusual behaviour of the protein could be possible due to two reasons; firstly, RGC-32 has only one cysteine residue. Cysteine residues are involved in formation of disulfide bonds which are often crucial for protein folding and stability. However, free cysteine residues can cause unwanted intramolecular disulfide bonds resulting in oligomerisation (Trivedi *et al.*, 2009). Secondly, RGC-32 protein is highly disordered which makes it an elongated molecule and susceptible to aggregation. It remains to be tested whether RGC-32 forms higher order oligomers *in vivo* and structural studies would be useful here. Our attempts to obtain crystals for X-ray diffraction were however unsuccessful (**Figure 3.3C**). This could again be explained by the fact that RGC-32 protein is likely to be highly disordered (54%) which makes it very challenging to crystallise the protein in its apo-state. A better strategy would be to co-crystallise RGC-32 with a binding partner, perhaps CDK1, as unstructured proteins such as RGC-32 tend to fold upon binding to another protein allowing them to attain a structure and aiding their crystallisation.

Initial pull-down studies in our laboratory using B cell lysates showed GST-RGC-32 precipitated CDK1 but not cyclin B. This led us to investigate whether RGC-32 competes with cyclin B for CDK1 binding. SPR studies in collaboration with Prof. Jane Endicott (Newcastle University) provided the first evidence that RGC-32 could bind directly to CDK1, however, it bound to CDK1-Cyclin B with higher affinity (**Figure 3.5C & D**). The binding kinetics of RGC-32 to CDK1 and CDK1-CyclinB were different to that of Cks1 (positive control) as it showed slow association and dissociation (**Figure 3.5A & B**). The slow binding kinetics suggest a folding-upon-binding mechanism for RGC-32, which might be possible due to its high degree of disorder. The interaction of RGC-32 with CDK1 and CDK1-Cyclin B was further confirmed using another biophysical technique, Microscale thermophoresis (MST) (**Figure 3.8**). Thus confirming a clear role of cyclin B in the interaction between RGC-32 and CDK1 and ruling out the possibility of RGC-32 competing with cyclin B as we had initially hypothesised. Moreover, RGC-32 was unable to bind CDK2-Cyclin A using MST studies confirming the previous studies about specificity of RGC-32 towards CDK1 (**Figure 3.9**) (Badea *et al.*, 2002). A possible explanation for this specific binding could be structural differences in the CDK1-Cyclin B and CDK2-Cyclin A complex (**Figure 1.3A & B**). The crystal structure of human CDK1-Cyclin B (PDB 4YC3) shows CDK1 to make fewer interactions with cyclin B as compared to CDK2-Cyclin A (PDB 1FIN). Moreover, the activation segment of CDK1 which provides a surface for peptide substrate recognition has a disordered region after binding to cyclin B. This region requires considerable rearrangement for substrate recognition by CDK1 as compared to the CDK2 activation segment that requires little rearrangement (Jeffrey *et al.*, 1995, Brown *et al.*, 2015). As the CDK1-Cyclin B complex is not tightly closed, it may provide a surface for RGC-32 binding which CDK2-

Cyclin A does not. Thus binding of RGC-32 to CDK1 may aid substrate recognition by rearranging the activation segment. Additionally, binding of cyclin B to CDK1 might create allosteric effects that assist in RGC-32 binding to CDK1 with a higher affinity.

Preliminary studies in our laboratory identified Spc24 as a potential binding partner of RGC-32. In this work we showed that RGC-32 can directly bind to chicken Spc24-25 globular domains with high affinity by MST studies, indicating a specific interaction between the two partner proteins (**Figure 3.16**). Immunoprecipitation assays in HEK 293 cells further confirmed the binding of RGC-32 to the Spc24-25 heterodimer (**Figure 3.17 & 3.18**). As mentioned earlier, the interaction of CNN-1 with Spc24-25 is dependent on the presence of hydrophobic residues (F69, L70, and L73) (**Figure 3.19A**). To determine whether the conserved residues of RGC-32 (F106, I107 and L110) are involved in this interaction similar to CNN-1, we generated a tertiary model for RGC-32. The RGC-32 model formed a three-helix bundle and the 3rd α-helix showed similarity to the N-terminal receptor motif of CNN-1. The model also showed that the α-helix of RGC-32 and the conserved residues occupies similar position to CNN-1 and buries nicely onto other hydrophobic residues from Spc24-25 (**Figure 3.19B & C**). Mutation analysis of each of the conserved residues (F106, I107 and L110), as well as a cumulative mutation of all the three residues of RGC-32, will need to be carried out to properly test this model. Interaction of RGC-32 with PLK1 has been well documented by pull-down studies (Saigusa *et al.*, 2007). This observation was further confirmed by using pull-down assays in our laboratory showing RGC-32 to precipitate PLK1 from B cell lysates (Dr Lina Chen).

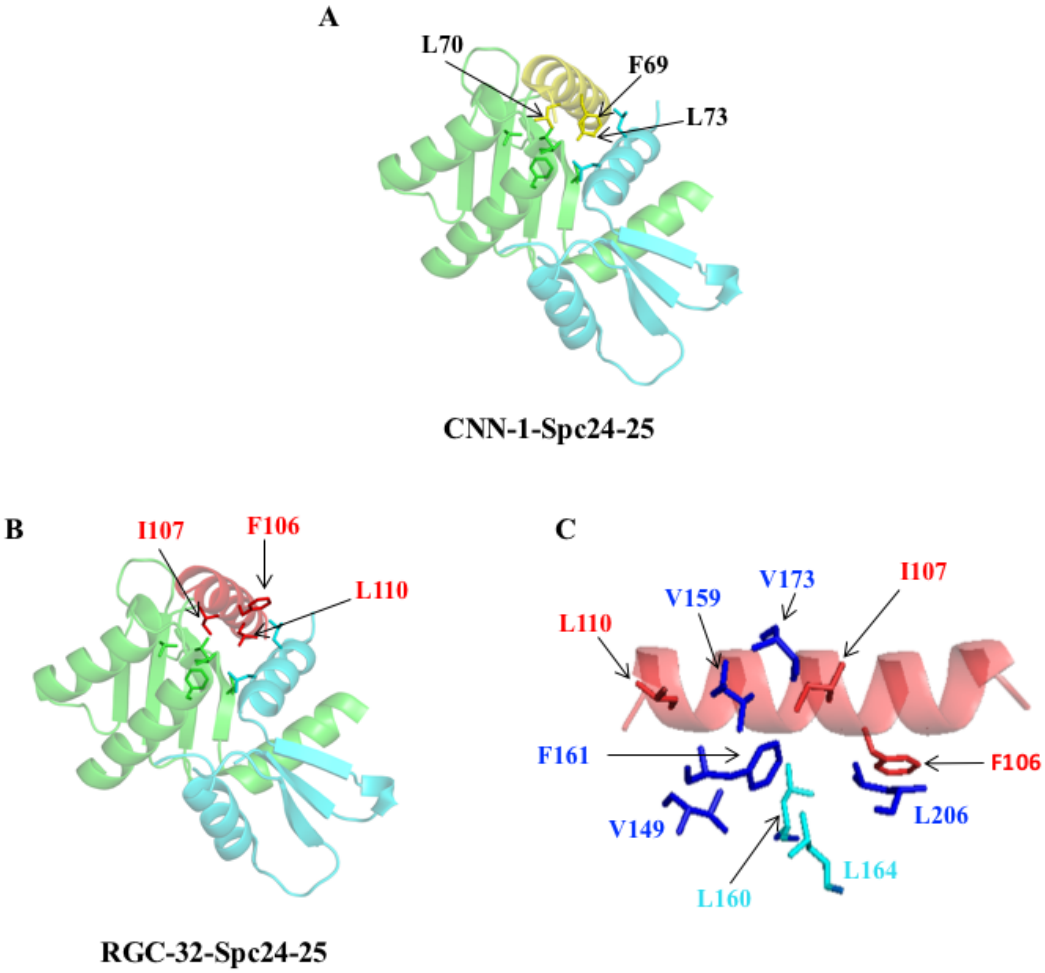

Figure 3.19 Structural model substituting CNN-1 N-terminal receptor with the α-helix of RGC-32.
(A) Structure of the CNN-1-Spc24-25 complex (PDB 4GEQ) coloured in pale yellow, cyan and green respectively. Residues involved in interaction are shown with arrows (Malvezzi *et al*., 2013). (B) Modelled RGC-32 residues form an **α**-helix (red) similar to CNN-1 and can be superimposed on to the CNN-1 in the CNN-1-Spc24-25 tertiary complex. The **α**-helix of RGC-32 and the three residues (F106, I107 and L110) occupies a similar position to CNN-1. (C) Model showing a zoom-in of the potential interacting amino acid residues of Spc24 (cyan) and Spc25 (blue) in close proximity to the conserved amino acid residues in the third helix of RGC32 (F106, I107 and L110). The RGC-32 model was generated using RaptorX structure prediction.

PLK1 is a crucial regulator of mitosis and its activity at kinetochores is reported for stable attachment of kinetochores to microtubules (Liu *et al.*, 2012). As RGC-32 bind to and is phosphorylated by PLK1 it will be interesting to examine how the interaction of RGC-32 with Spc24-25 kinetochore subunit affects the activity of PLK1 at the kinetochore. Understanding the molecular details of RGC-32 interaction with Spc24-25 will also allow us to address the role of RGC-32 at the kinetochores for example by testing if mutation of key interacting residues abrogates PLK1 mediated stabilisation of kinetochore-microtubule attachments.

Overall, this chapter provides an insight into the molecular functions of RGC-32. We showed the binding of RGC-32 with two different proteins from the cell cycle machinery. This provides further evidence for a role for RGC-32 in regulating the cell cycle specifically at the G2/M transition and mitosis as CDK1 and Spc24-25 are active during these phases. The role of cyclin B in the interaction of RGC-32 with CDK1 would be interesting to pursue as a future piece of research. Important aspects of RGC-32 function can further be revealed by co-crystallising RGC-32 with CDK1-Cyclin B. Additionally, mutational analysis and co-localisation studies by imaging could be carried out to probe whether RGC-32 localises at the centromeres and the underlying mechanism of interaction with Spc24-25 heterodimer.

4 Functional analysis of RGC-32

4.1 Introduction

RGC-32 mRNA is ubiquitously expressed in most tissues including brain, bladder, colon, heart, kidney, lung, breast and pancreas. Previous research has reported that RGC-32 mRNA is also upregulated in numerous cancers (Fosbrink *et al.*, 2005) and the RGC-32 protein appears to play an important role in cell cycle regulation. This was first demonstrated by Badea *et al.* who identified the role of RGC-32 in promoting progression of the cell cycle in rat oligodendrocytes (Badea *et al.*, 1998). The group later reported expression of RGC-32 to promote S-phase and M-phase entry of G1 arrested human aortic smooth muscle cells (Badea *et al.*, 2002). Moreover, siRNA knockdown of endogenous RGC-32 in human endothelial cells showed sub-lytic complement C5b-9 and growth factor induced cell proliferation to be abolished and CDK1 activation to be reduced. These data indicate a role of RGC-32 in C5b-9 induced cell cycle activation (Fosbrink *et al.*, 2009). Conversely, knockdown of RGC-32 showed an opposite effect on cell cycle in T-cells. The proliferative rate of $CD4^+$ T-cells from RGC-32 knockout mice was higher than in wild type mice. This suggests that RGC-32 may have different roles in regulating the cell cycle based on the cell type involved (Tegla *et al.*, 2015).

Previous studies performed in our laboratory to investigate the effect of EBV on cellular genes identified RGC-32 protein to be upregulated in EBV-infected Latency III cell lines (which express all latent genes). Interestingly, RGC-32 protein was not detectable in EBV-negative B cells and EBV-infected Latency I cell lines (which express only EBNA1). Cell cycle regulation by RGC-32 in B cells was investigated by stably expressing RGC-32 in EBV-negative B cells. Induction of RGC-32 expression in etoposide-treated cells led to G2/M checkpoint disruption. This demonstrated that RGC-

32 expression can disrupt cell cycle arrest in B cells (Schlick *et al.*, 2011). Therefore, in this chapter, we set out to further investigate the role of RGC-32 in the G2/M transition and mitosis and to examine its role in promoting the growth and proliferation of EBV-infected B cells.

4.2 Subcellular localization of RGC-32 during Mitosis

Previous studies in U-87 MG cells (a glioma cell line) showed that ectopically expressed RGC-32 protein was localized in the cytoplasm during interphase. Progression of these cells into prophase led to an increased RGC-32 signal at the centrosomes and spindle poles with the strongest signal observed during prometaphase and metaphase (Saigusa *et al.*, 2007).

PLK1 is also known to accumulate at the centromere and kinetochores during prometaphase and provide stabilisation of the initial kinetochore-microtubule attachment for error-free chromosome alignment (Lenart *et al.*, 2007, Liu *et al.*, 2012). Since, we observed a direct interaction of RGC-32 with Spc24-25 heterodimer in chapter 3 (**Figure 3.17B**) and RGC-32 binds to PLK1, it was important for us to investigate whether RGC-32 localised at the kinetochores and perhaps plays a role in the recruitment or activity of PLK1 at kinetochores. To do this, HeLa cells were transiently transfected with plasmids expressing GFP-RGC-32 (pEGFP-C3-RGC-32) and mCherry-CENP-A (mCherry-CENP-A). CENP-A is a Histone 3 (H3) variant that replaces the conventional H3 at the centromeric chromatin at the inner plate of the kinetochore. Time-lapse imaging showed RGC-32 to localise in the cytoplasm during interphase and translocate to the nucleus during prophase **(Figure 4.1A)** which is consistent with the data previously published by the Inazawa group (Saigusa *et al.*, 2007). However, it was not clear whether RGC-32 co-

localises with the kinetochore because CENP-A did not localise to the kinetochores but marked the entire chromosome making it difficult to study co-localisation of these proteins.

As the percentage of mitotic cells is very low (~10%) in an asynchronous population at any given point of time, we wanted to enrich the mitotic population for localisation studies. Therefore, HeLa cdk1as (analogue sensitive) cells were used in subsequent studies as these cells can be arrested in G2 by specifically inhibiting CDK1 activity. The HeLa cdk1as cell line (provided by Dr W.C. Earnshaw's laboratory) was generated by replacing endogenous CDK1 with analogue-sensitive *Xenopus laevis* cdk1as. CDK1as can be specifically inhibited by the bulky ATP analogue 1NM-PP1 as it has an F80G mutation in its active site which generates a pocket-like structure for bulky ATP analogue 1NM-PP1 binding (Gravells *et al.*, 2013). HeLa cdk1as cells were transiently transfected with pEGFP-C3-RGC-32 and mCherry-CENP-A. Transfected cells were arrested in G2 using 1NM-PP1 (1 μM). After 16 hours, the drug was washed off to release the cells into medium containing the proteasome inhibitor MG132 (25 μM) to stop the cells from exiting mitosis by preventing the degradation of cyclin B1 and other ubiquitin-conjugated proteins. Time-lapse imaging showed the RGC-32 protein signal to be higher at the spindle poles. However, it was not clear whether it localised at the kinetochore as CENP-A had again localised to the entire chromosome (**Figure 4.1B**).

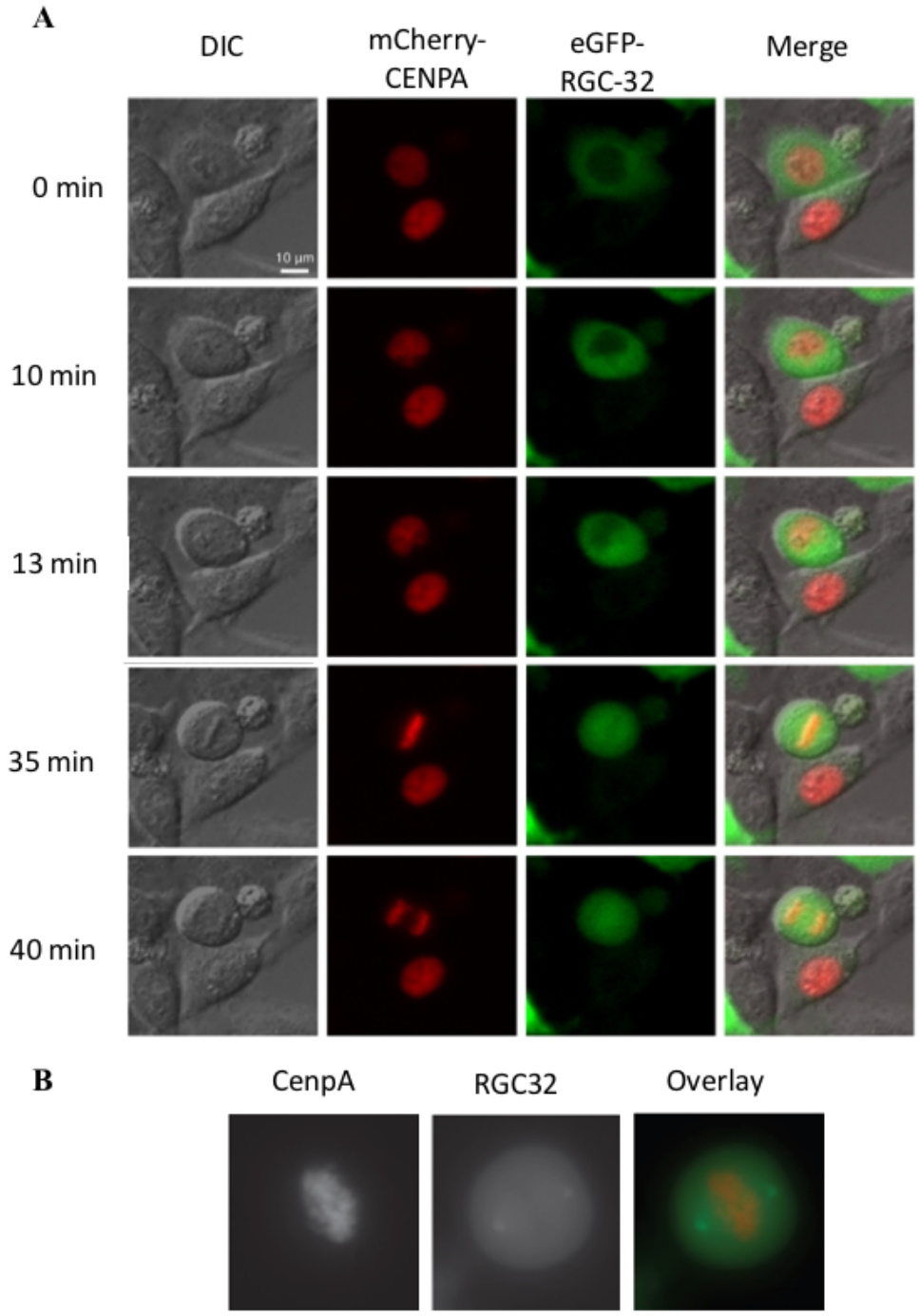

Figure 4.1 The localisation of RGC-32 in HeLa cells during mitosis.
(A) Selected frames of video from HeLa cells transiently expressing mCherry-CENP-A (red) and eGFP-RGC-32 (green). Channels were merged to study the co-localization of CENP-A and RGC-32. The time (in minutes) from the first image captured is shown on left side of each image. (B) HeLa cdk1as cells transiently expressing mCherry-CENP-A (red) and eGFP-RGC-32 (green) were arrested in G2 using an ATP analogue CDK1 inhibitor, 1NM-PP1 (1 µM) for 16 hours followed by washing off the drug to release the cells in media containing proteasome inhibitor MG132 (25 µM) to block mitotic exit. Images were captured using an Olympus IX73 microscope. Scale bar: 10 µM.

In the absence of another available kinetochore marker and time constraints, we did not pursue the potential kinetochore function of RGC-32 any further.

From the initial localisation studies, it appeared that RGC-32 translocated to the nucleus during mitosis in a similar manner to cyclin B. It has been previously reported that activation of cyclin B takes place in the cytoplasm followed by its translocation to the nucleus during late prophase just before the breakdown of the nuclear envelope (Pines and Hunter, 1991). This translocation is dependent on phosphorylation on serine residues in the cytoplasmic retention sequence (CRS). Additionally, PLK1 mediated phosphorylation of cyclin B on Ser133 and Ser147 in the nuclear export signal (NES) leads to nuclear translocation of cyclin B (Toyoshima-Morimoto *et al.*, 2001).

Since initial localisation studies suggested similarity between RGC-32 and cyclin B in their nuclear translocation behaviour, we performed temporal studies in order to investigate the exact timing of RGC-32 nuclear entry during mitosis. For this, HeLa cdk1as Cyclin B-RFP cells expressing endogenous mCherry-cyclin B (generated by the Hochegger laboratory, University of Sussex) were transiently transfected with pEGFP-C3-RGC-32. The HeLa cdk1as cyclin B-RFP cells were arrested in G2 phase using 1NM-PP1 (1 μM). After 16 hours, the drug was washed off into medium containing proteasome inhibitor MG132 (25 μM) to stop cells from exiting mitosis. Translocation of both proteins in the nucleus was studied by time-lapse imaging soon after G2 release. We observed that very few cells expressed eGFP-RGC-32 and mCherry-cyclin B together. This could be possibly due to low transfection efficiency. We found both RGC-32 and cyclin B translocated into the nucleus in a similar manner at the same time which appeared to be before nuclear envelope breakdown **(Figure 4.2)**.

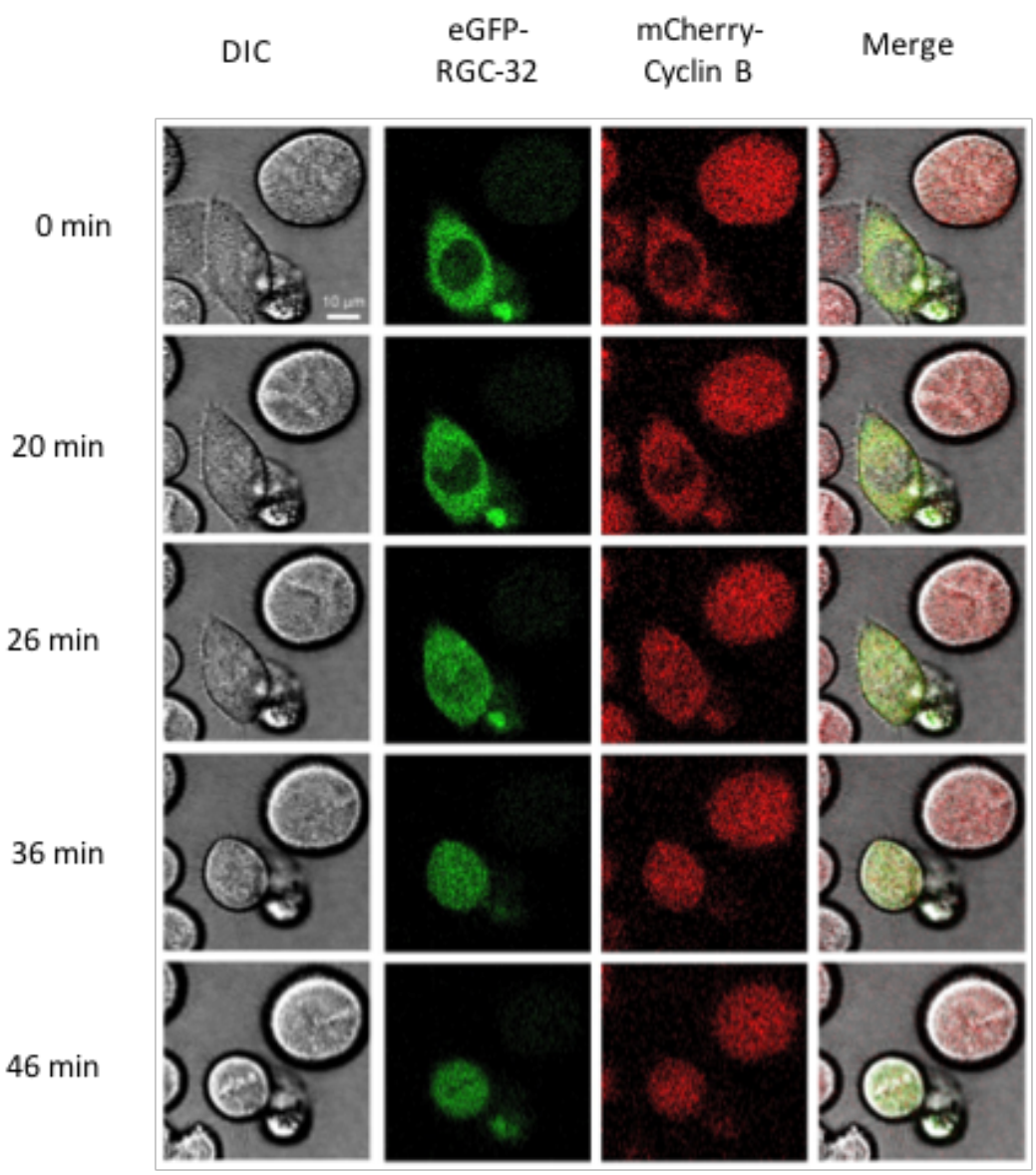

Figure 4.2 Nuclear translocation of cyclin B and RGC-32 in HeLa CDK1as mCherry-Cyclin B cells during mitosis.
Selected frames of video from HeLa cdk1as mCherry-cyclin B cells transiently expressing eGFP-RGC-32 (green). These cells express endogenous cyclin B tagged to mCherry (red). Merge shows the co-localisation of RGC-32 and cyclin B. Cells were arrested in G2 using 1NM-PP1 (1 μM) for 16 hours followed by washing off the drug to release the cells in media containing proteasome inhibitor MG132 (25 μM) to block mitotic exit. Images were captured at 2-minute intervals for 2 hours using Leica TCS SP8 confocal microscope. The time (in minutes) from the first image capture is shown on left side of each image. Scale bar: 10 μM.

Interestingly, cells expressing eGFP-RGC-32 were observed to remain in early mitosis for a longer duration as compared to the untransfected cells.

4.3 The role of RGC-32 in mitotic entry

The ability of RGC-32 to specifically activate CDK1 has been well established by *in vitro* kinase assays. Previous studies by our laboratory showed G2/M checkpoint disruption in B cells by RGC-32 overexpression as well as the activation of CDK1 *in vitro* by RGC-32 (Schlick *et al.*, 2011). This led us to dissect the role of RGC-32 in activation of CDK1 *in vivo* and in the G2/M transition. Our initial experiments aimed to reproduce RGC-32 and CDK1 binding in cells. Since B cells are difficult to transfect and synchronise reversibly in different phases, we performed these experiments in an adherent cell line, U2OS (osteosarcoma). U2OS cells were transiently transfected with plasmids expressing FLAG-RGC-32 (pFLAG-CMV2-RGC-32) and empty vector (pFLAG-CMV2). Immunocomplexes were analyzed by western blot for FLAG-RGC-32 and pull down of CDK1. We found that CDK1 associated with FLAG-RGC-32 (**Figure 4.3**). Because the levels of CDK1 detected were very low, we investigated whether immunoprecipitation studies using formaldehyde cross-linked cells may improve CDK1 detection. Immunoprecipitation demonstrated increased levels of CDK1 were bound to FLAG-RGC-32 in cross-linked cells.

Next, we sought to investigate the effect of RGC-32 expression on mitotic entry *in vivo*. As B cells cannot be efficiently synchronised for cell cycle studies, we performed this study in the well-established U2OS cdk1as cell line. For mitotic entry studies, the percentage of mitotic cells was determined using MATLAB. The algorithm counted the

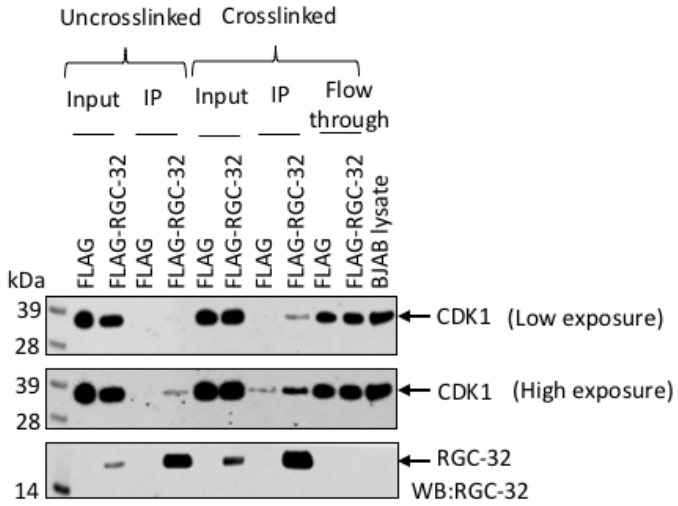

Figure 4.3 Investigating whether RGC-32 interacts with CDK1 *in vivo*.
U2OS cells transiently expressing pFLAG-CMV2 (negative control) or pFLAG-CMV2-RGC-32 were harvested with or without formaldehyde crosslinking as indicated. Western Blot analysis for CDK1 and RGC-32 proteins was then performed. Low exposure and high exposure are shown. BJAB (EBV negative cell line) lysate was used as a control for CDK1 expression.

number of total cells using the nuclear stain, SiRDNA, and the cells with a rounded morphology (DIC) were counted as mitotic cells (**Figure 4.4)**. In order to improve transfection efficiency, U2OS cdk1as cells were transfected soon after treating with trypsin (reverse transfection) with plasmid expressing FLAG-RGC-32 (pFLAG-CMV2-RGC-3) or empty vector (pFLAG-CMV2) along with empty GFP expressing vector (pEGFP-C3) (to monitor transfected cells). The CDK1 inhibitor, 1NM-PP1 (2 μM) was added to cells for 20 hours to arrest them in G2. Cells were washed into media with MG132 (25 μM) to prevent mitotic exit (**Figure 4.5A**). To study the effect of RGC-32 when CDK1 was partially inhibited, different concentrations of 1NM-PP1 (0.1 μM, 0.2 μM and 0.3 μM) were also re-added to the media and time-lapse imaging was carried out. From four hours of imaging, we observed that when the cells were arrested with 1NM-PP1 and then washed out, an increased proportion of RGC-32 expressing cells (~15%) entered mitosis (**Figure 4.5B**). This indicated that RGC-32 can push cells into mitosis consistent with its ability to activate CDK1. However, the effects of RGC-32 were reduced in the presence of increasing concentrations of CDK1 inhibitor indicating that RGC-32 cannot overcome 1NM-PP1 inhibition.

As these mitotic entry studies were performed using transient expression of RGC-32 which didn't always give reproducible transfection efficiency and was associated with some toxicity, we set out to generate a stable cell line expressing inducible RGC-32. eGFP-RGC-32 was cloned into pROSA26-MCS, which had the right arm and left arm homologous to the commonly used integration site, the *ROSA26* locus (**Figure 4.6A**). The *ROSA26* locus allows insertion of gene sequences with ease without any gene

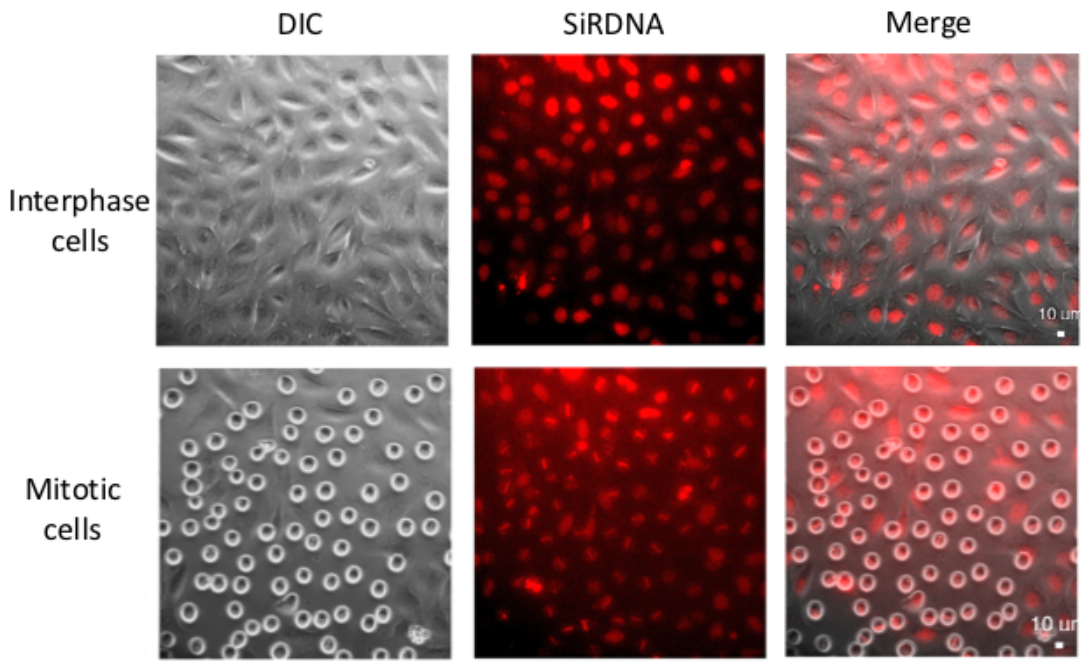

Figure 4.4 Mitotic entry of G2 arrested U2OS cdk1as cells transiently expressing RGC-32. U2OS cdk1as cells were arrested in G2 using an ATP analogue CDK1 inhibitor, 1NM-PP1 (2 μM) for 20 hours followed by washing off the drug to release the cells in media containing proteasome inhibitor MG132 (25 μM) to block mitotic exit. DNA was visualised using SiRDNA (Red). Images were captured after G2 release using an Olympus IX73 microscope using a 20x lens. Scale bar: 10 μM.

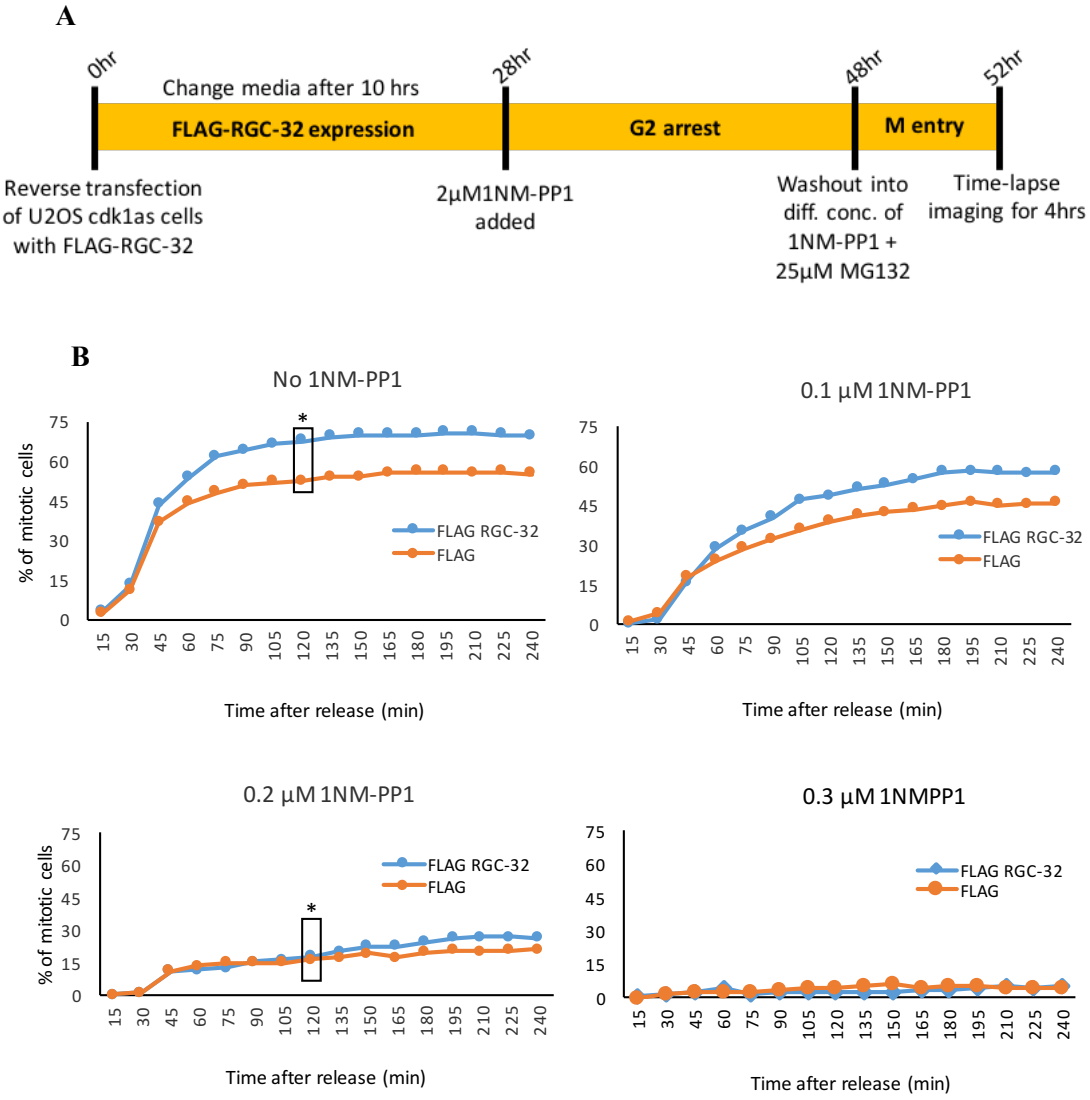

Figure 4.5 The effect of transient RGC-32 expression on mitotic entry of G2 arrested U2OS cdk1as cells.

(A) Schematic representation of the mitotic entry experiment. Trypsinised U2OS cdk1as cells were transiently transfected with either 2.5 μg of pFLAG_CMV2 or pFLAG_CMV2-RGC-32 along with empty pEGFP-C3 plasmid to calculate transfection efficiency. Cells were arrested in G2 using the ATP analogue CDK1 inhibitor 1NM-PP1 (2 μM). After complete arrest, cells were washed into media with proteasome inhibitor MG132 (25 μM) to block mitotic exit in addition to different concentrations of 1NM-PP1 (0-0.3 μM) to study mitotic entry. (B) Quantification of cells that entered mitosis -/+ RGC-32 expression with varying concentration of 1NM-PP1. Images were captured at 15-minute intervals for 4 hours with an Olympus IX73 microscope using a 20x lens. Graphs show the percentage of cells that have entered mitosis over time. 500 cells were examined for each condition. Results shown are representative of two independent experiments. Students's T-test for cells expressing FLAG-RGC-32 compared to control for 120 minutes after G2 release is shown for each condition where $P < 0.05$ (*).

silencing effects thereby making it a preferred site for studying gain-of-function and loss-of-function (Irion *et al.*, 2007). Using this vector system, the expression of eGFP-RGC-32 could be switched on by adding doxycycline (Dox). In addition, the plasmid also has a selection marker (zeocin) to select for transfected cells (**Figure 4.6B**). To target homologous recombination at *ROSA26* locus, U2OS cdk1as cells were transfected with pROSA26-eGFP-RGC-32 along with a guide RNA (gRNA) that has a complementary sequence to the target region and a 'PAM' (Protospacer adjacent motif) sequence recognised by the Cas9 nuclease. Single cell dilutions were performed in order to select for a zeocin-resistant clonal population (**Figure 4.6C**) and after expansion, PCR primers (P1 & P2) were used to check both the ROSA26 alleles were recombined with RGC-32. The gel showed one amplified product running at ~2000 bp (intact allele) and another one running at ~5000 bp (recombined ROSA26 allele with RGC-32) (**Figure 4.7A**). As the amplification of the recombined allele was not clearly visible using the previous primer pair, we carried out PCR amplification using forward primer specific to RGC-32 sequence (P3) and reverse primer for *ROSA26* locus (P2). The gel showed the amplified product at the right size (~5000 bp) confirming one recombined ROSA26 allele in the clonal cell lines (**Figure 4.7B**). Selected positive clones (D12, F4, G4, and G8) were then further screened for inducible expression of eGFP-RGC-32 after addition of doxycycline (1 μg/ml) for 48 hours. Western blot analysis showed that eGFP-RGC-32 was expressed in the presence of doxycycline for all the clones with the best induction observed for clone F4 (**Figure 4.7C**). Therefore, clone F4 was used for further experiments. This cell line was further screened for reversible arrest in G2 by 1NM-PP1 using flow cytometry.

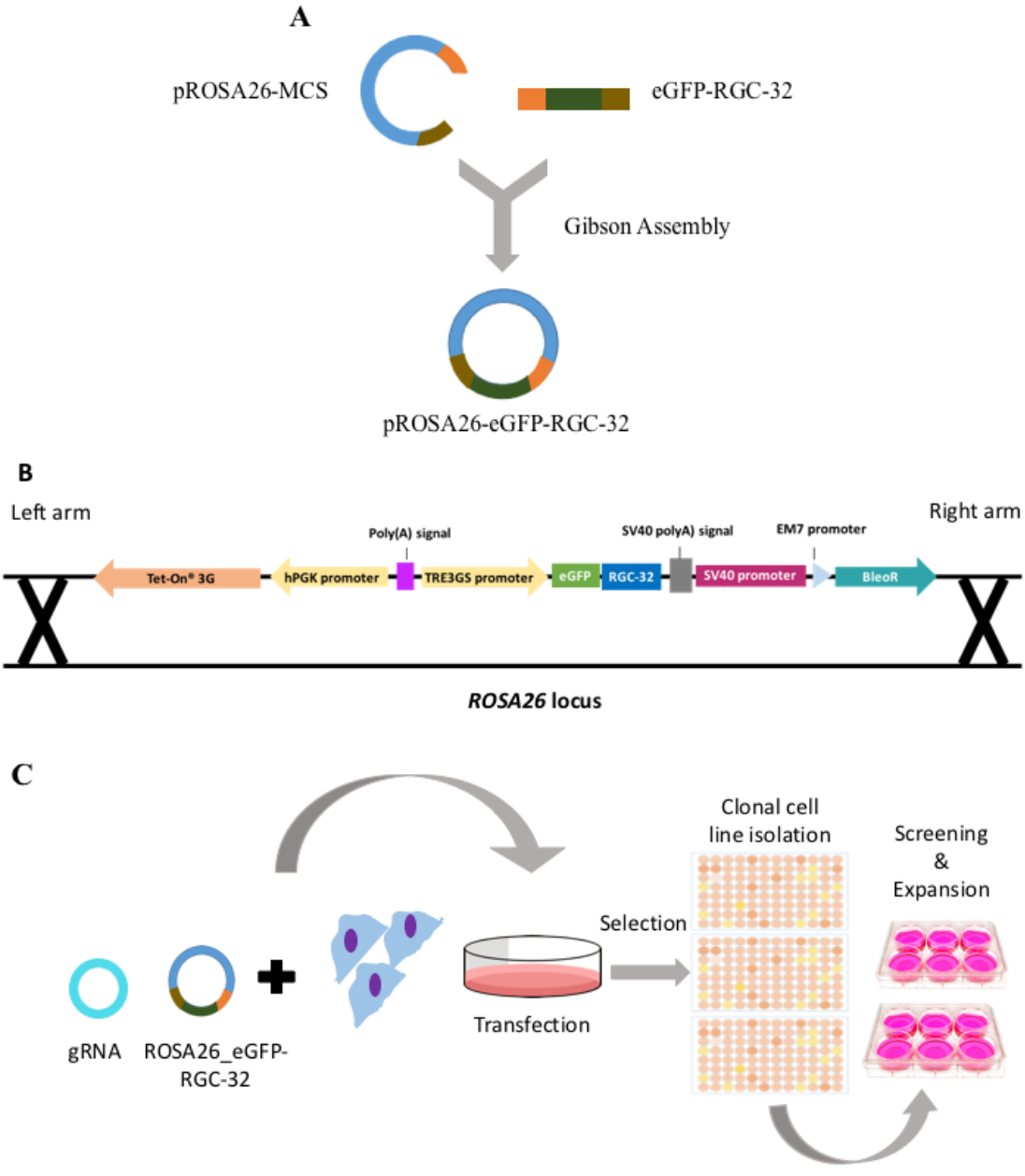

Figure 4.6 Generation of an inducible U2OS cdk1as eGFP-RGC-32 cell line.
(A) Gibson assembly ligation to generate pROSA26_eGFP-RGC-32 plasmid. eGFP-RGC-32 was amplified from pEGFP-C3-RGC-32 plasmid generating overhangs homologous to the pROSA26 MCS plasmid. Both the plasmid and insert were digested with AgeI followed by Gibson assembly at 50^{O}C. (B) Diagram of the inducible eGFP-RGC-32 construct under the control of TRE3GS promoter. The *ROSA26* locus was targeted by homologous recombination to knock in the inducible eGFP-RGC-32 construct. (C) U2OS cdk1as cells were transfected with pROSA26_eGFP-RGC-32 plasmid along with the guide RNA (gRNA) which is complementary to the mRNA sequence within the *ROSA26* locus allowing the insertion at a particular site. Transfected cells were diluted in selection media to give single cells per well in 96-well plates and resistant cells were screened for the integration and expression of eGFP-RGC-32.

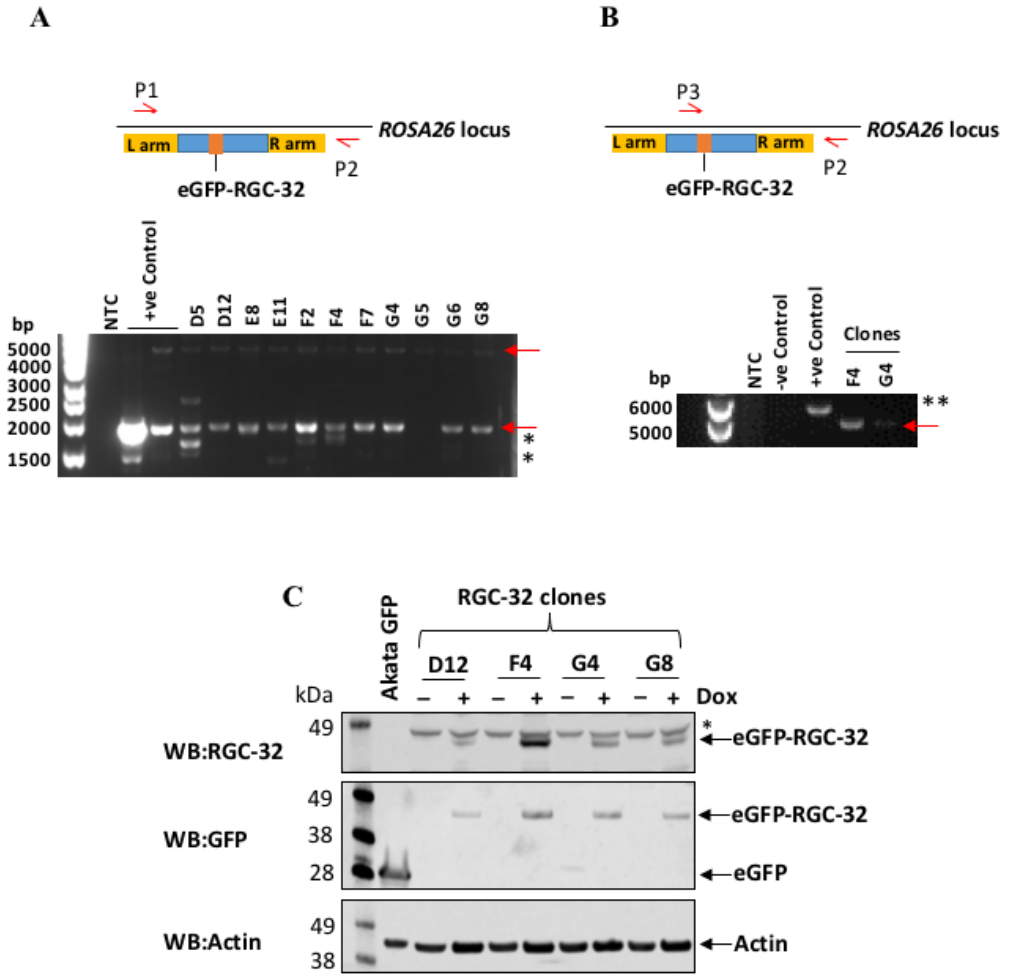

Figure 4.7 Screening of U2OS cdk1as eGFP-RGC-32 stable clones for integration and expression of eGFP-RGC-32.

Genomic DNA from different clones was analysed for the integration of eGFP-RGC-32 at the *ROSA26* locus. (A) PCR amplification of *ROSA26* locus using primers P1 (forward) & P2 (reverse) in all the clones. Genomic DNA of the Retinal Pigment Epithelium (RPE) cells was used as a positive control for the locus. The red arrow indicates the amplified product of ~2000 bp (no RGC-32) and ~5000 bp (with RGC-32). * Non-specific band (B) PCR amplification of the RGC-32 integrated in the *ROSA26* locus using a forward primer (P3) specific to insert and a reverse primer (P2) for *ROSA26* locus. Genomic DNA of RPE cells with and without the insertion of another gene at *ROSA26* locus were used as a positive and negative control for region of integration in U2OS cdk1as eGFP-RGC-32 cells respectively. The red arrow indicates amplification product of right size with RGC-32 integrated (~5000 bp). ** Amplified product from RPE cells with insertion of a different gene at *ROSA26* locus (~5800 bp). (C) Cells from clone D12, F4, G4 and G8 were treated with Doxycycline (Dox) for 48 hours followed by western blot analysis for expression of eGFP-RGC-32. Lysate from Akata pRTS-1 cells expressing eGFP was used as a positive control for GFP expression. Actin was used as a loading control. NTC: Non template control.

Cells were arrested in G2 upon treatment with the CDK1 inhibitor, 1NM-PP1 (2 μM) for 20 hours, with only ~14% of cells remaining in G1 (**Figure 4.8A**). Expression of eGFP-RGC-32 (~46%) was confirmed by wide-field microscopy of arrested cells (**Figure 4.8B**). We next repeated the mitotic entry experiment using this inducible cell line. Cells were grown in the presence of Dox for 28 hours to induce the expression of eGFP-RGC-32.

Both the control and RGC-32 expressing cells were then arrested in G2 by 1NM-PP1 (2 μM) for 20 hours following which they were washed into media with proteasome inhibitor MG132 (25 μM) to block mitotic exit in the absence or presence of low concentrations of 1NM-PP1. Cells were examined by time-lapse imaging (**Figure 4.9A**). The percentage of cells expressing eGFP-RGC-32 upon Dox treatment was ~30%. We observed more cells entering mitosis in the presence of RGC-32 when the CDK1 inhibitor was completely washed off. RGC-32 was not able to override the partial inhibition of CDK1 as observed previously (**Figure 4.9B**). Also this cell line responded differently from U2OS cdk1as cells transiently expressing FLAG-RGC-32 to different concentrations of the inhibitor. We observed the inhibition to be stronger in U2OS cdk1as cells expressing inducible RGC-32 even at 0.1 μM and less number of cells entered mitosis in the absence of INM-PP1 compared to U2OS cdk1as cells with transient RGC-32 expression (**Figure 4.4B and 4.9B**). Nevertheless, these data confirm the previous observation of the ability of RGC-32 to drive cells into mitosis in U2OS cdk1as cells.

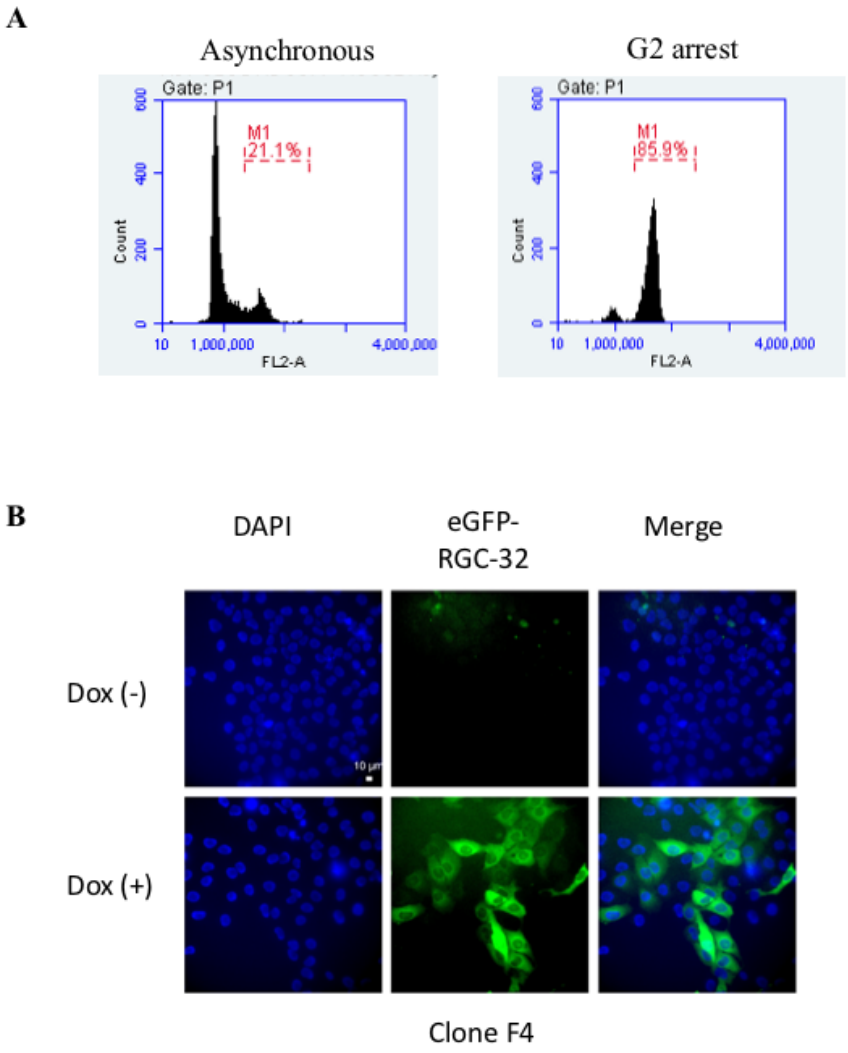

Figure 4.8 Analysis of the U2OS cdk1as eGFP-RGC-32 stable cell line (clone F4).
(A) Flow cytometry histogram of PI (propidium iodide) stained U2OS cdk1as eGFP-RGC-32 cells treated with and without the ATP analogue inhibitor 1NM-PP1 (2 µM) for 20 hours to arrest cells in G2. (B) Wide-field microscopy of cells which were cultured in Dox to induce the expression of eGFP-RGC-32 (Green) and arrested in G2 by 1NM-PP1 treatment for 20 hours. DNA was visualised using DAPI (Blue). Images were taken using an Olympus IX73 microscope. Scale bar: 10 µM.

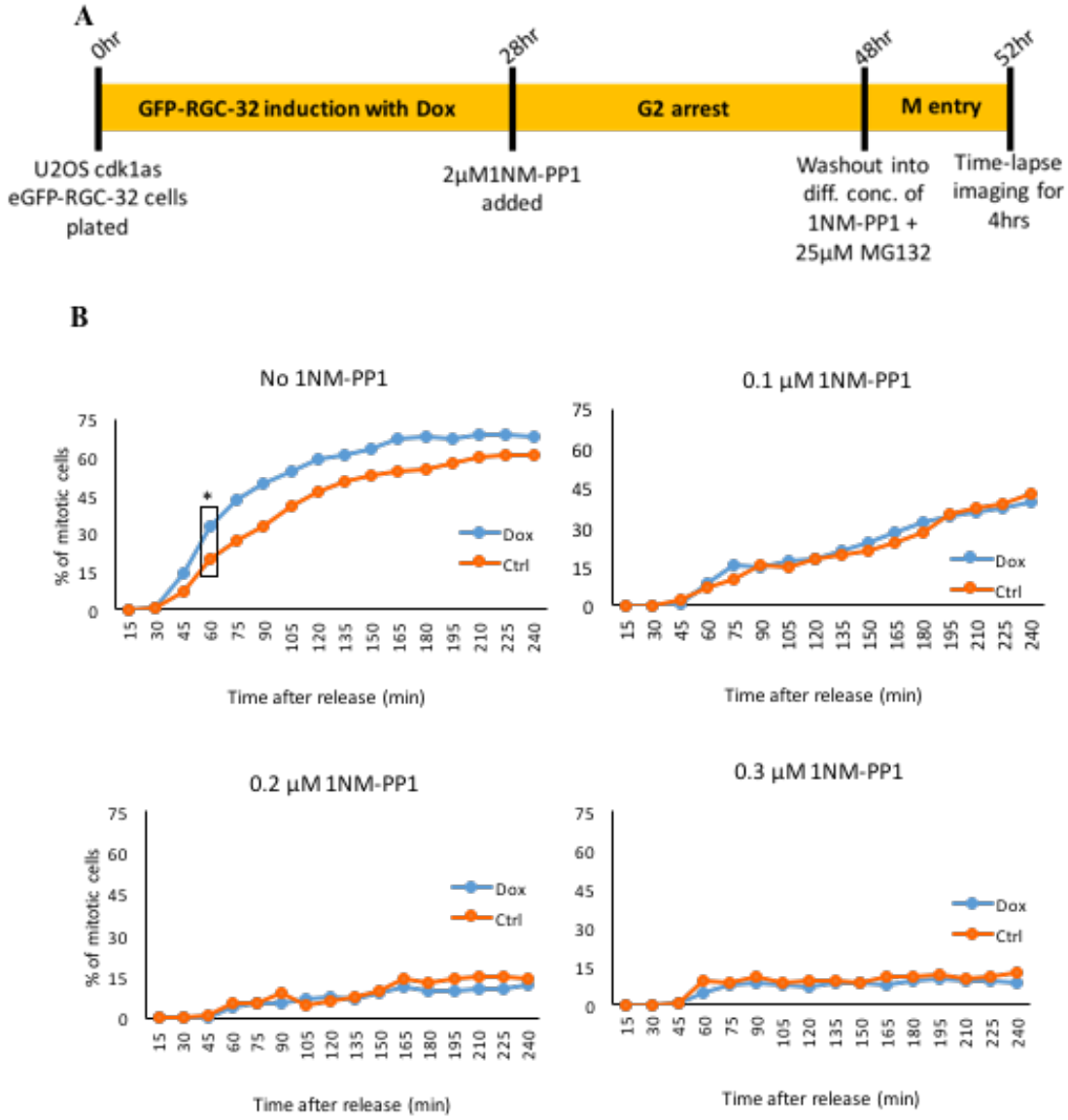

Figure 4.9 The effect of eGFP-RGC-32 expression on mitotic entry of G2 arrested U2OS cdk1as eGFP-RGC-32 cells.

A) Schematic representation of the mitotic entry experiment. U2OS cdk1as eGFP-RGC-32 cells were cultured in Dox followed by treatment with the ATP-analogue inhibitor of CDK1, 1NM-PP1 (2 µM) to arrest cells in G2. After complete arrest, cells were washed into media with proteasome inhibitor MG132 (25 µM) to block mitotic exit. Low concentrations of 1NM-PP1 (0-0.3 µM) were also included during wash out as indicated. (B) Quantification of cells that entered mitosis with varying concentration of 1NM-PP1 was judged by cell rounding. Images were captured at a 15-minute interval for 4 hours with an Olympus IX73 microscope using a 20x lens. Graphs show the percentage of cells that have entered mitosis over time. 500 cells were examined for each experiment. Results shown are representative of two independent experiments. Student's T-test for cells expressing eGFP-RGC-32 compared to control for 60 minutes after G2 release is shown for each condition where $P < 0.05$ (*).

As our results were consistent with activation of CDK1 by RGC-32, we investigated the effects of RGC-32 on CDK1 further using this system. During interphase, the CDK1-Cyclin B complex remains inactive due to inhibitory phosphorylation on Tyrosine (Tyr) 15 and Threonine (Thr) 14 by Wee1 and Myt1 kinases (McGowan and Russell, 1993, Fattaey and Booher, 1997). These inhibitory phosphorylation marks are removed by the Cdc25 phosphatase in the late G2, thus activating the CDK1-Cyclin B complex and promoting mitotic entry (Gautier *et al.*, 1991) (**Figure 1.2**). In order to characterise the mechanism of CDK1 activation by RGC-32, the mitotic entry assay was performed in the presence of an inhibitor of the Wee1 kinase (MK-1775). This is a small molecule inhibitor that selectively targets Wee1 preventing phosphorylation on Y15 of CDK1 (Hirai *et al.*, 2009). Treatment with the Wee1 inhibitor therefore results in activation of CDK1 and increases the number of cells entering mitosis (Parker and Piwnica-Worms, 1992). We wanted to determine whether the effects of RGC-32 could further enhance mitotic entry in the presence of the Wee1 inhibitor or whether they were mediated through effects on Tyr15 phosphorylation. U2OS cdk1as eGFP-RGC-32 cells were cultured in media containing Dox and arrested in G2. Cells were treated with MK-1775 (0.5 μM) (Kreahling *et al.*, 2013) for 30 minutes prior to 1NM-PP1 wash-off as these conditions were optimised by Hochegger laboratory in HeLa cdk1as and RPE cdk1as cell lines (University of Sussex). Cells were then washed into media with MG132 (25 μM) to block mitotic exit without any 1NM-PP1 followed by time-lapse imaging (**Figure 4.10A**). Consistent with our previous observations more cells entered mitosis in the presence of RGC-32. Unfortunately, uninduced cells (control) treated with MK-1775 did not show a very large increase in the number of cells entering mitosis. The inhibitor had very little effect on the proportion of RGC-32 expressing cells entering mitosis (**Figure 4.10B**), but

from these experiments we could not make a clear conclusion. Upon repeating the experiment, we saw an effect of the inhibitor for RGC-32 expressing cells. However, the effect of RGC-32 on mitotic entry in this experiment was lower than in previous experiment (**Figure 4.11**) making it is difficult to determine whether the effects of RGC-32 involved removal of Try15 phosphorylation. Due to time constraints, we could not optimise these experiments further.

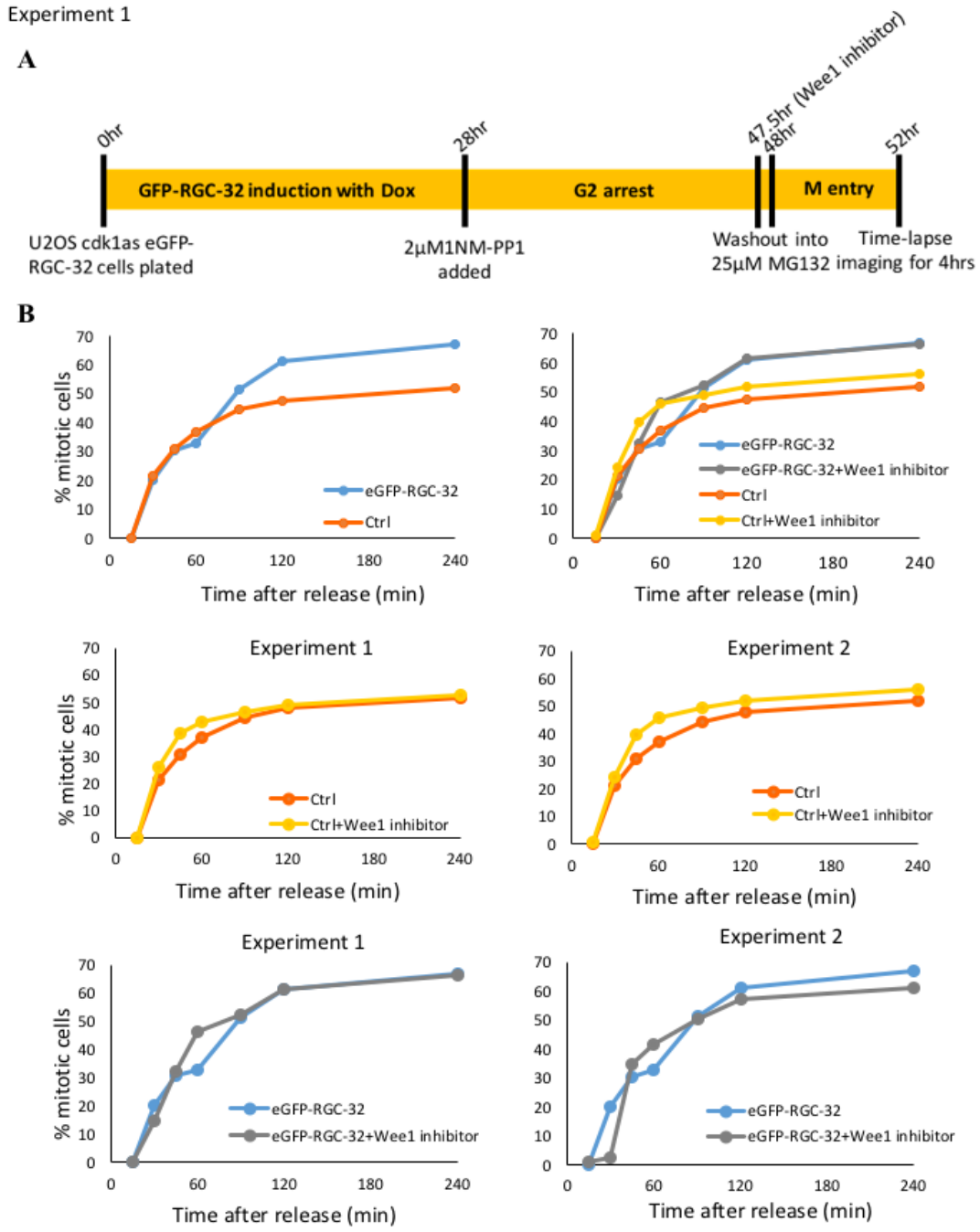

Figure 4.10 The effect of Wee1 inhibition on mitotic entry of G2 arrested U2OS cdk1as eGFP-RGC-32 cells expressing eGFP-RGC-32.
(A) Schematic representation of the mitotic entry experiment. U2OS cdk1as eGFP-RGC-32 cells were cultured in Dox followed by treatment with the ATP-analogue inhibitor of CDK1, 1NM-PP1 (2 µM) to arrest cells in G2. Cells were treated with Wee1 inhibitor (500 nM) 30 minutes prior to wash-off into media with proteasome inhibitor MG132 (25 µM) to block mitotic exit. (B) Quantification of cells entering mitosis -/+ Wee1 inhibitor was judged by cell rounding. Images were captured at 15-minute intervals for 4 hours with an Olympus IX73 microscope using a 20x lens. Graphs show the percentage of cells that have entered mitosis over time. 500 cells were examined for each experiment.

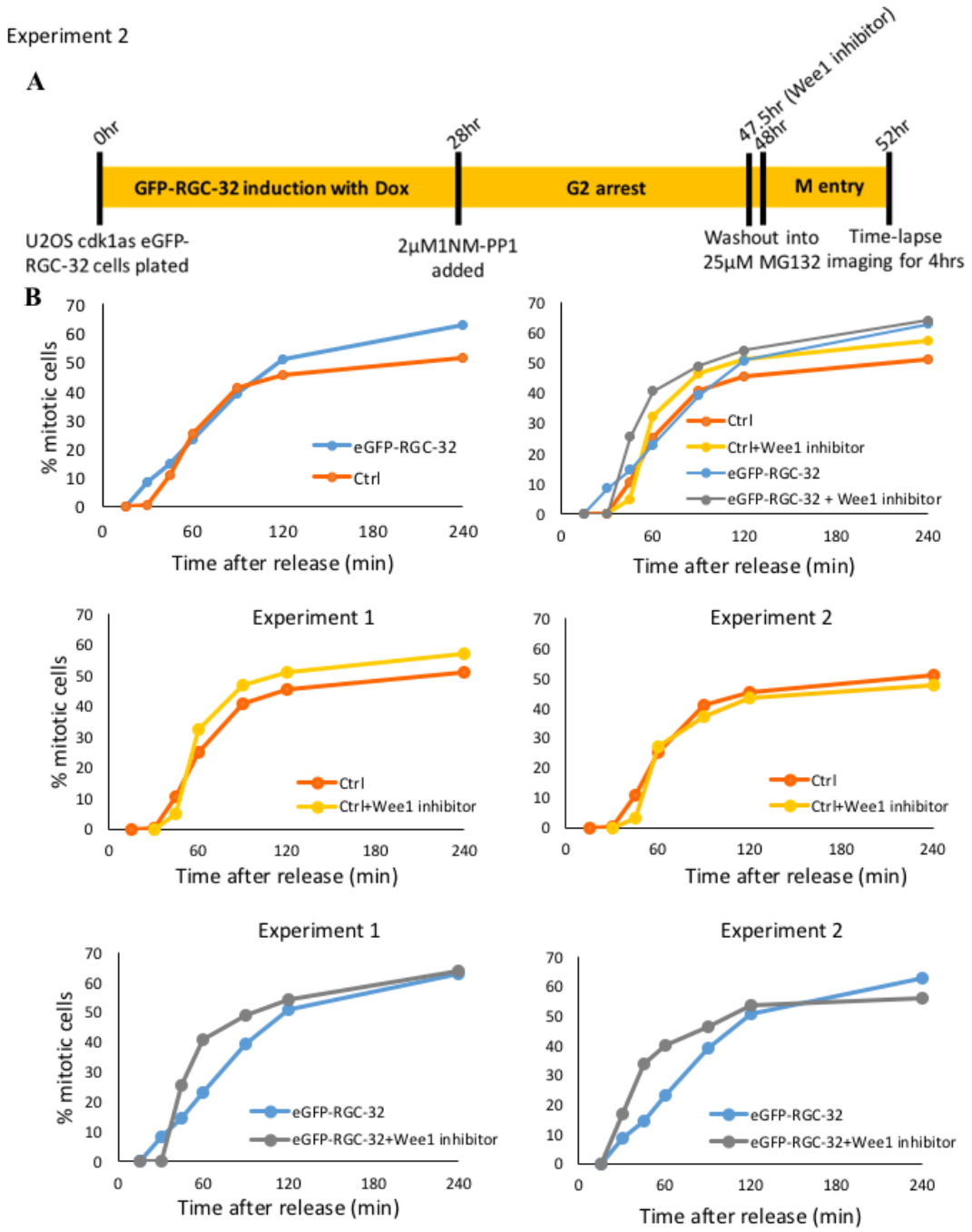

Figure 4.11 The effect of Wee1 inhibition on mitotic entry of G2 arrested U2OS cdk1as eGFP-RGC-32 cells expressing eGFP-RGC-32.
(A) Schematic representation of the mitotic entry experiment. U2OS cdk1as eGFP-RGC-32 cells were cultured in Dox followed by treatment with the ATP-analogue inhibitor of CDK1, 1NM-PP1 (2 µM) to arrest cells in G2. Cells were treated with Wee1 inhibitor (500 nM) 30 minutes prior to wash-off into media with proteasome inhibitor MG132 (25 µM) to block mitotic exit. (B) Quantification of cells entering mitosis -/+ Wee1 inhibitor was judged by cell rounding. Images were captured at 15-minute intervals for 4 hours with an Olympus IX73 microscope using a 20x lens. Graphs show the percentage of cells that have entered mitosis over time. 500 cells were examined for each experiment.

4.4 Effect of RGC-32 on CDK1 Tyrosine 15 phosphorylation

As the mitotic entry experiment with Wee1 inhibition was not conclusive, we investigated the effect of RGC-32 on inhibitory phosphorylation on Y15 of CDK1 using an immunofluorescence (IF) approach. We first performed immunostaining to check the Tyr (Y)15 phosphorylation specific antibody. U2OS cdk1as eGFP-RGC-32 cells were arrested in G2 with 1NM-PP1 (2 μM) where phosphorylation of Y15 will be high, fixed with paraformaldehyde and stained with an anti-Y15 (P) monoclonal antibody. Specific staining was obtained (**Figure 4.12**) allowing us to further proceed with the experiment in RGC-32 expressing cells.

U2OS cdk1as eGFP-RGC-32 cells were cultured in media in the absence and presence of Dox and arrested in G2 by 1NM-PP1 (2 μM). Y15 phosphorylation was examined at different time points (0, 5, 30, and 120 minutes) after release following washing of the cells into media with MG132 (25 μM) to block mitotic exit. Cells were fixed and stained with CDK1 Y15 phosphorylation specific primary antibody and then with fluorescence-conjugated (TRITC) secondary antibody. As the samples for each time point had mixed population of mitotic and interphase cells, we performed immunofluorescence analysis using a ScanR microscope and selected the population of interphase cells by gating for cells with nuclei with intact nuclear membranes (visualized with Hoechst stain). The level of CDK1 Y15 phosphorylation was measured for the gated interphase population for each sample. Each histogram shows the distribution of intensity of Y15 phosphorylation vs the number of cells whereas the box plot shows the mean fluorescence intensity for each sample.

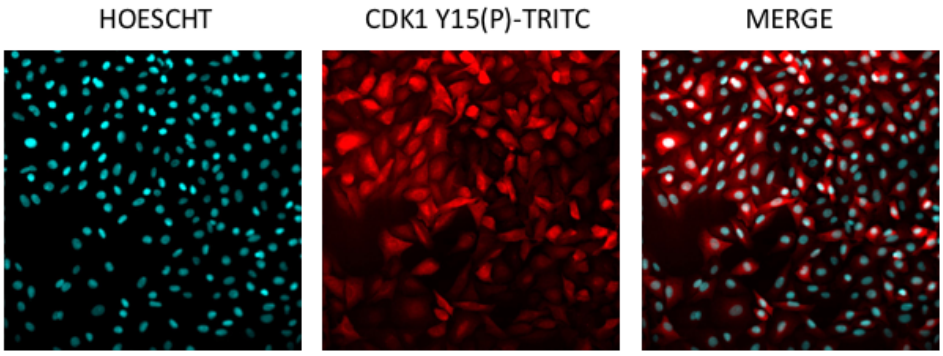

Figure 4.12 Immunostaining of CDK1 pY15 in U2OS cdk1as eGFP-RGC-32 cells.
U2OS cdk1as eGFP-RGC-32 cells were arrested in G2 by 1NM-PP1 (2 µM). Cells were fixed and immunostained for CDK1 Y15 phosphorylation (Red). DNA was visualized using Hoechst 33342 (Cyan). Images were taken using an Olympus IX73 microscope using a 20x lens. Scale bar: 10 µM.

As expected in control uninduced cells, Y15 phosphorylation staining decreased during mitotic entry as increasing number of cells entered mitosis (**Figure 4.13)**. Interestingly, we observed a reduction in Y15 phosphorylation in cells expressing RGC-32 for all the time points, including at the start of wash-off (0 min) as compared to the control cells indicating that RGC-32 reduces CDK1 Y15 phosphorylation. When this experiment was repeated, the staining did not work as well and the cell density was lower. We also observed different kinetics of mitotic entry, with most cells in mitosis by 30 minutes. Nonetheless, we saw a reduction in Y15 phosphorylation at the 5 min time point (**Figure 4.14**). Overall, it appears that RGC-32 promotes removal of inhibitory phosphorylation on Y15 of CDK1.

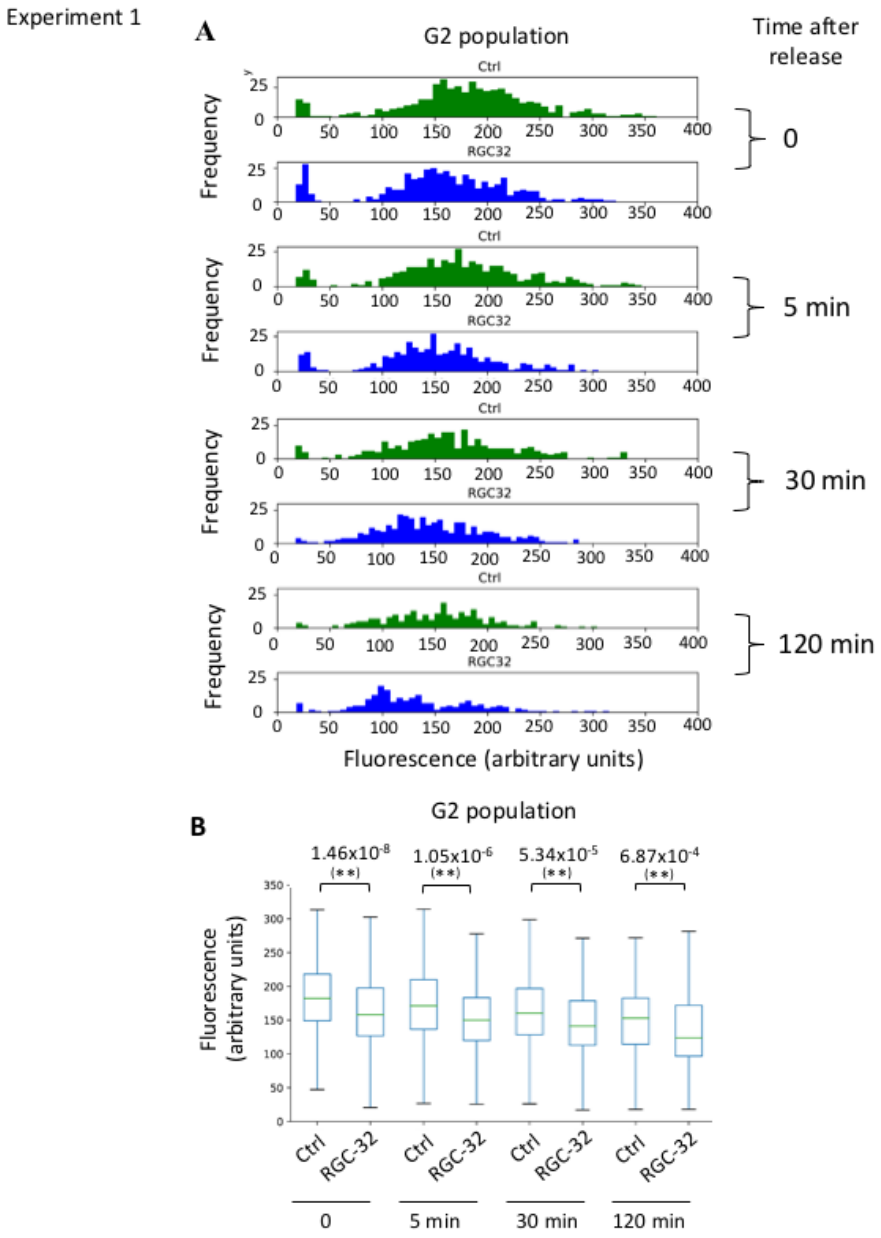

Figure 4.13 The effect of RGC-32 on Tyrosine 15 phosphorylation of CDK1.
U2OS cdk1as eGFP-RGC-32 cells were cultured -/+ Dox to induce the expression of eGFP-RGC-32. Cells were arrested in G2 for 20 hours with 1NM-PP1 (2 µM) and washed into media with proteasome inhibitor MG132 (25 µM) to block mitotic exit. Samples were collected at 0, 5, 30 and 120 minutes post wash-off. Cell were fixed and immunostained for CDK1 Y15 phosphorylation (Red) and DNA was visualized using Hoechst 33342 (Blue). Images were taken on an Olympus ScanR microscope using a 20x lens. Analysis was carried out using the ScanR image analysis software. (A) Histogram showing the number of cells with different fluorescent intensity of Y15 phosphorylation in G2 population of each sample for every time point after releasing the cells from G2 arrest. (B) Box plot shows the median, lower and upper values for the mean intensity of Y15 phosphorylation and the top and bottom bar show the overall range of intensity for Y15 phosphorylation in the selected population of control and eGFP-RGC-32 expressing cells for G2 population. Both the graphs were generated using PyCharm. T-test for cells expressing eGFP-RGC-32 compared to control for each time point is shown where $P < 0.001$ (**).

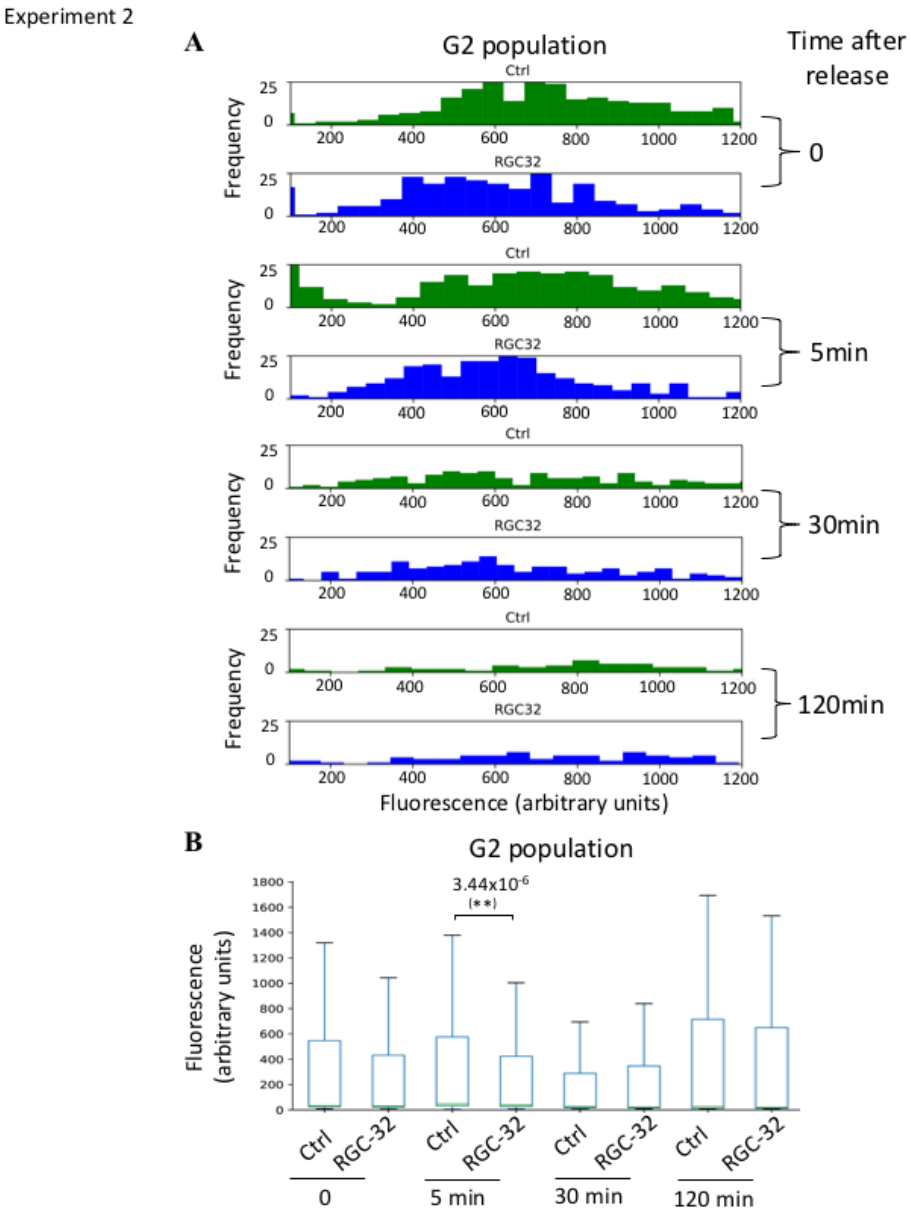

Figure 4.14 The effect of RGC-32 on Tyrosine 15 phosphorylation of CDK1.
U2OS cdk1as eGFP-RGC-32 cells were cultured -/+ Dox to induce the expression of eGFP-RGC-32. Cells were arrested in G2 for 20 hours with 1NM-PP1 (2 µM) and washed into media with proteasome inhibitor MG132 (25 µM) to block mitotic exit. Samples were collected at 0, 5, 30 and 120 minutes post wash-off. Cell were fixed and immunostained for CDK1 Y15 phosphorylation (Red) and DNA was visualized using Hoechst 33342 (Blue). Images were taken on an Olympus ScanR microscope using a 20x lens. Analysis was carried out using the ScanR image analysis software. (A) Histogram showing the number of cells with different fluorescent intensity of Y15 phosphorylation in G2 population of each sample for every time point after releasing the cells from G2 arrest. (B) Box plot shows the median, lower and upper values for the mean intensity of Y15 phosphorylation and the top and bottom bar show the overall range of intensity for Y15 phosphorylation in the selected population of control and eGFP-RGC-32 expressing cells for G2 population. Both the graphs were generated using PyCharm. T-test for cells expressing eGFP-RGC-32 compared to control for each time point is shown where $P < 0.001$ (**).

4.5 Effect of RGC-32 on CDK substrate phosphorylation

Next, we investigated the effect of RGC-32 on CDK1 mediated substrate phosphorylation at Serine/ Proline (S/P) residues upon mitotic entry. Cells were arrested in G2 followed by wash-off in media with MG132 (25 μM) to block mitotic exit. Cells were fixed 2 hours after releasing from G2 arrest and immunostained using primary antibody that detects phosphorylation at Serine/ Proline residues in the (K/H) S*P motif and then with fluorescence-conjugated (Cy5) secondary antibody in mitotic cells (**Figure 4.15**). By using this antibody, we determined whether phosphorylation of CDK substrates in mitosis increases in the presence of RGC-32. Immunofluorescence was performed using the ScanR microscope to measure the Serine/Proline phosphorylation in the mitotic cells. U2OS cdk1as eGFP-RGC-32 cells were arrested in G2 by 1NM- PP1 (2 μM) -/+ Dox followed by wash-off into media with MG132 (25 μM) to block mitotic exit. Samples were collected at different time points (5, 30, 60, and 120 minutes) after releasing the cells from G2 arrest. The mitotic population for each sample was gated by selecting for cells with metaphase plates with high Hoechst intensity. An overall increase in substrate phosphorylation was observed as cells moved into mitosis during the time-course of the experiment as expected. Substrate phosphorylation increased significantly in cells expressing RGC-32 after 30 and 60 minutes of wash-off and equalised to control levels after 120 minutes (**Figure 4.16**). Upon repeating the experiment, cells appeared to move more slowly into mitosis but significant increase in CDK substrate phosphorylation at 60 minutes was observed in cells expressing RGC-32 (**Figure 4.17**). In conclusion, our data indicates that RGC-32 increases phosphorylation of CDK substrates in mitosis consistent with activation of CDK1 kinase activity by RGC-32.

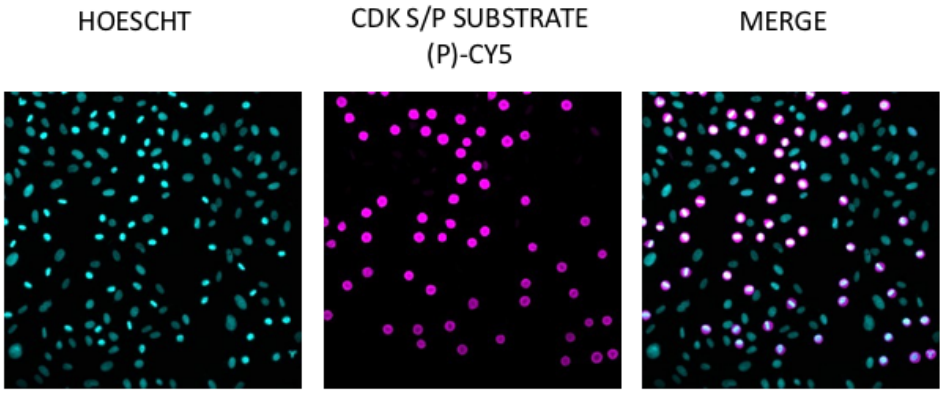

Figure 4.15 Immunostaining of CDK phospho S/P substrates in U2OS cdk1as eGFP-RGC-32 cells.
U2OS cdk1as eGFP-RGC-32 cells were arrested in G2 by 1NM-PP1 (2 μM) followed by wash-off into media with proteasome inhibitor MG132 (25 μM) to block mitotic exit. Cells were fixed 2 hours after wash-off and immunostained for CDK S/P substrate phosphorylation (Magenta). DNA was visualized using Hoechst 33342 (Cyan). Images were taken using an Olympus IX73 microscope using a 20x lens. Scale bar: 10 μM.

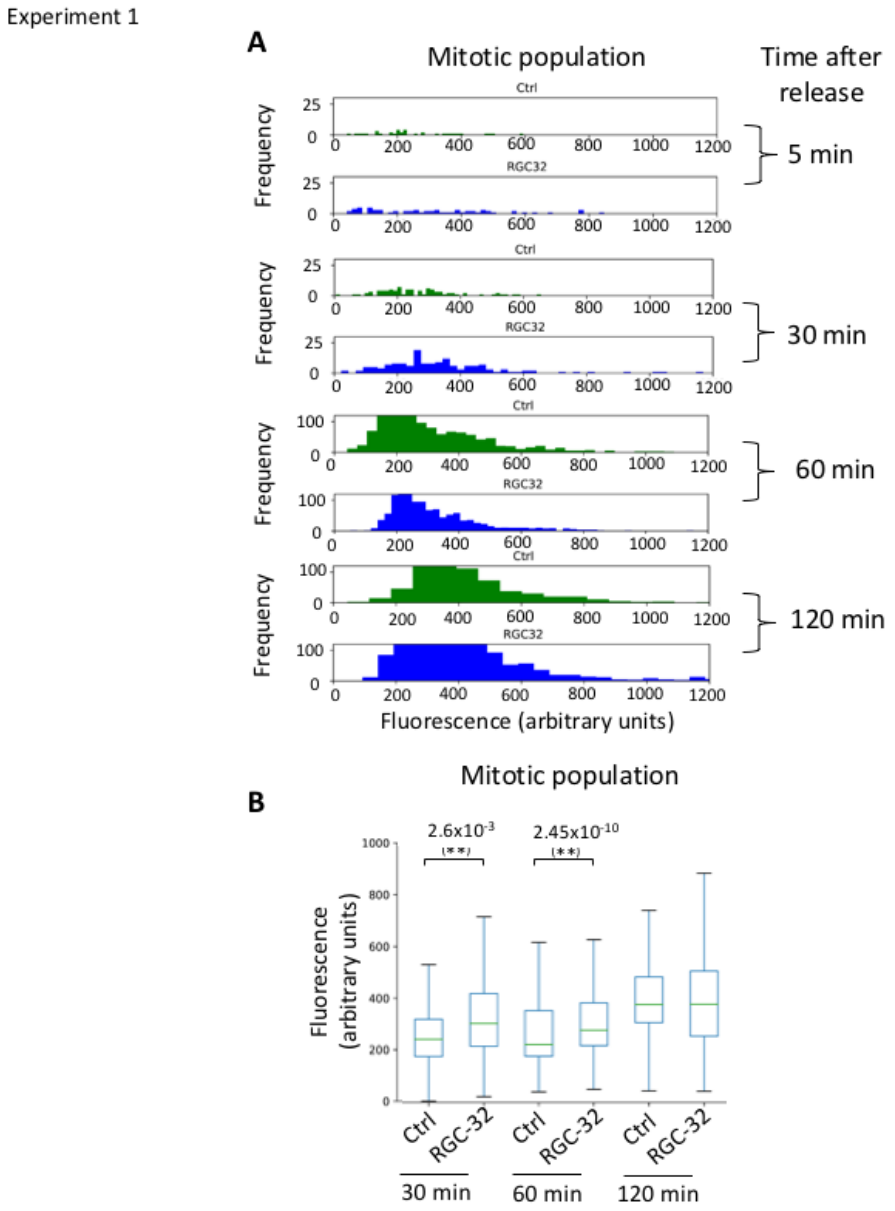

Figure 4.16 The effect of RGC-32 on phosphorylation of CDK1 targets.
U2OS cdk1as eGFP-RGC-32 cells were cultured -/+ Dox to induce the expression of eGFP-RGC-32. Cells were arrested in G2 for 20 hours with 1NM-PP1 (2 µM) and washed into media with proteasome inhibitor MG132 (25 µM) to block mitotic exit. Samples were collected at 5, 30, 60 and 120 minutes post wash-off. Cell were fixed and immunostained for CDK substrate phosphorylation at serine/ proline residues (Red) and DNA was visualized using Hoechst 33342 (Blue). Images were taken on an Olympus ScanR microscope using a 20x lens. ScanR image analysis was carried out to gate for G2 and mitotic population and to calculate the mean fluorescence intensity. (A) Histogram showing the number of cells with different fluorescent intensity of CDK target phosphorylation in mitotic population of each sample for every time point after releasing the cells from G2 arrest. (B) Box plot shows the median, lower and upper values for the mean intensity of CDK target phosphorylation and the top and bottom bar show the overall range of intensity for CDK S/P phosphorylation in the selected population of control and eGFP-RGC-32 expressing cells for mitotic population. Both the graphs were generated using PyCharm. T-test for cells expressing eGFP-RGC-32 compared to control for each time point is shown where $P < 0.001$ (**).

Experiment 2

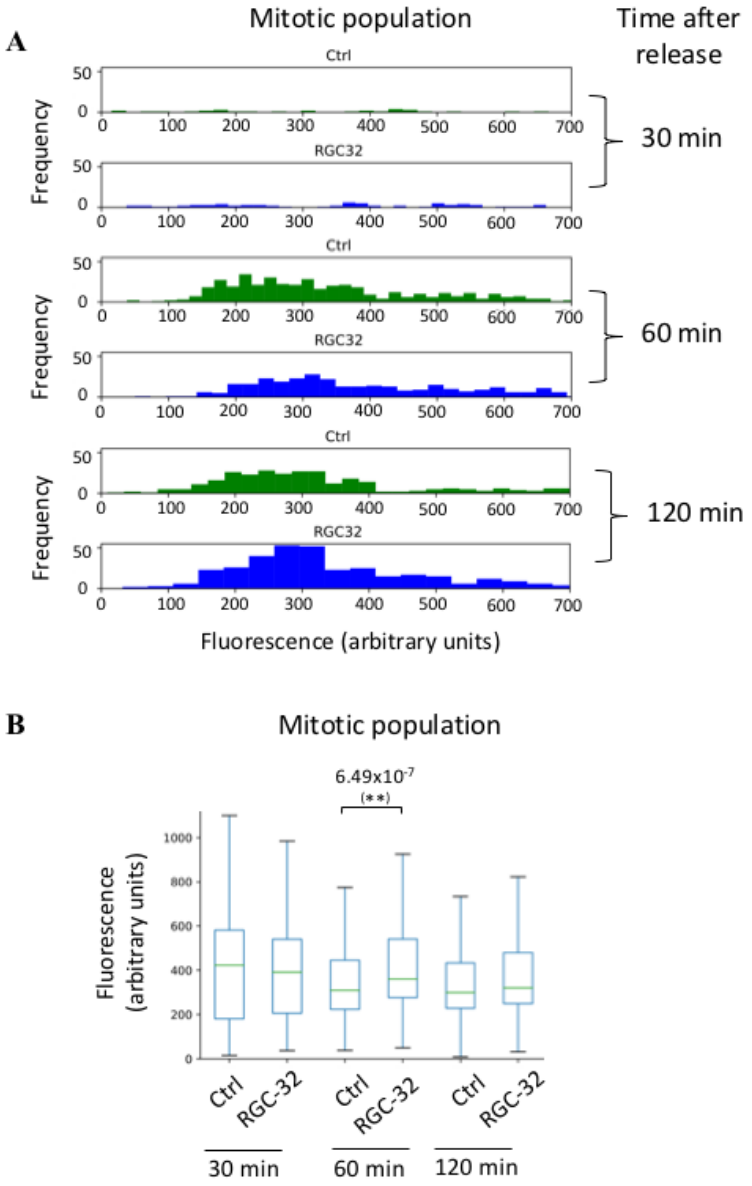

Figure 4.17 The effect of RGC-32 on phosphorylation of CDK1 targets.
U2OS cdk1as eGFP-RGC-32 cells were cultured -/+ Dox to induce the expression of eGFP-RGC-32. Cells were arrested in G2 for 20 hours with 1NM-PP1 (2 µM) and washed into media with proteasome inhibitor MG132 (25 µM) to block mitotic exit. Samples were collected at 5, 30, 60 and 120 minutes post wash-off. Cell were fixed and immunostained for CDK substrate phosphorylation at serine/ proline residues (Red) and DNA was visualized using Hoechst 33342 (Blue). Images were taken on an Olympus ScanR microscope using a 20x lens. ScanR image analysis was carried out to gate for G2 and mitotic population and to calculate the mean fluorescence intensity. (A) Histogram showing the number of cells with different fluorescent intensity of CDK target phosphorylation in mitotic population of each sample for every time point after releasing the cells from G2 arrest. (B) Box plot shows the median, lower and upper values for the mean intensity of CDK target phosphorylation and the top and bottom bar show the overall range of intensity for CDK S/P phosphorylation in the selected population of control and eGFP-RGC-32 expressing cells for mitotic population. Both the graphs were generated using PyCharm. T-test for cells expressing eGFP-RGC-32 compared to control for each time point is shown where $P < 0.001$ (**).

4.6 Can RGC-32 promote mitotic entry upon depletion of Cyclin B1/B2?

The ability of RGC-32 to bind to CDK1 directly and activate it both *in vitro* and *in vivo* led us to study whether RGC-32 is sufficient for mitotic entry in the absence of cyclin B. To study this we transfected U2OS cdk1as eGFP-RGC-32 cells with either cyclin B1 and B2 targeting siRNAs (Dharmacon smartpool) or control siRNA (Qiagen). We confirmed that cyclin B1 and B2 were depleted by western blot analysis 48 hours post transfection (**Figure 4.18**). Once the depletion of cyclin B was established using siRNA, we next investigated the effect of RGC-32 on mitotic entry in the absence of cyclin B. U2OS cdk1as eGFP-RGC-32 cells were transfected with either control siRNA or cyclin B1/B2 targeting siRNAs. Expression of eGFP-RGC-32 was induced by culturing the transfected cells in media containing Dox followed by treatment with 1NM-PP1 (2 μM) to arrest the cells in G2. After 20 hours, cells were washed into media with proteasome inhibitor MG132 (25 μM) to block mitotic exit (**Figure 4.19A**). The effect of RGC-32 on mitotic entry in the presence of cyclin B was consistent with more cells entering mitosis compared to control. However, this effect of RGC-32 was not observed in cells transfected with either the control siRNA or the cyclin B targeting siRNAs (**Figure 4.19B**). Since the effect of RGC-32 was not observed in control siRNA treated cells possibly due to toxicity effects, we could not derive any definite conclusion for the effect of RGC-32 on mitotic entry in the absence of cyclin B. Due to time constraints; this experiment could not be repeated.

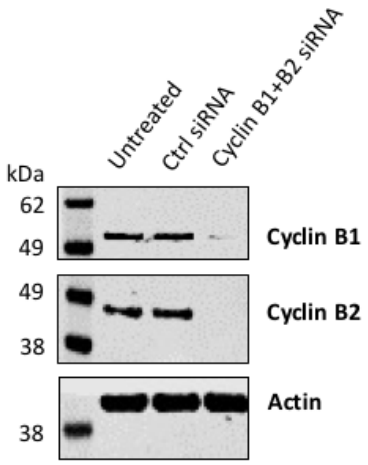

Figure 4.18 siRNA mediated depletion of Cyclin B1 and B2.
U2OS cdk1as eGFP-RGC-32 cells were transfected with control (Ctrl) or Cyclin B1 and Cyclin B2 (Cyclin B1+B2) siRNA using Lipofectamine® RNAiMAX. Western Blot analysis showed the depletion of Cyclin B1 and Cyclin B2 protein by the Cyclin B1+B2 siRNA. Actin was used as the loading control.

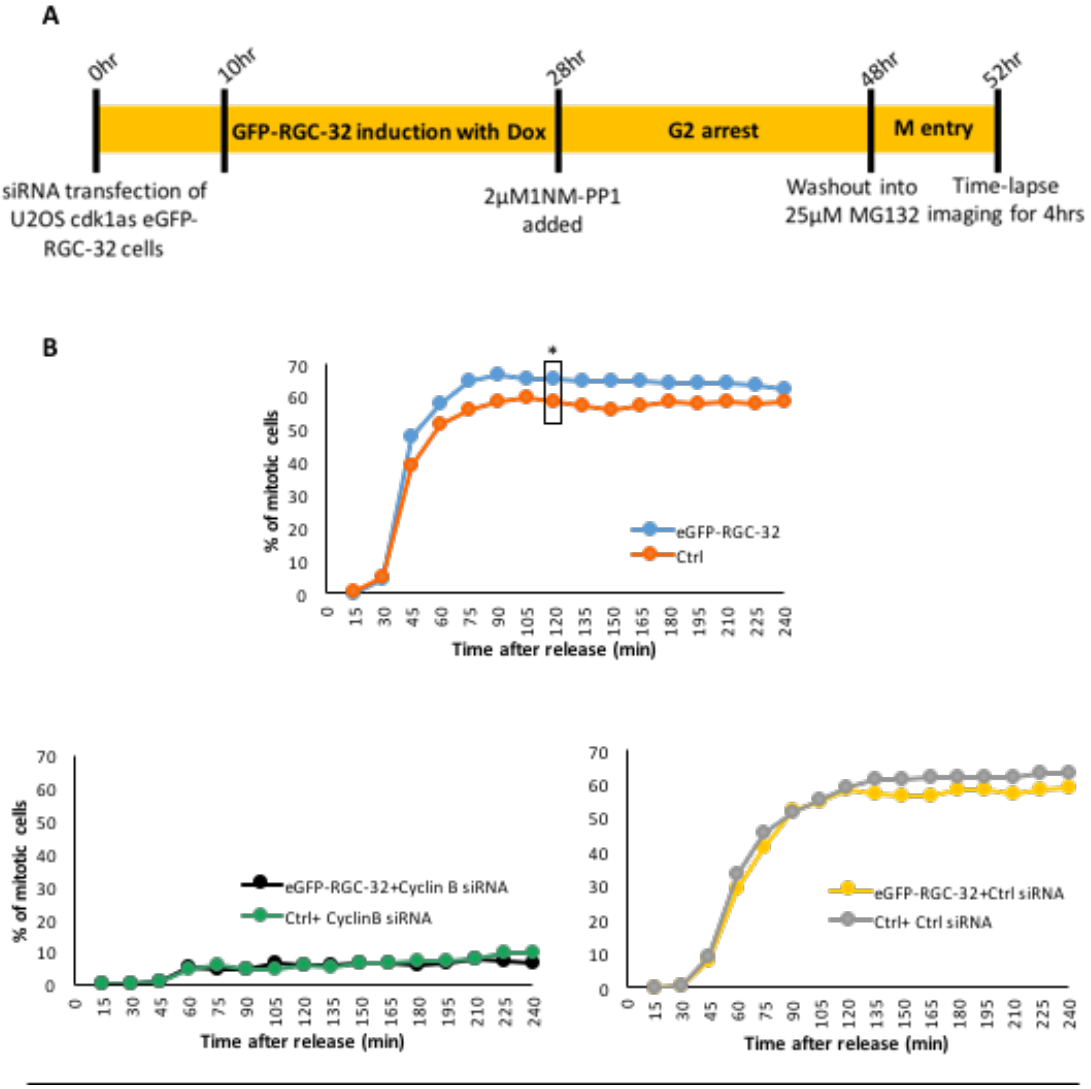

Figure 4.19 The effect of Cyclin B knockdown on mitotic entry of G2 arrested U2OS cdk1as eGFP-RGC-32 cells expressing eGFP-RGC-32.

(A) Schematic representation of the mitotic entry experiment. U2OS cdk1as eGFP-RGC-32 cells were transfected with either control siRNA or Cyclin B1/B2 siRNA. Media was changed after 10 hours and cells were cultured in Dox followed by treatment with ATP-analogue inhibitor of CDK1, 1NM-PP1 (2 µM) to arrest cells in G2. Cells were washed-off into media with proteasome inhibitor MG132 (25 µM) to block mitotic exit. (B) Quantification of cells entering mitosis +/- Cyclin B1/B2 expression was judged by cell rounding. Images were captured at a 15-minute interval for 4 hours with an Olympus IX73 microscope using a 20x lens. Graphs show the percentage of cells that have entered mitosis over time. 500 cells were examined for each experiment. Results shown are representative of two independent experiments. Student's T-test for cells expressing eGFP-RGC-32 compared to control for 120 minutes after G2 release is shown for each condition where $P < 0.05$ (*).

4.7 RGC-32 is required for the survival of EBV-infected B cells

To determine the role of RGC-32 in the growth of EBV-infected cells, where we first showed its expression to be activated, the expression of RGC-32 was silenced in EBV-positive Latency III (GM12878 & IB4) cells and cell viability assays were conducted. To confirm that the shRNA specifically targeted RGC-32, Dr Michèle Brocard from our laboratory transduced GM12878 cells with lentiviruses expressing shRNA specific to RGC-32 (shRNA 3-7) at a multiplicity of infection (MOI) of 1. As the scrambled control was not available, lentivirus expressing the GFP sequence was used as a control. Western blot analysed reduced protein expression in transduced cells as compared to untransduced (Untr) cells after 3 weeks of selection in puromycin. RGC-32 protein levels were reduced 50% - 78% in week 3 (**Figure 4.20A**) (Brocard *et al.*, 2018). However, the depletion of protein expression was not sustained in these longer-term puromycin-selected cells which indicated reduced RGC-32 expression was toxic to cells (**Figure 4.20B)**. To explore this further, knockdown studies were carried out by using combinations of RGC-32 targeting shRNA expressing lentiviruses as well as increasing the MOI to achieve higher transduction efficiency. Cell viability studies of IB4 cells transduced at a MOI of 5 with RGC-32 targeting shRNA showed the number of live cells in the culture decreased rapidly over 8 days of puromycin selection as compared to untransduced cells. Moreover, increased cell death was observed with increasing the combination of RGC-32 targeting shRNA (**Figure 4.20C**). These data suggests that silencing of RGC-32 leads to cell death of EBV-infected cells (Brocard *et al.*, 2018).

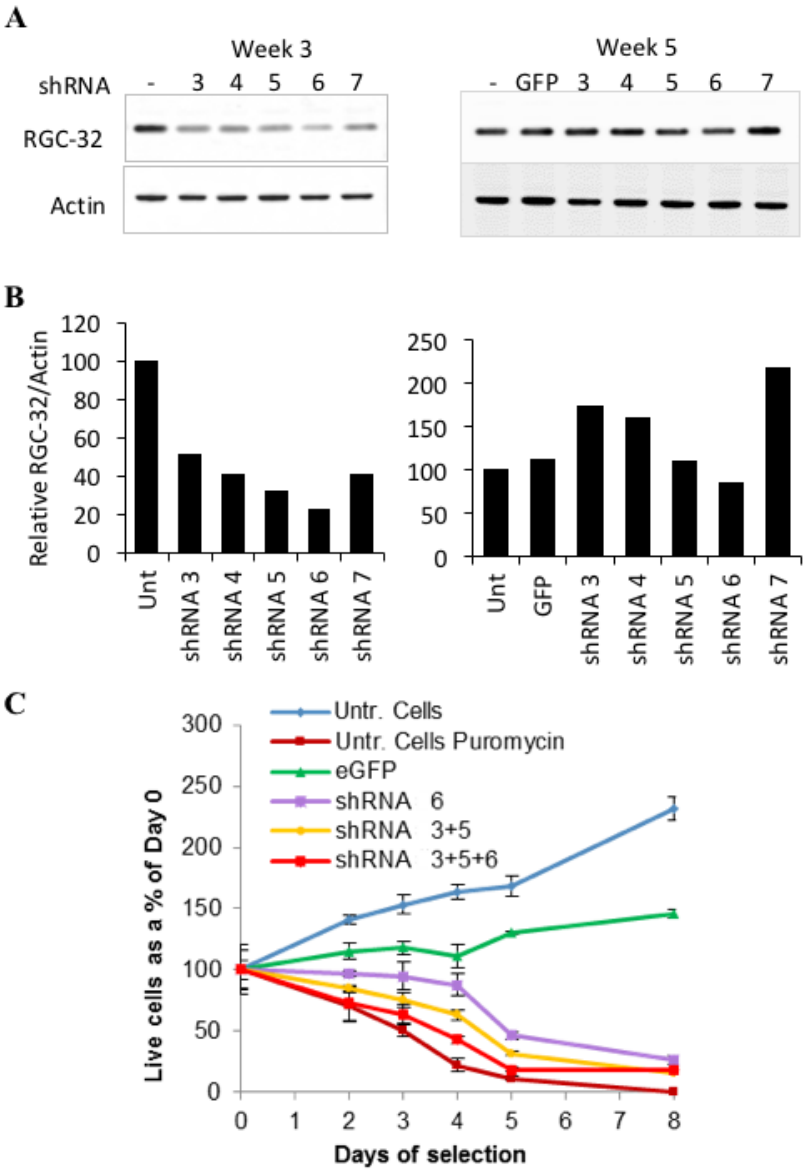

Figure 4.20 Depletion of RGC-32 mRNA in cells using lentiviruses expressing shRNA.
(A) GM12878 cells were transduced at MOI of 1 with either Mission (Sigma) lentiviral particle carrying the GFP coding sequence (eGFP) as a control or shRNAs targeting RGC-32 open reading frame or 3'UTR (shRNA 3 to 7). Western blot analysis shows depletion of RGC-32 protein in transduced cells after 3 and 5 weeks of selection in puromycin. Actin was used as a loading control. (B) Quantification of RGC-32 protein normalised to actin and expressed relative to the untransduced control showing the reduction in RGC-32 protein in transduced cells. (C) IB4 cells were transduced at MOI 5 with Mission lentiviral particles. The untransduced (Untr.) cells -/+ puromycin (Untr. + Puro) were used as controls for growth and selection respectively. Number of live cells was determined by trypan blue exclusion. Graph show the mean of four independent cell counts ± standard deviation and are expressed relative to the number of live cells at day 0 (Brocard *et al*., 2018).

To confirm that cell death was specific to RGC-32 depletion and not due to general toxicity of the lentiviruses or shRNA, a rescue experiment was performed by inducibly overexpressing exogenous RGC-32 in cells transduced with lentiviruses. To do this, IB4 cells were transfected with either pRTS-1 (control) or pRTS-1 RGC-32 allowing inducible expression of RGC-32 and hygromycin resistant cells were selected to establish a stable cell line (**Figure 4.21A**). The plasmid has a bidirectional promoter which drives the GFP expression in one direction and RGC-32 expression in other direction (IB4 pRTS-1 RGC-32) upon doxycycline treatment. In the control cell line, firefly luciferase is expressed instead of RGC-32 in the opposite direction to GFP (IB4 pRTS-1). Both stable cell lines were screened by flow cytometry to monitor the induction of GFP upon treatment with Dox for 48 hours. IB4 pRTS-1 cells showed an induction of ~86% and in IB4 pRTS-1 RGC-32 cells it was ~54% (**Figure 4.21B**). In addition, IB4 stable cell lines were screened for overexpression of RGC-32 mRNA 48 hours by qPCR. We observed some leaky expression of RGC-32 mRNA in IB4 pRTS-1 RGC-32 cells without doxycycline, however, treatment with dox increased the expression by ~230 fold compared to cells without dox (**Figure 4.22A**). The induction of RGC-32 protein expression was also analysed in these cells. However, we could not detect any increase in protein expression upon treatment with doxycycline as these cells already expressed high levels of RGC-32. To check that the inability to detect RGC-32 protein expression was not because of a problem with the plasmid being used, the Akata pRTS-1 RGC-32 (Latency I) stable cell line made by Dr Lina Chen using the same plasmid was also analysed. Here, RGC-32 protein expression was observed to be specifically induced in cells containing the pRTS-1 RGC-32 plasmid (**Figure 4.22B**).

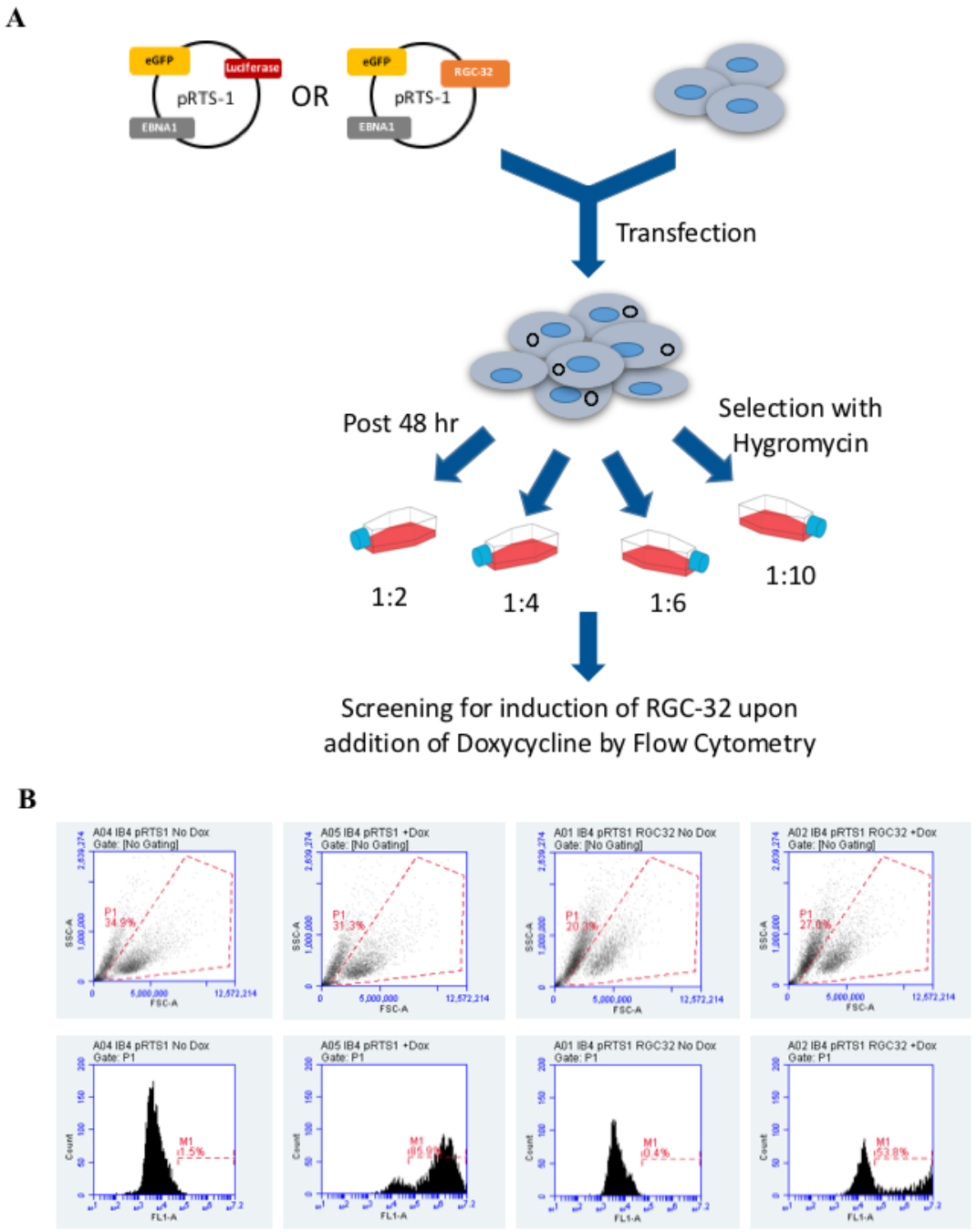

Figure 4.21 Generation of an IB4 stable cell lines expressing inducible eGFP and RGC-32. (A) Schematic diagram of IB4 (EBV-positive latency III) cells transfected with pRTS-1 or pRTS-1 RGC-32 followed by hygromycin selection of resistant cells stably expressing the inducible plasmids. (B) Flow cytometry analysis to determine the number of cells expressing eGFP and Luciferase (pRTS-1) or eGFP and RGC-32 (pRTS-1 RGC-32) 48 hours after treatment with doxycycline (Dox). The GFP positive cells were gated (M1) from the total events showing the percentage of positive cells (Brocard *et al*., 2018).

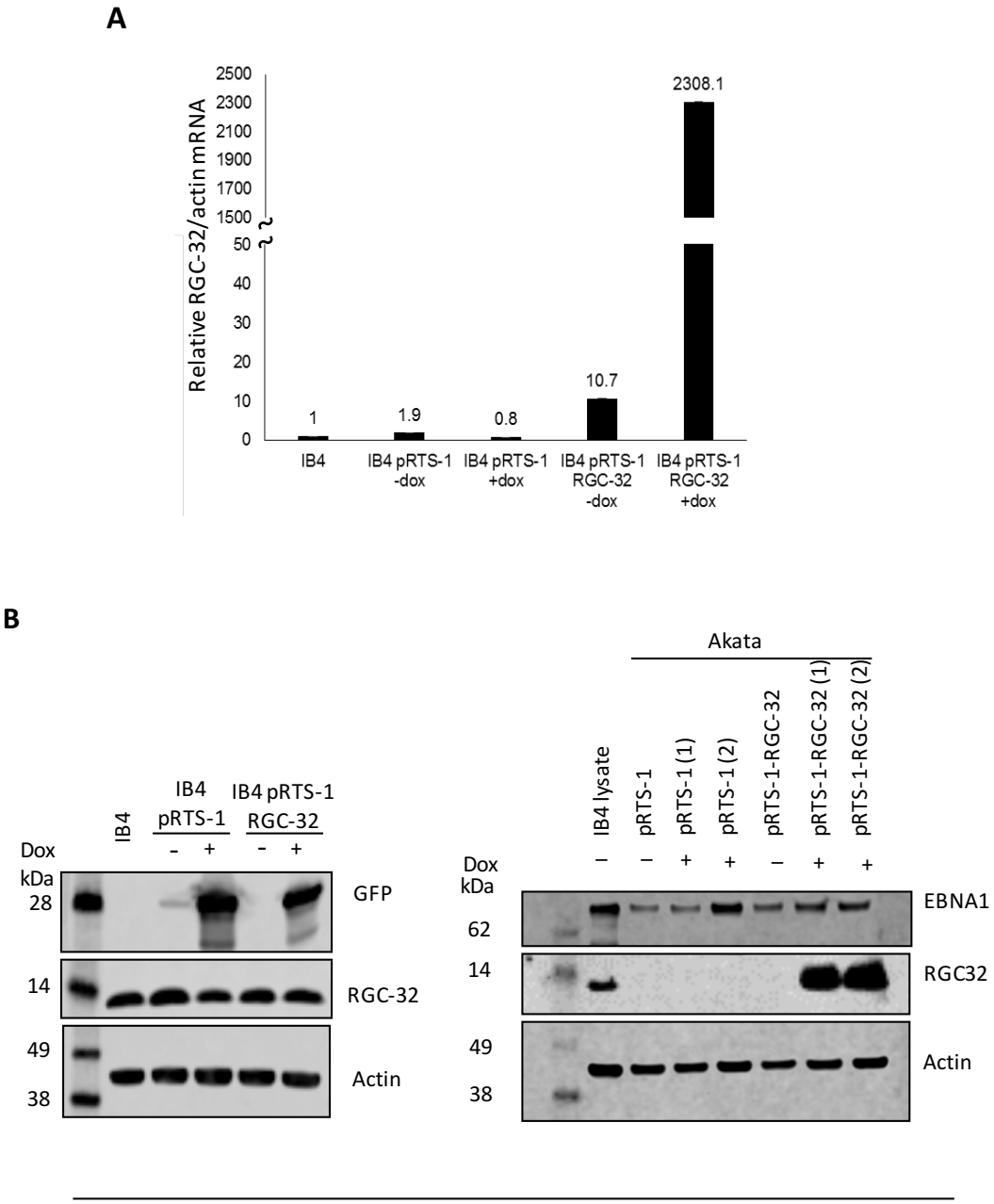

Figure 4.22 Analysis of inducible expression of RGC-32 in IB4 pRTS-1 RGC-32 stable cell line.

IB4 pRTS-1 and pRTS-1 RGC-32 cells were treated with Dox for 48 hours. (A) QPCR analysis of RGC-32 mRNA expression using cDNA from cell lines +/- Dox. RGC-32 mRNA levels were normalized to endogenous actin levels and expressed relative to RGC-32 mRNA levels in parental IB4 cell line. (B) Western blot analysis of GFP, EBNA1 and RGC-32 protein expression in IB4 pRTS-1 and pRTS-1 RGC-32 cells and Akata pRTS-1 and pRTS-1 RGC-32 cells +/- Dox. GFP expression was used as a positive control for induction as the plasmid has a bidirectional promoter expressing RGC-32 in one direction and GFP in other. Also, EBNA1 protein expression was used as a positive control for the plasmid replication. Actin was used as a loading control (Brocard *et al.*, 2018).

Expression of EBNA1 was used as a positive control for plasmid expression as the pRTS-1 vector backbone has the EBV origin of replication (*oriP*) and latent protein EBNA1 which binds to *OriP* and allows episomal replication and segregation of the plasmid (Bornkamm *et al.*, 2005). This suggests that there could be translational control that prohibits the overexpression of RGC-32 in IB4 cells. Since we confirmed that RGC-32 mRNA was overexpressed in these cells and rescue of shRNA effect would be expected to result from squelching of the effects by excess mRNA, we continued with the experiment.

For the rescue experiment, IB4 pRTS-1 and IB4 pRTS-1 RGC-32 cell lines were treated with doxycycline for 24 hours to induce the expression of GFP in the absence and presence of RGC-32. Cells were transduced with lentiviruses expressing either non-targeting shRNA or shRNA targeting the open reading frame of RGC-32. Transduced cells were selected in puromycin and the percentage of GFP positive cells was determined by flow cytometry. In the IB4 pRTS-1 control cell line, we observed that the percentage of GFP positive cells reduced substantially over time as compared to cells transduced with non-targeting shRNA. However, the percentage of GFP positive cells in IB4 pRTS-1 RGC-32 did not decrease to the same extent indicating that they were resistant to death induced by RGC-32 targeting shRNA (**Figure 4.23**). The percentage of GFP positive cells in IB4 pRTS-1 RGC-32 was observed to be 50% on day 5 as compared to 6% in IB4 pRTS-1 upon selection of transduced cells expressing shRNA specific to RGC-32. Although, the loss in percentage of GFP positive cells could be due to the loss of GFP expression in cells and not necessarily cell death, the GFP expression in cells transduced with Non-targeting shRNA did not reduce to the extent observed in cells transduced with

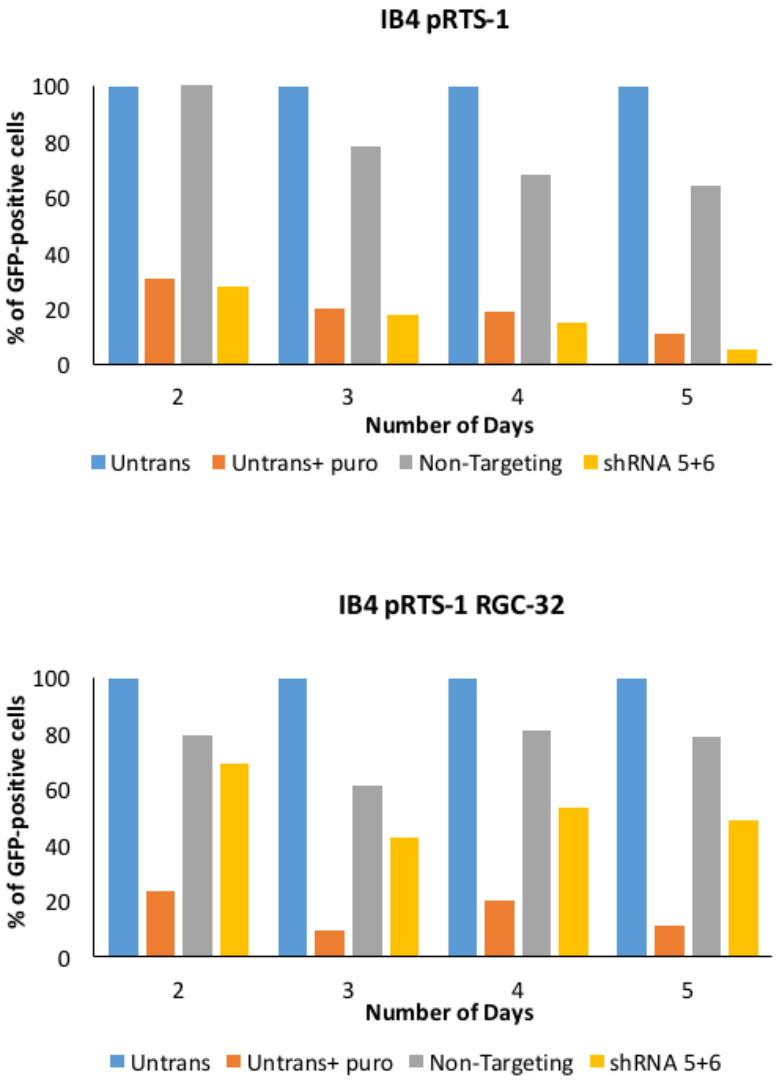

Figure 4.23 The effect of RGC-32 overexpression on cell death of IB4 cells transduced with lentiviruses expressing shRNA targeting RGC-32.
IB4 pRTS-1 (expressing GFP only) and IB4 pRTS-1 RGC-32 (expressing GFP and RGC-32) cells were cultured in doxycycline for 24 hours followed by transduction with either Mission (Sigma) non-targeting shRNA expressing lentiviruses or a mix of lentiviruses expressing shRNA targeting RGC-32 (shRNA 5+6) at MOI of 5. The untransduced (Untrans) cells -/+ puromycin (Untrans + Puro) were used as controls for growth and selection respectively. The number of GFP positive cells in lentivirus transduced cells relative to GFP positive cells in untransduced cells was calculated for each time point (Brocard *et al*., 2018).

RGC-32 targeting shRNA in the absence of RGC-32 expression. These data demonstrate that the cell death in IB4 cells was specific to RGC-32 silencing. Together, our studies confirm the crucial role of RGC-32 in survival of EBV-infected cells (Brocard *et al.*, 2018).

4.8 Discussion

Our initial interaction studies presented in chapter 3 showed that RGC-32 binds to the Spc24-25 heterodimer, part of the NDC80 complex of kinetochore. To further understand this, localisation of RGC-32 at kinetochores by virtue of its interaction with Spc24-25 heterodimer was investigated in HeLa and HeLa cdk1as cells. However, the plasmid m-Cherry-CENP-A, used for localization studies marked the entire chromosome instead of kinetochores making the observation non-conclusive (**Figure 4.1**). To address this issue, localization studies by staining the endogenous kinetochore marker in synchronized population of cells that overexpress RGC-32 could be performed in the future. During prometaphase, PLK1 mediates the stable attachment of kinetochores to the microtubules (Liu *et al.*, 2012). Therefore, investigating the exact timing of RGC-32 localisation during mitosis will provide information on its role in kinetochore-microtubule attachment. Interestingly, localization studies in HeLa cdk1as cells expressing endogenous cyclin B tagged to m-Cherry showed RGC-32 to translocate in the nucleus similar to cyclin B before the breakdown of nuclear envelope (**Figure 4.2**). Interestingly, RGC-32 does not have a nuclear localization signal in its sequence. This suggests RGC-32 could bind to the activated the CDK1-Cyclin B complex as shown by our interaction studies (**chapter 3**) leading to its translocation in the nucleus before the breakdown of nuclear envelope.

Several studies have reported a role of RGC-32 in disrupting the G2/M checkpoint. Our laboratory showed that overexpression of RGC-32 disrupts the G2/M checkpoint in two different B-cell backgrounds suggesting its role in EBV-mediated cell cycle deregulation (Schlick *et al.*, 2011). Therefore, to investigate the role of RGC-32 in G2/M transition, mitotic entry experiments in U2OS cdk1as cells by transiently expressing FLAG-RGC-32 were carried out. In these cells, the endogenous CDK1 has been disrupted and its function is provided by exogenous expression of an analogue-sensitive (AS) F80G mutant (cdk1as). Thus, allowing these cells to be reversibly arrested in G2 by inhibiting CDK1 using a bulky ATP-analogue, 1NM-PP1. We observed more cells to be pushed into mitosis following wash-off from G2 arrest in the presence of RGC-32 as compared to control. This observation was recapitulated in a stable cell line expressing doxycycline inducible RGC-32, U2OS cdk1as eGFP-RGC-32. However, RGC-32 was not able to override the partial inhibition of CDK1 by 1NM-PP1 (**Figure 4.5**). One possible explanation for this could be the binding of 1NM-PP1, a bulky ATP-analogue, in ATP binding pocket of CDK1 which inhibits substrate phosphorylation (Coudreuse and Nurse, 2010). Previous studies have shown that activation of CDK1 kinase activity by RGC-32 is mediated by phosphorylation on Thr91 of RGC-32 by CDK1 (Badea *et al.*, 2002) suggesting RGC-32 to be a CDK1 substrate. As RGC-32-mediated CDK1 activation and phosphorylation of RGC-32 at Thr91 are interdependent, inhibition of CDK1 by INM-PP1 could prohibit it from phosphorylation of RGC-32 thereby blocking the activation of CDK1 by RGC-32 (**Figure 4.9**). During these experiments we observed low expression of RGC-32 in stable cell line over time; this could be a result of gene silencing or the non-transfected cells developing resistance towards the selection drug. In order to address

this issue, sub-cloning of the cell line and screening for clones with better induction can be pursued in future.

Next, to determine the mechanism by which RGC-32 activates CDK1, mitotic entry studies were performed by inhibition of Wee1 kinase, which acts as a negative regulator of CDK1 (McGowan and Russell, 1993). Both the experiments for Wee1 inhibition did not show a consistent effect on mitotic entry in the control cell population suggesting that the concentration of Wee1 inhibitor used in these studies may not be sufficient to completely inhibit the activity of the kinase. Therefore, the concentration of Wee1 inhibitor needs to be addressed in future experiments by titrating the drug concentration to achieve optimum drug concentration and then revisit these experiments (**Figure 4.10-4.11**). Further, immunofluorescence studies showed the intensity of inhibitory phosphorylation of Y15 by Wee1 on CDK1 reduced significantly in the presence of RGC-32 as compared to control cells (**Figure 4.13-4.14**). In addition, the substrate phosphorylation at Serine/ Proline residues in the (K/H) S*P motif by CDK was also increased with the expression of RGC-32 (**Figure 4.16-4.17**). Therefore, these data combined with the mitotic entry studies suggest that RGC-32 may activate CDK1 *in vivo* by behaving as an epistatic inhibitor of Wee1 kinase. This means RGC-32 depends on the initial activation of CDK1-Cyclin B complex to further amplify the activity of CDK1 by a feedback loop leading to increased substrate phosphorylation and mitotic entry (**Figure 4.24**).

Cyclin B1/B2 knockdown studies in HeLa cells by another group showed that cyclin A2 could initiate mitosis in the absence of cyclin B1/B2 but the mitotic state in these cells could not be maintained suggesting an important role of cyclin B1/ B2 in maintaining

mitotic state (Gong and Ferrell, 2010). Although, we showed the binding affinity of RGC-32 to be higher for the CDK1-Cyclin B complex, we wanted to investigate whether RGC-32 could activate CDK1 in the absence of cyclin B1/ B2 and initiate mitosis as RGC-32 could also bind to CDK1 alone. However, mitotic entry study in U2OS cdk1as eGFP-RGC32 cells upon depletion of cyclin B was not conclusive as RGC-32 was not able to push more cells into mitosis when treated with control siRNA rendering the observation in cyclin B1/B2 siRNA treated cells as false negative (**Figure 4.19**). Therefore, this experiment needs to be further optimized to retain the effect of RGC-32 on mitotic entry in control cells.

Previous studies by our laboratory have shown RGC-32 is not only upregulated in EBV-infected cells expressing full panel of latent genes (Latency III) but this gene is also differentially regulated in Latency I and Latency III cells with the protein expression being detectable only in Latency III (Schlick *et al.*, 2011). Recently our laboratory showed that this differential regulation is due to translation repression of RGC-32 mediated by binding of Pumilio (an RNA-binding protein) to the RGC-32 3'UTR (Brocard *et al.*, 2018). Pumilio proteins have shown to repress several cell-cycle regulatory proteins including cyclin B1 and RINGO (atypical activator of CDK1 in *Xenopus*) by binding to their 3'UTR (Nakahata *et al.*, 2001, Padmanabhan and Richter, 2006). Knockdown studies using lentiviruses carrying shRNA targeting RGC-32 showed rapid cell death in IB4 (Latency III) cells as compared to GFP control (**Figure 4.20**) and this effect could be relieved upon exogenously overexpressing RGC-32 in cells (**Figure 4.23**). Thus, suggesting a crucial role of RGC-32 in survival of EBV-infected cells (Brocard *et al.*, 2018).

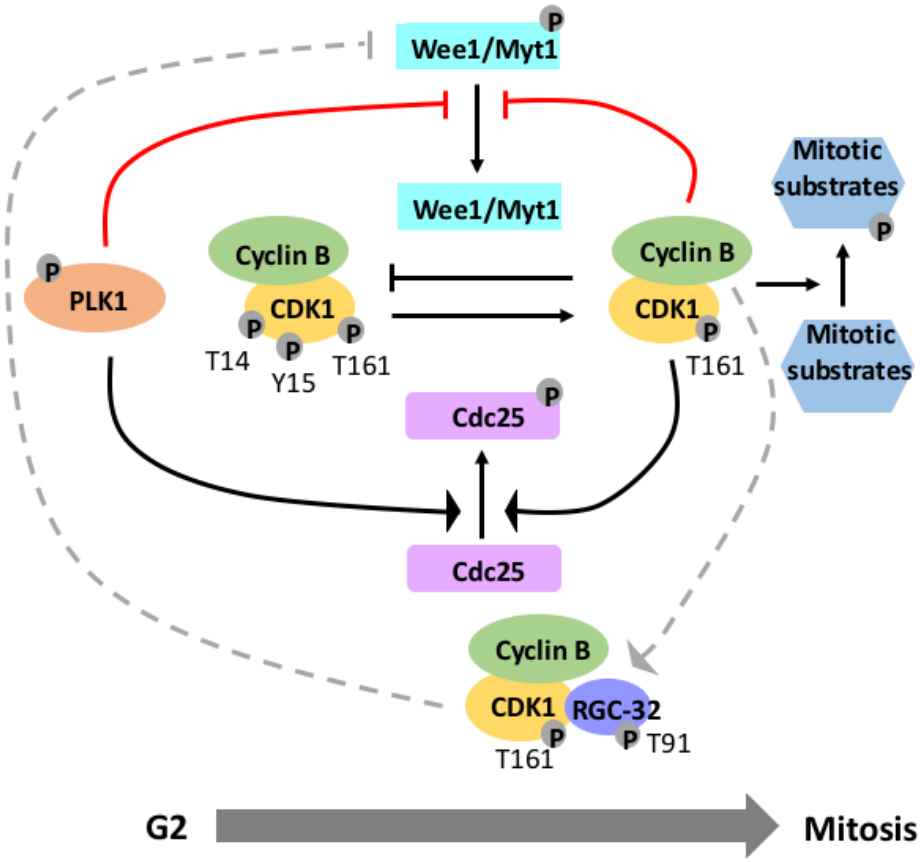

Figure 4.24 Model showing the regulation of G2/M transition by RGC-32.
Schematic representation showing the activation of CDK1 by RGC-32 is mediated via removal of inhibitory Tyr15 phosphorylation thereby acting as a epistatic inhibitor of Wee1 kinase. RGC-32 binds to active CDK1-Cyclin B1 complex and facilitates the activation of its feedback loop.

Overall this chapter provides insights into the role of RGC-32 in CDK1 activation *in vivo* to be mediated by removal of inhibitory Tyr (Y) 15 phosphorylation of CDK1. Moreover, increased CDK substrate phosphorylation in the presence of RGC-32 confirms the function of RGC-32 of as an atypical activator CDK1 thereby driving cells in mitosis. RGC-32 knockdown studies point to the crucial role of RGC-32 in the survival of EBV-infected cells and the possible role it plays in the cell cycle deregulation by EBV.

5 Regulation of the B-cell receptor signalling pathway by EBV transcription factors

5.1 Introduction

Several studies have shown EBV to deregulate the expression of host cell genes from multiple growth and survival pathways and to hijack the cell cycle machinery to efficiently transform and immortalise B cells. In order to understand the mechanism of EBNA2 and EBNA3 regulation of host cell genes, ChIP-sequencing (ChIP-seq) experiments were carried out in our laboratory by a previous PhD student (Michael McClellan) using an EBV-positive Burkitt's Lymphoma (BL) cell line that expresses all EBV latent proteins (Mutu III) (McClellan *et al.*, 2013). EBNA2 ChIP-seq was carried out using an EBNA2 specific monoclonal antibody and EBNA 3 ChIP-seq was carried out using a polyclonal antibody initially raised against EBNA3C, but that cross-reacts with EBNA3A and EBNA3B and thus identifies all EBNA3 binding sites (McClellan *et al.*, 2013). Significant binding sites (p-value $<10^{-7}$) for EBNA2 and EBNA3 were identified using the peak calling algorithm MACS (Zhang *et al.*, 2008). To identify cell genes that may be regulated by EBNA binding, three different criteria were used to link binding sites to potential target genes. The first criterion selected cellular genes that had significant EBNA binding sites with 2 Kb of their transcription start sites (promoter-proximal). It was reasoned that genes with promoter-proximal binding sites had a high chance of being regulated genes. The second criterion identified genes that were the closest to the top most significant EBNA binding sites. The top 300 most significant EBNA3 binding sites were used for this analysis. For EBNA2, where a higher number of highly significant binding sites had identical p-values, binding sites with a p-value of 10^{-310} or lower (526 sites) were used for analysis. It was reasoned that the most significant

(often the largest) binding sites were more likely to represent functional gene regulatory elements. Genes closest to these top significant binding sites in either direction were manually identified by Michael McClellan assisted by three undergraduate project students. The third criterion was less stringent and simply identified target genes that were closest to any significant binding site (p-value $<10^{-7}$). Pathway analysis on these gene lists was carried out by Prof. Michelle West. Analysis of promoter-proximal gene lists for EBNA2 and EBNA3 using the bioinformatic tool (DAVID) identified the B-cell receptor (BCR) signalling pathway as the only significantly enriched pathway using a widely-used cut off of Bonferonni<0.01 (**Table 5.1**). Using the lists of genes closest to a top significant EBNA2 binding site, the BCR signalling pathway was again the only significantly enriched pathway (Bonferonni<0.01) (**Table 5.1**). For genes closest to top significant EBNA3 binding sites no pathways were significantly enriched. Some genes in these lists overlap as top significant binding sites may also be promoter-proximal peaks. EBNA2 and EBNA3 proteins are also known to compete for binding to the same human genome binding sites and to target the same genes through distinct binding sites as a result of which some target genes may be shared (Harth-Hertle *et al.*, 2013, McClellan *et al.*, 2013, Wang *et al.*, 2015). In total these first two criteria identified 25 unique BCR signalling pathway genes that could be targeted by EBNA2 or EBNA3 proteins (*IFITM1*, *NFKBIA*, *CD72*, *RASGRP3*, *CD22*, *PIK3AP1*, *NFATC4*, *INPP5D*, *PIK3R1*, *NFATC1*, *PIK3R2*, *SYK*, *PTPN6*, *CR2*, *VAV3*, *LYN*, *PIK3CD*, *VAV2*, *PRKCB*, *MAPK1*, *CD19*, *CD81*, *PLCG2*, *CD79B*, *CD79A*). **Figure 5.1** shows their position in the BCR signalling pathway.

Gene list	Term	P value	Genes	Bonferroni	Benjamini	FDR
EBNA2 Promoter-proximal	hsa04662: B cell receptor signaling pathway	1.39E-05	PTPN6, CD19, RASGRP3, NFKBIA, CD22, CD79B, NFATC4, CD79A, CD72, PIK3R1, SYK	0.001759	0.001759	0.016079
EBNA3 Promoter-proximal	hsa04662: B cell receptor signaling pathway	1.87E-06	PTPN6, VAV3, NFKBIA, CD72, PRKCB, MAPK1, CD19, RASGRP3, CD22, NFATC4, CD79B, CD79A, PIK3R1, SYK	2.82E-04	2.82E-04	0.002233
EBNA2 Top significant	hsa04662: B cell receptor signaling pathway	2.61E-09	PTPN6, CR2, IFITM1, LYN, PIK3CD, VAV2, CD19, CD81, PLCG2, CD22, CD79B, PIK3AP1, NFATC4, CD79A, INPP5D, NFATC1, PIK3R2	3.50E-07	3.50E-07	3.06E-06
EBNA2 closest	hsa04662: B cell receptor signaling pathway	1.95E-12	HRAS, NFKB1, BTK, FOS, PIK3CA, PIK3AP1, SYK, AKT2, PIK3CG, BCL10, LYN, PIK3CB, RELA, LOC646626, PIK3CD, PRKCB, CARD11, MAPK1, JUN, CD81, IFITM1, NFKBIE, GRB2, PPP3R1, NFKBIA, CD72, LOC407835, KRAS, RASGRP3, DAPP1, RAC2, SOS1, RAC1, PPP3CB, NFAT5, PPP3CC, CD22, NFATC4, PIK3R5, PPP3CA, INPP5D, PIK3R3, NFATC2, NFATC3, PIK3R1, NFATC1, PIK3R2, BLNK, PTPN6, VAV3, CR2, MAP2K1, MAP2K2, MALT1, VAV2, VAV1, CD19, GSK3B, PLCG2, CD79B, CD79A, IKBKB	3.73E-10	1.87E-10	2.42E-09
EBNA3 closest	hsa04662: B cell receptor signaling pathway	3.96E-10	NFKBIA, CD72, LOC407835, FOS, KRAS, RASGRP3, DAPP1, RAC2, SOS1, PPP3CC, CD22, NFATC4, PIK3AP1, PPP3CA, INPP5D, PIK3R3, NFATC3, AKT3, PIK3R1, NFATC1, BLNK, SYK, PIK3CG, PTPN6, BCL10, VAV3, CR2, LYN, PIK3CB, MAP2K2, LOC646626, VAV2, PRKCB, CARD11, MAPK1, CD19, CD81, PLCG2, CD79B, CD79A, IKBKB	7.40E-08	3.70E-08	4.90E-07

Table 5.1 DAVID analysis of ChIP-seq from Mutu III cells showing enrichment of the BCR signalling pathway for genes that are within 2 Kb of EBNA2 and EBNA3 binding sites (promoter-proximal), closest to top most significant EBNA2 binding site (p-value $\leq 10^{-310}$) or genes that are closest to any significant binding site of EBNA2 and EBNA3 (p-value $<10^{-7}$) irrespective of the distance (McClellan *et al.*, 2013) .

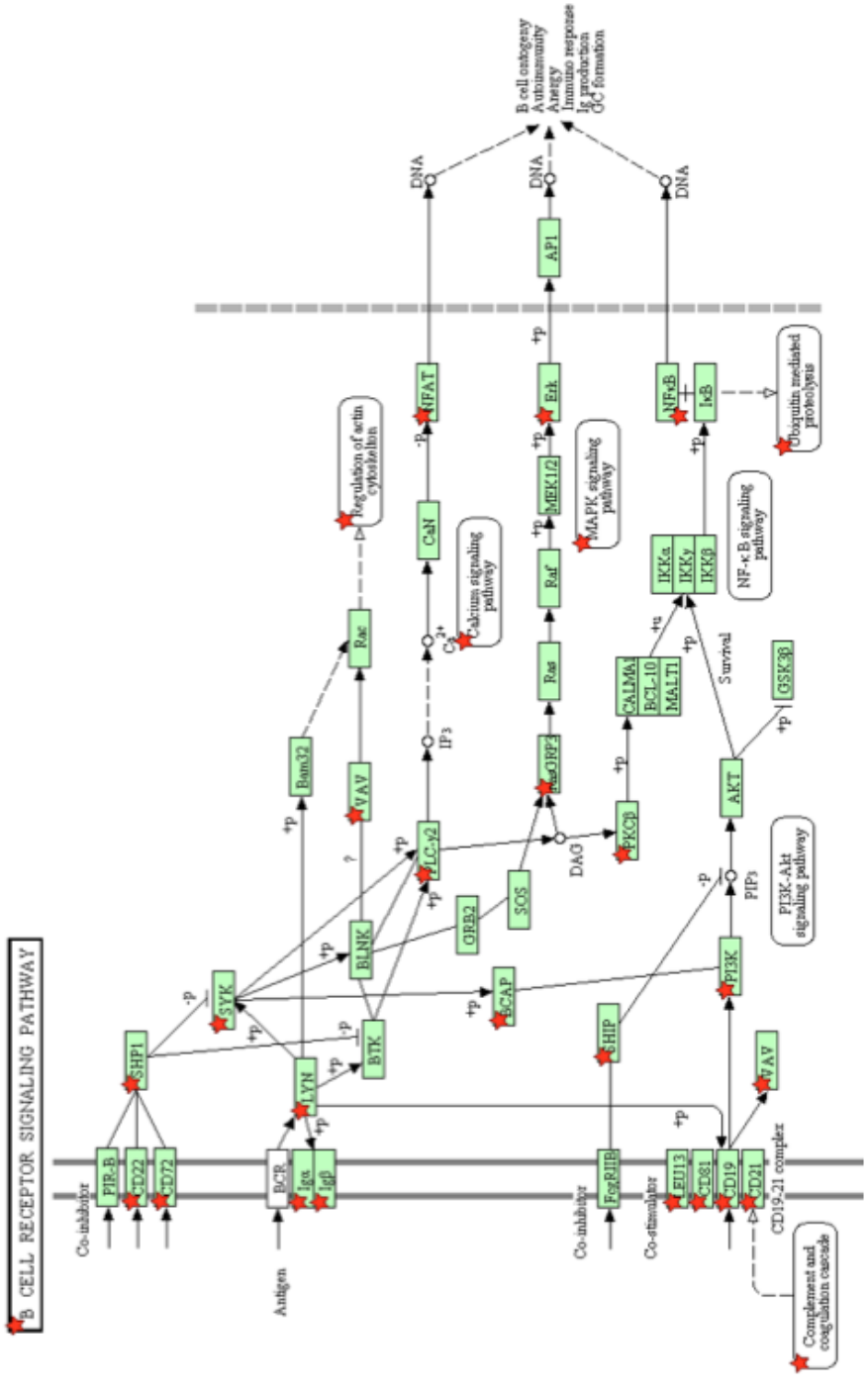

Figure 5.1 Regulation of B-cell receptor signalling pathway.
KEGG analysis showing the genes (with red stars) from BCR signalling pathway located within 2kb of an EBNA2 or EBNA3A, 3B and 3C binding site or genes which are closest to top most significant (p-value $\leq 10^{-310}$) EBNA2 binding site. The B-cell receptor consists of two heavy chains (IgH), two light chains (IgL) and two heterodimers Igα (CD79A) and Igβ (CD79B). Binding of antigen to BCR leads to the activation of protein tyrosine kinases Lyn, Syk and BTK which in turn initiate the downstream signalling pathways such as calcium signalling, MAPK, PI3K, Akt, NF-κB and RAS.

Pathway analysis of less stringently identified genes that were closest to any significant EBNA binding site also identified the BCR signalling pathway as a significantly enriched pathway for both EBNA2 and EBNA3 gene lists (**Table 5.1**). For EBNA2, BCR signalling was the second most enriched pathway (**Table 5.1**), with the first being T-cell receptor signalling (it is worth mentioning that many genes in these two pathways are the same). For EBNA3s, BCR signalling was also the second most enriched pathway (**Table 5.1**), with the first being JAK-STAT signalling. Again, as expected a number of these genes were identified in the analysis of promoter-proximal or top significant closest gene lists (**Table 5.1**). Taken together, all three criteria identified 63 unique genes in the BCR signalling pathway that could represent target genes of EBNA2 or EBNA3 proteins (**Table 5.2 and 5.3**).

Gene expression analysis from published microarray studies from our own and other laboratories was examined by Dr Michael McClellan for evidence of regulation of these potential BCR pathway target genes by EBNA2 or EBNA3 proteins (Chen *et al.*, 2005, Maier *et al.*, 2006, Spender *et al.*, 2006, Zhao *et al.*, 2006, Lucchesi *et al.*, 2008, Hertle *et al.*, 2009, White *et al.*, 2010, Zhao *et al.*, 2011b, McClellan *et al.*, 2012) (**Table 5.2**). Importantly he found that a number of these BCR pathway genes had been previously identified as regulated genes by gene expression arrays. However, for the majority of the genes, this regulation had not been confirmed in follow up analysis in other cell lines. In addition, he found that many of the BCR pathway potential target genes identified by our criteria had not previously been identified as regulated genes (**Table 5.3**).

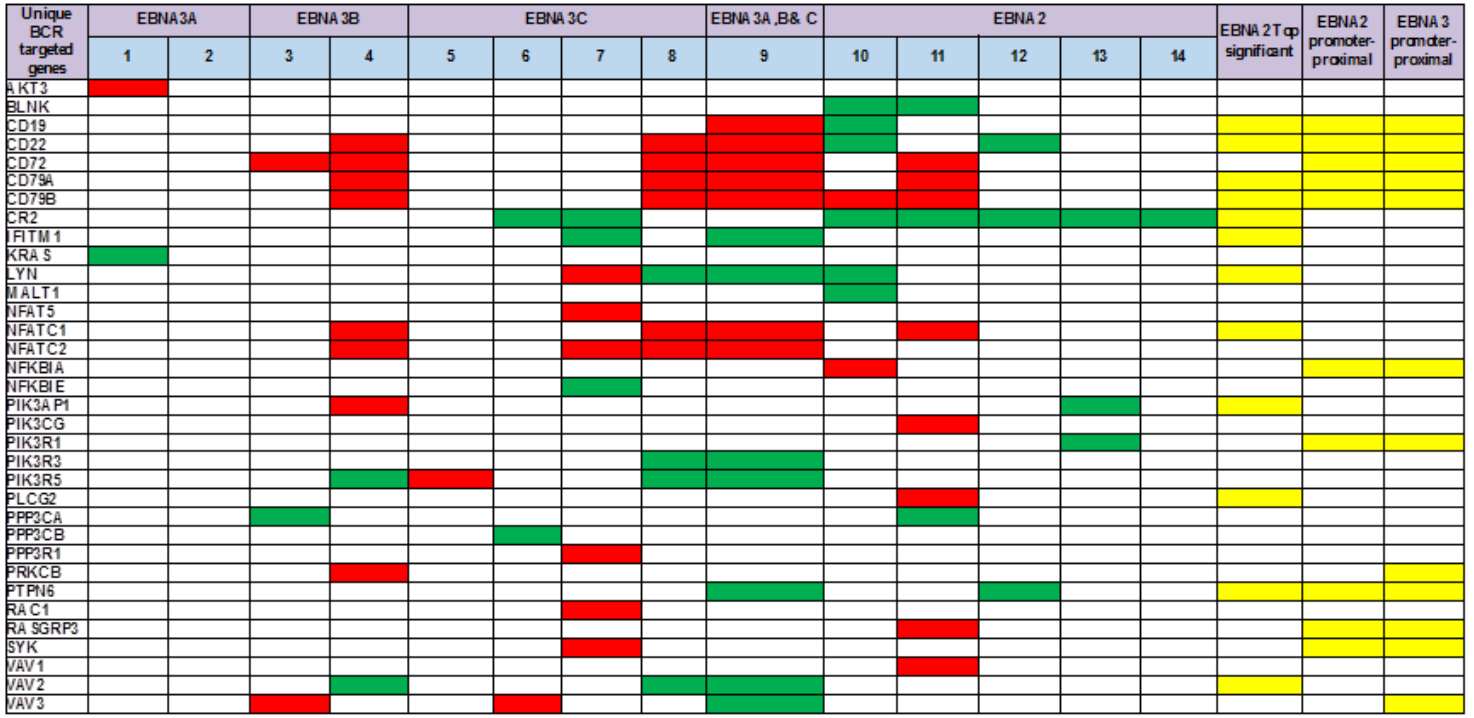

Table 5.2 showing 34 genes from the BCR signalling pathway that have been previously reported to be regulated by EBNA3s and EBNA2 in cell lines from different cell backgrounds (see below for description). The table also shows whether these genes were bound by EBNA2 or EBNA3 within 2 Kb (promoter-proximal) and genes that were closest to a top significant EBNA2 peak (p-value $\leq 10^{-310}$). Uncoloured cells indicate genes that are closest to any EBNA2 and EBNA3 binding peak (MACS $<10^{-7}$) irrespective of distance. The binding data was generated from the ChIP-seq data from Mutu III cells by the West laboratory. Green represents upregulation and red represents downregulation of the target genes by EBNA3s and EBNA2. **References : (1)** EBNA3A KO LCL **(Hertle *et al.*, 2009); (2)** EBNA3A KO BL31 (**White *et al.*, 2010); (3)** EBNA3B KO LCL (**White *et al.*, 2010); (4)** EBNA3B KO BL31 (**White *et al.*, 2010); (5)** EBNA3B-/3C_{low} LCL (**Chen *et al.*, 2006);** (6) EBNA3C BJAB (**McClellan *et al.*, 2012); (7)** EBNA 3CHT LCL (**Zhao *et al.*, 2011b); (8)** EBNA3C KO BL31 (**White *et al.*, 2010); (9)** EBNA3's KO BL31 (**White *et al.*, 2010); (10)** ER/EBNA2 BL41 (**Maier *et al.*, 2006**); (11) ER/EBNA2 BJAB (**Maier *et al.*, 2006);** (12) EBNA2 E2HTF LCL (**Zhao *et al.*, 2006); (13)** EBNA2 EREB 2.5 (**Spender *et al.*, 2006); (14)** EBNA2 EREB 2.5 (**Spender *et al.*, 2002).**

Unique BCR targeted genes	EBNA2 Top significant	EBNA2 promoter-proximal	EBNA3 promoter-proximal
BCL10			
BTK			
CARD11			
CD81			
DAPP1			
FOS			
GRB2			
GSK3B			
HRAS			
IKBKB			
INPP5D			
JUN			
MAPKK2 pseudogene			
LOC646626 (uncharacterised RNA)			
MAP2K1			
MAP2K2			
MAPK1			
NFATC3			
NFATC4			
NFKB1			
PIK3CA			
PIK3CB			
PIK3CD			
PIK3R2			
PPP3CC			
RAC2			
RELA			
SOS1			

Table 5.3 showing genes from the BCR signalling pathway included in TaqMan array cards that have not been previously reported to be regulated by EBNA3s and EBNA2. The table also show whether these genes were bound by EBNA2 or EBNA3 in close proximity to the gene promoter (within 2 Kb) or if they closest to a top significant EBNA2 (p-value $\leq 10^{-310}$) binding site. Uncoloured cells indicate genes that are closest to any EBNA2 and EBNA3 binding peak (MACS $<10^{-7}$) irrespective of distance. The binding data was generated from the ChIP-seq experiment in Mutu III cells by the West laboratory (McClellan *et al.*, 2013).

In this chapter, I set out to determine whether the BCR pathway genes that were identified by their association with EBNA2 or EBNA3 binding sites show evidence of regulation at the RNA and protein level and whether this has an impact on BCR signalling.

5.2 High throughput gene expression analysis for EBNA2 and EBNA3 regulated genes.

TaqMan array cards were previously designed in our laboratory by Dr Michael McClellan and loaded with pre-made or custom TaqMan assays for 55 of the 63 BCR pathway genes plus four control genes (*GAPDH*, *RPLP0*, *GUSB*, and *HPRT1*) for normalisation of target gene expression. Given the limited number of genes that can be loaded into the card, eight genes were not included on the array cards. These were LOC407835 (a MAPKK2 pseudogene), and LOC646626 (an uncharacterised non-coding RNA). Additionally, *NFKBIE*, *HRAS*, *MAP2K1*, *MAP2K2*, *PIK3CB* and *PPP3CC* were also excluded due to the presence of only very small EBNA2 or EBNA3 binding sites.

To examine the regulation of BCR pathway genes by EBNA2 and individual EBNA3 proteins, we used cell lines that either expressed these proteins conditionally or cell lines infected with viruses carrying a deletion of individual EBNA genes. To study gene regulation by EBNA2, we used an EBV-infected LCL (EREB 2.5) that was generated by the Kempkes group (Kempkes *et al.*, 1995). This cell line has the endogenous EBNA2 replaced with conditionally active estrogen receptor-EBNA2 (ER-EBNA2) fusion protein. Expression of active EBNA2 protein was achieved by culturing cells in media supplemented with β-estradiol which activates the estrogen receptor (Safe, 2001). In order to verify the conditional activation of EBNA2 in this cell line, the expression of the well-characterised EBNA2 target genes, *MYC* and *CR2* (*CD21)* was studied (Wang *et al.*, 1990, Kaiser *et al.*, 1999). QPCR analysis showed that as expected *MYC* and *CR2*

expression was upregulated after re-addition of β-estradiol to the cells cultured for 4 days in the absence of β-estradiol (**Figure 5.2**). A higher level of gene induction by EBNA2 was observed after 17 hrs, therefore, this time-point was used in the TaqMan array card assay. A heatmap was generated using unsupervised hierarchical clustering with Pearson correlation coefficient to visualise the data obtained using two biological replicates for each condition (**Figure 5.3**). Interestingly, even though best characterised as an activator, EBNA2 repressed majority of the target genes analysed (~68%). Only a few genes showed induced expression (~7%) while the remaining (25%) genes showed no regulation or inconsistent results were observed between replicates. **Table 5.4** shows the list of genes that we confirmed as target genes regulated by EBNA2. Our TaqMan array card data confirmed the activation of *CR2* and *PIK3R1* and repression of *CD72*, *CD79A*, *CD79B*, *NFATC1*, *VAV1*, *PLCG2*, *PIK3CG* and *RASGRP3* by EBNA2 independent of the cell background. Whereas, repression of *PTPN6*, *CD22*, *CD19*, *LYN*, *BLNK*, *PPP3CA* and activation of *NFKBIA* by EBNA2 in our TaqMan array card data contradicted with the previously reported regulation either in a different cell line or a different cell background (**Table 5.2 and 5.4**). Our data also identified *NFATC3*, *NFATC4*, *DAPP1*, *SOS1*, *IFITM1*, *VAV2*, *PIK3R3*, *PIK3R5*, *RAC2*, *NFAT5* and *FOS* as new target genes of EBNA2.

For regulation by EBNA3 proteins, the first set of cell lines used were EBV-negative Burkitt's lymphoma (BL31) infected with either wild-type recombinant EBV (wtBAC), EBNA3A knock-out EBV (BL31 3AKO), EBNA3B knock-out EBV (BL31 3BKO),

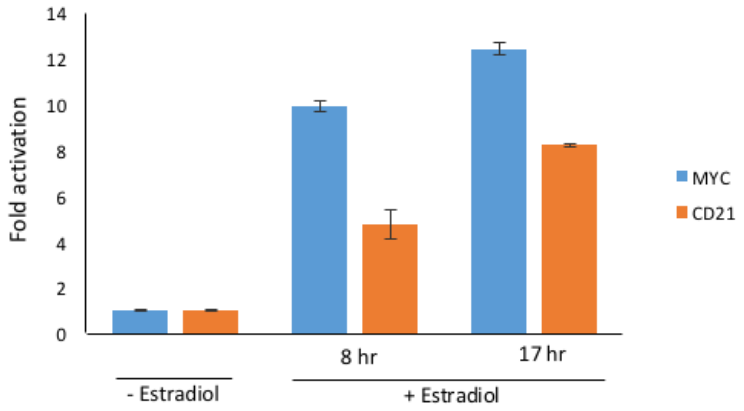

Figure 5.2 *MYC* and *CD21* mRNA induction in EREB2.5 cells.
QPCR analysis of *MYC* and *CD21* mRNA expression in EREB2.5 cell that were cultured in the absence of β-estradiol (-ER, -EBNA2) for 4 days and then for a further 8 hr and 17 hr with β-estradiol (+ER, +EBNA2). Signals were normalised to *GAPDH* signals. Results show the mean mRNA levels relative to EREB2.5 (-ER) ± standard deviation of qPCR duplicates.

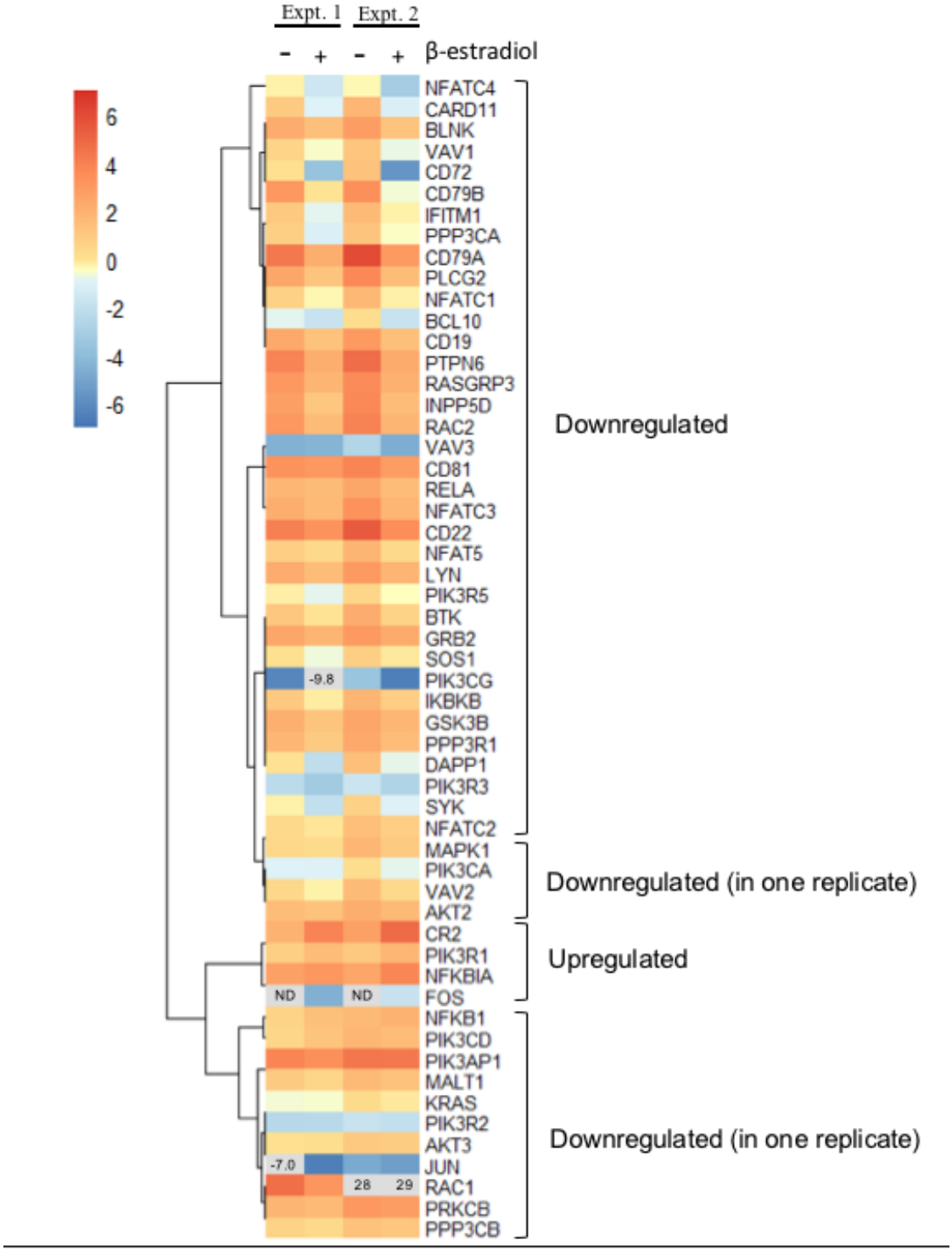
Expt. 1
Expt. 2
- + - +
β-estradiol
6
4
2
0
-2
-4
-6
NFATC4
CARD11
BLNK
VAV1
CD72
CD79B
IFITM1
PPP3CA
CD79A
PLCG2
NFATC1
BCL10
CD19
PTPN6
RASGRP3
INPP5D
RAC2
VAV3
CD81
RELA
NFATC3
CD22
NFAT5
LYN
PIK3R5
BTK
GRB2
SOS1
-9.8
PIK3CG
IKBKB
GSK3B
PPP3R1
DAPP1
PIK3R3
SYK
NFATC2
MAPK1
PIK3CA
VAV2
AKT2
CR2
PIK3R1
NFKBIA
ND
ND
FOS
NFKB1
PIK3CD
PIK3AP1
MALT1
KRAS
PIK3R2
AKT3
-7.0
JUN
28
29
RAC1
PRKCB
PPP3CB
Downregulated
Downregulated (in one replicate)
Upregulated
Downregulated (in one replicate)

Figure 5.3 Regulation of genes from BCR signalling by EBNA2 in a conditional LCL.
Heatmap showing gene expression normalised to the housekeeping gene, *GUSB*, in the lymphoblastoid cell line EREB 2.5 expressing conditionally active EBNA2. For inactivation and reactivation of EBNA2, cells were maintained in the absence of β-estradiol for 4 days and 1 μM β-estradiol was re-added for 17 hr prior to cell harvest. Normalised gene expression (*Δ*Ct) was obtained after deducting the Ct value of *GUSB* for each cell line from the Ct value of the gene in question. These values for each gene are shown as pseudocolour with blue being downregulated and orange being upregulated gene expression as shown by the scale. Hierarchical clustering was performed using Pearson correlation as a measure of similarity between genes with complete linkage as the clustering allocation. Genes are grouped as being upregulated or downregulated and the genes that are not grouped, are either not regulated or the replicates show opposite regulation thereby making the regulation inconclusive. Each column represents a cell line, and each row represents one gene. The cut off value for *Δ*Ct for upregulated and downregulated genes is 7 and -7 respectively. Genes with *Δ*Ct value higher than the cut off are shown in grey with their respective *Δ*Ct value whereas the genes whose expression was not detectable are shown in grey with ND (not determined). Heatmap was generated using Rstudio.

Genes	Molecular or Biological function	Regulated by EBNA2
Lymphoblastoid cell lines (LCLs)		
NFATC1*	Transcription regulation	
NFATC3		
NFATC4*		
BCL10		
FOS*		
BTK SYK* IKBKB*	Protein kinase	
PIK3CG* LYN*		
CD21 (CR2)*	Cell differentiation markers	
CD79A* CD79B* CD19* CD72* CD22*		
CARD11*		
INPP5D*	Hydrolase	
PTPN6*	Cell adhesion	
IFITM1*	Receptor	
BLNK	Adaptor	
SOS1* NFAT5	DNA binding	
NFKBIA*	Enzyme binding	
RAC2*	GTPase activity	
RASGRP3		
VAV2*	Guanine-nucleotide releasing factor	
VAV1		
PIK3R1*	Tumour suppressor	
PIK3R3* PIK3R5*		
PPP3CA*	Phosphatase	
DAPP1*		
PLCG2*	Transmembrane signalling	

Table 5.4 confirming the TaqMan array card data for cellular target genes by EBNA2 in a conditional LCL where green represent upregulation and red represent downregulation respectively. Newly identified target genes are highlighted in grey. Genes that were also regulated by EBNA3s (refer Table 5.5) are shown by (*).

EBNA3C knock-out EBV (BL31 3CKO), EBNA3A, 3B and 3C knock-out (BL31 E3KO) which will be referred as EBNA3KO from here on, or by the respective revertant virus to restore the deleted gene (BL31 3A rev2, BL31 3B rev2.2, BL31 3C rev2, BL31 E3 rev). These cell lines were generated by the Allday group to study gene regulation by EBNA3 proteins (Anderton *et al.*, 2007). In the initial experiments, we used western blot analysis for EBNA3A, EBNA3B and EBNA3C to check that the cell lines were carrying the expected viruses and that KO lines showed no expression of the specific gene in question. We confirmed the presence of all three EBNA3 proteins in the cell line infected with wild-type EBV (wtBAC) and in the BL31 E3 revertant (**Figure 5.4**). Expression of EBNA3A, EBNA3B and EBNA3C was absent as expected in the respective knock-out cell lines. We observed no expression of EBNA3A, EBNA3B and EBNA3C proteins in the BL31 E3KO cell line confirming the deletion of the internal regions for EBNA3A, EBNA3B and exon 2 for EBNA3C. The regulation of BCR genes by EBNA3 was investigated by TaqMan array cards. A heatmap was generated using unsupervised hierarchical clustering with Pearson correlation coefficient to visualise data obtained using the following cell lines: 1-two clones of wtBAC and individual EBNA3 gene deletion; 2- one clone of EBNA3 KO; 3- individual revertant compared to EBV-negative BL31 cell line (**Figure 5.5**). Consistent with the best characterised function as a repressor, EBNA3A, EBNA3B and EBNA3C proteins repressed ~50% of the targets analysed. Most of these genes were repressed by cooperation among all three EBNA3 proteins which is a widely reported regulation mechanism for the EBNA3 proteins seen in the majority of the genes previously reported. Only a few genes showed induced expression (~4%) while the remaining (~46%) genes showed no regulation or inconsistent results between clones.

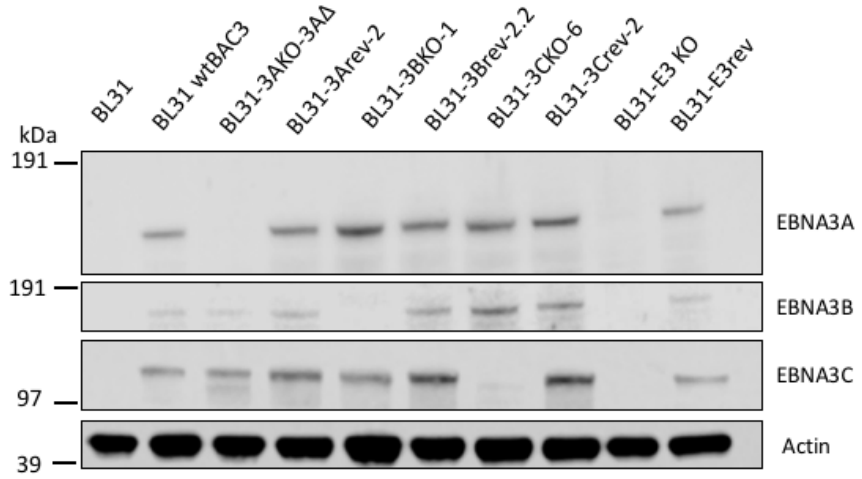

Figure 5.4 Expression of EBV nuclear antigen 3 (EBNA3) proteins in BL31 cell lines. Western blot analysis for expression of EBV latent genes (EBNA3A, EBNA3B and EBNA3C) in EBV-negative BL cell line BL31 and in BL31 cells infected with either wild-type recombinant EBV (wt BAC3), EBNA3A knock-out EBV (BL31 3AKO-3AΔ), EBNA3B knock-out EBV (BL31-3BKO-1), EBNA3C knock-out EBV (BL31-3CKO-6), EBNA3 knock-out EBV (BL31-E3KO) or with their respective revertant viruses to restore gene expression (BL31-3A rev-2, BL31-3B rev-2.2, BL31-3B rev-2.2 and BL31-3B rev-2.2). Actin was used as a loading control.

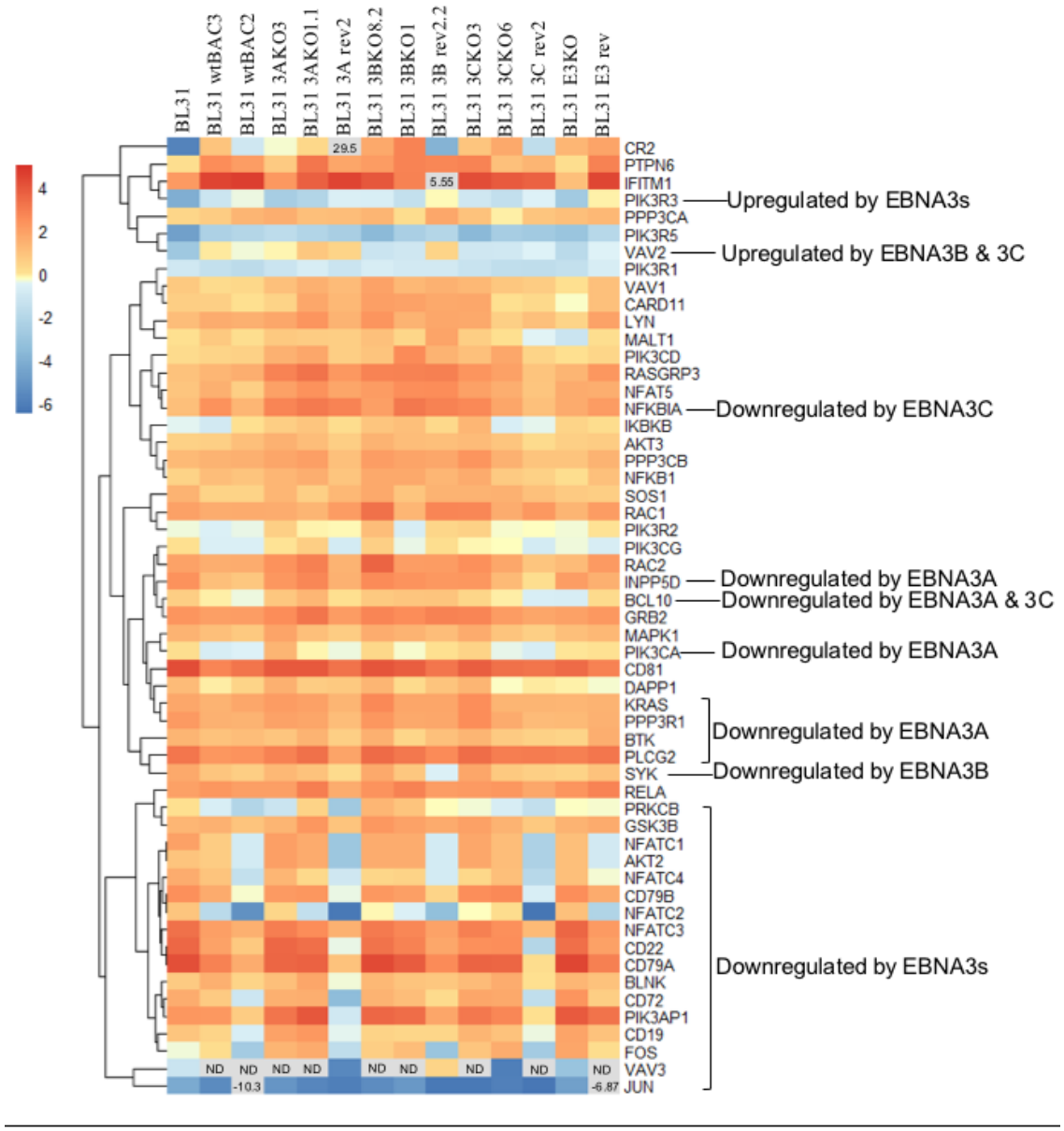
BL31
BL31 wtBAC3
BL31 wtBAC2
BL31 3AKO3
BL31 3AKO1.1
BL31 3A rev2
BL31 3BKO8.2
BL31 3BKO1
BL31 3B rev2.2
BL31 3CKO3
BL31 3CKO6
BL31 3C rev2
BL31 E3KO
BL31 E3 rev
29.5
5.55
ND
-10.3
-6.87
4
2
0
-2
-4
-6
CR2
PTPN6
IFITM1
PIK3R3
PPP3CA
PIK3R5
VAV2
PIK3R1
VAV1
CARD11
LYN
MALT1
PIK3CD
RASGRP3
NFAT5
NFKBIA
IKBKB
AKT3
PPP3CB
NFKB1
SOS1
RAC1
PIK3R2
PIK3CG
RAC2
INPP5D
BCL10
GRB2
MAPK1
PIK3CA
CD81
DAPP1
KRAS
PPP3R1
BTK
PLCG2
SYK
RELA
PRKCB
GSK3B
NFATC1
AKT2
NFATC4
CD79B
NFATC2
NFATC3
CD22
CD79A
BLNK
CD72
PIK3AP1
CD19
FOS
VAV3
JUN
Upregulated by EBNA3s
Upregulated by EBNA3B & 3C
Downregulated by EBNA3C
Downregulated by EBNA3A
Downregulated by EBNA3A & 3C
Downregulated by EBNA3A
Downregulated by EBNA3A
Downregulated by EBNA3B
Downregulated by EBNA3s

Figure 5.5 Regulation of genes from BCR signalling by EBNA3s in BL31s.
Heatmap showing gene expression normalised to the housekeeping gene, *GUSB*, in EBV-ve BL cells (BL31) cells infected with either wild-type recombinant EBV (wt BAC), EBNA3A knock-out EBV (BL31 3AKO), EBNA3B knock-out EBV (BL31 3BKO), EBNA3C knock-out EBV (BL31 3CKO), EBNA3 knock-out EBV (BL31 EBNA3KO) or their respective revertant virus (BL31 3A rev2, BL31 3Brve2.2, BL31 3Crev2, BL31 EBNA3 rev). Normalised gene expression (*Δ*Ct) is obtained after deducting the Ct value of *GUSB* for each cell line from the Ct value of the genes in question. These values for each gene are shown as pseudocolour with blue being downregulated and orange being upregulated gene expression as shown by the scale. Hierarchical clustering was performed using Pearson correlation as a measure of similarity between genes with complete linkage as the clustering allocation. Genes are grouped as being upregulated or downregulated and the genes that are not grouped, are either not regulated or the replicates show opposite regulation thereby making the regulation inconclusive. Each column represents a cell line, and each row represents one gene. The cut off value for *Δ*Ct for upregulated and downregulated genes is 5 and -6.5 respectively. Genes with *Δ*Ct value higher than the cut off are shown in grey with their respective *Δ*Ct value whereas the genes whose expression was not detectable are shown in grey with ND (not determined). Heatmap was generated using Rstudio.

Another set of cell lines from lymphoblastoid cell background was also used to study the regulation of BCR genes. This was important because several pathways are known to be distorted in BL during the outgrowth which may affect the regulation of the genes in question. For example, *LYN* has been reported to be differentially regulated by EBNA3C in BL and LCLs (White *et al.*, 2010, Zhao *et al.*, 2011a). For gene regulation by EBNA3A, LCL cell lines generated by the Kempkes laboratory by infecting primary B cells (different donors, D1 & D3) with either wild-type EBV (LCL wtBAC) or with a recombinant virus lacking the entire coding region of EBNA3A (LCL3A mtB) were used (Hertle *et al.*, 2009). The EBNA3B knock-out cell lines were generated by the Allday laboratory by infecting EBV-negative peripheral B cells from a donor (donor 2, D2) with either wild-type EBV (LCL wtBAC), EBNA3B knock-out (LCL 3BKO) or EBNA3B revertant virus (LCL 3B rev) (White *et al.*, 2010). Since EBNA3C is essential for immortalisation and outgrowth of LCLs (reviewed in (Young *et al.*, 2016)), a stable cell line with conditionally active EBNA3C (LCL 3CHT) was established by the Allday laboratory (Skalska *et al.*, 2013). This cell line was generated by infecting peripheral B cells with a recombinant virus containing EBNA3C fused to an estrogen receptor at the C-terminus. Expression of EBNA3C was achieved by culturing cells in media supplemented with 4-hydroxytamoxifen (HT) which interacts with and activates the estrogen receptor (Sasson and Notides, 1988). In order to confirm the cell lines have EBNA3A and EBNA3B deletion, qPCR analysis using RNA from LCL EBNA3A mtB and LCL 3BKO cell lines was carried out. There was no EBNA3A and EBNA3B mRNA expression in LCL EBNA3A mtB and LCL 3BKO cell line respectively (**Figure 5.6 A&B**).

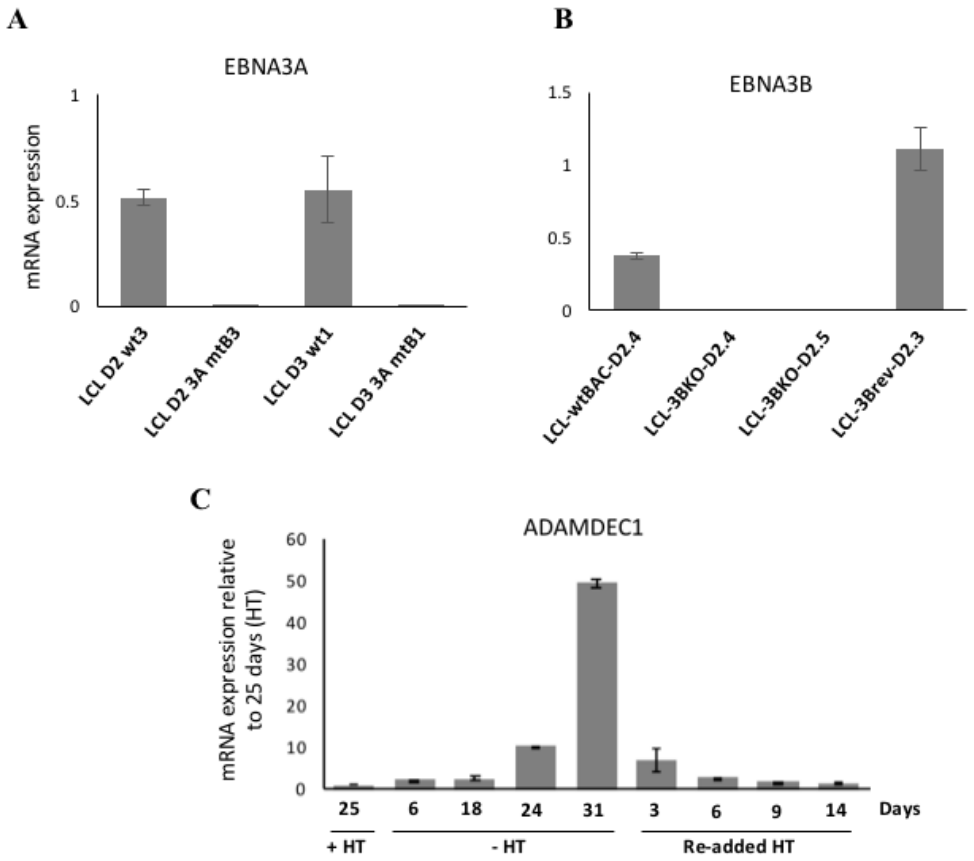

Figure 5.6 Investigating *EBNA3A*, *EBNA3B* and *ADAMDEC1* mRNA expression in LCLs. (A) QPCR analysis of *EBNA3A* mRNA expression in LCLs infected with either wild-type recombinant EBV (LCL D2 WT3, LCL D3 wt1) or EBNA3A mutant EBV (LCLD2 3AmtB3, LCLD3 3AmtB1). (B) QPCR analysis of *EBNA3B* mRNA expression in LCLs infected with either wild-type recombinant EBV (LCL-wtBAC-D2.4), EBNA3B knock-out EBV (LCL-3BKO-D2.4, LCL-3BKO-D2.5) or EBNA3B revertant virus (LCL-3Brev-D2.3). (C) QPCR analysis of *ADAMDEC1* mRNA expression. LCL3CHT were grown in the presence of HT (4-hydroxytamoxifen) for 25 days (EBNA3C active) and the HT was washed off and cells were cultured in the absence of HT for 21 days (EBNA3C inactive). Cells were then cultured either with HT (re-instate EBNA3C) for 14 days or were maintained without HT for a further 10. Signals for *EBNA3A* mRNA and *EBNA3B* mRNA were normalized to *β2 microglobin* mRNA levels and *ADAMDEC1* mRNA signals were normalized to *GAPDH* mRNA levels. Results show the mean ± standard deviation of qPCR duplicates.

For LCL 3CHT cell line, samples for RNA analysis were harvested at different time points from cells cultured with HT, without HT and after re-adding HT. To verify the activation of EBNA3C in LCL 3CHT cell line, expression of a known EBNA3C repressed target gene *ADAMDEC1* was studied (McClellan *et al.*, 2012, McClellan *et al.*, 2013, Kalchschmidt *et al.*, 2016a). QPCR analysis confirmed that *ADAMDEC1* expression increased in LCL 3CHT cells cultured in media without HT thereby confirming the loss of EBNA3C in this cell line on HT withdrawal (**Figure 5.6C**). TaqMan array card analysis in lymphoblastoid cell background showed EBNA3A to repress (~24%) less number of target genes and activate more (~25%) target genes compared to BL (**Figure 5.7**). Similarly, EBNA3B and EBNA3C showed less number of target genes regulated as compared to BL by activating (~4%) and (~17%) and repressing (~16%) and (~30%) target genes respectively (**Figure 5.8 and 5.9**). Majority of the target genes (~51%, EBNA3A; ~80%, EBNA3B; 53%, EBNA3C) showed no regulation by EBNA3 in LCLs or inconsistent regulation was observed between different clones. As the number of activated genes by EBNA3A, EBNA3B and EBNA3C was higher in LCLs compared to BL, it suggests a difference in the regulation of BCR signalling genes between these two cell backgrounds. **Table 5.5** shows the list of target genes confirmed by TaqMan array card analysis. There was co-regulation observed for most of the genes by EBNA3 proteins in the lymphoblastoid cell background similar to BL.

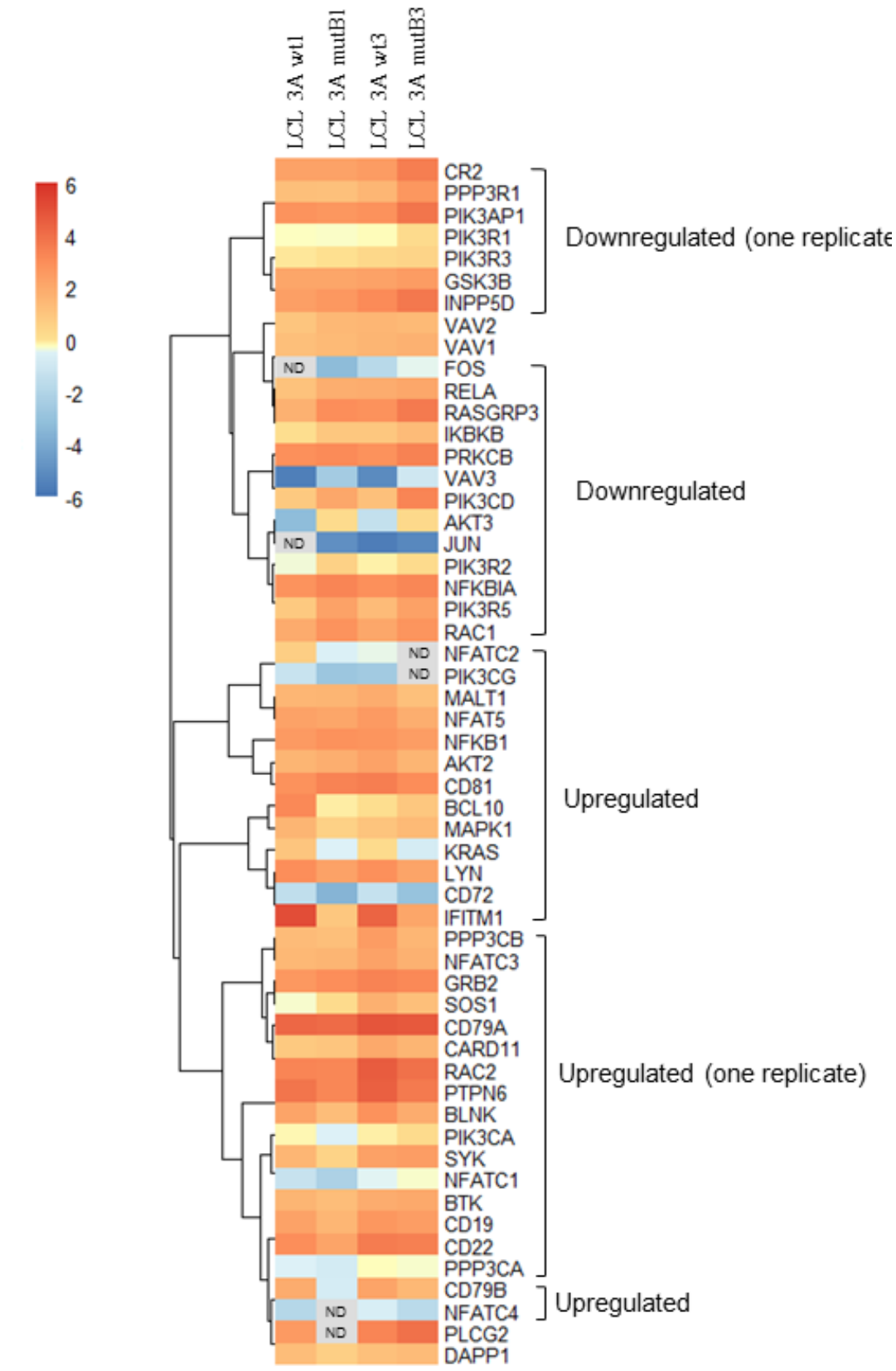
LCL 3A wt1
LCL 3A mutB1
LCL 3A wt3
LCL 3A mutB3
6
4
2
0
-2
-4
-6
CR2
PPP3R1
PIK3AP1
PIK3R1
PIK3R3
GSK3B
INPP5D
VAV2
VAV1
FOS
RELA
RASGRP3
IKBKB
PRKCB
VAV3
PIK3CD
AKT3
JUN
PIK3R2
NFKBIA
PIK3R5
RAC1
NFATC2
PIK3CG
MALT1
NFAT5
NFKB1
AKT2
CD81
BCL10
MAPK1
KRAS
LYN
CD72
IFITM1
PPP3CB
NFATC3
GRB2
SOS1
CD79A
CARD11
RAC2
PTPN6
BLNK
PIK3CA
SYK
NFATC1
BTK
CD19
CD22
PPP3CA
CD79B
NFATC4
PLCG2
DAPP1
ND
Downregulated (one replicate
Downregulated
Upregulated
Upregulated (one replicate)
Upregulated

Figure 5.7 Regulation of genes from BCR signalling by EBNA3A in LCLs.
Heatmap showing the target gene expression normalised to the housekeeping gene, *GUSB*. Regulation by EBNA3A was studied in LCLs established by infecting primary B cells from donor 1 & 3 with either wild-type EBV (wt BAC) or mutant virus lacking the coding sequence for EBNA3A (LCL 3A mutB). Normalised gene expression (*Δ*Ct) is obtained after deducting the Ct value of *GUSB* for each cell line from Ct value of genes in question. These values for each gene are shown as pseudocolour with blue being downregulated and orange being upregulated gene expression as shown by the scale. Hierarchical clustering was performed using Pearson correlation as a measure of similarity between genes with complete linkage as clustering allocation. Genes are grouped as being upregulated or downregulated and the genes that are not grouped, are either not regulated or the replicates show opposite regulation thereby making the regulation inconclusive. Each column represents cell lines, and each row represents one gene. The cut off value for *Δ*Ct for upregulated and downregulated genes is 6 and -6. Genes whose expression was not detectable are shown in grey with ND (not determined). Heatmap was generated using Rstudio.

Our TaqMan array card data confirmed the activation of *CR2*, *LYN*, *VAV2*, *IFITM1*, *PIK3R3*, *PTPN6* in BL and *KRAS*, *IFITM1*, *PPP3CA* in LCLs by EBNA3 proteins. It also confirmed the repression of *CD22*, *CD72*, *CD19*, *CD79A*, *CD79B*, *NFATC1*, *PIK3AP1*, *PRKCB* in BL and *PIK3R5* in LCLs by EBNA3 proteins (Chen *et al.*, 2005, Hertle *et al.*, 2009, White *et al.*, 2010, Zhao *et al.*, 2011a, McClellan *et al.*, 2012). However, repression of *CR2* and activation of *PPP3R1* by EBNA3C in LCL 3CHT cell line contradicted with the previously reported regulation (Zhao *et al.*, 2011a). Our data also identified new target genes *AKT2*, *NFATC3*, *NFATC4*, *FOS*, *AKT2*, *PIK3CG*, *PLCG2*, *INPP5D*, *NFKBIA*, *CARD11* in BL and *IKBKB*, *DAPP1*, *CARD11*, *RAC2*, *FOS*, *NFATC4* in LCLs (**Table 5.5**). Extensive overlap for the newly identified target genes regulated by EBNA2 and EBNA3 was observed. Although for some genes EBNA2 and EBNA3 showed antagonist effect, for example, EBNA2 activated *PIK3R1* in LCL which was found to be repressed by EBNA3C in the same cell background. Furthermore, based on TaqMan array card analysis, the genes that were identified as EBNA2 and EBNA3 targets could be mainly categorised by their molecular/biological function such as transcription regulation, adhesion, cell differentiation marker, protein kinases and tumour suppressors. Majority of these genes were found to be involved mainly in calcium signalling, PI3K-Akt signalling as well as genes that are upstream of these two signalling pathways. These two pathways are involved in cellular signalling, survival and proliferation of B cells (reviewed in (Rickert, 2013)). As the effects of gene regulation by EBNA2 and EBNA3 have not been studied previously, I set out to investigate the functional consequence of EBNA2 and EBNA3 mediated gene regulation from the PI3K-Akt pathway.

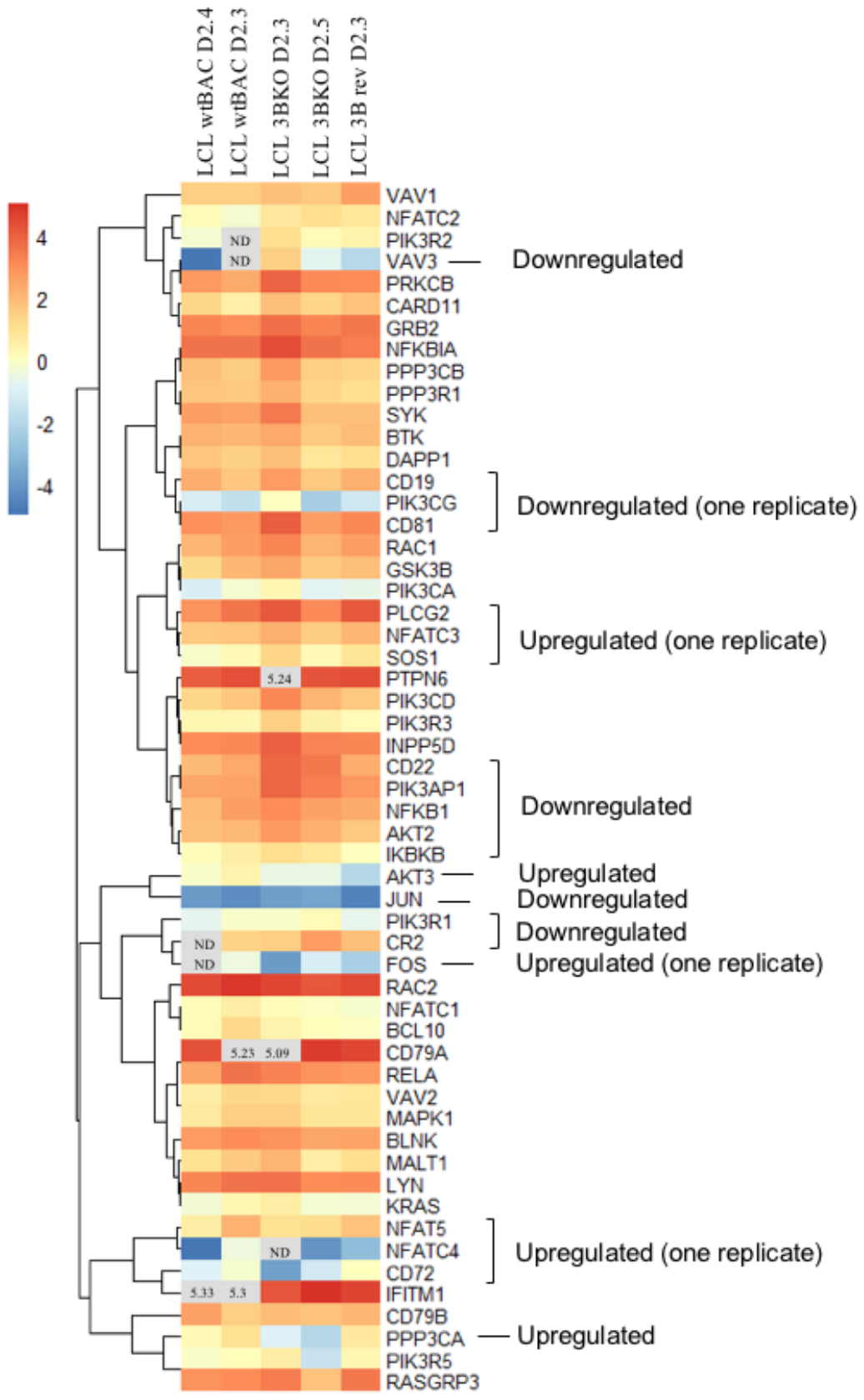
LCL wtBAC D2.4
LCL wtBAC D2.3
LCL 3BKO D2.3
LCL 3BKO D2.5
LCL 3B rev D2.3
4
2
0
-2
-4
VAV1
NFATC2
PIK3R2
VAV3
PRKCB
CARD11
GRB2
NFKBIA
PPP3CB
PPP3R1
SYK
BTK
DAPP1
CD19
PIK3CG
CD81
RAC1
GSK3B
PIK3CA
PLCG2
NFATC3
SOS1
PTPN6
PIK3CD
PIK3R3
INPP5D
CD22
PIK3AP1
NFKB1
AKT2
IKBKB
AKT3
JUN
PIK3R1
CR2
FOS
RAC2
NFATC1
BCL10
CD79A
RELA
VAV2
MAPK1
BLNK
MALT1
LYN
KRAS
NFAT5
NFATC4
CD72
IFITM1
CD79B
PPP3CA
PIK3R5
RASGRP3
ND
5.24
5.23
5.09
5.33
5.3
Downregulated
Downregulated (one replicate)
Upregulated (one replicate)
Downregulated
Upregulated
Downregulated
Downregulated
Upregulated (one replicate)
Upregulated (one replicate)
Upregulated

Figure 5.8 Regulation of genes from BCR signalling by EBNA3B in LCLs.
Heatmap showing the target gene expression normalised to the housekeeping gene, *GUSB*. Regulation by EBNA3B was studied in LCLs established by infecting primary B cells from donor 2 with either wild-type EBV (wt BAC), EBNA3B knockout EBV (LCL 3BKO) or revertant virus for EBNA3B (LCL 3B rev). Normalised gene expression (*Δ*Ct) is obtained after deducting the Ct value of *GUSB* for each cell line from Ct value of genes in question. These values for each gene are shown as pseudocolour with blue being downregulated and orange being upregulated gene expression as shown by the scale. Hierarchical clustering was performed using Pearson correlation as a measure of similarity between genes with complete linkage as clustering allocation. Genes are grouped as being upregulated or downregulated and the genes that are not grouped, are either not regulated or the replicates show opposite regulation thereby making the regulation inconclusive. Each column represents cell lines, and each row represents one gene. The cut off value for *Δ*Ct for upregulated and downregulated genes is 5 and -5. Genes with *Δ*Ct value higher than the cut off are shown in grey with their respective *Δ*Ct value whereas the genes whose expression was not detectable are shown in grey with ND (not determined). Heatmap was generated using Rstudio.

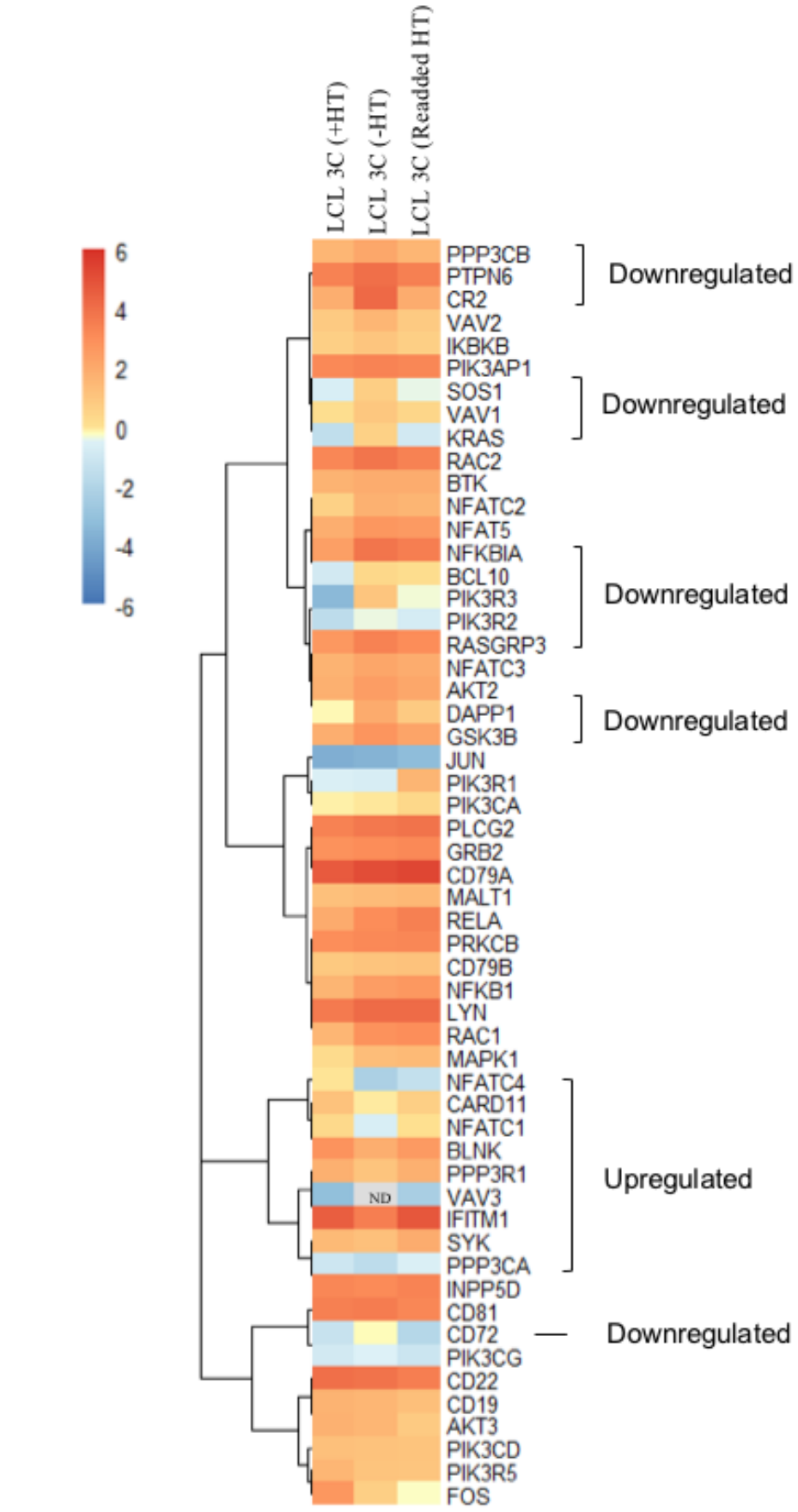
LCL 3C (+HT)
LCL 3C (-HT)
LCL 3C (Readded HT)
6
4
2
0
-2
-4
-6
PPP3CB
PTPN6
CR2
VAV2
IKBKB
PIK3AP1
SOS1
VAV1
KRAS
RAC2
BTK
NFATC2
NFAT5
NFKBIA
BCL10
PIK3R3
PIK3R2
RASGRP3
NFATC3
AKT2
DAPP1
GSK3B
JUN
PIK3R1
PIK3CA
PLCG2
GRB2
CD79A
MALT1
RELA
PRKCB
CD79B
NFKB1
LYN
RAC1
MAPK1
NFATC4
CARD11
NFATC1
BLNK
PPP3R1
VAV3
ND
IFITM1
SYK
PPP3CA
INPP5D
CD81
CD72
PIK3CG
CD22
CD19
AKT3
PIK3CD
PIK3R5
FOS
Downregulated
Downregulated
Downregulated
Downregulated
Upregulated
Downregulated

Figure 5.9 Regulation of genes from BCR signalling by EBNA3C in a conditional LCL.
Heatmap showing the target gene expression normalised to the housekeeping gene, *GUSB*. Regulation by EBNA3C was studied in LCL 3CHT established by infecting peripheral B cells with recombinant virus containing EBNA3C fused to estrogen receptor. LCL3CHT were grown in the presence of HT (4-hydroxytamoxifen) for 25 days (EBNA3C active) and the HT was washed off from cells and they were cultured in the absence of HT for 21 days (EBNA3C inactive). Cells were then either cultured with HT (re-instate EBNA3C) for 14 days or without HT for another 10 days (31 days in total). Normalised gene expression (*Δ*Ct) is obtained after deducting the Ct value of *GUSB* for each cell line from Ct value of genes in question. These values for each gene are shown as pseudocolour with blue being downregulated and orange being upregulated gene expression as shown by the scale. Hierarchical clustering was performed using Pearson correlation as a measure of similarity between genes with complete linkage as clustering allocation. Genes are grouped as being upregulated or downregulated and the genes that are not grouped, are either not regulated or the replicates show opposite regulation thereby making the regulation inconclusive. Each column represents cell lines, and each row represents one gene. The cut off value for *Δ*Ct for upregulated and downregulated genes is 6 and -6. Genes whose expression was not detectable are shown in grey with ND (not determined). Heatmap was generated using Rstudio.

Genes	Molecular or Biological function	Regulated by			
		EBNA 3A	EBNA 3B	EBNA 3C	All EBNA3
Burkitt's lymphoma cell lines (BL31)					
NFATC1* NFATC2 NFATC3 NFATC4*	Transcription regulation				
FOS*					
AKT2	Protein kinase				
SYK* PRKCB					
PIK3CG*					
LYN					
CR2 (CD21)*	Cell differentiation markers				
CARD11*					
CD79B* CD79A* CD22*					
CD72* CD19*					
PIK3AP1	Signalling adaptor				
NFKBIA*	Enzyme binding				
INPP5D*	Hydrolase				
PTPN6*	Cell adhesion				
IFITM1*	Receptor				
PLCG2*	Transmembrane signalling				
VAV2*	Guanine-nucleotide releasing factor				
PIK3R3*	Tumour suppressor				
Lymphoblastoid cell lines (LCLs)					
CD72*	Cell differentiation markers				
CARD11*					
CR2 (CD21)*					
CD22*					
VAV3	Guanine-nucleotide releasing factor				
LYN*	Protein kinase				
IKBKB*					
FOS*	Transcription regulation				
NFATC1*					
NFATC4*					
IFITM1*	Receptor				
PTPN6*	Cell adhesion				
SOS1*	DNA binding				
RAC2*	GTPase activity				
PPP3CA*	Phosphatase				
PPP3R1					
DAPP1*					
PIK3AP1	Signalling adaptor				
PIK3R1* PIK3R3*	Tumour suppressor				
PIK3R5*					

Table 5.5 confirming the Taqman array card data for cellular target genes by EBNA3s in BL and LCLs where green represent upregulation and red represent downregulation respectively. Newly identified target genes are highlighted in grey. Genes that were also regulated by EBNA2 are shown by (*).

5.3 EBNA2 and EBNA3 proteins repress the PI3K-Akt pathway through inactivation of Akt.

A majority of genes in this pathway showed regulation by both EBNA2 and EBNA3 proteins. The PI3K-Akt pathway promotes proliferation and growth of B cells and is one of the most frequently deregulated pathways in human cancers (reviewed in (Martini *et al.*, 2014)). **Figure 5.10** shows the genes that were identified as targets of EBNA2 and EBNA3 in the PI3K-Akt pathway from TaqMan array card analysis.

We observed the upstream components, *SYK* and *CD19* were mainly repressed by EBNA2 and EBNA3, with the exception of *LYN* being repressed by EBNA2 and activated by EBNA3 (**Table 5.4 & 5.5, Figure 5.10**). The PI3K regulatory subunits (*PIK3R1*, *PIK3R3* and *PIK3R5*) were differentially regulated by EBNA2 and EBNA3 whereas the negative regulator of PI3K, *INPP5D*, was repressed by EBNA2, EBNA3A and EBNA3C. As these data showed downregulation of upstream components and repression of the negative regulator of PI3K-Akt signalling by EBNA2 and EBNA3 proteins it was difficult to deduce the overall effect of EBNA2 and EBNA3 on this pathway.

Therefore, to further understand the regulation of PI3K-Akt signalling, binding data for genes that were regulated by either EBNA2 or EBNA3 was examined in more detail. We also aligned the binding data of ChIP-seq from GM12878 cells (LCLs, Latency III) with the binding data of ChIP-seq from Mutu III cells that was used for initial target gene analysis.

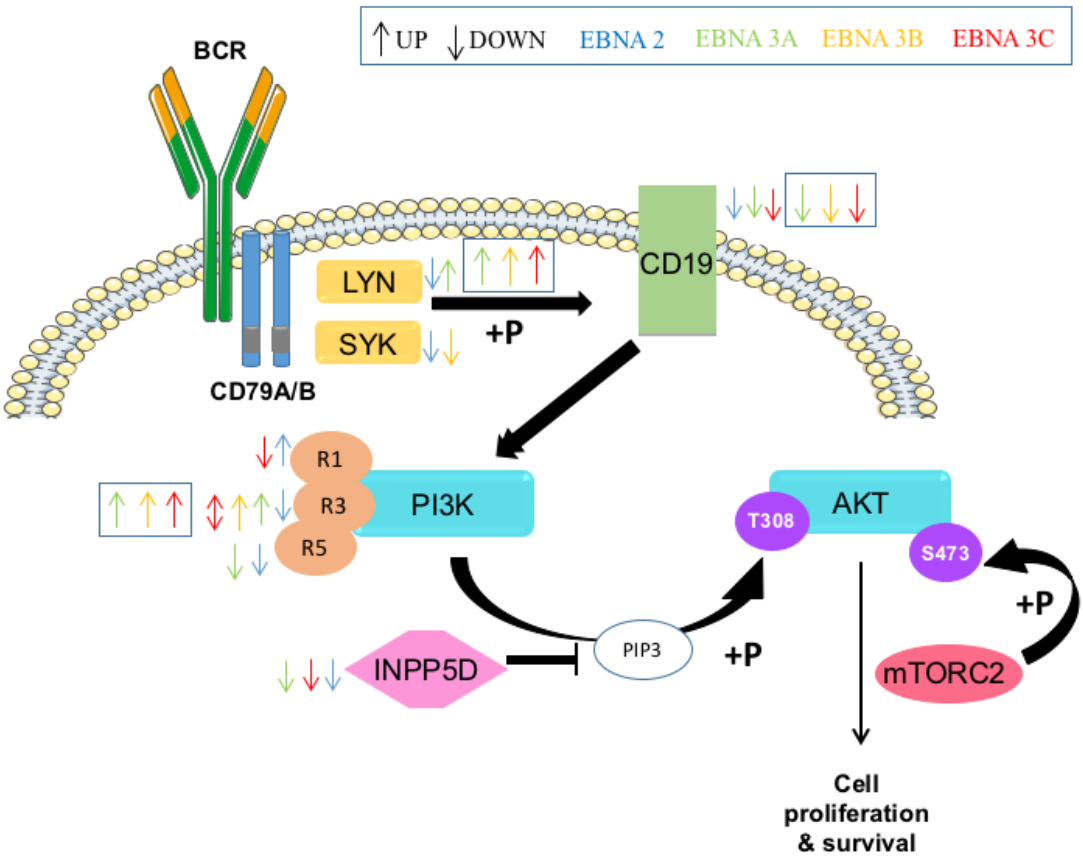

Figure 5.10 Schematic diagram of regulation of the PI3K-Akt signalling pathway by EBNA2 and EBNA3s.
This diagram shows the PI3K-Akt pathway downstream of BCR. A black arrow with +P indicates activation by phosphorylation, double headed arrow indicates activation by an unspecified mechanism. Black arrow without +P indicates activation of downstream signalling pathway whereas inhibition is represented by black perpendicular lines. Based on the TaqMan array card analysis, genes that have been reported to be regulated by EBNA2 and EBNA3s in this pathway are shown using arrows for upregulation and downregulaion. The arrows enclosed in a box represent co-operative regulation by EBNA3A, 3B and 3C. Arrows are colour coded according to which EBNA is regulating them.

ChIP in GM12878 cells was carried out using antibodies for EBNA2, EBNA3A, EBNA3B and EBNA3C as previously described in Mutu III experiment (Gunnell *et al.*, 2016), however, we did not have this data during the start of the study. Comparing the ChIP-seq data between cell backgrounds used in our TaqMan array cards will allow us to compare the overall binding pattern of EBNA2 and EBNA3 in these cell lines. However, it should be noted that the ChIP-seq data from GM12878 was not of good quality due to the low number of background subtracted reads per million. The binding data showed *LYN*, *CD19*, *SYK*, *INPP5D* and *PIK3R1* to be either bound by EBNA2 or EBNA3 at a promoter-proximal site or had a top significant EBNA2 binding site confirming the initial DAVID analysis (**Figure 5.11-5.15**). *PIK3R5* and *PIK3R3* were identified as genes close to a significant EBNA2 and EBNA3 binding site irrespective of the distance by the initial DAVID analysis, however, the binding data showed EBNA2 to bind at the *PIK3R3* promoter suggesting it to be a promoter-proximally bound gene (**Figure 5.16-5.17, Table 5.1**). This could be due to some issue with DAVID analysis as it did not list *PIK3R3* as a BCR target for genes that were promoter-proximally bound. We also investigated commonly bound sites by EBNA2 and EBNA3 for these genes. EBNA2 and EBNA3 bound to a common site in the downstream intragenic site for *SYK* and at the gene promoter for *PIK3R1* (**Figure 5.11-5.12**). For *LYN* and *INPP5D*, top significant EBNA2 binding site at the downstream intragenic region was found in addition to EBNA2 promoter-proximal binding sites (**Figure 5.13-5.14**).

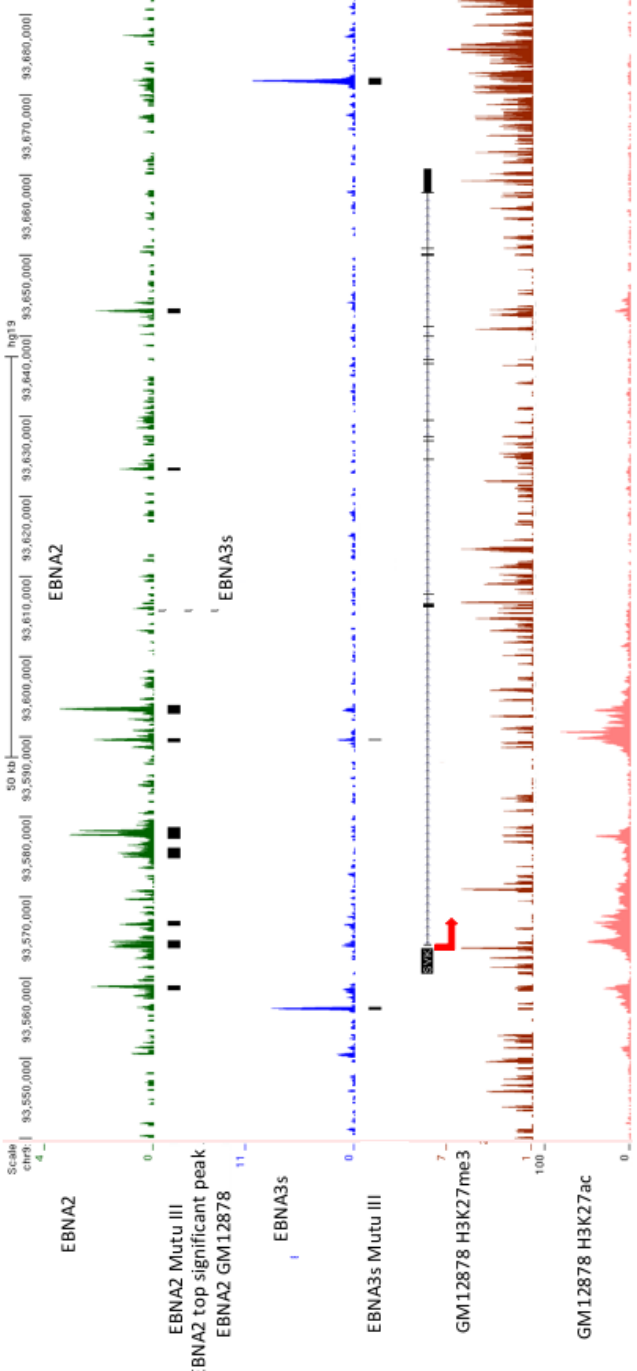

Figure 5.11 EBNA2 and EBNA3 binding sites at the *SYK* locus.
The number of EBNA2 and EBNA3 sequencing reads from immunoprecipitated Mutu III and GM12878 DNA are plotted per million background-subtracted total reads and aligned with human genome. MACS peak (Black box) called 'peaks' represent the binding sites of EBNA2 and EBNA3. Both EBNA2 and EBNA3 bind to a promoter proximal site at *SYK*. The red arrow indicates the direction of gene transcription. GM12878 H3K27ac and H3K27me3 ChIP-seq data from ENCODE are shown at the bottom of the panel.

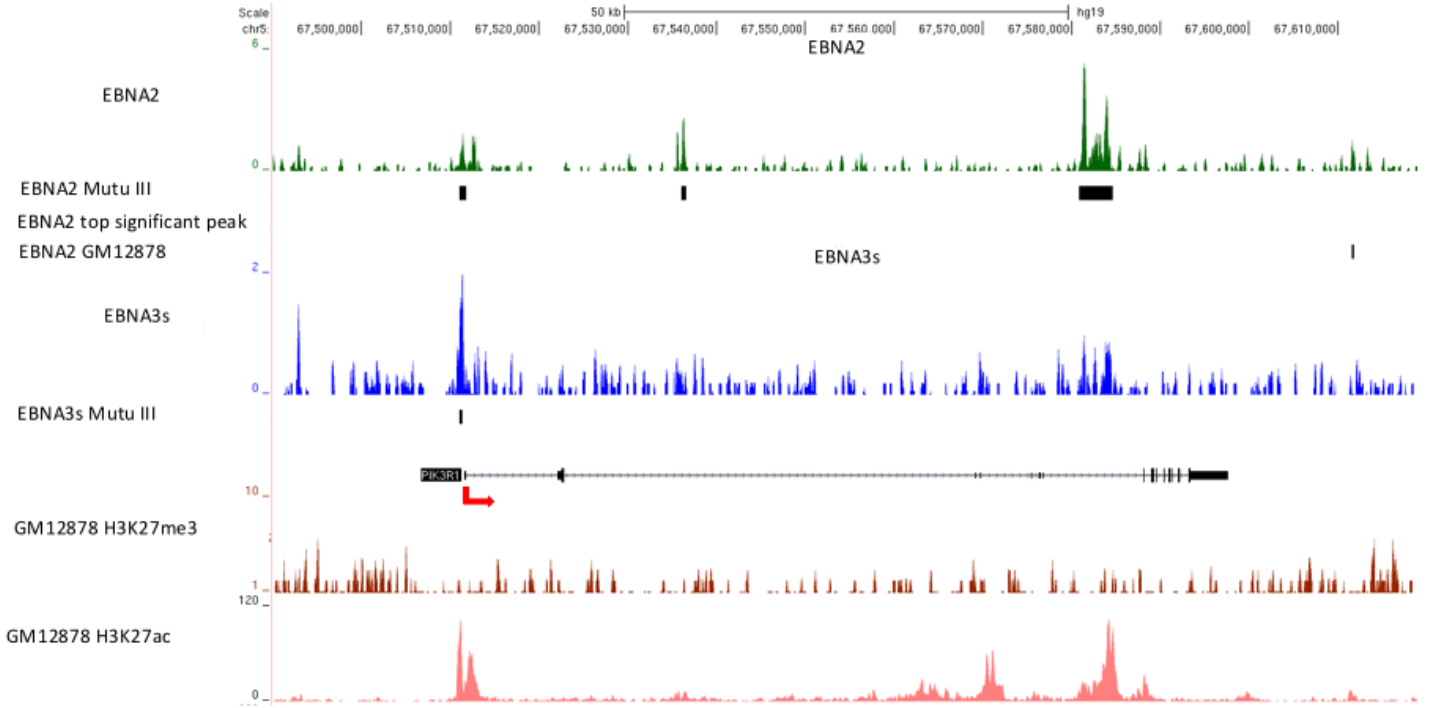

Figure 5.12 EBNA2 and EBNA3 binding sites at the *PIK3R1* locus.
The number of EBNA2 and EBNA3 sequencing reads from immunoprecipitated Mutu III and GM12878 DNA are plotted per million background-subtracted total reads and aligned with human genome. MACS peak (Black box) called 'peaks' represent the binding sites of EBNA2 and EBNA3. Both EBNA2 and EBNA3 bind to a promoter proximal site at *PIK3R1*. The red arrow indicates the direction of gene transcription. GM12878 LCL H3K27ac and H3K27me3 ChIP-seq data from ENCODE are shown at the bottom of the panel.

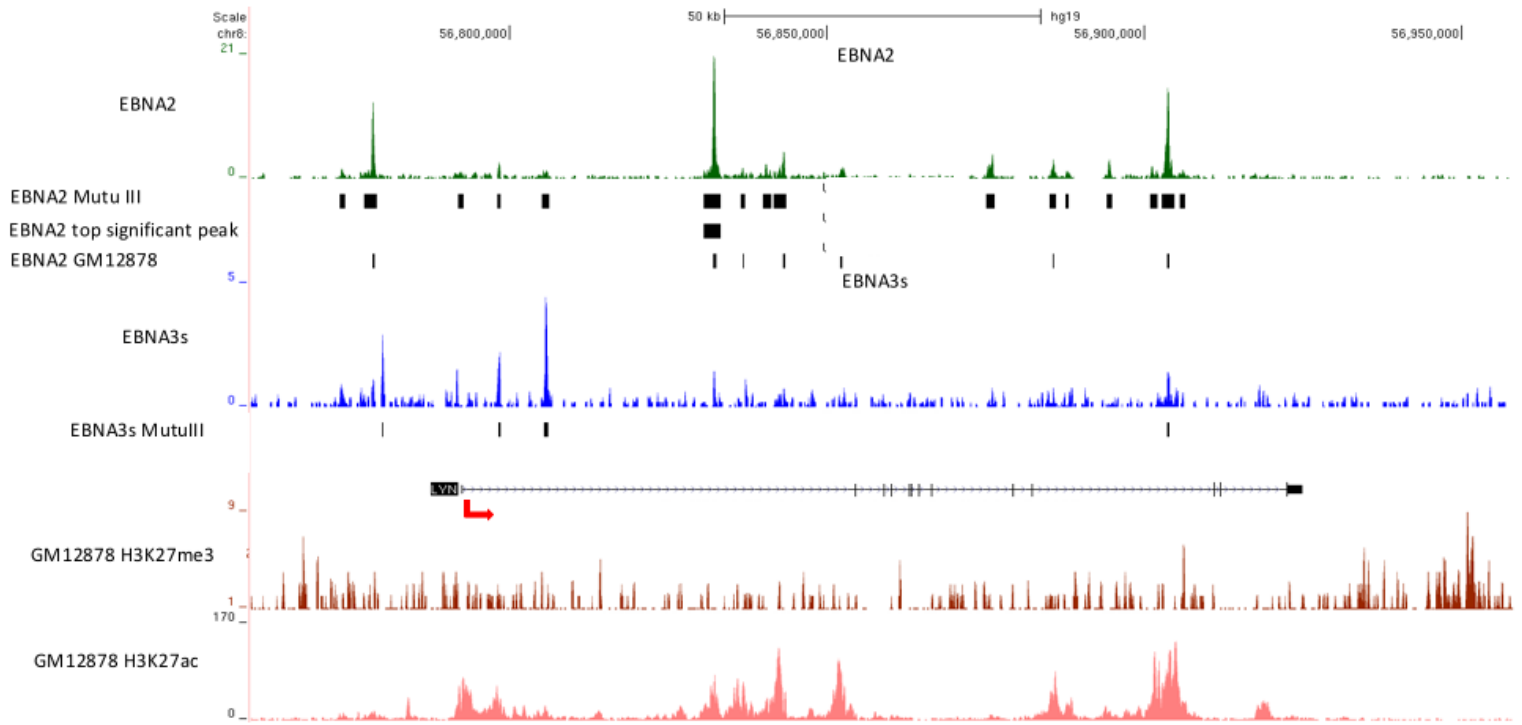

Figure 5.13 EBNA2 and EBNA3 binding sites at the *LYN* locus.
The number of EBNA2 and EBNA3 sequencing reads from immunoprecipitated Mutu III and GM12878 DNA are plotted per million background-subtracted total reads and aligned with human genome. MACS peak (Black box) called 'peaks' represent the binding sites of EBNA2 and EBNA3. Both EBNA2 and EBNA3 bind to a promoter proximal site at *LYN*. Top significant EBNA2 binding site found in the intragenic region downstream of *LYN*. The red arrow indicates the direction of gene transcription. GM12878 LCL H3K27ac and H3K27me3 ChIP-seq data from ENCODE are shown at the bottom of the panel.

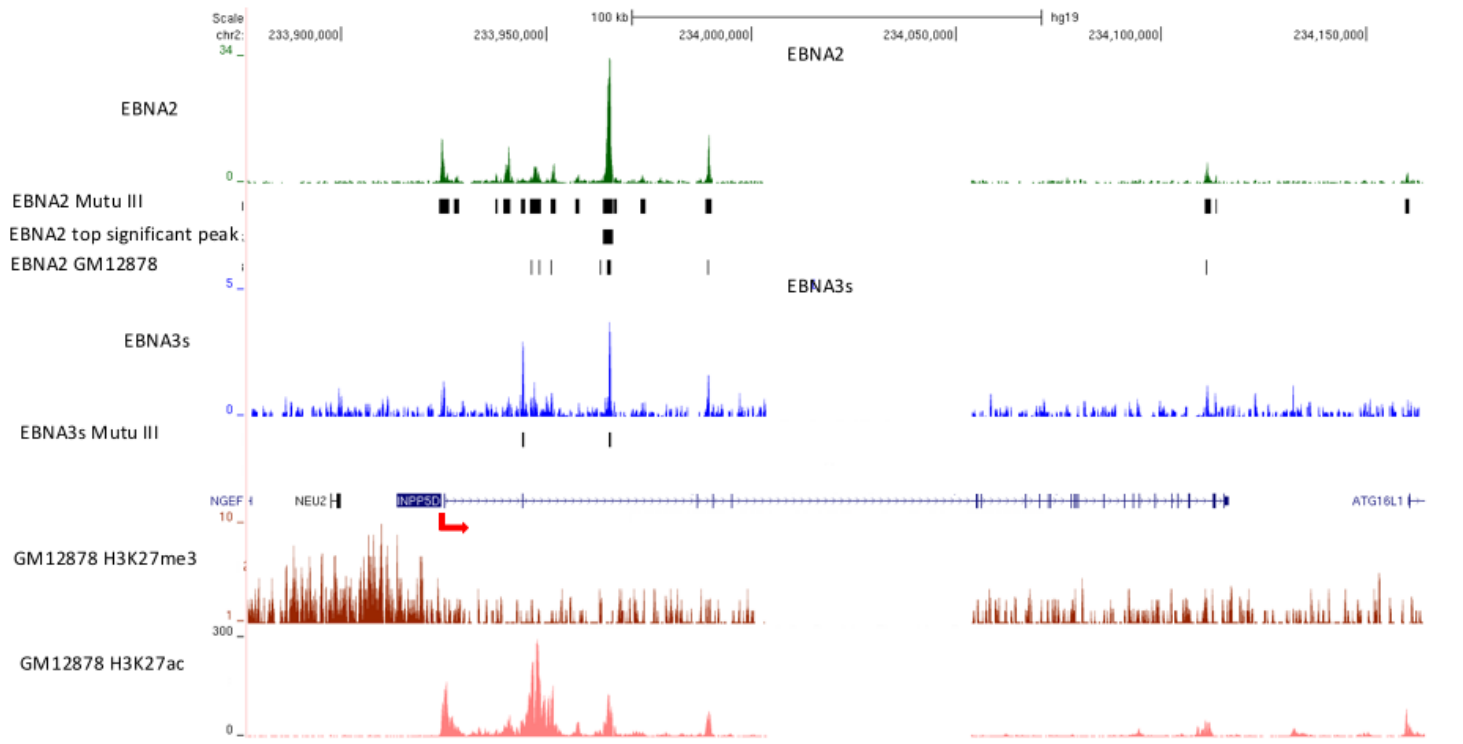

Figure 5.14 EBNA2 and EBNA3 binding sites at the *INPP5D* locus.
The number of EBNA2 and EBNA3 sequencing reads from immunoprecipitated Mutu III and GM12878 DNA are plotted per million background-subtracted total reads and aligned with human genome. MACS peak (Black box) called 'peaks' represent the binding sites of EBNA2 and EBNA3. Both EBNA2 and EBNA3 bind to a promoter proximal site at *INPP5D*. Top significant EBNA2 binding site found in the intragenic region downstream of *INPP5D*. The red arrow indicates the direction of gene transcription. GM12878 LCL H3K27ac and H3K27me3 ChIP-seq data from ENCODE are shown at the bottom of the panel.

Majority of the EBNA2 binding sites for these two genes in Mutu III were found to overlap with the EBNA2 binding sites in GM12878 and EBNA3 in Mutu III. *CD19* also had a top significant EBNA2 binding site in both Mutu III and GM12878 cells at the gene promoter that overlapped with the significant EBNA3 binding site (**Figure 5.15**). For *PIK3R3*, EBNA3 bound to only one site which overlapped with an EBNA2 binding site (**Figure 5.16)**. Whereas, *PIK3R5* only showed EBNA2 binding in both Mutu III and GM12878 cells which supports our TaqMan array card analysis as we did not see EBNA3 mediated regulation of *PIK3R5* in BL (**Figure 5.17**). Overall, the binding data showed most of these genes to have common sites for EBNA2 and EBNA3 binding further supporting the observation of these genes to be co-regulated by EBNA2 and EBNA3 proteins.

All the EBNA2 and EBNA3 binding peaks for these genes coincided with H3K27ac mark suggesting these sites to be potentially an active regulatory element (**Figure 5.11-5.17**). However, the genes that were repressed by either EBNA2 or EBNA3 did not show an increase in the repressive mark, H3K27me3, implicating repression of these genes to be independent of Polycomb repressor complex 2 (PRC2) which represses transcription by trimethylation of histone H3 lysine 27 (H3K27me3) and plays a role in the initial silencing of genes (reviewed in (Simon and Kingston, 2009)).

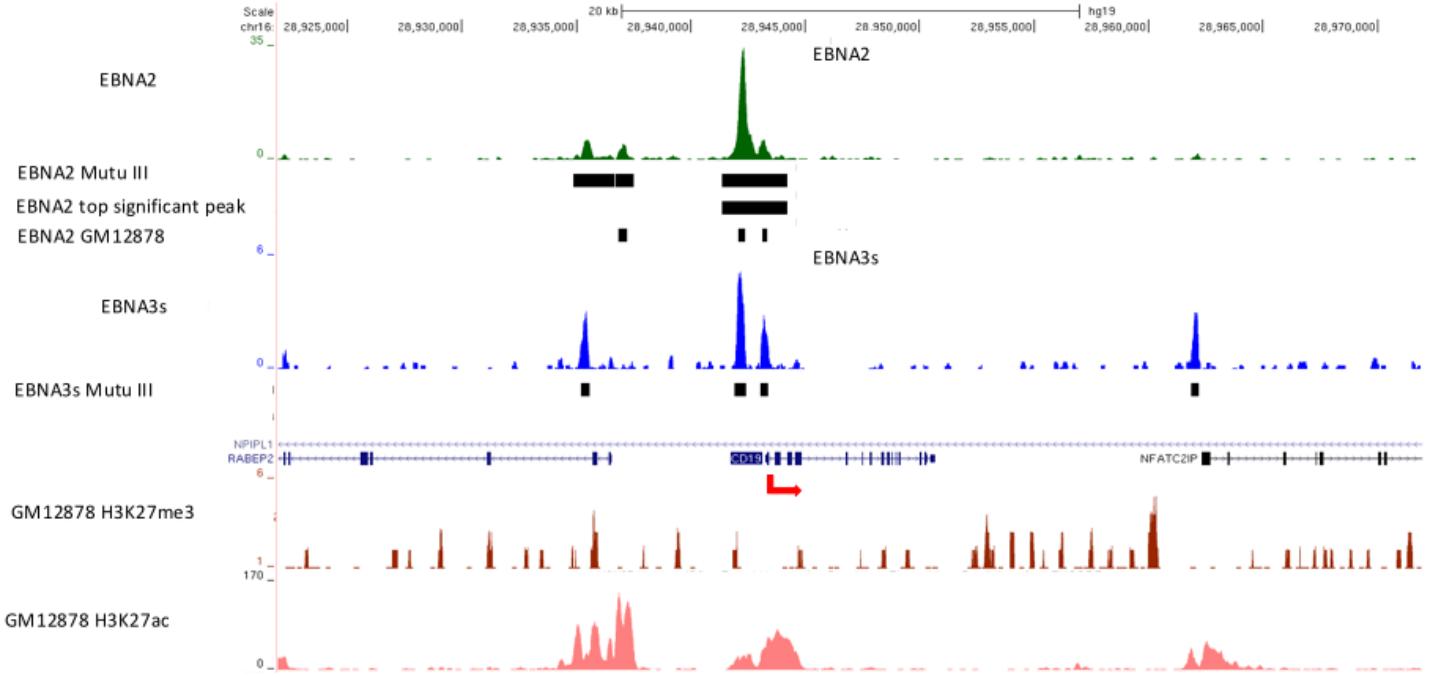

Figure 5.15 EBNA2 and EBNA3 binding sites at the *CD19* locus.
The number of EBNA2 and EBNA3 sequencing reads from immunoprecipitated Mutu III and GM12878 DNA are plotted per million background-subtracted total reads and aligned with human genome. MACS peak (Black box) called 'peaks' represent the binding sites of EBNA2 and EBNA3. Both EBNA2 and EBNA3 bind at the promoter of *CD19*. The EBNA2 binding site at the promoter is also a top significant peak. The red arrow indicates the direction of gene transcription. GM12878 LCL H3K27ac and H3K27me3 ChIP-seq data from ENCODE are shown at the bottom of the panel.

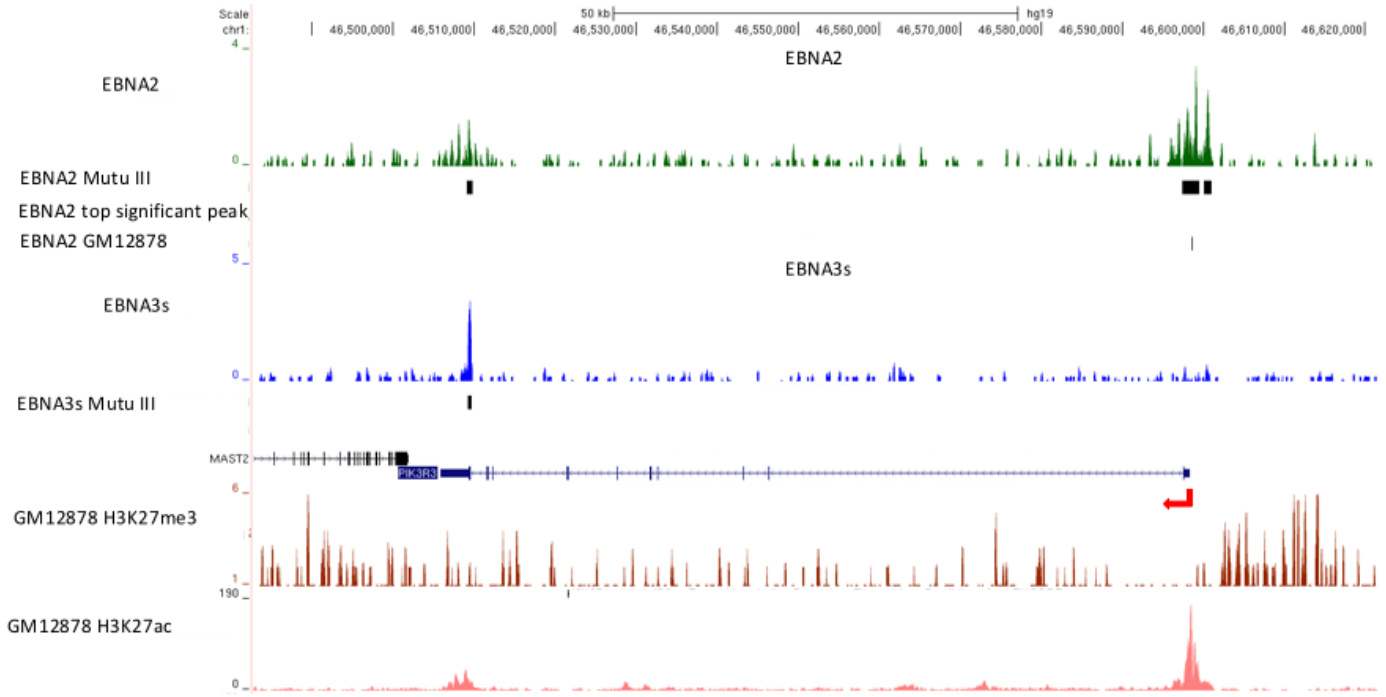

Figure 5.16 EBNA2 and EBNA3 binding sites at the *PIK3R3* locus.
The number of EBNA2 and EBNA3 sequencing reads from immunoprecipitated Mutu III and GM12878 DNA are plotted per million background-subtracted total reads and aligned with human genome. MACS peak (Black box) called 'peaks' represent the binding sites of EBNA2 and EBNA3. *PIK3R3* was the nearest gene to an EBNA2 and EBNA3 binding site (MACS $<10^{-7}$) according to initial DAVID analysis, however, the significant EBNA2 peak binds at the promoter of *PIK3R3*. The red arrow indicates the direction of gene transcription. GM12878 LCL H3K27ac and H3K27me3 ChIP-seq data from ENCODE are shown at the bottom of the panel.

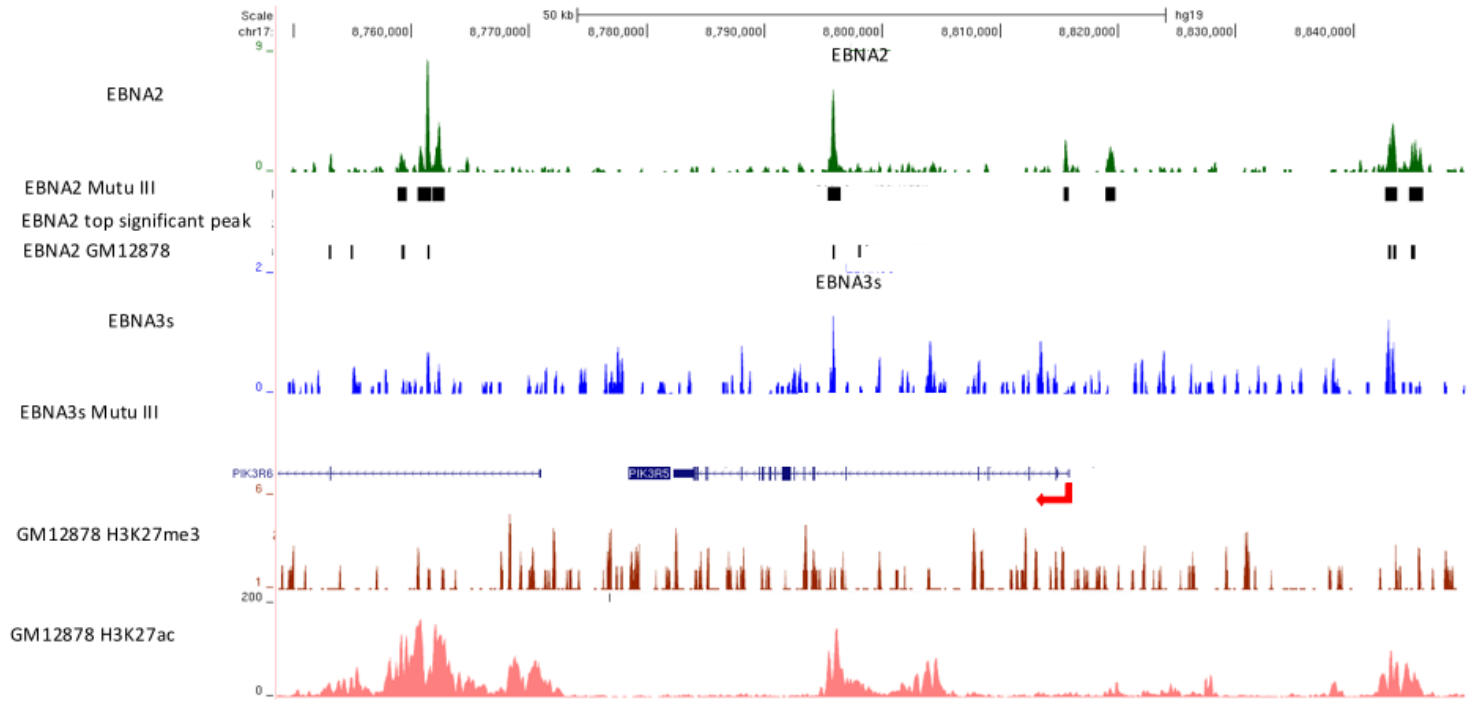

Figure 5.17 EBNA2 and EBNA3 binding sites at the *PIK3R5* locus.
The number of EBNA2 and EBNA3 sequencing reads from immunoprecipitated Mutu III and GM12878 DNA are plotted per million background-subtracted total reads and aligned with human genome. MACS peak (Black box) called 'peaks' represent the binding sites of EBNA2 and EBNA3. *PIK3R5* is near to an EBNA2 binding site (MACS $<10^{-7}$) with one peak in the intragenic region. The red arrow indicates the direction of gene transcription. GM12878 LCL H3K27ac and H3K27me3 ChIP-seq data from ENCODE are shown at the bottom of the panel.

Heatmap analysis was used to visualise gene expression between different cell lines. We further studied the relative quantification of PI3K-Akt signalling genes to determine the significance of the EBNA2 and EBNA3 mediated gene regulation. For EBNA2, mRNA expression was studied relative to EREB 2.5 (-ER, inactive EBNA2) cell line (**Figure 5.18**). *SYK*, *LYN*, *INPP5D*, *PIK3R1* and *PIK3R3* were significantly repressed by EBNA2 with the exception of PIK3R1 which was activated by EBNA2. Whereas, *CD19* although repressed by EBNA2, it was not found to be significant. For EBNA3 in BL, mRNA expression of genes was studied relative to EBV-negative BL31 cell line (**Figure 5.19**). Only *CD19* was significantly repressed by EBNA3A whereas *SYK*, *LYN*, *INPP5D*, *PIK3R1*, *PIK3R3* and *PIK3R5* were not significantly regulated. EBNA3KO cells did show repression of *PIK3R3* and *PIK3R5* but the significance of their regulation could not be determined as we did not have another clone/replicate for this deletion. In LCLs, mRNA expression for EBNA3A and EBNA3B regulated genes was studied relative to their respective wtBAC cell lines and for EBNA3C, LCL 3CHT grown in the presence of HT (active EBNA3C) was used to study the relative mRNA expression (**Figure 5.20**). The relative quantification showed only *LYN* to be significantly activated by EBNA3A in LCLs. Although robust repression of *PIK3R1* and *PIK3R3* by EBNA3C was observed, we could not determine the significance for these genes as we did not have a biological replicate for each sample in this cell line. Altogether, the relative quantification data confirmed the regulation of PI3K-Akt signalling genes by EBNA2 whereas only a few target genes for EBNA3 could be confirmed due to the lack of biological replicates or big error bars.

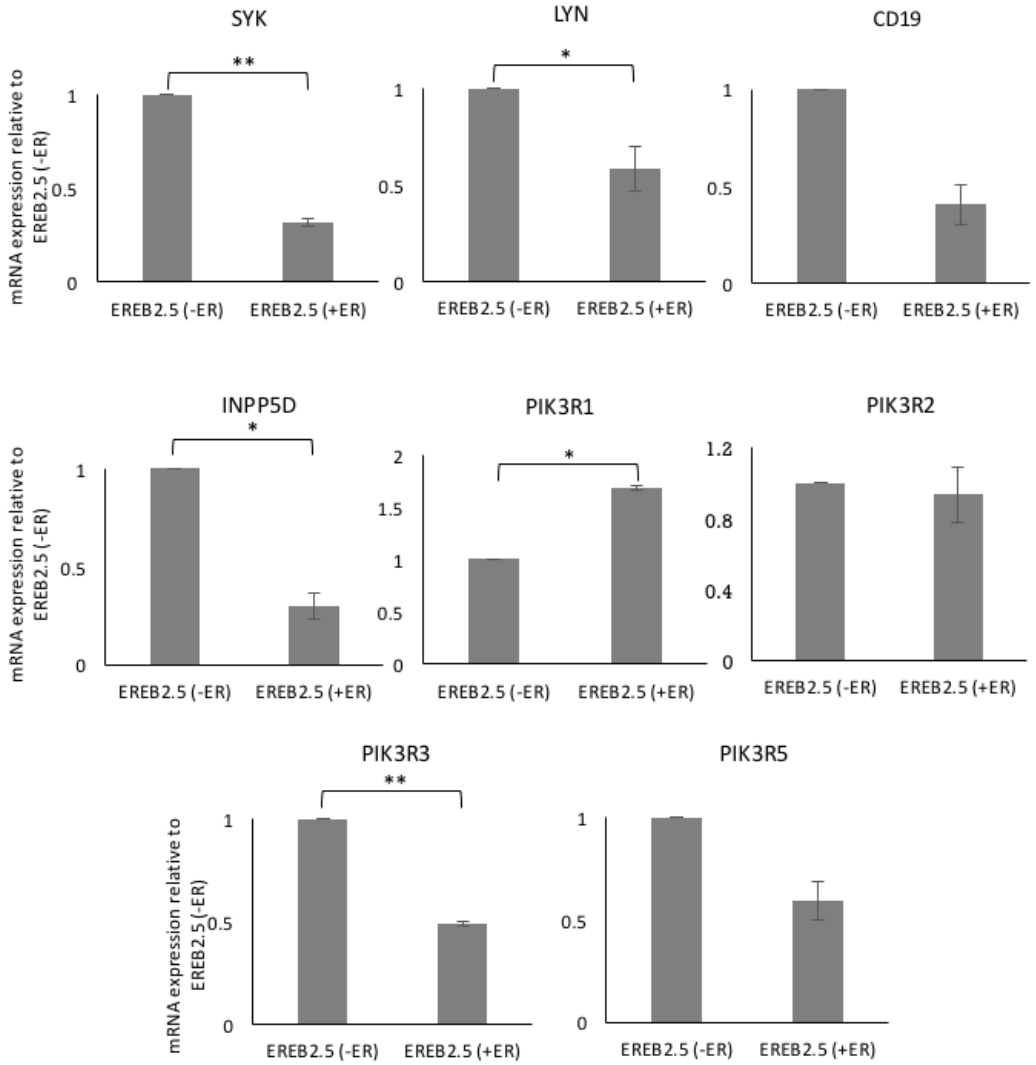

Figure 5.18 Gene regulation by EBNA2 in LCLs (EREB 2.5).
QPCR analysis of *SYK, LYN, CD19, INPP5D, PIK3R1, PIK3R2, PIK3R3* and *PIK3R5* mRNA expression in EREB2.5 cells. Signals were normalised to *GUSB* mRNA levels. Results show the mean mRNA levels relative to EREB2.5 (-ER) ± standard deviation of two independent experiments. Student's t-test for mRNA expression in EREB2.5 (+ER) compared to EREB2.5 (-ER) shown $P < 0.05$ (*) and $P < 0.01$ (**).

Next, we investigated the functional consequence of transcriptional regulation of these genes on the PI3K-Akt pathway. Phosphorylation of Akt on Thr308 by PDK1 lead to its partial activation and complete activation is achieved by phosphorylation on Ser473 by mTORC2. On the other hand, INPP5D represses the PI3K-Akt signalling by hydrolysing PIP_3 (phosphatidylinositol (3,4,5) triphosphate) to PIP_2 (phosphatidylinositol (3,4) diphosphate). PI3K PIP_3 is required for the recruitment of PDK1 and Akt to the plasma membrane and activation of mTOCRC2 thereby leading to Akt phosphorylation on Thr308 and Ser473 (reviewed in (Liu and Cohen, 2015)). As EBNA2 and EBNA3 repress *INPP5D* and differentially regulate PI3K regulatory subunits, we studied the phosphorylation of Akt to understand the overall impact of EBNA2 and EBNA3 proteins on Akt activity. To address this, western blotting using phospho-specific antibodies for Akt (Thr308 & Ser473) was carried out. Expression of the EBV latent membrane protein, LMP1, was also monitored as it has been shown to increase the basal activity of Akt through phosphorylation on Ser473 in HEK 293 cells (Dawson *et al.*, 2003). LMP1 expression was induced in EREB 2.5 cells with active EBNA2 consistent with it being a transcriptional target of EBNA2 (Wang *et al.*, 1990) (**Figure 5.21**). The active phosphorylation on Ser473 and Thr308 of Akt in EREB 2.5 cells with active EBNA2 was reduced despite a small increase in the total Akt protein level confirming repression of Akt phosphorylation by EBNA2 despite increased LMP1 expression. We also analysed the expression of EBNA3C in these cells as initial TaqMan array card analysis showed downregulation of *PIK3R1* and *PIK3R3* by EBNA3C in LCLs (**Table 5.5**). EBNA3C expression did not change with the activation of EBNA2 thereby ruling out the effects of EBNA3C on the observed Akt dephosphorylation.

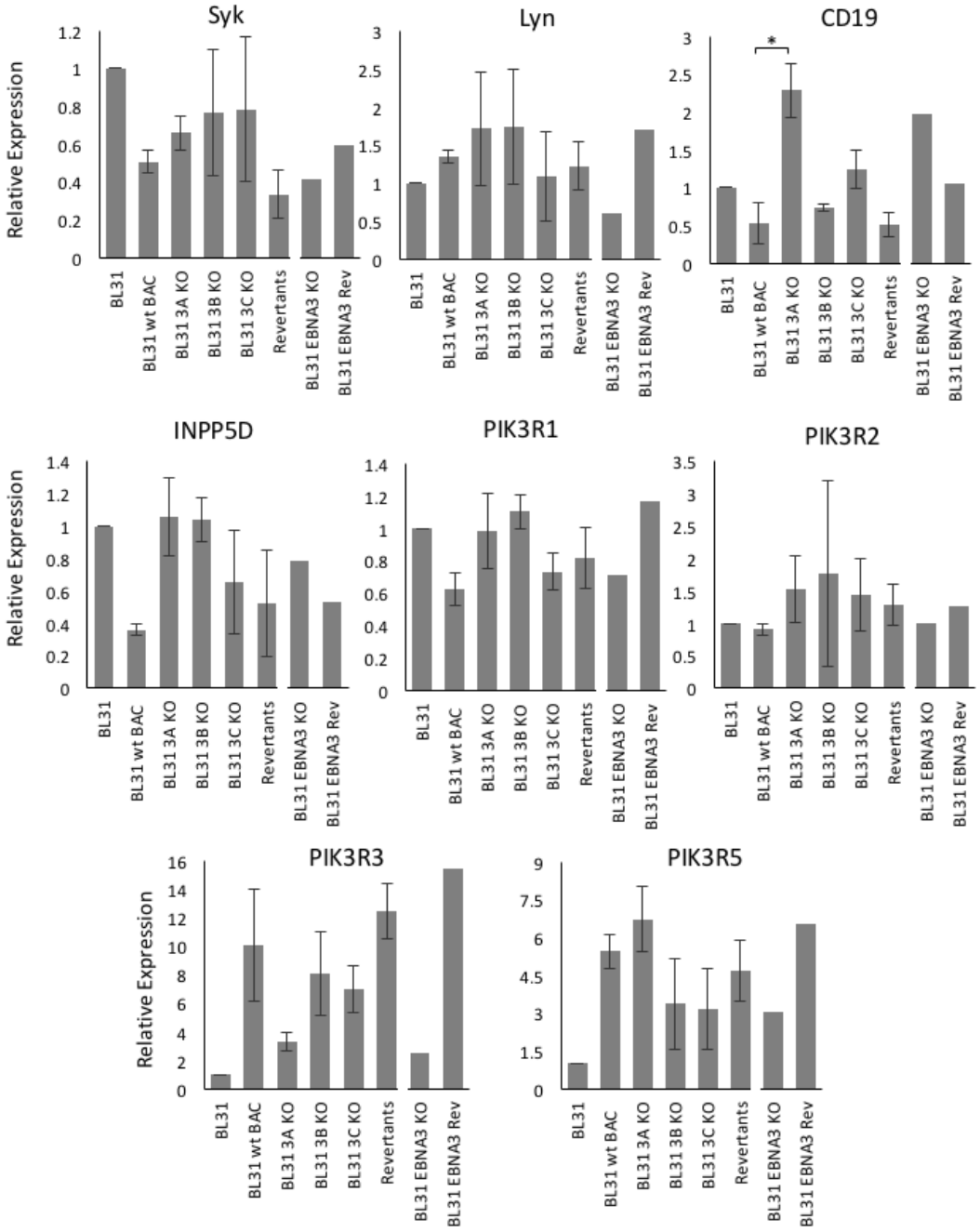

Figure 5.19 Gene regulation by EBNA3 in BL31 cell lines.
QPCR analysis of *SYK, LYN, CD19, INPP5D, PIK3R1, PIK3R2, PIK3R3* and *PIK3R5* mRNA expression in EBV-ve BL cells (BL31) and cells infected with either wild-type recombinant EBV (wtBAC), EBNA3A knock-out EBV (BL31 3AKO), EBNA3B knock-out EBV (BL31 3BKO), EBNA3C knock-out EBV (BL31 3CKO), EBNA3 knock-out EBV (BL31 EBNA3KO) or the revertant virus (Revertants (EBNA3A,3B & 3C), BL31 EBNA3 rev). Signals were normalised to *GUSB* mRNA levels. Results show the mean mRNA levels relative to EBV −ve BL cells (BL31) ± standard deviation of regulation in two different clones. Student's t-test for mRNA expression compared to BL31 wtBAC is shown $P < 0.05$ (*).

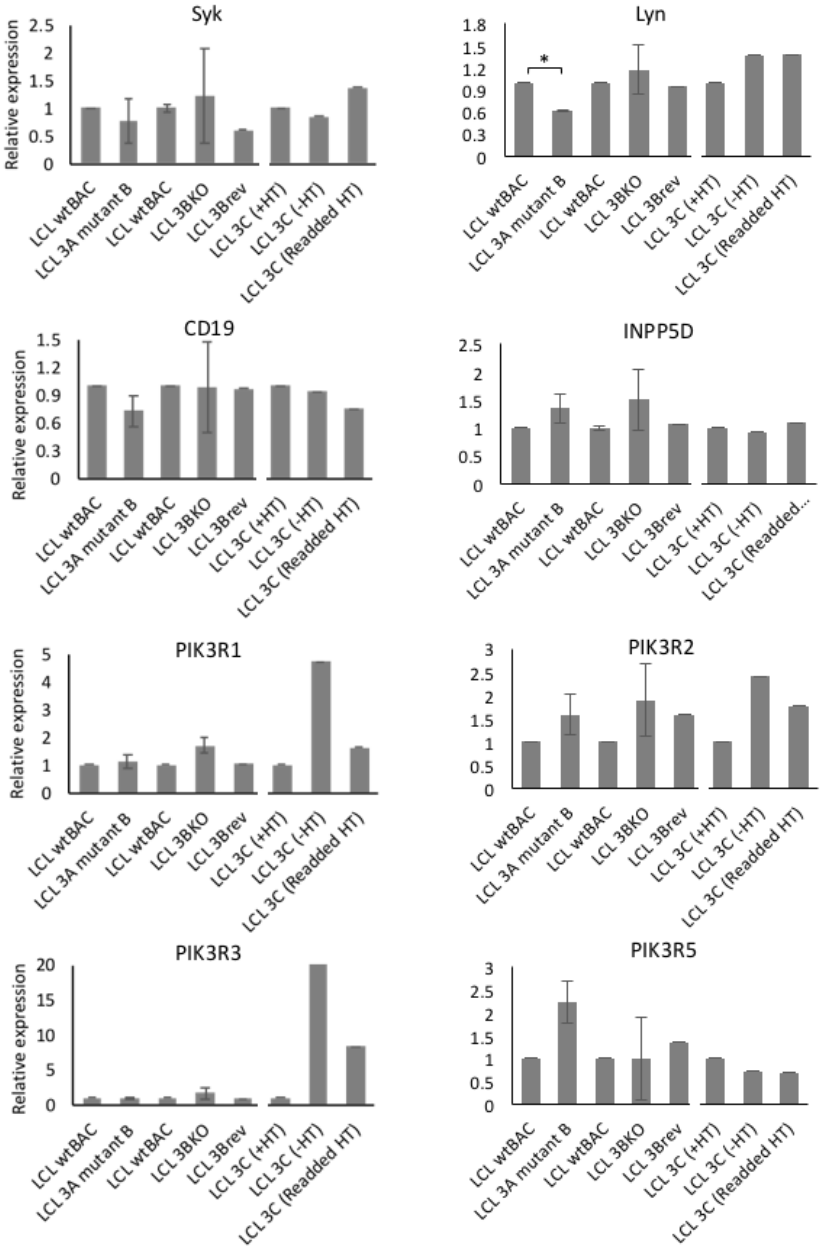

Figure 5.20 Regulation of gene expression by EBNA3 in LCLs.
QPCR analysis of *SYK, LYN, CD19, INPP5D, PIK3R1, PIK3R2, PIK3R3* and *PIK3R5* mRNA expression in LCLs. Regulation by EBNA3A and EBNA3B was studied in LCLs infected with either wild-type recombinant EBV or recombinant EBV lacking entire coding region of EBNA3A (LCL 3A mutant B), knock-out EBNA3B EBV (LCL3BKO) or recombinant revertant EBV (LCL 3Brev). Regulation by EBNA3C was studied in LCL 3CHT cells cultured in the presence of HT for 25 days (LCL 3C +HT) followed by wash-off and cells were either cultured in the absence of HT (LCL 3C -HT) or HT was re-added to some cells after 21 days for a further 14 days (LCL 3C readded HT) while the remaining cells were cultured without HT for another 10 days (31 days in total). Signals were normalised to *GUSB* mRNA levels. Results show the mean mRNA levels relative to LCLs infected with wild-type EBV for EBNA3A and EBNA3B ± standard deviation of expression in two clones. Student's t-test for mRNA expression compared to LCL wtBAC is shown $P < 0.05$ (*).

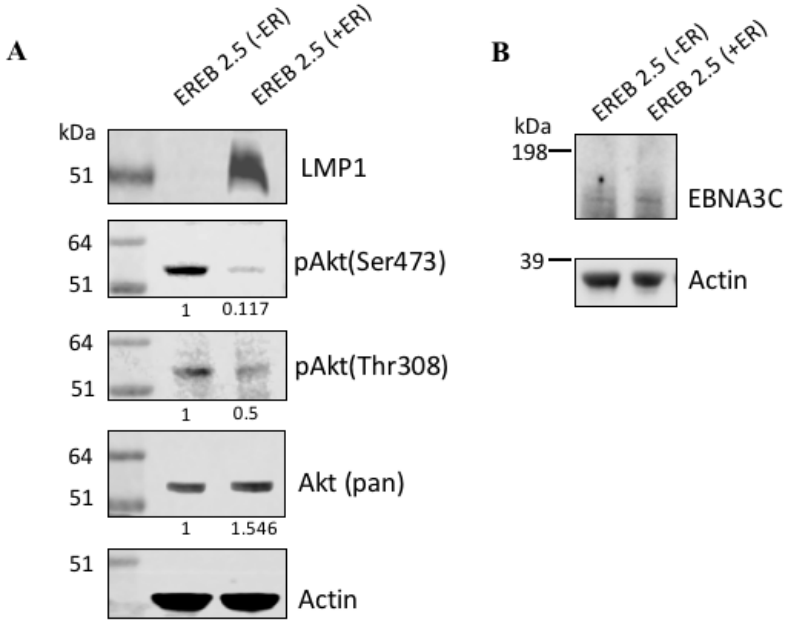

Figure 5.21 Repression of *Akt* by EBNA2 in EREB2.5 cells.
Western blot analysis for expression of (A) Akt at Ser473 and Thr308 phosphorylation, Akt (pan), LMP1 and (B) EBNA3C. Actin was used as a loading control. Numbers under panel show quantification of western blot signal for each antibody normalised to actin and expressed relative to EREB 2.5 (-ER).

Moreover, we observed reduced Akt (Thr308) phosphorylation even in the presence of high LMP1 expression in EREB 2.5 (+ER) suggesting EBNA2 to override the effect of LMP1 on Akt phosphorylation. This also implies transcriptional repression of upstream components overrides the effect of *INPP5D* repression by EBNA2. Together, these data suggest a net negative effect of EBNA2 on PI3K-Akt signalling arm as a result of reduced Akt phosphorylation.

We also examined the impact of EBNA3 expression on PI3K-Akt signalling by investigating Akt phosphorylation. Western blot analysis for effects of EBNA3 regulation in Burkitt's lymphoma showed dephosphorylation of Akt on Ser473 and Thr308 in EBV-infected BL31 cells (BL31 wtBAC3 & wtBAC2) (**Figure 5.22**). This was consistent with the dominant repressive effects of EBNA2 on upstream components of the Akt pathway resulting in inactivation of Akt. The active phosphorylation increases prominently in cells lacking EBNA3A expression without affecting total Akt protein expression (**Figure 5.22A**). Thereby, it confirms the role of EBNA3A in repression of PI3K-Akt signalling. Although variable LMP1 expression was observed across the cell panel, the increased phosphorylation on Ser473 in BL31 3AKO3 appears to be independent of high LMP1 levels since an increase in phosphorylation on Ser473 was also observed in another EBNA3A knock-out cell line (BL31 3AKO1.1) where LMP1 levels were lower (**Figure 5.22B**). In addition, high levels of LMP1 in BL31 3BKO1 and BL31 3CKO6 did not increase phosphorylation on Ser473 of Akt (**Figure 5.22**).

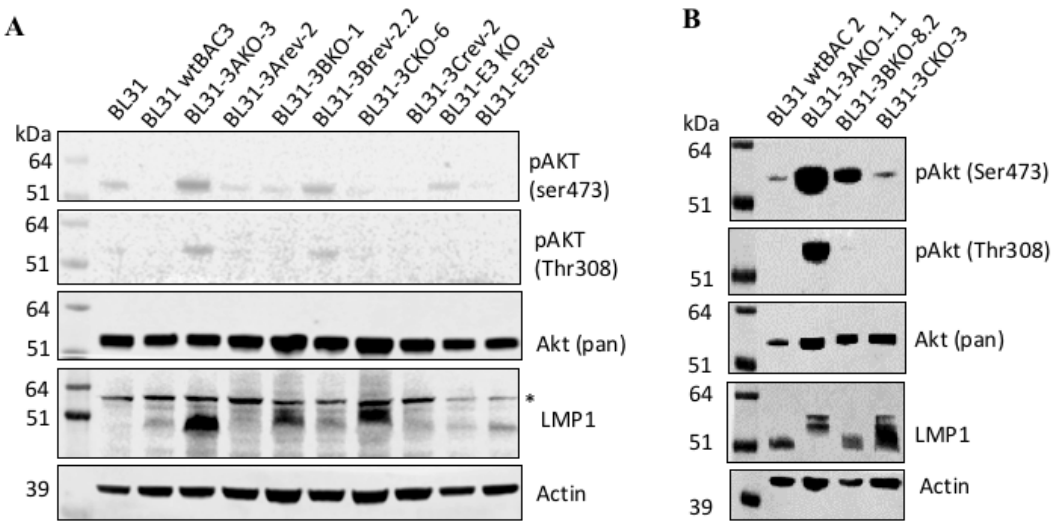

Figure 5.22 Repression of *Akt* by EBNA3A latent genes in BL31 cell lines.
(A & B) Western blot analysis for expression of Akt at Ser473 and Thr408 phosphorylation, Akt (total levels), LMP1 in EBV-negative BL cell-line BL31 and in BL31 cells infected with either wild-type recombinant EBV (BL31 wt BAC3, BL31 wt BAC2), EBNA3A knock-out EBV (BL31 3AKO-3AΔ, BL31-3AKO-1.1), EBNA3B knock-out EBV (BL31-3BKO-1, BL31-3BKO-8.2), EBNA3C knock-out EBV (BL31-3CKO-6, BL31-3CKO-3), EBNA3 knock-out EBV (BL31-E3KO) or with their respective revertant viruses (BL31-3A rev-2, BL31-3B rev-2.2, BL31-3B rev-2.2 and BL31-3B rev-2.2). Actin was used as a loading control. Non-specific band (*).

Analysis of Akt phosphorylation in LCLs was also carried out as EBNA3C was shown to repress *PIK3R1* and *PIK3R3* in the LCL 3CHT cell line (**Table 5.5**). Phosphorylation of Akt on Ser473 and Thr308 was reduced in cells with active EBNA3C (**Figure 5.23**). Consistent with repression of Akt by EBNA3C, Akt phosphorylation increased on inactivation of EBNA3C and was found to be reduced upon reactivation of EBNA3C. Although an increase in total Akt protein and LMP1 was observed upon inactivation of EBNA3C, the increase in Akt (Ser473) was increased ~ 3 fold more suggesting a relief in the repression of Akt in these cells. On the other hand, increased EBNA2 expression in LCL 3C (-HT) should have lead to reduced Akt phosphorylation as observed earlier. However, the increase in Akt phosphorylation in these cells suggests EBNA3C effects to be dominant on Akt regulation. Together in LCLs and BL, we observed reduced Akt phosphorylation by EBNA3C and EBNA3A implicating their role in suppression of PI3K-Akt signalling.

5.4 Discussion

To increase our understanding on the role of EBNA2 and EBNA3 transcription factors in growth and survival of infected B cells, we investigated transcriptional regulation of genes involved in BCR signalling, TaqMan array cards were used to perform gene expression analysis. Regulation by EBNA2 was studied in a lymphoblastoid cell line (LCL) with conditionally active EBNA2 (EREB 2.5). For gene regulation by EBNA3s, studies were undertaken in two cell backgrounds, EBV negative Burkitt's lymphoma cells (BL31) and LCLs. Our approach confirmed the regulation of majority of the BCR

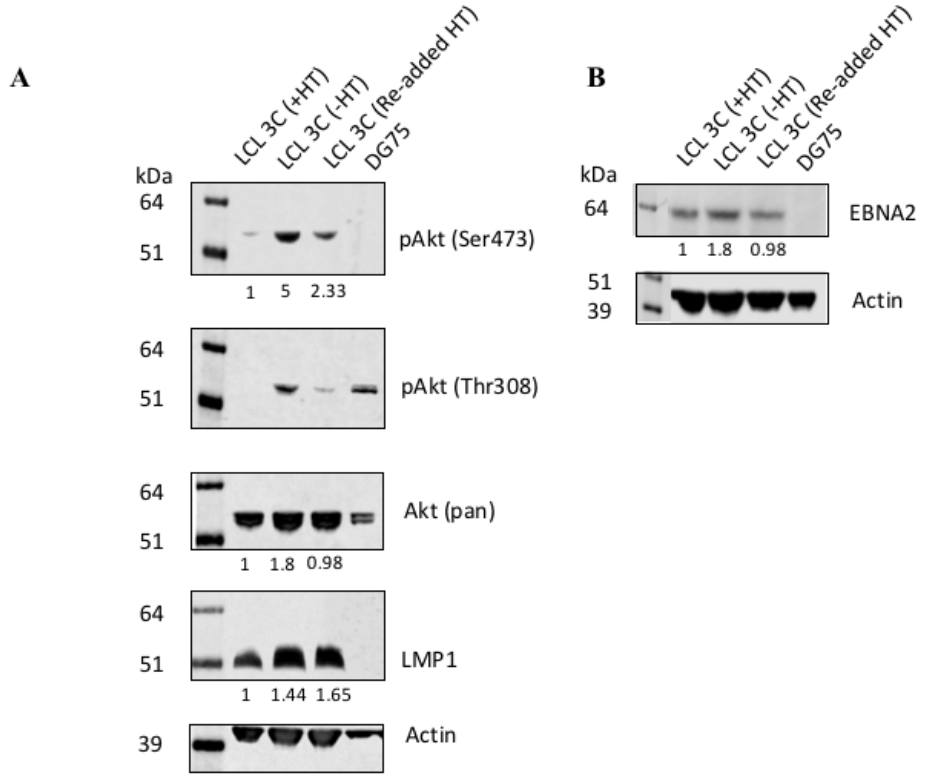

Figure 5.23 Repression of *Akt* by EBNA3C in LCL 3CHT cells.
Western blot analysis for expression of (A) Akt at Ser473 and Thr308 phosphorylation, Akt (pan), LMP1 and (B) EBNA2. DG75 (EBV-ve) cell lysate was used as a control for total Akt levels. Actin was used as a loading control. Numbers under panel show quantification of western blot signal for each antibody normalised to actin and expressed relative to LCL 3C (+HT).

signalling genes that have been previously reported as well as identified several new targets that could provide us with useful information of EBNA2 and EBNA3 mediated deregulation of this pathway (**Table 5.4 and 5.5**). Majority of the new target genes identified belong to the calcium signalling and the PI3K-Akt pathway. My studies were focussed on the effects of gene regulation on the PI3K-Akt pathway while effects on calcium signalling are being investigated by another PhD student in the laboratory (Hilda Veenstra). A comprehensive list of genes from PI3K-Akt signalling which has been previously identified along with the regulation observed by TaqMan array card analysis is shown in **Table 5.6**.

EBNA2 and EBNA3 share 25% of the binding sites in the human genome. Several studies have reported EBNA2 and EBNA3 to co-regulate genes and to antagonistically regulate genes. Re-ChIP analysis has also shown EBNA2 and EBNA3 proteins to compete for binding at all the shared sites as they were not found to co-occupy at any of their common binding sites (McClellan *et al.*, 2012, Harth-Hertle *et al.*, 2013, McClellan *et al.*, 2013). We observed EBNA2 and EBNA3 had overlapping binding sites at the target genes from the PI3K-Akt pathway. Activation of *PIK3R1* by EBNA2 was consistent with the previous study in EREB 2.5 cells. Spender *et al*. demonstrated EBNA2 to promote cell survival of infected cells through activation of *PIK3R1* (Spender *et al.*, 2006). However, we observed EBNA3C counteract this regulation in LCLs. ChIP-seq data for *PIK3R1* shows EBNA2 and EBNA3 binding to overlap at the gene promoter suggesting these two proteins to compete for binding at the promoter. *LYN* was also antagonistically regulated by EBNA2 and EBNA3A in LCLs.

Genes in PI3K-Akt	Previously reported									Microfluidics array card							
	EBNA 2		EBNA3A		EBNA3B		EBNA3C		EBNA3A,3B & 3C	EBNA2	EBNA3A		EBNA3B		EBNA3C		EBNA3A,3B & 3C
	BL	LCL	BL	LCL	BL	LCL	BL	LCL	BL	LCL	BL	LCL	BL	LCL	BL	LCL	BL
AKT2																	
AKT3																	
CD19																	
INPP5D																	
LYN																	
PIK3AP1																	
PIK3CA																	
PIK3CB																	
PIK3CD																	
PIK3CG																	
PIK3R1																	
PIK3R2																	
PIK3R3																	
PIK3R5												*					
SYK																	

Table 5.6 compares genes from the PI3K-Akt pathway that have been previously reported to be regulated by EBNA2 and EBNA3 with the genes confirmed to be regulated by EBNA2 and EBNA3 from TaqMan array card analysis in cell lines from Burkitt's lymphoma and Lymphoblastoid cell background. Green represent upregulation and red represent downregulation of the target genes by EBNA3 and EBNA2. '*' Regulation of *PIK3R5* by EBNA3A (LCL) is not direct. **Reference:** (Hertle *et al*., 2009; White *et al*., 2010; Chen *et al*., 2006; Zhao *et al*., 2011; Zhao *et al*., 2006; Spender et al., 2006; Maier *et al*., 2006).

This was further supported by the ChIP-seq data as EBNA3 binding overlapped with the small intragenic EBNA2 binding site downstream of the promoter as well as it overlapped with the EBNA2 peak at the 3' end of the gene. Thus suggesting EBNA2 and EBNA3 compete for binding at these sites. Moreover, one of the EBNA2 and EBNA3 overlapping site also showed the presence of a high H3K27ac signal (active mark) suggesting it to be a potential enhancer. Therefore, it will be interesting to investigate whether EBNA3A prevents active hub formation by enhancer-promoter looping or whether it promotes a repressive chromatin hub by chromosome conformation capture (CCC). Furthermore, ChIP-seq data showed no increase in H3K27me3 (repressive mark) at genes repressed by EBNA2 and EBNA3 in PI3K-Akt signalling (**Figure 5.11-5.17**). This is interesting because EBNA3 mediated repression often involves Polycomb repressor complexes (PRC) and leads to the silencing of genes by H3K27me3. Whereas, there is no evidence for EBNA2 mediated repression involving PRC. Therefore, the binding data suggests the repressive effect of EBNA3 on PI3K-Akt signalling genes to be independent of PRC.

We also observed cell type-specific regulation for some target genes from PI3K-Akt signalling by EBNA3 family members. For example, *PIK3R3* was activated by EBNA3A, EBNA3B and EBNA3C in BL whereas this gene was repressed by EBNA3C in LCLs based on the TaqMan array card analysis. Similar observation was shown for EBNA3 regulation of *CCL3* and *CCL4* (chemokines) wherein EBNA3A repress the expression of these genes in BL and activates them in LCLs (McClellan *et al.*, 2012). One possible reason for cell type-specific regulation could be a result of the relative expression of EBNA2 and EBNA3 family proteins in these cell backgrounds.

We also observed EBNA2, EBNA3A and EBNA3C repressed *INPP5D* (*SHIP-1*) in addition to the modulation of other genes such as *LYN*, *SYK*, *PIK3R1*, *PIK3R3* and *PIK3R5* in the PI3K-Akt pathway (**Table 5.4 and 5.5**). As mentioned earlier, INPP5D acts as a negative regulator of the PI3K-Akt pathway leading to reduced phosphorylation of Akt (Ser473, Thr308). Although we observed repression of INPP5D which would increase active Akt phosphorylation, the net effect of EBNA2 and EBNA3 in LCL and BL leads to removal of active phosphorylation on Akt thereby repressing PI3K-Akt mediated downstream signalling. One possible explanation for this could be the negative effects on upstream components and *PIK3R3* and *PIK3R5* which override the effects of *INPP5D* repression. To understand whether BCR signalling is repressed by EBNA2 and EBNA3 in cells, it will be important to examine their effects when BCR is activated by antigen, rather than looking at the steady state effects in the absence of stimulation.

Overall this chapter confirms the transcriptional regulation of previously identified EBNA2 and EBNA3 targets and also identified new targets from BCR signalling. It highlights the cooperative and antagonist effect of EBNA2 and EBNA3 proteins on cellular reprogramming. Moreover, downregulation of the PI3K-Akt pathway through reduced Akt (Ser473, Thr308) phosphorylation suggests a strategy used by EBV to bias survival outcomes.

6 Discussion

EBV is a gamma herpesvirus associated with numerous human cancers e.g. Burkitt's lymphoma, Diffuse large B cell lymphoma, Hodgkin's lymphoma, nasopharyngeal carcinoma, gastric carcinoma, AIDS-related lymphomas as well as post-transplant lymphoproliferative disease. The virus preferentially infects and immortalise B cells by modulating the expression of host genes from several growth and survival pathways such as NF-κB, PI3K-Akt, and chemokine receptor signalling pathways. Many cell cycle regulatory pathways are also deregulated by the EBNA3 family of proteins thereby driving EBV-mediated B-cell transformation. RGC-32, atypical CDK1 activator, is expressed in many tissues and has been reported to be deregulated in numerous cancers suggesting its role in tumorigenesis. Our laboratory identified RGC-32 expression to be upregulated in primary B cells upon EBV infection through relief of Pumilio-mediated translational repression. We have shown RGC-32 expression to be crucial for survival of EBV-infected cells. Pumilio proteins repress the expression of many cell-cycle regulatory proteins including the expression of atypical CDK1 activator, RINGO/Speedy protein which is a functional homologue of RGC-32 (Padmanabhan and Richter, 2006). In this study, we investigated the role of RGC-32 in regulating G2/M transition. We also characterised the molecular mechanism of interaction of RGC-32 with crucial cell-cycle regulatory proteins, CDK1 and Spc24-25. Our studies show RGC-32 to activate CDK1 *in vivo* through inhibition of Wee1 kinase thereby contributing to our understanding of cell cycle regulation by EBV. Interestingly, microarray studies identified *Wee1* repression by EBNA3C in EBV-infected cells further suggesting different mechanisms for suppression of the negative effects of Wee1 on G2/M transition in EBV-infected cells.

To further understand the role of EBNA2 and EBNA3 in promoting growth and survival of infected cells, ChIP-seq experiments were carried out in our laboratory that mapped binding sites for EBNA2 and EBNA3 in B cell genome. We found the B cell receptor (BCR) signalling as a top enriched pathway for genes close to EBNA2 and EBNA3 binding sites. We identified the key genes from the BCR signalling pathway that are regulated by EBNA2 and EBNA3 and studied the impact of this regulation on the PI3K-Akt pathway. Our study suggests EBNA2, EBNA3A and EBNA3C proteins to suppress PI3K-Akt signalling as a result of reduced active Akt phosphorylation in both Burkiit's lymphoma and Lymphoblastoid cell lines.

6.1 Molecular characterisation of RGC-32 interaction with cell cycle proteins.

In vitro pull-down studies showed RGC-32 to be able to bind CDK1 (Badea *et al.*, 2002). This observation was contradicted by another group as their immunoprecipitation studies did not show cyclin B to precipitate with RGC-32 in HEK 293T cells (Saigusa *et al.*, 2007). These two reports raise a question on whether RGC-32 bind to CDK1 alone rather than the CDK1-Cyclin B complex. However, this aspect has not been addressed to date. Preliminary studies in our laboratory confirmed the binding of RGC-32 to both CDK1 and PLK1 from B cell lysates. We further investigated the binding of RGC-32 with CDK1 using SPR in collaboration with Prof. Jane Endicott. Our results provide the first evidence that RGC-32 binds directly to CDK1 with the binding kinetics suggesting RGC-32 to fold upon binding which is consistent with the behaviour of a protein with no hydrophobic core (**Figure 3.5C**). However, the binding affinity of RGC-32 to CDK1 improved in the presence of cyclin B (**Figure 3.5D**). This observation was further confirmed by Microscale thermophoresis (MST) studies, an analogous biophysical technique that we

used to verify the interaction between RGC-32 and CDK1 (**Figure 3.8**). Importantly, RGC-32 could not bind to CDK2-Cyclin A complex confirming a previous observation by Badea *et al*. that RGC-32 does not interact with CDK2-Cyclin A and has specificity towards CDK1 (Badea *et al.*, 2002).

To understand the mode of binding of RGC-32 to CDK1 and a possible role of cyclin B in this interaction, a model of the ternary complex between RGC-32 and CDK1-Cyclin B (PDB 4YC3) was generated using Z-Dock, an online docking server (**Figure 6.1**) (Pierce *et al.*, 2014). The Z-dock program calculated the model based on every possible combination allowed in the translational and rotational space of the two structures, evaluating each of the model based on energy-minimising function. We observed RGC-32 (cyan) to interact exclusively with CDK1 (brown) and make no direct contact with cyclin B (green). Also, RGC-32 bound at the opposite side of the activation segment of CDK1 (146-173 amino acids). The activation segment of CDK1 provides a platform for peptide substrate recognition upon phosphorylation. Therefore, this model suggested that RGC-32 may influence CDK1 activity allosterically (**Figure 6.1**). A close-up of the interaction surface of RGC-32 with CDK1 revealed RGC-32 to interact with CDK1 via its region consisting of 26-50 amino acid, an observation that was previously identified by pull-down studies carried out by Dr Lina Chen in our laboratory as a region required for the RGC-32-CDK1 interaction (Unpublished data). The presence of charged residues at the interaction interface suggested an electrostatic interaction (e.g. salt-bridge, H-bonds) between RGC-32 and CDK1.

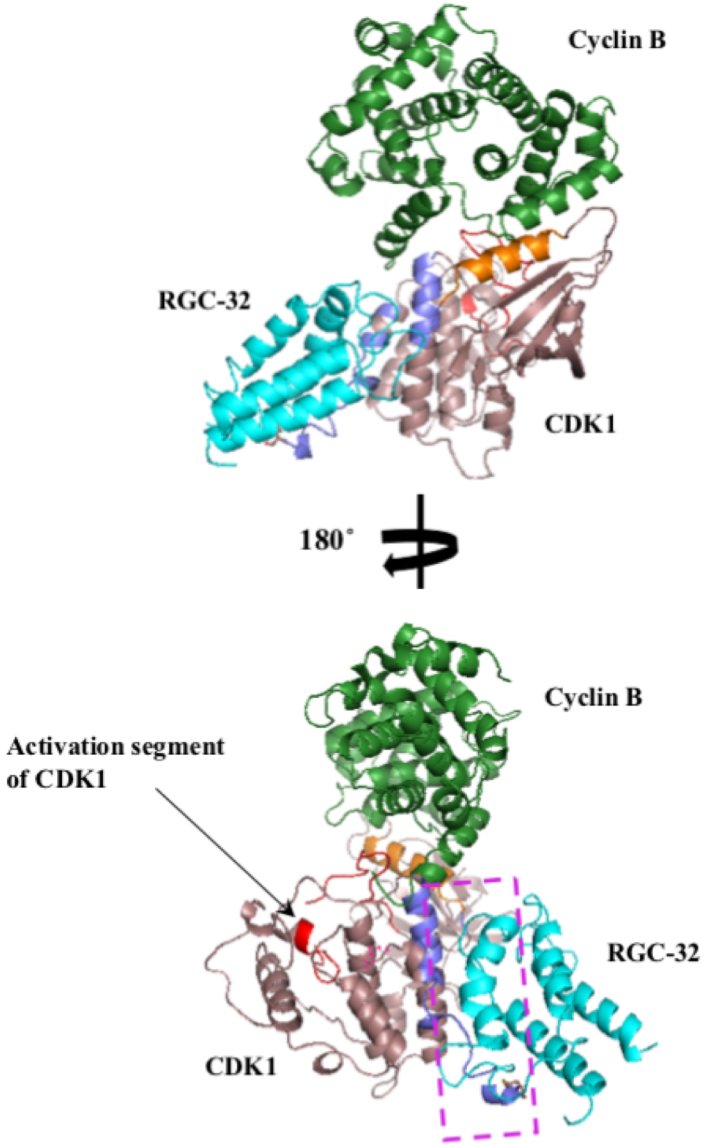

Figure 6.1 Model of RGC-32 binding to CDK1-Cyclin B complex.
Dock model of RGC-32-CDK1-Cyclin B ternary complex coloured in cyan, brown and green respectively. The activation segment of $CDK1_{(146\text{-}173\ aa)}$ is coloured in red, C-helix of $CDK1_{(45\text{-}59\ aa)}$ is coloured in orange and the blue region highlights the RGC-32 interaction interface on CDK1. The magenta dotted rectangle highlights the region 26-50 amino acids of RGC-32 that was observed to be crucial for CDK1 binding in mapping studies. The model shows possible mode of interaction of RGC32 with the CDK1-Cyclin B complex (PDB 4YC3). This model was generated using Z-dock (Pierce *et al*., 2014).

We observed potential salt-bridge formation between CDK1 K279 and RGC-32 E35, CDK1 D289 and RGC-32 K41 and CDK1 K296 and RGC-32 D10 (**Figure 6.2**).

Structural studies have shown conformational adjustments in CDK1 upon cyclin B binding (Brown *et al.*, 2015). Although most of this conformational change is not observed in the C-terminal loop of CDK1 (279-296 amino acids) to which RGC-32 mainly binds. Significant movement occurs in the C-helix (45-59 amino acids) that spans between the cyclin B and RGC-32 binding sites on CDK1 (highlighted by the red dotted oval, **Figure 6.3**). Interestingly, one amino acid residue (H60) from the loop (60-67 amino acids) was predicted to make contact with RGC-32. It is possible therefore to speculate that the conformational changes in this region as a result of cyclin B binding might allow positioning of the C-helix (45-59 amino acids) and the loop (60-67 amino acids) in a more favorable conformation for RGC-32 to bind. In future, it will be important to perform mutagenesis studies to test the model and determine the contribution of H60 residue of CDK1 in the interaction with RGC-32 and to mutate key residues in the C-terminal loop (276-296 amino acids) and in the 26-51 amino acid region of RGC-32 to validate their interaction and test their contribution.

To explore if our model exhibited an interaction of RGC-32 that is specific for CDK1, we performed sequence alignment of CDK1 with CDK2. Although CDK1 has 65% sequence identity with CDK2, the region of CDK1 that was predicted to interact with RGC-32 is not conserved in CDK2 (**Figure 6.4**). This supports our observation of RGC-32 binding specifically to CDK1-Cyclin B and not to CDK2-Cyclin A in MST studies.

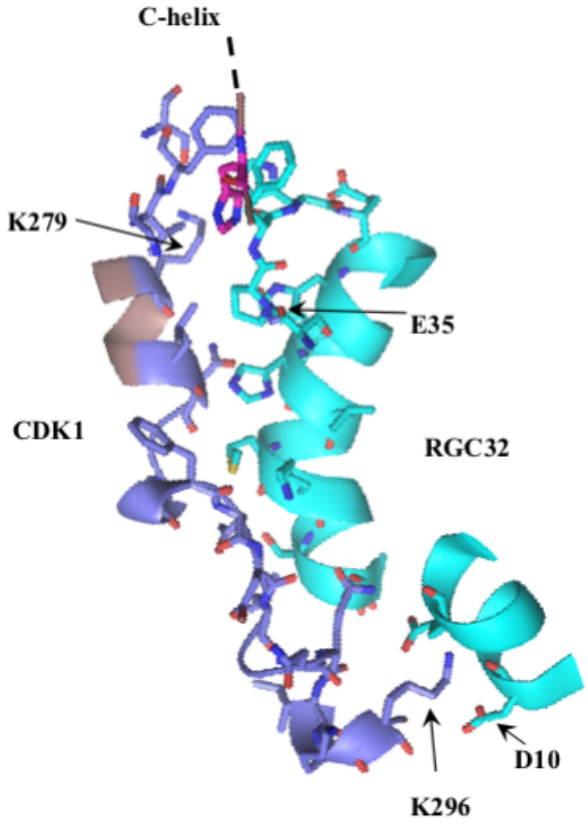

Figure 6.2 Close-up view of the RGC-32-CDK1 binding interface.
A zoom-in on the model of ternary complex showing the interaction interface between RGC-32 (cyan) and CDK1 (blue). The figure shows the interaction could be mediated by electrostatic interactions as highlighted by presence of lot of charged residues at the interface (CDK1 K279- RGC-32 E35, CDK K296- RGC-32 D10, CDK1 D289- RGC-32 K41*). Residue H60 in C-helix of CDK1 highlighted in magenta. This residue is present in the loop that undergoes conformational change when CDK1 is bound to Cyclin B. One pair of interacting residues '*' could not be shown in the figure as the residues are buried in the structure.

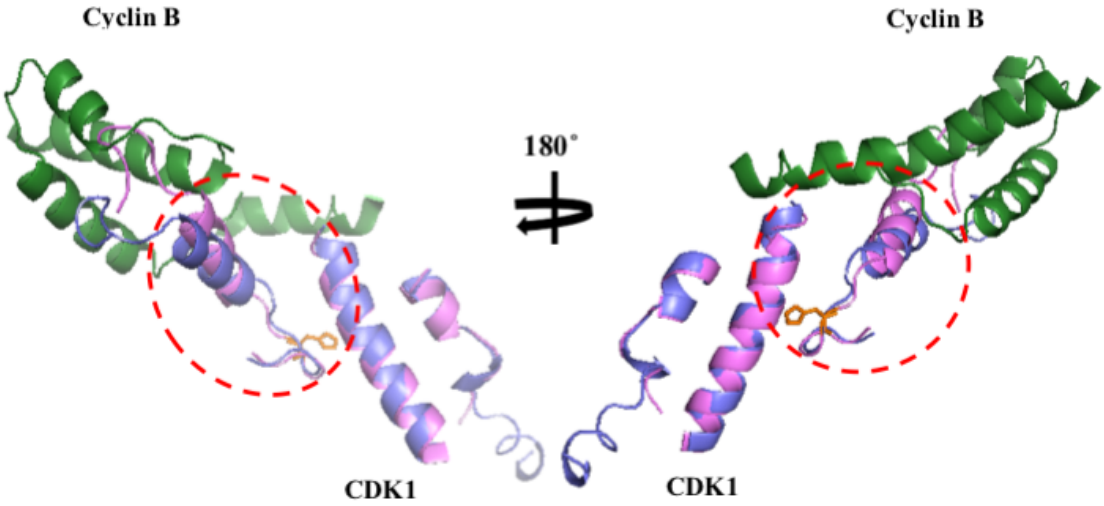

Figure 6.3 Conformational change in CDK1 when bound to Cyclin B.
Structure of CDK1 in unbound (blue, PDB 4YC6) and Cyclin B-bound (brown, PDB 4YC3) states. CDK1 interacting region of Cyclin B is highlighted in green. The red dotted circle highlights the region that undergoes conformational changes in CDK1 upon Cyclin B binding. The H60 residue in the CDK1 loop (60-67) that possibly makes contact with RGC-32 is coloured in orange.

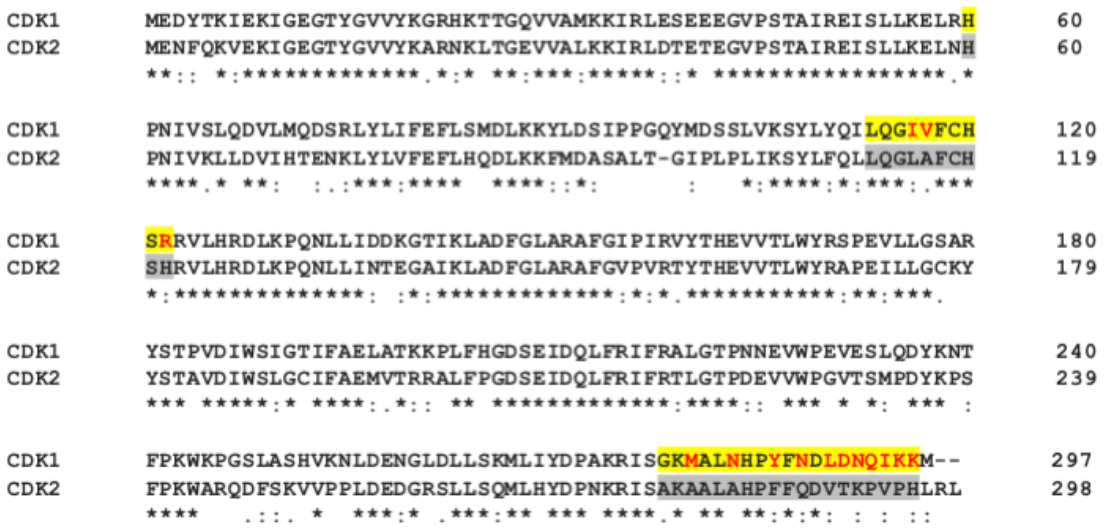

Figure 6.4 Sequence alignment of human CDK1 with CDK2 (65 % sequence identity).
Sequence alignment of human CDK1 with CDK2 using Clustal Omega online server. The potential RGC-32 binding sites on CDK1 are highlighted in yellow. The corresponding regions in CDK2 are highlighted in grey. The red amino acid residues show the differences between CDK1 and CDK2 within the RGC-32 binding region.

Overall, our model suggested that RGC-32 binds to CDK1 directly and not to cyclin B. However, cyclin B might play a role in the interaction between CDK1 and RGC-32 by causing a conformational change in the CDK1 structure upon binding which affects the RGC-32 interaction region. This would be in agreement with the observations from SPR and MST studies where we observed that the affinity of RGC-32 binding is higher in the presence of cyclin B. Moreover, the presence of charged residues also suggests that RGC-32 and CDK1 interact with each other predominantly through electrostatic interactions. It would be interesting to solve the three dimensional structure of this complex in collaboration with Endicott laboratory to validate the interaction between these proteins.

During the course of this study, we identified similarity (37 % sequence identity) between the 3rd predicted α-helix of RGC-32 and a receptor motif in the N-terminus of a histone-fold protein CNN-1 from *Saccharomyces cerevisiae* (**Figure 3.10**). CNN-1 binds to the Spc24-25 heterodimer of the NDC80 complex, a microtubule binding component of kinetochore, as a 'molecular hook' ensuring the attachment of microtubules to the kinetochores (Malvezzi *et al.*, 2013). The interaction of CNN-1 with Spc24-25 requires three hydrophobic residues F69, L70 and L73 which bind in a hydrophobic pocket present in the yeast Spc24-25 globular domains. The alignment between CNN-1 and RGC-32 highlighted that two of the interacting residues were conserved in RGC-32 (F106, I107 and L110) whereas the central Leucine (L) in CNN-1 was an Isoleucine (I) in the corresponding position in RGC-32. As we could not express enough of human Spc24-25 recombinant protein, interaction studies were carried out using chicken Spc24-25 globular domains (~60 % identity to human) showing direct binding of RGC-32 to these heterodimers with high affinity therefore suggesting a specific interaction between these

proteins (**Figure 3.16**). This was further confirmed by immunoprecipitation studies in DG75 and HEK 293 cells (**Figure 3.17-3.18**).

The crystal structure of yeast CNN-1 in complex with Spc24-25 globular subunits shows CNN-1 to adopt a α-helical structure upon binding to Spc24-25 (Malvezzi *et al.*, 2013). CNN-1 helix binds in a hydrophobic pocket of Spc24-25 domains through interaction with the 1st helix of each Spc24 and Spc25 subunit resulting into a three-helix bundle (**Figure 6.5A**). The crystal structure of the phosphomimetic chicken homologue of CNN-1 (CENP-T) with chicken Spc24-25 shows CENP-T peptide to consist of two α-helices. The 2nd α-helix of CENP-T which has the conserved region with CNN-1 binds in the hydrophobic pocket of Spc24-25 similar to CNN-1 (**Figure 6.5B**) (Nishino *et al.*, 2013). Both CNN-1 and CENP-T have majority of binding interface associated with the β-sheet of Spc25. However, CENP-T makes an additional contact with the 1st helix of Spc24 which is not observed in CNN-1-Spc24-25 complex in yeast. Unlike CNN-1, CENP-T binds weakly to Spc24-25 and the affinity improves upon phosphorylation on its N-terminal residues (Thr72, Ser88). These residues are not directly involved in the interaction with Spc24-25 but they form a salt-bridge allowing orientation of hydrophobic residues of CENP-T towards Spc25 thereby increasing the affinity of their interaction (Nishino *et al.*, 2013). We showed RGC-32 to bind more efficiently to Spc25 than Spc24 in DG75 cells by immunprecipitation studies. This suggests that RGC-32 may behave more like CNN-1 in its mode of interaction to Spc24-25 rather than like CENP-T. This is further evidenced by the structural similarity between CNN-1 and RGC-32 with Spc24-25 globular domains (**Figure 3.19**).

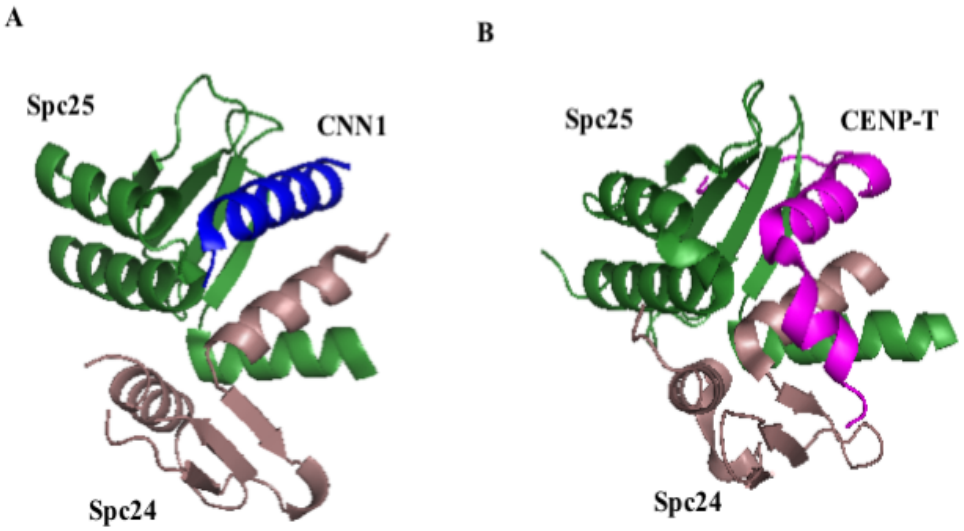

Figure 6.5 Crystal structure of CNN-1 (yeast) and CENP-T (chicken) with Spc24-25.
(A) CNN-1$_{(60\text{-}84\ aa)}$ (blue) in complex with Spc24$_{(155\text{-}213\ aa)}$ (brown) and Spc25$_{(133\text{-}221\ aa)}$ (green) (PDB 4GEQ). (B) Phospho-mimetic complex of chicken CENP-T$_{(69\text{-}93\ aa)}$ (magenta) with Spc24$_{(134\text{-}195\ aa)}$ (brown) and Spc25$_{(134\text{-}232\ aa)}$ (green) (PDB 3VZA). The crystal structure also highlights the orientation of the CNN1/CENP-T helix while in interaction with the Spc24-25 heterodimer.

Interestingly, the interaction of RGC-32 with CDK1 leads to phosphorylation of RGC-32 on Thr91 (Badea *et al.*, 2002). This residue lies in close vicinity of the Spc24-25 interaction surface of RGC-32. Although we observed efficient binding of unphosphorylated RGC-32 to Spc24-25, it would be interesting to determine whether phosphorylation on Thr91 of RGC-32 improves its affinity as a result of additional contacts similar to CENP-T.

6.2 Does RGC-32 localise to kinetochores through interaction with Spc24-25?

Ectopic expression of Myc-RGC-32 in glioma cells (U-87MG) showed the protein to be cytoplasmic during interphase. As these cells progressed into prophase, an increased RGC-32 signal was observed at the centrosomes and spindle poles with maximal signal observed during prometaphase and metaphase (Saigusa *et al.*, 2007). Our localisation studies in HeLa cells showed RGC-32 protein to be cytoplasmic during interphase and to translocate to the nucleus during prophase (**Figure 4.1A**). Consistent with the previous observation, RGC-32 was also observed at spindle poles during metaphase (**Figure 4.1B**). Live cell imaging studies showed RGC-32 to translocate into the nucleus in a similar manner to cyclin B before the breakdown of the nuclear envelope. Cyclin B is known to shuttle between the nucleus and cytoplasm as a result of phosphorylation of its serine residues in the cytoplasmic retention (CRS) and nuclear export signal (NES). PLK1, a key mitotic regulator, promotes this nuclear translocation by phosphorylating cyclin B on Ser133 and Ser147 (Toyoshima-Morimoto *et al.*, 2001). Interestingly, RGC-32 does not have a nuclear localisation signal (NLS), therefore the translocation of RGC-32 could possibly be mediated upon binding to the CDK1-Cyclin B complex. Live cell imaging studies were also carried out to determine whether RGC-32 co-localises with CENP-A, a

kinetochore marker, as a result of interaction with Spc24-25 kinetochore subunit. However, CENP-A did not localise to the kinetochores but marked the entire chromosome making it difficult to study co-localisation of these proteins.

Previous pull-down studies in our laboratory showed RGC-32 to bind both CDK1 and PLK1 in B-cell lysates. Further, mapping studies using C-terminal truncation constructs were carried out to determine the binding sites of PLK1 on RGC-32 (Dr Lina Chen). These pull-down studies showed PLK1 to bind to a distinct but adjacent region to the CDK1 interacting region. While the CDK1 interacting region was mapped to amino acids 26-50 on RGC-32, PLK1 binding was mapped to amino acids 51-75 on RGC-32 (unpublished data). However, we do not know yet whether these kinases bind simultaneously or sequentially to RGC-32. To address this a three-way pull-down or immunoprecipitation study could be carried out in future. Since PLK1 is known to stabilize the kinetochore-microtubule attachment, interaction of RGC-32 with PLK1 is interesting as RGC-32 has also been shown to bind directly to Spc24-25 heterodimer of kinetochore (**Figure 3.15B**). PLK1 localises to kinetochores during prometaphase to stabilise the initial kinetochore-microtubule attachments. During metaphase, PLK1 signal decreases dramatically at the kinetochores to relieve the PLK1-mediated suppression of bioriented kinetochore-microtubules dynamics (Liu *et al.*, 2012). Several studies have reported nuclear proteins that aid the recruitment of PLK1 to kinetochores are also a substrate of CDK1. A role for Bub1 (Budding uninhibited by benzimidazole 1) in the recruitment of PLK1 to the kinetochores has been reported. Bub1 is a serine/threonine kinase that localises to kinetochores during mitosis and plays a role in the spindle checkpoint (Taylor *et al.*, 2001, Qi *et al.*, 2006). The recruitment of PLK1 by Bub1 at kinetochores is dependent on CDK1 phosphorylation of Bub1 at Thr609 and binding of

Bub1 to the polo-box domain (PBD) of PLK1 (Qi *et al.*, 2006). Another group reported recruitment of PLK1 to kinetochores to be mediated by a cytoplasmic linker protein (CLIP) 170. The interaction between CLIP-170 and PLK1 is dependent on the binding of CLIP-170 to the PBD of PLK1 and phosphorylation of CLIP-170 on Thr287 by CDK1 (Amin *et al.*, 2014). Recently, a role of PLK1 in the maintenance of spindle assembly checkpoint (SAC) has also been reported. This function of PLK1 is dependent on binding of PLK1 to Bub1 and not CLIP-170 (Ikeda and Tanaka, 2017). RGC-32 has the ability to bind PLK1 via its PBD and has been shown to be phosphorylated by PLK1 (Saigusa *et al.*, 2007). Since RGC-32 act as a substrate of CDK1 and interacts with Spc24-25 subunit of the kinetochore, it would be interesting to investigate whether RGC-32 plays a similar role to Bub1 and CLIP-170 in the recruitment of PLK1 to the kinetochore. It will also be interesting to examine whether the interaction of RGC-32 with CDK1 and PLK1 is temporal and occur as a two-stage process. For example, RGC-32 could first interact with CDK1 during the G2/M transition leading to RGC-32 phosphorylation and subsequent activation of CDK1. RGC-32 could then translocate to the nucleus in complex with CDK1-Cyclin B. Following translocation and during early prophase, RGC-32 may then dissociate from the CDK1-Cyclin B complex and interact with PLK1 during prometaphase thereby promoting the recruitment of PLK1 at kinetochores through interaction with Spc24-25 subunit (**Figure 6.6**). This model could be tested by studying co-localisation of RGC-32 with PLK1 at the kinetochores during prometaphase using the U2OS cdk1as eGFP-RGC-32 stable cell line.

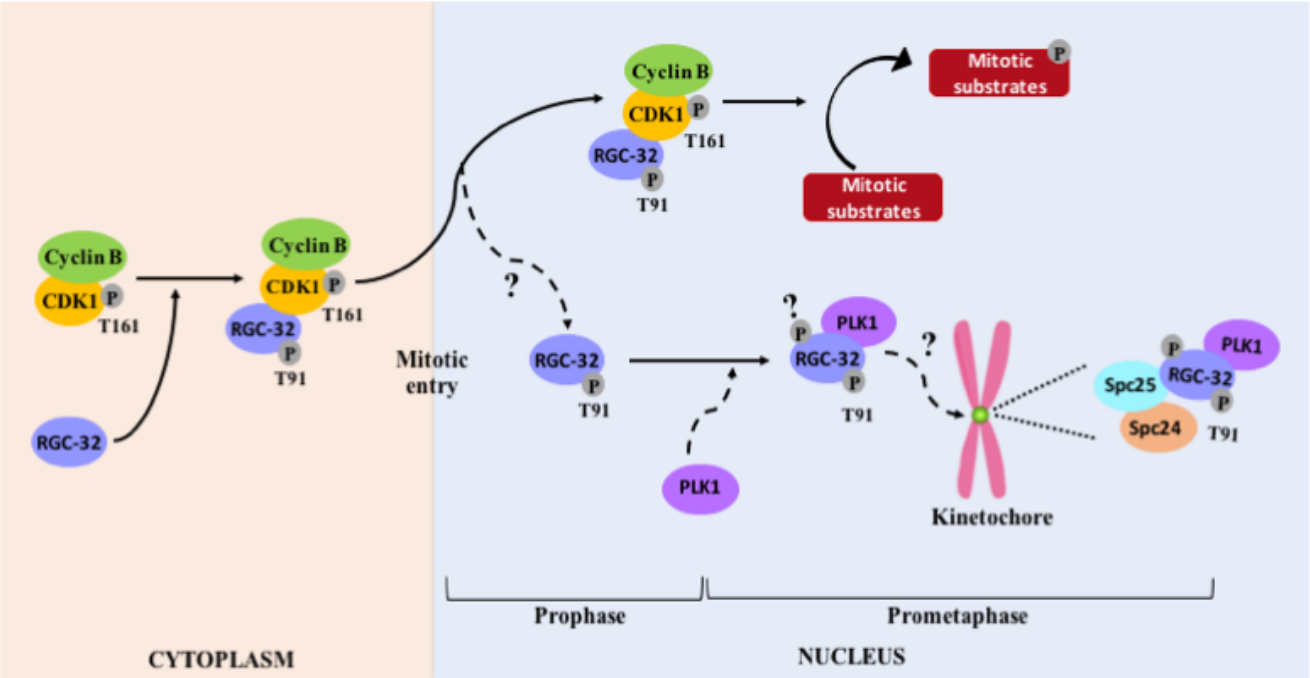

Figure 6.6 Model for temporal interaction of RGC-32 with mitotic kinase, CDK1 and PLK1.
RGC-32 binds to the CDK1-Cyclin B complex which leads to the phosphorylation of RGC-32. Phospho RGC-32 further enhances the activation of CDK1-Cyclin B. Upon complete activation, the CDK1-Cyclin B-RGC-32 complex translocates to the nucleus during prophase where CDK1 substrate phosphorylation leads to the onset of mitosis. It is possible that RGC-32 either remains bound to CDK1 mediating its substrate phosphorylation or it dissociates from CDK-Cyclin B complex and binds to PLK1 at the Polo box domain. PLK1 phosphorylates RGC-32 upon binding which may be followed by recruitment of PLK1 to kinetochores through interaction of RGC-32 with the Spc24-24 subunit from the NDC80 complex

6.3 What is the mechanism of RGC-32 mediated activation of CDK1?

RGC-32 is not homologous to any other human protein but is functionally similar to the RINGO/Speedy protein family in *Xenopus*. RGC-32 increases CDK1 kinase activity *in vitro* similar to RINGO family proteins (Badea *et al.*, 2002). RINGO has the ability to bind and induce CDK1 activation in the absence of cyclin B both *in vitro* and *in vivo* (Ferby *et al.*, 1999). Previous *in vitro* kinase assays by our laboratory using recombinant RGC-32 confirmed the activation of CDK1 (Schlick *et al.*, 2011). However, RGC-32 binds to CDK1 with higher affinity in the presence of cyclin B suggesting the possibility of RGC-32 and RINGO proteins to activate CDK1 could be different. Previous studies have reported the inability of RGC-32 to activate CDK1 in the presence of the CDK inhibitor $p27^{KIPI}$ (Badea *et al.*, 2002). $p27^{KIPI}$ binds inside the catalytic cleft of CDK mimicking ATP thereby leading to cell cycle arrest as a result of inhibition of CDK enzymatic activity (Russo *et al.*, 1996, Lloyd *et al.*, 1999). This could mean that binding of $p27^{KIPI}$ to CDK1 possibly inhibits CDK1 mediated phosphorylation of RGC-32 in addition to other substrates. As phosphorylation of RGC-32 at Thr91 and RGC-32-mediated activation of CDK1 are interdependent, it would explain the inability of RGC-32 to activate CDK1 in the presence of $p27^{KIPI}$. In contrast, RINGO proteins have been shown to activate CDK1 in the presence of $p27^{KIPI}$ (Lenormand *et al.*, 1999, Porter *et al.*, 2002, Barnes *et al.*, 2003). This further supports different modes of atypical activation of CDK1 adopted by RGC-32 and RINGO.

RINGO/Speedy proteins have been shown to promote G2/M progression in *Xenopus* oocytes (Ferby *et al.*, 1999). We carried out mitotic entry studies by specifically inhibiting CDK1 activity using an ATP-analogue, 1NM-PP1 in U2OS cdk1as cells inducibly expressing eGFP-RGC-32 to investigate RGC-32 mediated CDK1 activation *in vivo*. In

these mitotic entry studies, we showed that there are increased number of mitotic cells in the presence of RGC-32 soon after removal of CDK1 inhibition by 1NM-PP1 (**Figure 4.9**). Thus implicating a role of RGC-32 in driving cells into mitosis by activation of CDK1. Further investigation into the mechanism of activation showed reduced inhibitory phosphorylation on Tyr15 of CDK1 in the presence of RGC-32 (**Figure 4.13 and 4.14)**. Therefore, the activation of CDK1 by RGC-32 could be a result of inhibition of the Wee1 kinase which is responsible for inactivating CDK1 by Try15 phosphorylation. During G2/M transition, phosphorylation on Ser123 and Ser53 of Wee1 by CDK1-Cyclin B and PLK1 respectively initiates a cascade of events leading to degradation of the Wee1 kinase (reviewed in (Perry and Kornbluth, 2007)). It would be interesting to determine whether RGC-32 inactivates Wee1 kinase by phosphorylation on either of these serine residues by fixed cell immunofluorescence using antibodies specific to phosphorylation of serine residues of Wee1 kinase.

Increased phosphorylation on Ser/Thr substrates of CDK was also detected in the presence of RGC-32. Binding of small regulatory proteins to CDK1 plays an important role in controlling critical events of the cell cycle. Cyclin-dependent kinase subunit (Cks) proteins, Cks1 and Cks2, bind to CDKs and cyclins (Zhang *et al.*, 2004). Binding of Cks proteins to CDK1 enhances the phosphorylation of selected substrates at mitosis (Patra *et al.*, 1999). It is possible that RGC-32 could play a similar role to Cks proteins resulting in increased phosphorylation of particular CDK substrates. Saigusa *et al*. reported overexpression of RGC-32 to delay mitotic progression in HeLa cells suggesting a role of RGC-32 in inhibition of mitotic exit (Saigusa *et al.*, 2007). Interestingly, preliminary localisation studies of RGC-32 in HeLa cdk1as cells showed cells expressing RGC-32 remained in early mitosis (prophase) for longer as compared to control population (data

not shown). During mitotic exit, active APC/C (Anaphase promoting complex/ cyclosome) degrades cyclin B by ubiquitination during the metaphase-anaphase transition (Hershko *et al.*, 1991). This leads to dephosphorylation of the mitotic substrate due to reduced CDK1 activity eventually resulting into mitotic exit (Wheatley *et al.*, 1997, Kramer *et al.*, 2000). It could be possible that RGC-32 delays mitotic exit by keeping CDK1 active for longer duration. We carried out preliminary experiment to address this phenomenon. Mitotic exit in cells expressing RGC-32 was studied by treating cells synchronised in mitosis with different concentration of 1NM-PP1, as inhibition of CDK1 should push cells out of mitosis. The percentage of cells exiting mitosis was obtained by counting the number of mitotic cells versus interphase cells using the nuclear stain (SiRDNA). The difference between control and RGC-32 expressing cells exiting mitosis was not very high (data not shown) and would need further optimization in future.

6.4 Role of BCR signalling in Leukemia and B cell lymphomas.

B-cell receptor decides the fate of B cells by guiding the development of immature B-cells either into Germinal center B-cell (Plasma and Memory) or Marginal zone B-cell (Yam-Puc *et al.*, 2018). BCR signalling is critical for promoting growth and survival of normal B cells and it can induce apoptosis of malignant B cells (Niiro and Clark, 2003). There has been increasing evidence of the BCR signalling pathway being involved in a variety of B cell lymphomas such as activated B-cell like (ABC) Diffuse large B-cell lymphoma (DLBCL) and follicular lymphoma. It has been shown to play a central role in the genesis of Chronic lymphocytic leukaemia (CLL) and therapeutic studies using kinase inhibitors for SYK, BTK and PI3K (Fostamatinib, Ibrutinib and Idelalisib) have shown to be effective in the treatment of CLL (reviewed in (Burger and Chiorazzi, 2013) therefore suggesting activation of the PI3K-Akt pathway in CLL.

We have now shown EBNA2 and EBNA3 to target multiple pathways downstream of BCR highlighting their role in the regulation of BCR mediated survival and growth of infected cells. TaqMan array card analysis in Burkitt's lymphoma (BL) and Lymphoblastoid cell lines (LCLs) showed majority of the genes from calcium signalling and PI3K-Akt signalling to be repressed by EBNA2 and EBNA3 proteins (**Table 5.4 and 5.5**). This thesis focused on the effects of EBAN2 and EBNA3 on the PI3K-Akt pathway in which regulation of some of the target genes was observed to be cell-type specific for example *PIK3R3*, which could be due to the difference in signalling pathways between cell backgrounds. In Burkitt's lymphoma, several signalling pathways are distorted during the outgrowth of cell line especially the constitutive activation of *MYC* via translocation. Whereas, LCLs are established by EBV-infection of naïve B cells *in vitro*, providing more physiological relevance to EBV-infection of B cells. Irrespective of the differences in mRNA regulation between different cell backgrounds, we found the net effect of EBNA2, EBNA3A and EBNA3C proteins in both cell background lead to the suppression of the PI3K-Akt pathway as a result of reduced active phosphorylation of Akt (Thr308, Ser473) (**Figure 5.21-5.23**). EBV also exploits BCR signalling through the function of its latent membrane proteins LMP1 and LMP2A. LMP2A mimics active BCR by associating with SYK and LYN protein tyrosine kinases as well as it has the ability to block active BCR through recruitment of E3 ubiquitin ligase which leads to degradation of SYK and LYN tyrosine kinases (Burkhardt *et al.*, 1992, Miller *et al.*, 1993). Blocking of BCR by LMP2A reduces intracellular calcium mobilization in cells. LMP1 is known to activate the PI3K-Akt pathway by phosphorylation of Akt on Ser473 (Dawson *et al.*, 2003). This positive and negative modulation of BCR signalling by EBV latent proteins could be a strategy employed by the virus to promote growth-survival balance of EBV-

infected cells. Additionally, as BCR signalling plays a role in differentiation, suppression of BCR-mediated downstream signalling may enable the virus to maintain viral persistence without the activated blasts undergoing differentiation into plasma cells.

BCR-mediated PI3K-Akt signalling has generally been reported to be activated in B-cell lymphomas which contradicts with our observation in BL and LCLs. A possible explanation for this could be the steady state of BCR in these cell lines. It will be important to stimulate BCR signalling by antigen in these cells and examine the effects of EBNA2 and EBNA3 regulation on PI3K-Akt signalling. A role of the microenvironment in controlling BCR signalling in B-cell malignancies has also been reported (reviewed in (Rickert, 2013)) which could not be investigated in our studies. Therefore, it would be important to take into account the effect of cross-talk between the BCR signalling and various microenvironment factors. Moreover, PI3K and Akt are involved in many other signalling pathways and can be induced by various receptors such as Integrin, RTK (receptor tyrosine kinase) and Cytokine in addition to BCR. EBV is known to downregulate genes from integrin receptor signalling pathway (McClellan *et al.*, 2012). Therefore, the net effect of EBNA2 and EBNA3 observed on PI3K-Akt signalling may not be specific to BCR pathway and will need further examination of upstream signalling molecules to fully elucidate EBNA2 and EBNA3 mediated regulation of the PI3K-Akt pathway.

In summary, our studies have unravelled some of the important aspects of EBV-mediated growth and survival of infected cells. We identified a key function of RGC-32 in G2/M transition by activation of CDK1 through the removal of ‘inactivating’ phosphorylation on Tyr15 of CDK1. We also identified a new pathway regulated by EBNA2 and EBNA3

and showed negative regulation of the PI3K-Akt pathway through decreased ‘activating’ phosphorylation of Akt by EBNA2, EBNA3A and EBNA3C. These findings from our study help us increase our understanding of how EBV immortalises B cells and promotes lymphoma development.

7 Appendix

7.1 Antibodies (Western Blotting)

Antibody	Host	Dilution	Type	Reference/Company
Anti-PLK1	Mouse	1:1000	monoclonal	Abcam (#ab 14210)
Anti-Spc24	Rabbit	1:500	monoclonal	Abcam (#ab 157184)
Anti-Spc25	Rabbit	1:250	polyclonal	Abcam (#ab 20679)
Anti-RGC-32	Rabbit	1:2000	polyclonal	In-house (#ab 2818)
Anti-Cyclin B1	Rabbit	1:200	polyclonal	Santa cruz biotechnology (#SC752)
Anti-Cyclin B2	Mouse	1:500	monoclonal	Santa cruz biotechnology (#SC28303)
Anti-CDK1	Rabbit	1:1000	monoclonal	Abcam (#ab133327)
	Mouse	1:1000	monoclonal	Invitrogen (#33-1800)
Anti-Cyclin A2	Mouse	1:200	monoclonal	Abcam (#ab 38)
Anti-GFP	Rabbit	1:1000	polyclonal	Life technologies (#A6455)
Anti-FLAG M2	Mouse	1:1000	monoclonal	Sigma (#F1804)
Anti-IRF4	Goat	1:2000	polyclonal	Santa cruz biotechnology (#SC6059x)
Anti-LMP1	Mouse	1:300	monoclonal	Abcam (#ab78113)

Antibody	Host	Dilution	Type	Reference/Company
Anti-Akt (pan)	Rabbit	1:500	monoclonal	Cell signalling technologies (#C67E7)
Anti-Akt (phospho T308)	Rabbit	1:500	monoclonal	Cell signalling technologies (#13038)
Anti-Akt (phospho S473)	Rabbit	1:400	monoclonal	Cell signalling technologies (#4060)
Anti-Actin	Rabbit	1:2000	polyclonal	Sigma (#A2066)
Anti-EBNA1 (M. Stacey serum)	Human	1:200	polyclonal	Gift from M. Rowe.
Anti-EBNA3C	Mouse	1:300	monoclonal	E3CA10 (Gift from M. Rowe, (Maunders *et al.*, 1994)
Anti-EBNA3A	Sheep	1:500	polyclonal	Exalpha Biologicals (#F115P)
Anti-EBNA3B	Sheep	1:500	polyclonal	Exalpha Biologicals (#F120P)
Anti-Actin	Rabbit	1:2000	polyclonal	Sigma (#A2066)

7.2 HRP-conjugated Antibodies

Substance	Dilution	Reference/Company
Anti-mouse IgG	1:3000	Cell signalling technologies
Anti-rabbit IgG	1:3000	Cell signalling technologies
Protein A	1:1000	Amersham

7.3 Primary Antibodies (Immunofluorescence)

Antibody	Host	Dilution	Information	Reference/Company
Anti-Phospho CDK1(Tyr15)	Rabbit	1:50	monoclonal	Cell signalling technologies (#4539)
Anti Phospho- CDK substrate Motif (K/H) pSP	Rabbit	1:100	monoclonal	Cell signalling technologies (#9477)
Anti-FLAG M2	Mouse	1:500	monoclonal	Sigma (#F1804)

7.4 Fluorescence-conjugated Antibodies

Substance	Dilution	Reference/Company
Alexa594 anti-mouse	1:2000	Life Technologies (#A31624)
Alexa594 anti-rabbit	1:2000	Life Technologies (#A31632)
Alexa647 anti-mouse	1:2000	Life Technologies (#A21235)
Alexa647 anti-rabbit	1:2000	Thermofisher (#A31573)

7.5 Primer sets for real-time PCR analysis

Target gene		Sequence
GAPDH	MW 84 (forward)	TCA AGA TCA TCA GCA ATG CC
	MW 85 (reverse)	CAT GAG TCC TTC CAC GAT ACC
ADAMDEC1	MW 486 (forward)	AGA TCC ACG ACC ATG CTC AGC T
	MW 487 (reverse)	GTG ACA TCA CTC CTA CAA GAG CC
Actin	MW 417 (forward)	CTG GCA CCA CAC CTT CTA CA
	MW 418 (reverse)	TAG CAC AGC CTG GAT AGC AA
RGC-32 (exon 3)	MW 86 (forward)	TTA TAG GAA CAG CTT CAG CTT C
	MW 87 (reverse)	CTG AGG AGT GAC AGT GGC AG
β-globlin	MW 1447 (forward)	TTA GCT GTG CTC GCG CTA CTC T
	MW 1448 (reverse)	TGG TTC ACA CGG CAG GCA TAC T
CD21 (CR2)	MW 1132 (forward)	TCT TGG CTC TCG TCG CAC
	MW 1133 (reverse)	TTA TCA CGG TAC CAA CAG CAA TG
MYC	MW 1127 (forward)	TCA AGA GGT GCC ACG TCT CC
	MW 1128 (reverse)	TCT TGG CAG CAG GAT AGT CCT T
EBNA 3A	MW 1816 (forward)	CCC CTT AAC TCA ACC CAT TAA CC

Target gene		Sequence
	MW 1817 (reverse)	CCC CTT AAC TCA ACC CAT TAA CC
EBNA 3B	MW 405 (forward)	CCC CTT AAC TCA ACC CAT TAA CC
	MW 406 (reverse)	CCC CTT AAC TCA ACC CAT TAA CC

7.6 Primer sets for PCR

Gene		Sequence
ROAS26 left arm	P1 (forward)	CTA GCC TCT TGT CGC CGA TT
	P2 (reverse)	GCC AGT AAT GGA GTT TCA CCT GTC ATT TTC
ROSA26_eGFP-RGC-32	MW 1632 (forward)	CGC ACG CGT ATC GAT AAT GGT GAG CAA GGG CGA G
	MW 1633 (reverse)	CAG AGA TCT GGA TCC ATC ACA TAC TTG CTA AAG TTT TGT CAA G
ROSA26_integration	MW 1739, P3 (forward)	GAG TTT CCT TGT CGT CAG GCC T
pGEX6P3_FLAG RGC-32	MW 1787 (forward)	CTG TTC CAG GGG CCC CTG GGA TCC ATG GAC TAC AAA GAC GAT GAC GAC
	MW 1788 (reverse)	TCG TCA GTC AGT CAC GAT GCG GCC GCT CAC ATA CTT GCT AAA GTT TTG TCA AGA TCA GC
SfiIRGC-32 ORF	MW 592 (forward)	CGG GCC TCA CTG GCC TCA CAT ACT TGC TAA AGT
	MW 593 (reverse)	GCG GCC TCA CTG GCC TCT AGA ATG AAG CCG
pEGFPN1-RGC-32	MW 1769 (forward)	CGA ATT CTG CAG TCG ACG GTA CCA GTC GAC TCT AGA ATG AAG CCG C
	MW 1772 (reverse)	CAC CAT GGT GGC GAC CGG TCC GGT ACC GGA TCC GCA CAT ACT TGC TAA AGT TTT

7.7 siRNA Sequences

Gene Name	RNA Accessions	Reference/Company
Cyclin B1	NM_031966.3	Dharmacon SMARTpool (#L-003206-00-0005)
Cyclin B2	NM_004701.3	Dharmacon SMARTpool (#L-003207-00-0005)
AllStars Negative control siRNA	-	Qiagen (#1027280)

7.8 Plasmids

Plasmid	Information	Generated by/ Company
pEGFPC3	Mammalian expression vector for N-terminal GFP-tagged protein.	Clontech
pEGFPC3_RGC-32	RGC-32 was amplified from pFLAG RGC-32 and cloned into pEGFPC3 as a KpnI/BamHI fragment.	Generated by Sarika Khasnis
ROSA26_eGFP RGC-32	eGFP-RGC-32 was amplified by PCR from pEGFPC3RGC-32 using ROSA26_eGFP-RGC-32 primer set. Both insert and ROSA26 MCS vector were digested with AgeI followed by Gibson assembly, allowing the insert to anneal to single-stranded regions of the vector.	Generated by Sarika Khasnis
pRTS-1_RGC-32	RGC-32 open reading frame was amplified by PCR from pFLAG RGC-32 using primers SfiI RGC-32 ORF primer set. The PCR product with the SfiI site introduced was then cloned into the SfiI sites of pUC19 SfiI (gift from Prof. G. Bornkamm). An SfiI fragment containing the RGC-32 ORF was then excised and cloned into the SfiI sites of pRTS-1 (gift from Prof G. Bornkamm) replacing the luciferase gene.	Generated by Sarika Khasnis
pFLAG_RGC-32	RGC-32 was amplified from BJAB E3C-4 (Wang *et al.*, 1990) cDNA using the RGC-32 primer set and cloned into pFLAG-CMV-2 as an Xba1/BamH1 fragment.	Generated by Helen Webb
pGEX6P3_RGC-32	RGC-32 was amplified from pFLAG RGC-32 and cloned into pGEX-6P3 as a BamHI/NotI fragment	Generated by Lina Chen

Plasmid	Information	Generated by/ Company
pGEX6P3_pFLAG-RGC-32	pFLAG-RGC-32 was amplified by PCR from pFLAG-RGC-32 using primers containing vector and insert sequences. T4 DNA polymerase was then used to resect regions of the pGEX6P3 vector, allowing the insert to anneal to single-stranded regions of the vector.	Generated by Sarika Khasnis
P3E (Amp)	Bacterial expression vector for N-terminal GST tagging.	Gift from Dr Chrisostomos Prodromou
p3E (Kan)	Bacterial expression vector for N-terminal GST tagging.	Gift from Dr Chrisostomos Prodromou
p3E (Amp)_ChSpc24	ChSpc24 was amplified from p2E (Amp)-ChSpc24 into p3E (Amp) as a NdeI/HindIII fragment	Generated by Sarika Khasnis
p3E (Kan)_ChSpc25	ChSpc25 was amplified from pET28b (Kan)-ChSpc25 into p3E (Kan) as a NdeI/HindIII fragment	Generated by Sarika Khasnis
p3E (Amp)_HSpc24	HSpc24 was amplified from p2E (Amp)-HSpc24 into p3E (Amp) as a NdeI/HindIII fragment	Generated by Sarika Khasnis
p3E (Kan)_HSpc25	HSpc25 was amplified from pET28b (Kan)-HSpc25 into p3E (Kan) as a NdeI/HindIII fragment	Generated by Sarika Khasnis

7.9 Cell Lines

Cell line	EBV status	Description	Reference
HeLa	Negative	Human cervical carcinoma from a 31-year old woman transformed by HPV-8.	(Scherer *et al.*, 1953)
U2OS	Negative	Human osteosarcoma cell line cultivated from the bone tissue of a fifteen-year-old Female suffering from sarcoma of tibia.	-
HEK 293	Negative	Human embryonic kidney (HEK) cells with sheared fragments of human adenovirus type 5 (Ad5) DNA	-
BJAB	Negative	African lymphoma originally classed as BL but lacks c-myc translocation.	(Menezes *et al.*, 1975)
DG75	Negative	BL from the pleural effusion of a 10-year- old boy with Burkitt's lymphoma.	(Ben-Bassat *et al.*, 1977)
IB4	Positive (Latency III)	Umbilical cord B-lymphocytes infected with EBV strain B95-8 carrying a deletion of EBV C promoter (Cp).	(Yandava and Speck, 1992)
Mutu III	Positive (Latency III)	African BL derived from a 7-year-old black male. Mutu BL drifted in culture to express a latency III pattern.	(Gregory *et al.*, 1990)
GM12878	Positive (Latency III)	Lymphoblastoid cell line transformed by EBV from the blood of a female donor with northern and western European ancestry.	-

7.10 List of cell lines used for microarrays

Cell line	Description	Reference
EBNA3A KO LCL	LCLs established by infecting with a recombinant virus lacking entire ORF of EBNA3A.	(Hertle *et al.*, 2009)
EBNA3A KO BL31	EBV-negative BL31 infected with recombinant virus lacking EBNA3A.	(White *et al.*, 2010)
EBNA3B KO BL31	EBV-negative BL31 infected with recombinant virus lacking EBNA3B.	
EBNA3C KO BL31	EBV-negative BL31 infected with recombinant virus lacking exon 2 of EBNA3C.	
EBNA3 KO BL31	EBV-negative BL31 infected with recombinant virus lacking EBNA3A,3B and 3C.	
EBNA3B KO LCL	LCLs established by infecting with a recombinant virus lacking entire ORF of EBNA3B.	
EBNA3B-/3C low LCL	LCLs established by infecting with a recombinant virus lacking EBNA3B and the expression of EBNA3C is low in these cells.	(Chen *et al.*, 2005)
EBNA3C BJAB	EBV-negative B cell lymphoma transfected with plasmid stably expressing EBNA3C.	(McClellan *et al.*, 2012)
EBNA3C HT LCL	LCLs established by infecting with a recombinant virus with EBNA3C fused to oestrogen receptor that can b induced by hydroxytamoxifen (HT).	(Zhao *et al.*, 2011b)
EBNA E2HTF LCL	LCLs established by infecting with mutant recombinant EcoA cosmid-rescued P3HR1 EBV.	(Zhao *et al.*, 2006)

Cell line	Description	Reference
ER/EBNA2 BL41	EBV-negative BL41 transfected with a plasmid expressing a ß-estradiol conditional EBNA2.	(Maier *et al.*, 2006)
ER/EBNA2 BJAB	EBV-negative B cell lymphoma transfected with a plasmid expressing a ß-estradiol conditional EBNA2.	
EREB 2.5	EBV-immortalised LCL that expresses a conditionally-active oestrogen receptor (ER)-EBNA2 fusion protein.	(Spender *et al.*, 2006)

8 References

Adams, H., Campidelli, C., Dirnhofer, S., Pileri, S.A. & Tzankov, A. (2009) Clinical, phenotypic and genetic similarities and disparities between post-transplant and classical Hodgkin lymphomas with respect to therapeutic targets. *Expert Opin Ther Targets,* 13 (10)**,** 1137-45.

Adldinger, H.K., Delius, H., Freese, U.K., Clarke, J. & Bornkamm, G.W. (1985) A putative transforming gene of Jijoye virus differs from that of Epstein-Barr virus prototypes. *Virology,* 141 (2)**,** 221-34.

Agarwal, M.L., Taylor, W.R., Chernov, M.V., Chernova, O.B. & Stark, G.R. (1998) The p53 network. *Journal of Biological Chemistry,* 273 (1)**,** 1-4.

Allan, G.J., Inman, G.J., Parker, B.D., Rowe, D.T. & Farrell, P.J. (1992) Cell growth effects of Epstein-Barr virus leader protein. *J Gen Virol,* 73 (Pt 6)**,** 1547-51.

Allday, M.J., Bazot, Q. & White, R.E., (2015) The EBNA3 family: Two oncoproteins and a tumour suppressor that are central to the biology of EBV in B cells. *Current Topics in Microbiology and Immunology.* Springer Verlag, 61-117.

Allday, M.J. & Farrell, P.J. (1994) Epstein-Barr virus nuclear antigen EBNA3C/6 expression maintains the level of latent membrane protein 1 in G1-arrested cells. *J Virol,* 68 (6)**,** 3491-8.

AlQarni, S., Al-Sheikh, Y., Campbell, D., Drotar, M., Hannigan, A., Boyle, S., Herzyk, P., Kossenkov, A., Armfield, K., Jamieson, L., Bailo, M., Lieberman, P.M., Tsimbouri, P. & Wilson, J.B. (2018) Lymphomas driven by Epstein-Barr virus nuclear antigen-1 (EBNA1) are dependant upon Mdm2. *Oncogene,* 37 (29)**,** 3998-4012.

Ambinder, R.F., Shah, W.A., Rawlins, D.R., Hayward, G.S. & Hayward, S.D. (1990) Definition of the sequence requirements for binding of the EBNA-1 protein to its palindromic target sites in Epstein-Barr virus DNA. *J Virol,* 64 (5)**,** 2369-79.

Amin, M.A., Itoh, G., Iemura, K., Ikeda, M. & Tanaka, K. (2014) CLIP-170 recruits PLK1 to kinetochores during early mitosis for chromosome alignment. *Journal of Cell Science,* 127 (13)**,** 2818-2824.

Anderson, L.J. & Longnecker, R. (2008) An auto-regulatory loop for EBV LMP2A involves activation of Notch. *Virology,* 371 (2)**,** 257-66.

Anderton, E., Yee, J., Smith, P., Crook, T., White, R.E. & Allday, M.J. (2007) Two Epstein-Barr virus (EBV) oncoproteins cooperate to repress expression of the proapoptotic tumour-suppressor Bim: clues to the pathogenesis of Burkitt's lymphoma. *Oncogene,* 27 (4)**,** 421-433.

Anderton, E., Yee, J., Smith, P., Crook, T., White, R.E. & Allday, M.J. (2008) Two Epstein-Barr virus (EBV) oncoproteins cooperate to repress expression of the proapoptotic tumour-suppressor Bim: clues to the pathogenesis of Burkitt's lymphoma. *Oncogene,* 27 (4)**,** 421-33.

Awasthi, P., Foiani, M. & Kumar, A., (2016) ATM and ATR signaling at a glance. *J Cell Sci.* England, 1285.

Badea, T., Niculescu, F., Soane, L., Fosbrink, M., Sorana, H., Rus, V., Shin, M.L. & Rus, H. (2002) RGC-32 increases p34CDC2 kinase activity and entry of aortic smooth muscle cells into S-phase. *Journal of Biological Chemistry,* 277 (1)**,** 502-508.

Badea, T.C., Niculescu, F.I., Soane, L., Shin, M.L. & Rus, H. (1998) Molecular cloning and characterization of RGC-32, a novel gene induced by complement activation in oligodendrocytes. *Journal of Biological Chemistry,* 273 (41)**,** 26977-26981.

Baer, R., Bankier, A.T., Biggin, M.D., Deininger, P.L., Farrell, P.J., Gibson, T.J., Hatfull, G., Hudson, G.S., Satchwell, S.C., Seguin, C. & et al. (1984) DNA sequence and expression of the B95-8 Epstein-Barr virus genome. *Nature,* 310 (5974)**,** 207-11.

Balfour, H.H., Jr., Odumade, O.A., Schmeling, D.O., Mullan, B.D., Ed, J.A., Knight, J.A., Vezina, H.E., Thomas, W. & Hogquist, K.A. (2013) Behavioral, virologic, and immunologic factors associated with acquisition and severity of primary Epstein-Barr virus infection in university students. *J Infect Dis,* 207 (1)**,** 80-8.

Banerjee, S., Lu, J., Cai, Q., Sun, Z., Jha, H.C. & Robertson, E.S. (2014) EBNA3C augments Pim-1 mediated phosphorylation and degradation of p21 to promote B-cell proliferation. *PLoS Pathog,* 10 (8)**,** e1004304.

Barnes, E.A., Porter, L.A., Lenormand, J.L., Dellinger, R.W. & Donoghue, D.J. (2003) Human Spy1 promotes survival of mammalian cells following DNA damage. *Cancer Res,* 63 (13)**,** 3701-7.

Barnum, K.J. & O'Connell, M.J. (2014) Cell cycle regulation by checkpoints. *Methods Mol Biol,* 1170**,** 29-40.

Bazot, Q., Paschos, K., Skalska, L., Kalchschmidt, J.S., Parker, G.A. & Allday, M.J. (2015) Epstein-Barr Virus Proteins EBNA3A and EBNA3C Together Induce Expression of the Oncogenic MicroRNA Cluster miR-221/miR-222 and Ablate Expression of Its Target p57KIP2. *PLOS Pathogens,* 11 (7)**,** e1005031.

Ben-Bassat, H., Goldblum, N., Mitrani, S., Goldblum, T., Yoffey, J.M., Cohen, M.M., Bentwich, Z., Ramot, B., Klein, E. & Klein, G. (1977) Establishment in continuous culture of a new type of lymphocyte from a "Burkitt like" malignant lymphoma (line D.G.-75). *Int J Cancer,* 19 (1)**,** 27-33.

Bhatia, K., Raj, A., Guitierrez, M.I., Judde, J.G., Spangler, G., Venkatesh, H. & Magrath, I.T. (1996) Variation in the sequence of Epstein Barr virus nuclear antigen 1 in normal peripheral blood lymphocytes and in Burkitt's lymphomas. *Oncogene,* 13 (1)**,** 177-81.

Blagosklonny, M.V. & Pardee, A.B. (2002) The restriction point of the cell cycle. *Cell cycle (Georgetown, Tex.),* 1 (2)**,** 103-110.

Blomberg, I. & Hoffmann, I. (1999) Ectopic expression of Cdc25A accelerates the G(1)/S transition and leads to premature activation of cyclin E- and cyclin A-dependent kinases. *Mol Cell Biol,* 19 (9)**,** 6183-94.

Bodescot, M. & Perricaudet, M. (1986) Epstein-barr virus mRNAs produced by alternative splicing. *Nucleic Acids Research,* 14 (17)**,** 7103-7114.

Bornkamm, G.W., Berens, C., Kuklik-Roos, C., Bechet, J.-M., Laux, G., Bachl, J., Korndoerfer, M., Schlee, M., Hölzel, M., Malamoussi, A., Chapman, R.D., Nimmerjahn, F., Mautner, J., Hillen, W., Bujard, H. & Feuillard, J. (2005) Stringent doxycycline-dependent control of gene activities using an episomal one-vector system. *Nucleic Acids Research,* 33 (16)**,** e137-e137.

Borza, C.M. & Hutt-Fletcher, L.M. (2002) Alternate replication in B cells and epithelial cells switches tropism of Epstein-Barr virus. *Nature Medicine,* 8 (6)**,** 594-599.

Bourne, Y., Watson, M.H., Hickey, M.J., Holmes, W., Rocque, W., Reed, S.I. & Tainer, J.A. (1996) Crystal structure and mutational analysis of the human CDK2 kinase complex with cell cycle-regulatory protein CksHs1. *Cell,* 84 (6)**,** 863-74.

Brink, N.S., Sharvell, Y., Howard, M.R., Fox, J.D., Harrison, M.J. & Miller, R.F. (1998) Detection of Epstein-Barr virus and Kaposi's sarcoma-associated herpesvirus DNA in CSF from persons infected with HIV who had neurological disease. *J Neurol Neurosurg Psychiatry,* 65 (2)**,** 191-5.

Brocard, M., Khasnis, S., Wood, C.D., Shannon-Lowe, C. & West, M.J. (2018) Pumilio directs deadenylation-associated translational repression of the cyclin-dependent kinase 1 activator RGC-32. *Nucleic Acids Res,* 46 (7)**,** 3707-3725.

Brown, N.R., Korolchuk, S., Martin, M.P., Stanley, W.A., Moukhametzianov, R., Noble, M.E. & Endicott, J.A. (2015) CDK1 structures reveal conserved and unique features of the essential cell cycle CDK. *Nat Commun,* 6**,** 6769.

Burger, J.A. & Chiorazzi, N. (2013) B cell receptor signaling in chronic lymphocytic leukemia. *Trends Immunol,* 34 (12)**,** 592-601.

Burgess, A., Buck, M., Krauer, K. & Sculley, T. (2006) Nuclear localization of the Epstein-Barr virus EBNA3B protein. *J Gen Virol,* 87 (Pt 4)**,** 789-93.

Burkhardt, A.L., Bolen, J.B., Kieff, E. & Longnecker, R. (1992) An Epstein-Barr virus transformation-associated membrane protein interacts with src family tyrosine kinases. *Journal of Virology,* 66 (8)**,** 5161-5167.

Burkitt, D. (1958) A sarcoma involving the jaws in African children. *Br J Surg,* 46 (197)**,** 218-23.

Burkitt, D. & O'Conor, G.T. (1961) Malignant lymphoma in African children. I. A clinical syndrome. *Cancer,* 14**,** 258-69.

Burkitt, D.P. (1969) Etiology of Burkitt's lymphoma--an alternative hypothesis to a vectored virus. *J Natl Cancer Inst,* 42 (1)**,** 19-28.

Calderwood, M.A., Lee, S., Holthaus, A.M., Blacklow, S.C., Kieff, E. & Johannsen, E. (2011) Epstein-Barr Virus Nuclear Protein 3C binds to the N-terminal (NTD) and beta trefoil domains (BTD) of RBP/CSL; only the NTD interaction is essential for lymphoblastoid cell growth. *Virology,* 414 (1)**,** 19-25.

Campbell, K.S. (1999) Signal transduction from the B cell antigen-receptor. *Current Opinion in Immunology,* 11 (3)**,** 256-264.

Carbone, A., Gloghini, A. & Dotti, G. (2008) EBV-associated lymphoproliferative disorders: classification and treatment. *Oncologist,* 13 (5)**,** 577-85.

Carey, G.B. & Scott, D.W. (2001) Role of Phosphatidylinositol 3-Kinase in Anti-IgM- and Anti-IgD-Induced Apoptosis in B Cell Lymphomas. *The Journal of Immunology,* 166 (3)**,** 1618-1626.

Cesarman, E., Dalla-Favera, R., Bentley, D. & Groudine, M. (1987) Mutations in the first exon are associated with altered transcription of c-myc in Burkitt lymphoma. *Science,* 238 (4831)**,** 1272-5.

Chan, T.A., Hwang, P.M., Hermeking, H., Kinzler, K.W. & Vogelstein, B. (2000) Cooperative effects of genes controlling the G(2)/M checkpoint. *Genes Dev,* 14 (13)**,** 1584-8.

Chavez, J.C., Sahakian, E. & Pinilla-Ibarz, J. (2013) Ibrutinib: an evidence-based review of its potential in the treatment of advanced chronic lymphocytic leukemia. *Core Evid,* 8**,** 37-45.

Cheeseman, I.M. & Desai, A. (2008) Molecular architecture of the kinetochore-microtubule interface. *Nature Reviews Molecular Cell Biology,* 9 (1)**,** 33-46.

Chen, A., DiVisconte, M., Jiang, X., Quink, C. & Wang, F. (2005) Epstein-Barr Virus with the Latent Infection Nuclear Antigen 3B Completely Deleted Is Still Competent for B-Cell Growth Transformation In Vitro. *Journal of Virology,* 79 (7)**,** 4506-4509.

Chen, C., Chen, Y.H. & Lin, W.W. (1999) Involvement of p38 mitogen-activated protein kinase in lipopolysaccharide-induced iNOS and COX-2 expression in J774 macrophages. *Immunology,* 97 (1)**,** 124-9.

Chen, H.L., Lung, M.M., Sham, J.S., Choy, D.T., Griffin, B.E. & Ng, M.H. (1992) Transcription of BamHI-A region of the EBV genome in NPC tissues and B cells. *Virology,* 191 (1)**,** 193-201.

Chen, J., Sathiyamoorthy, K., Zhang, X., Schaller, S., Perez White, B.E., Jardetzky, T.S. & Longnecker, R. (2018) Ephrin receptor A2 is a functional entry receptor for Epstein-Barr virus. *Nat Microbiol,* 3 (2)**,** 172-180.

Chen, M.S., Hurov, J., White, L.S., Woodford-Thomas, T. & Piwnica-Worms, H. (2001) Absence of apparent phenotype in mice lacking Cdc25C protein phosphatase. *Mol Cell Biol,* 21 (12)**,** 3853-61.

Chen, S.Y., Lu, J., Shih, Y.C. & Tsai, C.H. (2002) Epstein-Barr virus latent membrane protein 2A regulates c-Jun protein through extracellular signal-regulated kinase. *J Virol,* 76 (18)**,** 9556-61.

Chen, Y.T., Tan, K.A., Pang, L.Y. & Argyle, D.J. (2012) The class I PI3K/Akt pathway is critical for cancer cell survival in dogs and offers an opportunity for therapeutic intervention. *BMC Vet Res,* 8**,** 73.

Chinnadurai, G. (2007) Transcriptional regulation by C-terminal binding proteins. *Int J Biochem Cell Biol,* 39 (9)**,** 1593-607.

Choudhuri, T., Verma, S.C., Lan, K., Murakami, M. & Robertson, E.S. (2007a) The ATM/ATR signaling effector Chk2 is targeted by Epstein-Barr virus nuclear antigen 3C to release the G2/M cell cycle block. *J Virol,* 81 (12)**,** 6718-30.

Choudhuri, T., Verma, S.C., Lan, K., Murakami, M. & Robertson, E.S. (2007b) The ATM/ATR signaling effector Chk2 is targeted by Epstein-Barr virus nuclear antigen 3C to release the G(2)/M cell cycle block. *Journal of Virology,* 81 (12)**,** 6718-6730.

Ciferri, C., Musacchio, A. & Petrovic, A. (2007) The Ndc80 complex: Hub of kinetochore activity. *FEBS Letters,* 581 (15)**,** 2862-2869.

Cohen, J.I., Mocarski, E.S., Raab-Traub, N., Corey, L. & Nabel, G.J. (2013) The need and challenges for development of an Epstein-Barr virus vaccine. *Vaccine,* 31 Suppl 2**,** B194-6.

Cohen, J.I., Wang, F., Mannick, J. & Kieff, E. (1989) Epstein-Barr virus nuclear protein 2 is a key determinant of lymphocyte transformation. *Proc Natl Acad Sci U S A,* 86 (23)**,** 9558-62.

Coleman, C.B., Daud, II, Ogolla, S.O., Ritchie, J.A., Smith, N.A., Sumba, P.O., Dent, A.E. & Rochford, R. (2017) Epstein-Barr Virus Type 2 Infects T Cells in Healthy Kenyan Children. *J Infect Dis,* 216 (6)**,** 670-677.

Coleman, C.B., Wohlford, E.M., Smith, N.A., King, C.A., Ritchie, J.A., Baresel, P.C., Kimura, H. & Rochford, R. (2015) Epstein-Barr virus type 2 latently infects T cells, inducing an atypical activation characterized by expression of lymphotactic cytokines. *J Virol,* 89 (4)**,** 2301-12.

Coudreuse, D. & Nurse, P. (2010) Driving the cell cycle with a minimal CDK control network. *Nature,* 468 (7327)**,** 1074-9.

Cuevas, B.D., Lu, Y., Mao, M., Zhang, J., LaPushin, R., Siminovitch, K. & Mills, G.B. (2001) Tyrosine phosphorylation of p85 relieves its inhibitory activity on phosphatidylinositol 3-kinase. *J Biol Chem,* 276 (29)**,** 27455-61.

Cui, X.B., Guo, X. & Chen, S.Y. (2013) Response gene to complement 32 deficiency causes impaired placental angiogenesis in mice. *Cardiovasc Res,* 99 (4)**,** 632-9.

Dawson, C.W., Tramountanis, G., Eliopoulos, A.G. & Young, L.S. (2003) Epstein-Barr virus latent membrane protein 1 (LMP1) activates the phosphatidylinositol 3-kinase/Akt pathway to promote cell survival and induce actin filament remodeling. *J Biol Chem,* 278 (6)**,** 3694-704.

Day, P.J., Cleasby, A., Tickle, I.J., O'Reilly, M., Coyle, J.E., Holding, F.P., McMenamin, R.L., Yon, J., Chopra, R., Lengauer, C. & Jhoti, H. (2009) Crystal structure of human CDK4 in complex with a D-type cyclin. *Proc Natl Acad Sci U S A,* 106 (11)**,** 4166-70.

De Matteo, E., Baron, A.V., Chabay, P., Porta, J., Dragosky, M. & Preciado, M.V. (2003) Comparison of Epstein-Barr virus presence in Hodgkin lymphoma in pediatric versus adult argentine patients. *Archives of Pathology & Laboratory Medicine,* 127 (10)**,** 1325-1329.

Decaussin, G., Sbih-Lammali, F., de Turenne-Tessier, M., Bouguermouh, A. & Ooka, T. (2000) Expression of BARF1 gene encoded by Epstein-Barr virus in nasopharyngeal carcinoma biopsies. *Cancer Res,* 60 (19)**,** 5584-8.

DeFranco, A.L., Chan, V.W. & Lowell, C.A. (1998) Positive and negative roles of the tyrosine kinase Lyn in B cell function. *Semin Immunol,* 10 (4)**,** 299-307.

Dirmeier, U., Neuhierl, B., Kilger, E., Reisbach, G., Sandberg, M.L. & Hammerschmidt, W. (2003) Latent membrane protein 1 is critical for efficient growth transformation of human B cells by epstein-barr virus. *Cancer Res,* 63 (11)**,** 2982-9.

Donninger, H., Bonome, T., Radonovich, M., Pise-Masison, C.A., Brady, J., Shih, J.H., Barrett, J.C. & Birrer, M.J. (2004) Whole genome expression profiling of advance

stage papillary serous ovarian cancer reveals activated pathways. *Oncogene,* 23 (49)**,** 8065-77.

Draetta, G. (1993) Cdc2 activation: the interplay of cyclin binding and Thr161 phosphorylation. *Trends Cell Biol,* 3 (9)**,** 287-9.

Drozdetskiy, A., Cole, C., Procter, J. & Barton, G.J. (2015) JPred4: a protein secondary structure prediction server. *Nucleic Acids Research*.

Duhren-von Minden, M., Ubelhart, R., Schneider, D., Wossning, T., Bach, M.P., Buchner, M., Hofmann, D., Surova, E., Follo, M., Kohler, F., Wardemann, H., Zirlik, K., Veelken, H. & Jumaa, H. (2012) Chronic lymphocytic leukaemia is driven by antigen-independent cell-autonomous signalling. *Nature,* 489 (7415)**,** 309-12.

Ellis-Connell, A.L., Iempridee, T., Xu, I. & Mertz, J.E. (2010) Cellular microRNAs 200b and 429 regulate the Epstein-Barr virus switch between latency and lytic replication. *J Virol,* 84 (19)**,** 10329-43.

Engelman, J.A. (2009) Targeting PI3K signalling in cancer: opportunities, challenges and limitations. *Nat Rev Cancer,* 9 (8)**,** 550-62.

Epstein, M.A., Achong, B.G. & Barr, Y.M. (1964) VIRUS PARTICLES IN CULTURED LYMPHOBLASTS FROM BURKITT'S LYMPHOMA. *The Lancet,* 283 (7335)**,** 702-703.

Erickson, K.D. & Martin, J.M. (1997) Early detection of the lytic LMP-1 protein in EBV-infected B-cells suggests its presence in the virion. *Virology,* 234 (1)**,** 1-13.

Erickson, K.D. & Martin, J.M. (2000) The late lytic LMP-1 protein of Epstein-Barr virus can negatively regulate LMP-1 signaling. *J Virol,* 74 (2)**,** 1057-60.

Farrell, P.J. (2015) Epstein-Barr Virus Strain Variation. *Curr Top Microbiol Immunol,* 390 (Pt 1)**,** 45-69.

Fattaey, A. & Booher, R.N. (1997) Myt1: a Wee1-type kinase that phosphorylates Cdc2 on residue Thr14. *Prog Cell Cycle Res,* 3**,** 233-40.

Ferby, I., Blazquez, M., Palmer, A., Eritja, R. & Nebreda, A.R. (1999) A novel p34(cdc2)-binding and activating protein that is necessary and sufficient to trigger G(2)/M progression in Xenopus oocytes. *Genes Dev,* 13 (16)**,** 2177-89.

Flavell, J.R., Baumforth, K.R., Wood, V.H., Davies, G.L., Wei, W., Reynolds, G.M., Morgan, S., Boyce, A., Kelly, G.L., Young, L.S. & Murray, P.G. (2008) Down-regulation of the TGF-beta target gene, PTPRK, by the Epstein-Barr virus encoded EBNA1 contributes to the growth and survival of Hodgkin lymphoma cells. *Blood,* 111 (1)**,** 292-301.

Foley, E.A. & Kapoor, T.M. (2013) Microtubule attachment and spindle assembly checkpoint signalling at the kinetochore. *Nat Rev Mol Cell Biol,* 14 (1)**,** 25-37.

Fosbrink, M., Cudrici, C., Niculescu, F., Badea, T.C., David, S., Shamsuddin, A., Shin, M.L. & Rus, H. (2005) Overexpression of RGC-32 in colon cancer and other tumors. *Experimental and Molecular Pathology,* 78 (2)**,** 116-122.

Fosbrink, M., Cudrici, C., Tegla, C.A., Soloviova, K., Ito, T., Vlaicu, S., Rus, V., Niculescu, F. & Rus, H. (2009) Response gene to complement 32 is required for C5b-9 induced cell cycle activation in endothelial cells. *Exp Mol Pathol,* 86 (2)**,** 87-94.

Frappier, L. (2012) The Epstein-Barr Virus EBNA1 Protein. *Scientifica (Cairo),* 2012**,** 438204.

Fujita, N., Sato, S., Katayama, K. & Tsuruo, T. (2002) Akt-dependent phosphorylation of p27Kip1 promotes binding to 14-3-3 and cytoplasmic localization. *J Biol Chem,* 277 (32)**,** 28706-13.

Gascoigne, K.E., Takeuchi, K., Suzuki, A., Hori, T., Fukagawa, T. & Cheeseman, I.M. (2011) Induced ectopic kinetochore assembly bypasses the requirement for CENP-A nucleosomes. *Cell,* 145 (3)**,** 410-422.

Gautier, J., Solomon, M.J., Booher, R.N., Bazan, J.F. & Kirschner, M.W. (1991) cdc25 is a specific tyrosine phosphatase that directly activates p34cdc2. *Cell,* 67 (1)**,** 197-211.

Gheghiani, L., Loew, D., Lombard, B., Mansfeld, J. & Gavet, O. (2017) PLK1 Activation in Late G2 Sets Up Commitment to Mitosis. *Cell Rep,* 19 (10)**,** 2060-2073.

Gires, O., Zimber-Strobl, U., Gonnella, R., Ueffing, M., Marschall, G., Zeidler, R., Pich, D. & Hammerschmidt, W. (1997) Latent membrane protein 1 of Epstein-Barr virus mimics a constitutively active receptor molecule. *Embo j,* 16 (20)**,** 6131-40.

Glaser, L.V., Rieger, S., Thumann, S., Beer, S., Kuklik-Roos, C., Martin, D.E., Maier, K.C., Harth-Hertle, M.L., Gruning, B., Backofen, R., Krebs, S., Blum, H., Zimmer, R., Erhard, F. & Kempkes, B. (2017) EBF1 binds to EBNA2 and promotes the assembly of EBNA2 chromatin complexes in B cells. *PLoS Pathog,* 13 (10)**,** e1006664.

Gong, D. & Ferrell, J.E., Jr. (2010) The roles of cyclin A2, B1, and B2 in early and late mitotic events. *Mol Biol Cell,* 21 (18)**,** 3149-61.

Gordon, L.I. & Longnecker, R. (2012) Off-targeting oft-targeted CD20 in cHL. *Blood,* 119 (18)**,** 4095-6.

Gravells, P., Tomita, K., Booth, A., Poznansky, J. & Porter, A.C.G. (2013) Chemical genetic analyses of quantitative changes in Cdk1 activity during the human cell cycle. *Human Molecular Genetics,* 22 (14)**,** 2842-2851.

Graves, J.D., Draves, K.E., Craxton, A., Saklatvala, J., Krebs, E.G. & Clark, E.A. (1996) Involvement of stress-activated protein kinase and p38 mitogen-activated protein kinase in mIgM-induced apoptosis of human B lymphocytes. *Proc Natl Acad Sci U S A,* 93 (24)**,** 13814-8.

Gregory, C.D., Rowe, M. & Rickinson, A.B. (1990) Different Epstein-Barr virus-B cell interactions in phenotypically distinct clones of a Burkitt's lymphoma cell line. *J Gen Virol,* 71 (Pt 7)**,** 1481-95.

Grossman, S.R., Johannsen, E., Tong, X., Yalamanchili, R. & Kieff, E. (1994) The Epstein-Barr virus nuclear antigen 2 transactivator is directed to response elements by the J kappa recombination signal binding protein. *Proc Natl Acad Sci U S A,* 91 (16)**,** 7568-72.

Gruhne, B., Kamranvar, S.A., Masucci, M.G. & Sompallae, R. (2009) EBV and genomic instability—A new look at the role of the virus in the pathogenesis of Burkitt's lymphoma. *Seminars in Cancer Biology,* 19 (6)**,** 394-400.

Gu, Y., Rosenblatt, J. & Morgan, D.O. (1992) Cell cycle regulation of CDK2 activity by phosphorylation of Thr160 and Tyr15. *Embo j,* 11 (11)**,** 3995-4005.

Gulley, M.L., Eagan, P.A., Quintanilla-Martinez, L., Picado, A.L., Smir, B.N., Childs, C., Dunn, C.D., Craig, F.E., Williams, J.W., Jr. & Banks, P.M. (1994) Epstein-Barr virus DNA is abundant and monoclonal in the Reed-Sternberg cells of Hodgkin's disease: association with mixed cellularity subtype and Hispanic American ethnicity. *Blood,* 83 (6)**,** 1595-602.

Gunnell, A., Webb, H.M., Wood, C.D., McClellan, M.J., Wichaidit, B., Kempkes, B., Jenner, R.G., Osborne, C., Farrell, P.J. & West, M.J. (2016) RUNX super-enhancer control through the Notch pathway by Epstein-Barr virus transcription factors regulates B cell growth. *Nucleic Acids Research,* 44 (10)**,** 4636-4650.

Hammerschmidt, W. & Sugden, B. (1988) Identification and characterization of oriLyt, a lytic origin of DNA replication of Epstein-Barr virus. *Cell,* 55 (3)**,** 427-33.

Harada, S. & Kieff, E. (1997) Epstein-Barr virus nuclear protein LP stimulates EBNA-2 acidic domain-mediated transcriptional activation. *J Virol,* 71 (9)**,** 6611-8.

Harth-Hertle, M.L., Scholz, B.A., Erhard, F., Glaser, L.V., Dolken, L., Zimmer, R. & Kempkes, B. (2013) Inactivation of intergenic enhancers by EBNA3A initiates and maintains polycomb signatures across a chromatin domain encoding CXCL10 and CXCL9. *PLoS Pathog,* 9 (9)**,** e1003638.

Hayles, J., Beach, D., Durkacz, B. & Nurse, P. (1986) The fission yeast cell cycle control gene cdc2: isolation of a sequence suc1 that suppresses cdc2 mutant function. *Mol Gen Genet,* 202 (2)**,** 291-3.

Henke, C.E., Kurland, L.T. & Elveback, L.R. (1973) Infectious mononucleosis in Rochester, Minnesota, 1950 through 1969. *American Journal of Epidemiology,* 98 (6)**,** 483-490.

Henkel, T., Ling, P.D., Hayward, S.D. & Peterson, M.G. (1994) Mediation of Epstein-Barr virus EBNA2 transactivation by recombination signal-binding protein J kappa. *Science,* 265 (5168)**,** 92-5.

Henle, G., Henle, W. & Diehl, V. (1968) Relation of Burkitt's tumor-associated herpes-ytpe virus to infectious mononucleosis. *Proc Natl Acad Sci U S A,* 59 (1)**,** 94-101.

Hermeking, H., Lengauer, C., Polyak, K., He, T.C., Zhang, L., Thiagalingam, S., Kinzler, K.W. & Vogelstein, B. (1997) 14-3-3sigma is a p53-regulated inhibitor of G2/M progression. *Mol Cell,* 1 (1)**,** 3-11.

Hershko, A., Ganoth, D., Pehrson, J., Palazzo, R.E. & Cohen, L.H. (1991) Methylated ubiquitin inhibits cyclin degradation in clam embryo extracts. *J Biol Chem,* 266 (25)**,** 16376-9.

Hertle, M.L., Popp, C., Petermann, S., Maier, S., Kremmer, E., Lang, R., Mages, J. & Kempkes, B. (2009) Differential Gene Expression Patterns of EBV Infected EBNA-3A Positive and Negative Human B Lymphocytes. *PLoS Pathogens,* 5 (7)**,** e1000506.

Hickabottom, M., Parker, G.A., Freemont, P., Crook, T. & Allday, M.J. (2002) Two nonconsensus sites in the Epstein-Barr virus oncoprotein EBNA3A cooperate to bind the co-repressor carboxyl-terminal-binding protein (CtBP). *J Biol Chem,* 277 (49)**,** 47197-204.

Hickey, S.M. & Strasburger, V.C. (1997) What every pediatrician should know about infectious mononucleosis in adolescents. *Pediatr Clin North Am,* 44 (6)**,** 1541-56.

Hirai, H., Iwasawa, Y., Okada, M., Arai, T., Nishibata, T., Kobayashi, M., Kimura, T., Kaneko, N., Ohtani, J., Yamanaka, K., Itadani, H., Takahashi-Suzuki, I., Fukasawa, K., Oki, H., Nambu, T., Jiang, J., Sakai, T., Arakawa, H., Sakamoto, T., Sagara, T., Yoshizumi, T., Mizuarai, S. & Kotani, H. (2009) Small-molecule inhibition of Wee1 kinase by MK-1775 selectively sensitizes p53-deficient tumor cells to DNA-damaging agents. *Mol Cancer Ther,* 8 (11)**,** 2992-3000.

Hoffmann, I., Draetta, G. & Karsenti, E. (1994) Activation of the phosphatase activity of human cdc25A by a cdk2-cyclin E dependent phosphorylation at the G1/S transition. *Embo j,* 13 (18)**,** 4302-10.

Holmes, R.D. & Sokol, R.J. (2002) Epstein-Barr virus and post-transplant lymphoproliferative disease. *Pediatr Transplant,* 6 (6)**,** 456-64.

Holowaty, M.N., Zeghouf, M., Wu, H., Tellam, J., Athanasopoulos, V., Greenblatt, J. & Frappier, L. (2003) Protein profiling with Epstein-Barr nuclear antigen-1 reveals an interaction with the herpesvirus-associated ubiquitin-specific protease HAUSP/USP7. *J Biol Chem,* 278 (32)**,** 29987-94.

Hong, J.Y., Yoon, D.H., Suh, C., Huh, J., Do, I.G., Sohn, I., Jo, J., Jung, S.H., Hong, M.E., Yoon, H., Ko, Y.H., Kim, S.J. & Kim, W.S. (2015) EBV-positive diffuse large B-cell lymphoma in young adults: is this a distinct disease entity? *Annals of Oncology,* 26 (3)**,** 548-555.

Hsieh, D.J., Camiolo, S.M. & Yates, J.L. (1993) Constitutive binding of EBNA1 protein to the Epstein-Barr virus replication origin, oriP, with distortion of DNA structure during latent infection. *Embo j,* 12 (13)**,** 4933-44.

Hsieh, J.J. & Hayward, S.D. (1995) Masking of the CBF1/RBPJ kappa transcriptional repression domain by Epstein-Barr virus EBNA2. *Science,* 268 (5210)**,** 560-3.

Hsu, C.Y., Yi, Y.H., Chang, K.P., Chang, Y.S., Chen, S.J. & Chen, H.C. (2014) The Epstein-Barr virus-encoded microRNA MiR-BART9 promotes tumor metastasis by targeting E-cadherin in nasopharyngeal carcinoma. *PLoS Pathog,* 10 (2)**,** e1003974.

Hudson, G.S., Farrell, P.J. & Barrell, B.G. (1985) Two related but differentially expressed potential membrane proteins encoded by the EcoRI Dhet region of Epstein-Barr virus B95-8. *J Virol,* 53 (2)**,** 528-35.

Hurley, E.A. & Thorley-Lawson, D.A. (1988) B cell activation and the establishment of Epstein-Barr virus latency. *Journal of Experimental Medicine,* 168 (6)**,** 2059-2075.

Ikeda, M. & Tanaka, K. (2017) Plk1 bound to Bub1 contributes to spindle assembly checkpoint activity during mitosis. *Sci Rep,* 7 (1)**,** 8794.

Inoue, D. & Sagata, N. (2005) The Polo-like kinase Plx1 interacts with and inhibits Myt1 after fertilization of Xenopus eggs. *Embo j,* 24 (5)**,** 1057-67.

Irion, S., Luche, H., Gadue, P., Fehling, H.J., Kennedy, M. & Keller, G. (2007) Identification and targeting of the ROSA26 locus in human embryonic stem cells. *Nat Biotechnol,* 25 (12)**,** 1477-82.

James, S.R., Downes, C.P., Gigg, R., Grove, S.J., Holmes, A.B. & Alessi, D.R. (1996) Specific binding of the Akt-1 protein kinase to phosphatidylinositol 3,4,5-trisphosphate without subsequent activation. *Biochem J,* 315 (Pt 3)**,** 709-13.

Jeffrey, P.D., Russo, A.A., Polyak, K., Gibbs, E., Hurwitz, J., Massague, J. & Pavletich, N.P. (1995) Mechanism of CDK activation revealed by the structure of a cyclinA-CDK2 complex. *Nature,* 376 (6538)**,** 313-20.

Ji, L. & T., K.E. (2013) *The evolution of CDK-Activating Kinases.* Landes Bioscience.

Jiang, S., Willox, B., Zhou, H., Holthaus, A.M., Wang, A., Shi, T.T., Maruo, S., Kharchenko, P.V., Johannsen, E.C., Kieff, E. & Zhao, B. (2014) Epstein-Barr Virus Nuclear Antigen 3C binds to BATF/IRF4 or SPI1/IRF4 composite sites and recruits Sin3A to repress CDKN2A. *Proceedings of the National Academy of Sciences of the United States of America,* 111 (1)**,** 421-426.

Jinno, S., Suto, K., Nagata, A., Igarashi, M., Kanaoka, Y., Nojima, H. & Okayama, H. (1994) Cdc25A is a novel phosphatase functioning early in the cell cycle. *Embo j,* 13 (7)**,** 1549-56.

Johannsen, E., Miller, C.L., Grossman, S.R. & Kieff, E. (1996) EBNA-2 and EBNA-3C extensively and mutually exclusively associate with RBPJkappa in Epstein-Barr virus-transformed B lymphocytes. *Journal of Virology,* 70 (6)**,** 4179-4183.

Johansson, P. (2007) *Regulation of the Epstein-Barr Virus Latent Membrane Protein 1 Expression.*

Jones, C.H., Hayward, S.D. & Rawlins, D.R. (1989) Interaction of the lymphocyte-derived Epstein-Barr virus nuclear antigen EBNA-1 with its DNA-binding sites. *J Virol,* 63 (1)**,** 101-10.

Kaiser, C., Laux, G., Eick, D., Jochner, N., Bornkamm, G.W. & Kempkes, B. (1999) The Proto-Oncogene c-myc Is a Direct Target Gene of Epstein-Barr Virus Nuclear Antigen 2. *Journal of Virology,* 73 (5)**,** 4481-4484.

Kalchschmidt, J.S., Gillman, A.C.T., Paschos, K., Bazot, Q., Kempkes, B. & Allday, M.J. (2016a) EBNA3C Directs Recruitment of RBPJ (CBF1) to Chromatin during the Process of Gene Repression in EBV Infected B Cells. *PLoS Pathog,* 12 (1)**,** e1005383.

Kalchschmidt, J.S., Gillman, A.C.T., Paschos, K., Bazot, Q., Kempkes, B. & Allday, M.J. (2016b) EBNA3C Directs Recruitment of RBPJ (CBF1) to Chromatin during the Process of Gene Repression in EBV Infected B Cells. *PLoS Pathogens,* 12 (1)**,** e1005383.

Kaldis, P. (1999) The cdk-activating kinase (CAK): from yeast to mammals. *Cell Mol Life Sci,* 55 (2)**,** 284-96.

Kang, M.S. & Kieff, E. (2015) Epstein-Barr virus latent genes. *Exp Mol Med,* 47**,** e131.

Kang, Y., Siegel, P.M., Shu, W., Drobnjak, M., Kakonen, S.M., Cordon-Cardo, C., Guise, T.A. & Massague, J. (2003) A multigenic program mediating breast cancer metastasis to bone. *Cancer Cell,* 3 (6)**,** 537-49.

Kapatai, G. & Murray, P. (2007) Contribution of the Epstein Barr virus to the molecular pathogenesis of Hodgkin lymphoma. *J Clin Pathol,* 60 (12)**,** 1342-9.

Kastan, M.B. & Bartek, J. (2004) Cell-cycle checkpoints and cancer. *Nature,* 432 (7015)**,** 316-323.

Katayama, K., Fujita, N. & Tsuruo, T. (2005) Akt/protein kinase B-dependent phosphorylation and inactivation of WEE1Hu promote cell cycle progression at G2/M transition. *Mol Cell Biol,* 25 (13)**,** 5725-37.

Kelley, L.A., Mezulis, S., Yates, C.M., Wass, M.N. & Sternberg, M.J. (2015) The Phyre2 web portal for protein modeling, prediction and analysis. *Nat Protoc,* 10 (6)**,** 845-58.

Kempkes, B. & Ling, P.D. (2015) EBNA2 and Its Coactivator EBNA-LP. *Curr Top Microbiol Immunol,* 391**,** 35-59.

Kempkes, B. & Robertson, E.S. (2015) Epstein-Barr virus latency: current and future perspectives. *Curr Opin Virol,* 14**,** 138-44.

Kempkes, B., Spitkovsky, D., Jansen-Durr, P., Ellwart, J.W., Kremmer, E., Delecluse, H.J., Rottenberger, C., Bornkamm, G.W. & Hammerschmidt, W. (1995) B-cell proliferation and induction of early G1-regulating proteins by Epstein-Barr virus mutants conditional for EBNA2. *Embo j,* 14 (1)**,** 88-96.

Kitay, M.K. & Rowe, D.T. (1996) Cell cycle stage-specific phosphorylation of the Epstein-Barr virus immortalization protein EBNA-LP. *J Virol,* 70 (11)**,** 7885-93.

Klein, G., Klein, E. & Kashuba, E. (2010) Interaction of Epstein-Barr virus (EBV) with human B-lymphocytes. *Biochemical and Biophysical Research Communications,* 396 (1)**,** 67-73.

Knight, J.S., Lan, K., Subramanian, C. & Robertson, E.S. (2003) Epstein-Barr virus nuclear antigen 3C recruits histone deacetylase activity and associates with the corepressors mSin3A and NCoR in human B-cell lines. *J Virol,* 77 (7)**,** 4261-72.

Knight, J.S., Sharma, N. & Robertson, E.S. (2005) SCFSkp2 complex targeted by Epstein-Barr virus essential nuclear antigen. *Mol Cell Biol,* 25 (5)**,** 1749-63.

Koncz, G., Bodor, C., Kovesdi, D., Gati, R. & Sarmay, G. (2002) BCR mediated signal transduction in immature and mature B cells. *Immunol Lett,* 82 (1-2)**,** 41-9.

Kondo, E., Harashima, A., Takabatake, T., Takahashi, H., Matsuo, Y., Yoshino, T., Orita, K. & Akagi, T. (2003) NF-ATc2 induces apoptosis in Burkitt's lymphoma cells through signaling via the B cell antigen receptor. *Eur J Immunol,* 33 (1)**,** 1-11.

Krabbe, S., Hesse, J. & Uldall, P. (1981) Primary Epstein-Barr virus infection in early childhood. *Arch Dis Child,* 56 (1)**,** 49-52.

Kramer, E.R., Scheuringer, N., Podtelejnikov, A.V., Mann, M. & Peters, J.M. (2000) Mitotic regulation of the APC activator proteins CDC20 and CDH1. *Mol Biol Cell,* 11 (5)**,** 1555-69.

Krauer, K., Buck, M., Flanagan, J., Belzer, D. & Sculley, T. (2004a) Identification of the nuclear localization signals within the Epstein-Barr virus EBNA-6 protein. *J Gen Virol,* 85 (Pt 1)**,** 165-72.

Krauer, K.G., Burgess, A., Buck, M., Flanagan, J., Sculley, T.B. & Gabrielli, B. (2004b) The EBNA-3 gene family proteins disrupt the G2/M checkpoint. *Oncogene,* 23 (7)**,** 1342-53.

Kreahling, J.M., Foroutan, P., Reed, D., Martinez, G., Razabdouski, T., Bui, M.M., Raghavan, M., Letson, D., Gillies, R.J. & Altiok, S. (2013) Wee1 inhibition by MK-1775 leads to tumor inhibition and enhances efficacy of gemcitabine in human sarcomas. *PLoS One,* 8 (3)**,** e57523.

Kumagai, A. & Dunphy, W.G. (1996) Purification and molecular cloning of Plx1, a Cdc25-regulatory kinase from Xenopus egg extracts. *Science,* 273 (5280)**,** 1377-80.

Kuppers, R. (2009) The biology of Hodgkin's lymphoma. *Nat Rev Cancer,* 9 (1)**,** 15-27.

Laherty, C.D., Hu, H.M., Opipari, A.W., Wang, F. & Dixit, V.M. (1992) The Epstein-Barr virus LMP1 gene product induces A20 zinc finger protein expression by activating nuclear factor kappa B. *J Biol Chem,* 267 (34)**,** 24157-60.

Lai, E.C. (2002) Keeping a good pathway down: transcriptional repression of Notch pathway target genes by CSL proteins. *EMBO Rep,* 3 (9)**,** 840-5.

Lampert, F. & Westermann, S., (2011) A blueprint for kinetochores - new insights into the molecular mechanics of cell division. *Nat Rev Mol Cell Biol.* England, 407-12.

Landais, E., Saulquin, X. & Houssaint, E. (2005) The human T cell immune response to Epstein-Barr virus. *Int J Dev Biol,* 49 (2-3)**,** 285-92.

Laux, G., Dugrillon, F., Eckert, C., Adam, B., Zimber-Strobl, U. & Bornkamm, G.W. (1994) Identification and characterization of an Epstein-Barr virus nuclear antigen 2-responsive cis element in the bidirectional promoter region of latent membrane protein and terminal protein 2 genes. *J Virol,* 68 (11)**,** 6947-58.

Laux, G., Economou, A. & Farrell, P.J. (1989) The terminal protein gene 2 of Epstein-Barr virus is transcribed from a bidirectional latent promoter region. *J Gen Virol,* 70 (Pt 11)**,** 3079-84.

Laux, G., Perricaudet, M. & Farrell, P.J. (1988) A spliced Epstein-Barr virus gene expressed in immortalized lymphocytes is created by circularization of the linear viral genome. *Embo j,* 7 (3)**,** 769-74.

Le Roux, A., Berebbi, M., Moukaddem, M., Perricaudet, M. & Joab, I. (1993) Identification of a short amino acid sequence essential for efficient nuclear targeting of the Epstein-Barr virus nuclear antigen 3A. *J Virol,* 67 (3)**,** 1716-20.

Le Roux, A., Kerdiles, B., Walls, D., Dedieu, J.F. & Perricaudet, M. (1994) The Epstein-Barr virus determined nuclear antigens EBNA-3A, -3B, and -3C repress EBNA-2-mediated transactivation of the viral terminal protein 1 gene promoter. *Virology,* 205 (2)**,** 596-602.

Lee, S., Sakakibara, S., Maruo, S., Zhao, B., Calderwood, M.A., Holthaus, A.M., Lai, C.Y., Takada, K., Kieff, E. & Johannsen, E. (2009) Epstein-Barr virus nuclear protein 3C domains necessary for lymphoblastoid cell growth: interaction with RBP-Jkappa regulates TCL1. *J Virol,* 83 (23)**,** 12368-77.

Lenart, P., Petronczki, M., Steegmaier, M., Di Fiore, B., Lipp, J.J., Hoffmann, M., Rettig, W.J., Kraut, N. & Peters, J.M. (2007) The small-molecule inhibitor BI 2536 reveals novel insights into mitotic roles of polo-like kinase 1. *Curr Biol,* 17 (4)**,** 304-15.

Lenormand, J.L., Dellinger, R.W., Knudsen, K.E., Subramani, S. & Donoghue, D.J. (1999) Speedy: a novel cell cycle regulator of the G2/M transition. *Embo j,* 18 (7)**,** 1869-77.

Lerner, M.R., Andrews, N.C., Miller, G. & Steitz, J.A. (1981) Two small RNAs encoded by Epstein-Barr virus and complexed with protein are precipitated by antibodies from patients with systemic lupus erythematosus. *Proc Natl Acad Sci U S A,* 78 (2)**,** 805-9.

Li, M., Chen, D., Shiloh, A., Luo, J., Nikolaev, A.Y., Qin, J. & Gu, W. (2002) Deubiquitination of p53 by HAUSP is an important pathway for p53 stabilization. *Nature,* 416 (6881)**,** 648-53.

Li, M.O., Wan, Y.Y. & Flavell, R.A. (2007) T cell-produced transforming growth factor-beta1 controls T cell tolerance and regulates Th1- and Th17-cell differentiation. *Immunity,* 26 (5)**,** 579-91.

Lin, A., Wang, S., Nguyen, T., Shire, K. & Frappier, L. (2008) The EBNA1 protein of Epstein-Barr virus functionally interacts with Brd4. *J Virol,* 82 (24)**,** 12009-19.

Lindqvist, A., Kallstrom, H., Lundgren, A., Barsoum, E. & Rosenthal, C.K. (2005) Cdc25B cooperates with Cdc25A to induce mitosis but has a unique role in activating cyclin B1-Cdk1 at the centrosome. *J Cell Biol,* 171 (1)**,** 35-45.

Lindqvist, A., van Zon, W., Karlsson Rosenthal, C. & Wolthuis, R.M. (2007) Cyclin B1-Cdk1 activation continues after centrosome separation to control mitotic progression. *PLoS Biol,* 5 (5)**,** e123.

Liu, D., Davydenko, O. & Lampson, M.A. (2012) Polo-like kinase-1 regulates kinetochore–microtubule dynamics and spindle checkpoint silencing. *The Journal of Cell Biology,* 198 (4)**,** 491-499.

Liu, J. & Kipreos, E.T. (2013) *The evolution of CDK-Activating Kinases.* Landes Bioscience.

Liu, L., Cavanaugh, J.E., Wang, Y., Sakagami, H., Mao, Z. & Xia, Z. (2003) ERK5 activation of MEF2-mediated gene expression plays a critical role in BDNF-promoted survival of developing but not mature cortical neurons. *Proc Natl Acad Sci U S A,* 100 (14)**,** 8532-7.

Liu, X. & Cohen, J.I. (2015) The role of PI3K/Akt in human herpesvirus infection: From the bench to the bedside. *Virology,* 479-480**,** 568-77.

Lloyd, R.V., Erickson, L.A., Jin, L., Kulig, E., Qian, X., Cheville, J.C. & Scheithauer, B.W. (1999) p27kip1: a multifunctional cyclin-dependent kinase inhibitor with prognostic significance in human cancers. *Am J Pathol,* 154 (2)**,** 313-23.

Lohka, M.J., Hayes, M.K. & Maller, J.L. (1988) Purification of maturation-promoting factor, an intracellular regulator of early mitotic events. *Proc Natl Acad Sci U S A,* 85 (9)**,** 3009-13.

Longnecker, R., Kieff, E. & Cohen, J.I. (2013) *Epstein-Barr virus.* 6th ed.1898–1959 Fields virology.

Lucchesi, W., Brady, G., Dittrich-Breiholz, O., Kracht, M., Russ, R. & Farrell, P.J. (2008) Differential gene regulation by Epstein-Barr virus type 1 and type 2 EBNA2. *J Virol,* 82 (15)**,** 7456-66.

Lupton, S. & Levine, A.J. (1985) Mapping genetic elements of Epstein-Barr virus that facilitate extrachromosomal persistence of Epstein-Barr virus-derived plasmids in human cells. *Mol Cell Biol,* 5 (10)**,** 2533-42.

Magrath, I. (1990) The pathogenesis of Burkitt's lymphoma. *Adv Cancer Res,* 55**,** 133-270.

Magrath, I., Jain, V. & Bhatia, K. (1992) Epstein-Barr virus and Burkitt's lymphoma. *Semin Cancer Biol,* 3 (5)**,** 285-95.

Maier, S., Staffler, G., Hartmann, A., Hock, J., Henning, K., Grabusic, K., Mailhammer, R., Hoffmann, R., Wilmanns, M., Lang, R., Mages, J. & Kempkes, B. (2006) Cellular target genes of Epstein-Barr virus nuclear antigen 2. *J Virol,* 80 (19)**,** 9761-71.

Malumbres, M. & Pérez De Castro, I. (2014) Aurora kinase A inhibitors: Promising agents in antitumoral therapy. *Expert Opinion on Therapeutic Targets,* 18 (12)**,** 1377-1393.

Malvezzi, F., Litos, G., Schleiffer, A., Heuck, A., Mechtler, K., Clausen, T. & Westermann, S. (2013) A structural basis for kinetochore recruitment of the Ndc80 complex via two distinct centromere receptors. *The EMBO Journal,* 32 (3)**,** 409-423.

Martini, M., De Santis, M.C., Braccini, L., Gulluni, F. & Hirsch, E. (2014) PI3K/AKT signaling pathway and cancer: an updated review. *Ann Med,* 46 (6)**,** 372-83.

Maruo, S., Johannsen, E., Illanes, D., Cooper, A., Zhao, B. & Kieff, E. (2005) Epstein-Barr virus nuclear protein 3A domains essential for growth of lymphoblasts: transcriptional regulation through RBP-Jkappa/CBF1 is critical. *J Virol,* 79 (16)**,** 10171-9.

Maruo, S., Wu, Y., Ishikawa, S., Kanda, T., Iwakiri, D. & Takada, K. (2006) Epstein-Barr virus nuclear protein EBNA3C is required for cell cycle progression and growth maintenance of lymphoblastoid cells. *Proc Natl Acad Sci U S A,* 103 (51)**,** 19500-5.

Maruo, S., Wu, Y., Ito, T., Kanda, T., Kieff, E.D. & Takada, K. (2009) Epstein-Barr virus nuclear protein EBNA3C residues critical for maintaining lymphoblastoid cell growth. *Proc Natl Acad Sci U S A,* 106 (11)**,** 4419-24.

Maruo, S., Zhao, B., Johannsen, E., Kieff, E., Zou, J. & Takada, K. (2011) Epstein-Barr virus nuclear antigens 3C and 3A maintain lymphoblastoid cell growth by repressing p16INK4A and p14ARF expression. *Proc Natl Acad Sci U S A,* 108 (5)**,** 1919-24.

Masui, Y. & Markert, C.L. (1971) Cytoplasmic control of nuclear behavior during meiotic maturation of frog oocytes. *J Exp Zool,* 177 (2)**,** 129-45.

Maunders, M.J., Petti, L. & Rowe, M. (1994) Precipitation of the Epstein-Barr virus protein EBNA 2 by an EBNA 3c-specific monoclonal antibody. *J Gen Virol,* 75 (Pt 4)**,** 769-78.

McCann, E.M., Kelly, G.L., Rickinson, A.B. & Bell, A.I. (2001) Genetic analysis of the Epstein-Barr virus-coded leader protein EBNA-LP as a co-activator of EBNA2 function. *J Gen Virol,* 82 (Pt 12)**,** 3067-79.

McClellan, M.J., Khasnis, S., Wood, C.D., Palermo, R.D., Schlick, S.N., Kanhere, A.S., Jenner, R.G. & West, M.J. (2012) Downregulation of integrin receptor-signaling genes by Epstein-Barr virus EBNA 3C via promoter-proximal and -distal binding elements. *J Virol,* 86 (9)**,** 5165-78.

McClellan, M.J., Wood, C.D., Ojeniyi, O., Cooper, T.J., Kanhere, A., Arvey, A., Webb, H.M., Palermo, R.D., Harth-Hertle, M.L., Kempkes, B., Jenner, R.G. & West, M.J. (2013)

Modulation of enhancer looping and differential gene targeting by Epstein-Barr virus transcription factors directs cellular reprogramming. *PLoS Pathog,* 9 (9), e1003636.

McGowan, C.H. & Russell, P. (1993) Human Wee1 kinase inhibits cell division by phosphorylating p34cdc2 exclusively on Tyr15. *Embo j,* 12 (1), 75-85.

Menezes, J., Leibold, W., Klein, G. & Clements, G. (1975) Establishment and characterization of an Epstein-Barr virus (EBC)-negative lymphoblastoid B cell line (BJA-B) from an exceptional, EBV-genome-negative African Burkitt's lymphoma. *Biomedicine,* 22 (4), 276-84.

Meselson, M. & Stahl, F.W. (1958) THE REPLICATION OF DNA IN ESCHERICHIA COLI. *Proc Natl Acad Sci U S A,* 44 (7), 671-82.

Miller, C.L., Longnecker, R. & Kieff, E. (1993) Epstein-Barr virus latent membrane protein 2A blocks calcium mobilization in B lymphocytes. *J Virol,* 67 (6), 3087-94.

Monroe, J.G. (2006) ITAM-mediated tonic signalling through pre-BCR and BCR complexes. *Nat Rev Immunol,* 6 (4), 283-94.

Moormann, A.M., Chelimo, K., Sumba, P.O., Tisch, D.J., Rochford, R. & Kazura, J.W. (2007) Exposure to holoendemic malaria results in suppression of Epstein-Barr virus-specific T cell immunosurveillance in Kenyan children. *J Infect Dis,* 195 (6), 799-808.

Morgan, D. (2007) *The Cell Cycle:Principles of Control.* New Science Press.

Morgan, D.O. (1997) Cyclin-dependent kinases: engines, clocks, and microprocessors. *Annu Rev Cell Dev Biol,* 13, 261-91.

Mueller, P.R., Coleman, T.R. & Dunphy, W.G. (1995) Cell cycle regulation of a Xenopus Wee1-like kinase. *Mol Biol Cell,* 6 (1), 119-34.

Murray, P. & Bell, A. (2015) Contribution of the Epstein-Barr Virus to the Pathogenesis of Hodgkin Lymphoma. *Curr Top Microbiol Immunol,* 390 (Pt 1), 287-313.

Murray, P.G. & Young, L.S. (2001) Epstein-Barr virus infection: basis of malignancy and potential for therapy. *Expert reviews in molecular medicine,* 3 (28), 1-20.

Nakahata, S., Katsu, Y., Mita, K., Inoue, K., Nagahama, Y. & Yamashita, M. (2001) Biochemical identification of Xenopus Pumilio as a sequence-specific cyclin B1 mRNA-binding protein that physically interacts with a Nanos homolog, Xcat-2, and a cytoplasmic polyadenylation element-binding protein. *J Biol Chem,* 276 (24), 20945-53.

Nguyen, L., Papenhausen, P. & Shao, H. (2017) The Role of c-MYC in B-Cell Lymphomas: Diagnostic and Molecular Aspects. *Genes (Basel),* 8 (4).

Niculescu, F., Badea, T. & Rus, H. (1999) Sublytic C5b-9 induces proliferation of human aortic smooth muscle cells: role of mitogen activated protein kinase and phosphatidylinositol 3-kinase. *Atherosclerosis,* 142 (1)**,** 47-56.

Niederman, J.C., Miller, G., Pearson, H.A., Pagano, J.S. & Dowaliby, J.M. (1976) Infectious mononucleosis. Epstein Barr virus shedding in saliva and the oropharynx. *New England Journal of Medicine,* 294 (25)**,** 1355-1359.

Niemann, C.U. & Wiestner, A. (2013) B-cell receptor signaling as a driver of lymphoma development and evolution. *Semin Cancer Biol,* 23 (6)**,** 410-21.

Niiro, H. & Clark, E.A. (2002) Regulation of B-cell fate by antigen-receptor signals. *Nature Reviews Immunology,* 2 (12)**,** 945-956.

Niiro, H. & Clark, E.A. (2003) Branches of the B cell antigen receptor pathway are directed by protein conduits Bam32 and Carma1. *Immunity,* 19 (5)**,** 637-40.

Nishino, T., Rago, F., Hori, T., Tomii, K., Cheeseman, I.M. & Fukagawa, T. (2013) CENP-T provides a structural platform for outer kinetochore assembly. *Embo j,* 32 (3)**,** 424-36.

Nonkwelo, C., Skinner, J., Bell, A., Rickinson, A. & Sample, J. (1996) Transcription start sites downstream of the Epstein-Barr virus (EBV) Fp promoter in early-passage Burkitt lymphoma cells define a fourth promoter for expression of the EBV EBNA-1 protein. *J Virol,* 70 (1)**,** 623-7.

Nurse, P. & Thuriaux, P. (1980) Regulatory genes controlling mitosis in the fission yeast Schizosaccharomyces pombe. *Genetics,* 96 (3)**,** 627-37.

Ok, C.Y., Li, L. & Young, K.H. (2015) EBV-driven B-cell lymphoproliferative disorders: from biology, classification and differential diagnosis to clinical management. *Exp Mol Med,* 47**,** e132.

Old, L.J., Boyse, E.A., Oettgen, H.F., Harven, E.D., Geering, G., Williamson, B. & Clifford, P. (1966) Precipitating antibody in human serum to an antigen present in cultured burkitt's lymphoma cells. *Proc Natl Acad Sci U S A,* 56 (6)**,** 1699-704.

Padmanabhan, K. & Richter, J.D. (2006) Regulated Pumilio-2 binding controls RINGO/Spy mRNA translation and CPEB activation. *Genes Dev,* 20 (2)**,** 199-209.

Pan, Y.R., Vatsyayan, J., Chang, Y.S. & Chang, H.Y. (2008) Epstein-Barr virus latent membrane protein 2A upregulates UDP-glucose dehydrogenase gene expression via ERK and PI3K/Akt pathway. *Cell Microbiol,* 10 (12)**,** 2447-60.

Parker, G.A., Crook, T., Bain, M., Sara, E.A., Farrell, P.J. & Allday, M.J. (1996) Epstein-Barr virus nuclear antigen (EBNA)3C is an immortalizing oncoprotein with similar properties to adenovirus E1A and papillomavirus E7. *Oncogene,* 13 (12)**,** 2541-9.

Parker, G.A., Touitou, R. & Allday, M.J. (2000) Epstein-Barr virus EBNA3C can disrupt multiple cell cycle checkpoints and induce nuclear division divorced from cytokinesis. *Oncogene,* 19 (5)**,** 700-9.

Parker, L.L., Atherton-Fessler, S., Lee, M.S., Ogg, S., Falk, J.L., Swenson, K.I. & Piwnica-Worms, H. (1991) Cyclin promotes the tyrosine phosphorylation of p34cdc2 in a wee1+ dependent manner. *Embo j,* 10 (5)**,** 1255-63.

Parker, L.L. & Piwnica-Worms, H. (1992) Inactivation of the p34cdc2-cyclin B complex by the human WEE1 tyrosine kinase. *Science,* 257 (5078)**,** 1955-7.

Paschos, K., Parker, G.A., Watanatanasup, E., White, R.E. & Allday, M.J. (2012) BIM promoter directly targeted by EBNA3C in polycomb-mediated repression by EBV. *Nucleic Acids Res,* 40 (15)**,** 7233-46.

Patra, D. & Dunphy, W.G. (1998) Xe-p9, a Xenopus Suc1/Cks protein, is essential for the Cdc2-dependent phosphorylation of the anaphase- promoting complex at mitosis. *Genes Dev,* 12 (16)**,** 2549-59.

Patra, D., Wang, S.X., Kumagai, A. & Dunphy, W.G. (1999) The xenopus Suc1/Cks protein promotes the phosphorylation of G(2)/M regulators. *J Biol Chem,* 274 (52)**,** 36839-42.

Pei, Y., Lewis, A.E. & Robertson, E.S. (2017) Current Progress in EBV-Associated B-Cell Lymphomas. *Adv Exp Med Biol,* 1018**,** 57-74.

Pellet, E.R. & Roizman, B. (2013) *Herpesviridae.* 6th ed.1803–1822 Fields virology.

Peng, R., Tan, J. & Ling, P.D. (2000) Conserved regions in the Epstein-Barr virus leader protein define distinct domains required for nuclear localization and transcriptional cooperation with EBNA2. *J Virol,* 74 (21)**,** 9953-63.

Penn, I. (2000) Cancers in renal transplant recipients. *Adv Ren Replace Ther,* 7 (2)**,** 147-56.

Perry, J.A. & Kornbluth, S. (2007) Cdc25 and Wee1: analogous opposites? *Cell Div,* 2**,** 12.

Peter, M. & Herskowitz, I. (1994) Joining the complex: cyclin-dependent kinase inhibitory proteins and the cell cycle. *Cell,* 79 (2)**,** 181-4.

Petri, E.T., Errico, A., Escobedo, L., Hunt, T. & Basavappa, R. (2007) The crystal structure of human cyclin B. *Cell Cycle,* 6 (11)**,** 1342-9.

Pierce, B.G., Wiehe, K., Hwang, H., Kim, B.H., Vreven, T. & Weng, Z. (2014) ZDOCK server: interactive docking prediction of protein-protein complexes and symmetric multimers. *Bioinformatics,* 30 (12)**,** 1771-3.

Pierce, S.K. (2002) Lipid rafts and B-cell activation. *Nat Rev Immunol,* 2 (2)**,** 96-105.

Pines, J. & Hunter, T. (1991) Human cyclins A and B1 are differentially located in the cell and undergo cell cycle-dependent nuclear transport. *J Cell Biol,* 115 (1)**,** 1-17.

Portal, D., Zhou, H., Zhao, B., Kharchenko, P.V., Lowry, E., Wong, L., Quackenbush, J., Holloway, D., Jiang, S., Lu, Y. & Kieff, E. (2013) Epstein-Barr virus nuclear antigen leader protein localizes to promoters and enhancers with cell transcription factors and EBNA2. *Proc Natl Acad Sci U S A,* 110 (46)**,** 18537-42.

Porter, L.A., Dellinger, R.W., Tynan, J.A., Barnes, E.A., Kong, M., Lenormand, J.L. & Donoghue, D.J. (2002) Human Speedy: a novel cell cycle regulator that enhances proliferation through activation of Cdk2. *J Cell Biol,* 157 (3)**,** 357-66.

Portis, T. & Longnecker, R. (2004) Epstein-Barr virus (EBV) LMP2A mediates B-lymphocyte survival through constitutive activation of the Ras/PI3K/Akt pathway. *Oncogene,* 23 (53)**,** 8619-28.

Qi, W., Tang, Z. & Yu, H. (2006) Phosphorylation- and polo-box-dependent binding of Plk1 to Bub1 is required for the kinetochore localization of Plk1. *Mol Biol Cell,* 17 (8)**,** 3705-16.

Quenault, T., Lithgow, T. & Traven, A. (2011) PUF proteins: repression, activation and mRNA localization. *Trends Cell Biol,* 21 (2)**,** 104-12.

Raab-Traub, N., Flynn, K., Pearson, G., Huang, A., Levine, P., Lanier, A. & Pagano, J. (1987) The differentiated form of nasopharyngeal carcinoma contains Epstein-Barr virus DNA. *Int J Cancer,* 39 (1)**,** 25-9.

Radkov, S.A., Bain, M., Farrell, P.J., West, M., Rowe, M. & Allday, M.J. (1997) Epstein-Barr virus EBNA3C represses Cp, the major promoter for EBNA expression, but has no effect on the promoter of the cell gene CD21. *J Virol,* 71 (11)**,** 8552-62.

Radkov, S.A., Touitou, R., Brehm, A., Rowe, M., West, M., Kouzarides, T. & Allday, M.J. (1999) Epstein-Barr virus nuclear antigen 3C interacts with histone deacetylase to repress transcription. *J Virol,* 73 (7)**,** 5688-97.

Reisman, D. & Sugden, B. (1986) trans activation of an Epstein-Barr viral transcriptional enhancer by the Epstein-Barr viral nuclear antigen 1. *Mol Cell Biol,* 6 (11)**,** 3838-46.

Rickert, R.C. (2013) New insights into pre-BCR and BCR signalling with relevance to B cell malignancies. *Nat Rev Immunol,* 13 (8)**,** 578-91.

Rickinson, A.B., Young, L.S. & Rowe, M. (1987) Influence of the Epstein-Barr virus nuclear antigen EBNA 2 on the growth phenotype of virus-transformed B cells. *J Virol,* 61 (5)**,** 1310-7.

Rieder, C.L. (1982) The formation, structure, and composition of the mammalian kinetochore and kinetochore fiber. *International Review of Cytology,* Vol. 79**,** 1-58.

Robertson, E. & Kieff, E. (1995) Reducing the complexity of the transforming Epstein-Barr virus genome to 64 kilobase pairs. *J Virol,* 69 (2)**,** 983-93.

Robertson, E.S., Grossman, S., Johannsen, E., Miller, C., Lin, J., Tomkinson, B. & Kieff, E. (1995) Epstein-Barr virus nuclear protein 3C modulates transcription through interaction with the sequence-specific DNA-binding protein J kappa. *J Virol,* 69 (5)**,** 3108-16.

Robertson, E.S., Lin, J. & Kieff, E. (1996) The amino-terminal domains of Epstein-Barr virus nuclear proteins 3A, 3B, and 3C interact with RBPJ(kappa). *J Virol,* 70 (5)**,** 3068-74.

Rochford, R., Cannon, M.J. & Moormann, A.M., (2005) Endemic Burkitt's lymphoma: a polymicrobial disease? *Nat Rev Microbiol.* England, 182-7.

Rossig, L., Jadidi, A.S., Urbich, C., Badorff, C., Zeiher, A.M. & Dimmeler, S. (2001) Akt-dependent phosphorylation of p21(Cip1) regulates PCNA binding and proliferation of endothelial cells. *Mol Cell Biol,* 21 (16)**,** 5644-57.

Rovedo, M. & Longnecker, R. (2007) Epstein-barr virus latent membrane protein 2B (LMP2B) modulates LMP2A activity. *J Virol,* 81 (1)**,** 84-94.

Rowe, D.T., Rowe, M., Evan, G.I., Wallace, L.E., Farrell, P.J. & Rickinson, A.B. (1986) Restricted expression of EBV latent genes and T-lymphocyte-detected membrane antigen in Burkitt's lymphoma cells. *Embo j,* 5 (10)**,** 2599-607.

Ruppert, J.G., Samejima, K., Platani, M., Molina, O., Kimura, H., Jeyaprakash, A.A., Ohta, S. & Earnshaw, W.C. (2018) HP1alpha targets the chromosomal passenger complex for activation at heterochromatin before mitotic entry. *Embo j,* 37 (6).

Rus, H.G., Niculescu, F. & Shin, M.L. (1996) Sublytic complement attack induces cell cycle in oligodendrocytes. *J Immunol,* 156 (12)**,** 4892-900.

Rus, V., Nguyen, V., Tatomir, A., Lees, J.R., Mekala, A.P., Boodhoo, D., Tegla, C.A., Luzina, I.G., Antony, P.A., Cudrici, C.D., Badea, T.C. & Rus, H.G. (2017) RGC-32 Promotes Th17 Cell Differentiation and Enhances Experimental Autoimmune Encephalomyelitis. *J Immunol,* 198 (10)**,** 3869-3877.

Russo, A.A., Jeffrey, P.D., Patten, A.K., Massague, J. & Pavletich, N.P. (1996) Crystal structure of the p27Kip1 cyclin-dependent-kinase inhibitor bound to the cyclin A-Cdk2 complex. *Nature,* 382 (6589)**,** 325-31.

Safe, S. (2001) Transcriptional activation of genes by 17 beta-estradiol through estrogen receptor-Sp1 interactions. *Vitam Horm,* 62**,** 231-52.

Saha, A., Murakami, M., Kumar, P., Bajaj, B., Sims, K. & Robertson, E.S. (2009) Epstein-Barr virus nuclear antigen 3C augments Mdm2-mediated p53 ubiquitination and degradation by deubiquitinating Mdm2. *J Virol,* 83 (9)**,** 4652-69.

Saigusa, K., Imoto, I., Tanikawa, C., Aoyagi, M., Ohno, K., Nakamura, Y. & Inazawa, J. (2007) RGC32, a novel p53-inducible gene, is located on centrosomes during mitosis and results in G2/M arrest. *Oncogene,* 26 (8)**,** 1110-21.

Sample, J., Liebowitz, D. & Kieff, E. (1989) Two related Epstein-Barr virus membrane proteins are encoded by separate genes. *J Virol,* 63 (2)**,** 933-7.

Sample, J., Young, L., Martin, B., Chatman, T., Kieff, E. & Rickinson, A. (1990) Epstein-Barr virus types 1 and 2 differ in their EBNA-3A, EBNA-3B, and EBNA-3C genes. *J Virol,* 64 (9)**,** 4084-92.

Santaguida, S. & Musacchio, A. (2009) The life and miracles of kinetochores. *EMBO Journal,* 28 (17)**,** 2511-2531.

Saridakis, V., Sheng, Y., Sarkari, F., Holowaty, M.N., Shire, K., Nguyen, T., Zhang, R.G., Liao, J., Lee, W., Edwards, A.M., Arrowsmith, C.H. & Frappier, L. (2005) Structure of the p53 binding domain of HAUSP/USP7 bound to Epstein-Barr nuclear antigen 1 implications for EBV-mediated immortalization. *Mol Cell,* 18 (1)**,** 25-36.

Sasson, S. & Notides, A.C. (1988) Mechanism of the estrogen receptor interaction with 4-hydroxytamoxifen. *Mol Endocrinol,* 2 (4)**,** 307-12.

Schepers, A., Pich, D., Mankertz, J. & Hammerschmidt, W. (1993) cis-acting elements in the lytic origin of DNA replication of Epstein-Barr virus. *J Virol,* 67 (7)**,** 4237-45.

Schepers, A., Ritzi, M., Bousset, K., Kremmer, E., Yates, J.L., Harwood, J., Diffley, J.F. & Hammerschmidt, W. (2001) Human origin recognition complex binds to the region of the latent origin of DNA replication of Epstein-Barr virus. *Embo j,* 20 (16)**,** 4588-602.

Scherer, W.F., Syverton, J.T. & Gey, G.O. (1953) Studies on the propagation in vitro of poliomyelitis viruses. IV. Viral multiplication in a stable strain of human malignant epithelial cells (strain HeLa) derived from an epidermoid carcinoma of the cervix. *J Exp Med,* 97 (5)**,** 695-710.

Schleiffer, A., Maier, M., Litos, G., Lampert, F., Hornung, P., Mechtler, K. & Westermann, S. (2012) CENP-T proteins are conserved centromere receptors of the Ndc80 complex. *Nat Cell Biol,* 14 (6)**,** 604-13.

Schlick, S.N., Wood, C.D., Gunnell, A., Webb, H.M., Khasnis, S., Schepers, A. & West, M.J. (2011) Upregulation of the cell-cycle regulator RGC-32 in Epstein-Barr virus-immortalized cells. *PLoS One,* 6 (12)**,** e28638.

Schmitz, R., Ceribelli, M., Pittaluga, S., Wright, G. & Staudt, L.M. (2014) Oncogenic mechanisms in Burkitt lymphoma. *Cold Spring Harb Perspect Med,* 4 (2).

Schmitz, R., Young, R.M., Ceribelli, M., Jhavar, S., Xiao, W., Zhang, M., Wright, G., Shaffer, A.L., Hodson, D.J., Buras, E., Liu, X., Powell, J., Yang, Y., Xu, W., Zhao, H., Kohlhammer, H., Rosenwald, A., Kluin, P., Muller-Hermelink, H.K., Ott, G., Gascoyne, R.D., Connors, J.M., Rimsza, L.M., Campo, E., Jaffe, E.S., Delabie, J., Smeland, E.B., Ogwang, M.D., Reynolds, S.J., Fisher, R.I., Braziel, R.M., Tubbs, R.R., Cook, J.R., Weisenburger, D.D., Chan, W.C., Pittaluga, S., Wilson, W., Waldmann, T.A., Rowe, M., Mbulaiteye, S.M., Rickinson, A.B. & Staudt, L.M. (2012) Burkitt lymphoma pathogenesis and therapeutic targets from structural and functional genomics. *Nature,* 490 (7418)**,** 116-20.

Shannon-Lowe, C. & Rowe, M. (2011) Epstein-Barr Virus Infection of Polarized Epithelial Cells Via the Basolateral Surface By Memory B Cell-Mediated Transfer Infection. *PLoS Pathogens,* 7 (5).

Sherr, C.J. & Roberts, J.M. (1999) CDK inhibitors: positive and negative regulators of G1-phase progression. *Genes Dev,* 13 (12)**,** 1501-12.

Simon, J.A. & Kingston, R.E. (2009) Mechanisms of polycomb gene silencing: knowns and unknowns. *Nat Rev Mol Cell Biol,* 10 (10)**,** 697-708.

Sinclair, A.J., Palmero, I., Peters, G. & Farrell, P.J. (1994) EBNA-2 and EBNA-LP cooperate to cause G0 to G1 transition during immortalization of resting human B lymphocytes by Epstein-Barr virus. *Embo j,* 13 (14)**,** 3321-8.

Sivachandran, N., Cao, J.Y. & Frappier, L. (2010) Epstein-Barr virus nuclear antigen 1 Hijacks the host kinase CK2 to disrupt PML nuclear bodies. *J Virol,* 84 (21)**,** 11113-23.

Sivachandran, N., Sarkari, F. & Frappier, L. (2008) Epstein-Barr nuclear antigen 1 contributes to nasopharyngeal carcinoma through disruption of PML nuclear bodies. *PLoS Pathog,* 4 (10)**,** e1000170.

Skalska, L., White, R.E., Franz, M., Ruhmann, M. & Allday, M.J. (2010) Epigenetic Repression of p16(INK4A) by Latent Epstein-Barr Virus Requires the Interaction of EBNA3A and EBNA3C with CtBP. *PLoS Pathogens,* 6 (6)**,** e1000951.

Skalska, L., White, R.E., Parker, G.A., Sinclair, A.J., Paschos, K. & Allday, M.J. (2013) Induction of p16(INK4a) Is the Major Barrier to Proliferation when Epstein-Barr Virus (EBV) Transforms Primary B Cells into Lymphoblastoid Cell Lines. *PLoS Pathogens,* 9 (2)**,** e1003187.

Smith, L.D. & Ecker, R.E. (1971) The interaction of steroids with Rana pipiens Oocytes in the induction of maturation. *Dev Biol,* 25 (2)**,** 232-47.

So, L. & Fruman, D.A. (2012) PI3K signalling in B- and T-lymphocytes: new developments and therapeutic advances. *Biochem J,* 442 (3)**,** 465-81.

Song, G., Ouyang, G. & Bao, S. (2005) The activation of Akt/PKB signaling pathway and cell survival. *J Cell Mol Med,* 9 (1)**,** 59-71.

Spender, L.C. & Inman, G.J. (2012) Phosphoinositide 3-kinase/AKT/mTORC1/2 signaling determines sensitivity of Burkitt's lymphoma cells to BH3 mimetics. *Mol Cancer Res,* 10 (3)**,** 347-59.

Spender, L.C., Lucchesi, W., Bodelon, G., Bilancio, A., Karstegl, C.E., Asano, T., Dittrich-Breiholz, O., Kracht, M., Vanhaesebroeck, B. & Farrell, P.J. (2006) Cell target genes of Epstein-Barr virus transcription factor EBNA-2: induction of the p55alpha regulatory subunit of PI3-kinase and its role in survival of EREB2.5 cells. *J Gen Virol,* 87 (Pt 10)**,** 2859-67.

Stewart, S., Dawson, C.W., Takada, K., Curnow, J., Moody, C.A., Sixbey, J.W. & Young, L.S. (2004) Epstein-Barr virus-encoded LMP2A regulates viral and cellular gene expression by modulation of the NF-kappaB transcription factor pathway. *Proc Natl Acad Sci U S A,* 101 (44)**,** 15730-5.

Stokoe, D., Stephens, L.R., Copeland, T., Gaffney, P.R., Reese, C.B., Painter, G.F., Holmes, A.B., McCormick, F. & Hawkins, P.T. (1997) Dual role of phosphatidylinositol-3,4,5-trisphosphate in the activation of protein kinase B. *Science,* 277 (5325)**,** 567-70.

Styles, C.T., Paschos, K., White, R.E. & Farrell, P.J. (2018) The Cooperative Functions of the EBNA3 Proteins Are Central to EBV Persistence and Latency. *Pathogens,* 7 (1).

Szymula, A., Palermo, R.D., Bayoumy, A., Groves, I.J., Ba Abdullah, M., Holder, B. & White, R.E. (2018) Epstein-Barr virus nuclear antigen EBNA-LP is essential for transforming naive B cells, and facilitates recruitment of transcription factors to the viral genome. *PLoS Pathog,* 14 (2)**,** e1006890.

Takacs, M., Banati, F., Koroknai, A., Segesdi, J., Salamon, D., Wolf, H., Niller, H.H. & Minarovits, J. (2010) Epigenetic regulation of latent Epstein-Barr virus promoters. *Biochimica et Biophysica Acta - Gene Regulatory Mechanisms,* 1799 (3-4)**,** 228-235.

Takaki, T., Echalier, A., Brown, N.R., Hunt, T., Endicott, J.A. & Noble, M.E. (2009) The structure of CDK4/cyclin D3 has implications for models of CDK activation. *Proc Natl Acad Sci U S A,* 106 (11)**,** 4171-6.

Taylor, S.S., Hussein, D., Wang, Y., Elderkin, S. & Morrow, C.J. (2001) Kinetochore localisation and phosphorylation of the mitotic checkpoint components Bub1 and BubR1 are differentially regulated by spindle events in human cells. *J Cell Sci,* 114 (Pt 24)**,** 4385-95.

Tegla, C.A., Cudrici, C.D., Nguyen, V., Danoff, J., Kruszewski, A.M., Boodhoo, D., Mekala, A.P., Vlaicu, S.I., Chen, C., Rus, V., Badea, T.C. & Rus, H. (2015) RGC-32 is a novel regulator of the T-lymphocyte cell cycle. *Exp Mol Pathol,* 98 (3)**,** 328-37.

Tempera, I., Klichinsky, M. & Lieberman, P.M. (2011) EBV latency types adopt alternative chromatin conformations. *PLoS Pathog,* 7 (7)**,** e1002180.

Tempera, I. & Lieberman, P.M. (2014) Epigenetic regulation of EBV persistence and oncogenesis. *Semin Cancer Biol,* 26**,** 22-9.

Thorley-Lawson, D.A. & Gross, A. (2004) Persistence of the Epstein-Barr Virus and the Origins of Associated Lymphomas. *New England Journal of Medicine,* 350 (13)**,** 1328-1337.

Tomkinson, B., Robertson, E. & Kieff, E. (1993) Epstein-Barr virus nuclear proteins EBNA-3A and EBNA-3C are essential for B-lymphocyte growth transformation. *J Virol,* 67 (4)**,** 2014-25.

Touitou, R., Hickabottom, M., Parker, G., Crook, T. & Allday, M.J. (2001) Physical and functional interactions between the corepressor CtBP and the Epstein-Barr virus nuclear antigen EBNA3C. *J Virol,* 75 (16)**,** 7749-55.

Toyoshima-Morimoto, F., Taniguchi, E., Shinya, N., Iwamatsu, A. & Nishida, E. (2001) Polo-like kinase 1 phosphorylates cyclin B1 and targets it to the nucleus during prophase. *Nature,* 410 (6825)**,** 215-20.

Trivedi, M.V., Laurence, J.S. & Siahaan, T.J. (2009) The role of thiols and disulfides on protein stability. *Curr Protein Pept Sci,* 10 (6)**,** 614-25.

Tsang, C.M., Deng, W., Yip, Y.L., Zeng, M.S., Lo, K.W. & Tsao, S.W. (2014) Epstein-Barr virus infection and persistence in nasopharyngeal epithelial cells. *Chin J Cancer,* 33 (11)**,** 549-55.

Tzellos, S. & Farrell, P.J. (2012) Epstein-barr virus sequence variation-biology and disease. *Pathogens (Basel, Switzerland),* 1 (2)**,** 156-74.

Valentine, R., Dawson, C.W., Hu, C., Shah, K.M., Owen, T.J., Date, K.L., Maia, S.P., Shao, J., Arrand, J.R., Young, L.S. & O'Neil, J.D. (2010) Epstein-Barr virus-encoded

EBNA1 inhibits the canonical NF-kappaB pathway in carcinoma cells by inhibiting IKK phosphorylation. *Mol Cancer,* 9**,** 1.

Vermeulen, K., Van Bockstaele, D.R. & Berneman, Z.N. (2003) The cell cycle: A review of regulation, deregulation and therapeutic targets in cancer. *Cell Proliferation,* 36 (3)**,** 131-149.

Waltzer, L., Bourillot, P.Y., Sergeant, A. & Manet, E. (1995) RBP-J kappa repression activity is mediated by a co-repressor and antagonized by the Epstein-Barr virus transcription factor EBNA2. *Nucleic Acids Res,* 23 (24)**,** 4939-45.

Waltzer, L., Logeat, F., Brou, C., Israel, A., Sergeant, A. & Manet, E. (1994) The human J kappa recombination signal sequence binding protein (RBP-J kappa) targets the Epstein-Barr virus EBNA2 protein to its DNA responsive elements. *Embo j,* 13 (23)**,** 5633-8.

Wang, A., Welch, R., Zhao, B., Ta, T., Keles, S. & Johannsen, E. (2015) Epstein-Barr Virus Nuclear Antigen 3 (EBNA3) Proteins Regulate EBNA2 Binding to Distinct RBPJ Genomic Sites. *J Virol,* 90 (6)**,** 2906-19.

Wang, F., Gregory, C., Sample, C., Rowe, M., Liebowitz, D., Murray, R., Rickinson, A. & Kieff, E. (1990) Epstein-Barr virus latent membrane protein (LMP1) and nuclear proteins 2 and 3C are effectors of phenotypic changes in B lymphocytes: EBNA-2 and LMP1 cooperatively induce CD23. *J Virol,* 64 (5)**,** 2309-18.

Wang, Z., Chen, W., Zhang, Y., Xu, L. & Wang, Q. (2014) Diagnostic value of circulating microRNAs for nasopharyngeal cancer: a systematic review and meta-analysis. *J Cancer Res Ther,* 10 Suppl**,** C173-8.

Ward, M.H., Pan, W.H., Cheng, Y.J., Li, F.H., Brinton, L.A., Chen, C.J., Hsu, M.M., Chen, I.H., Levine, P.H., Yang, C.S. & Hildesheim, A. (2000) Dietary exposure to nitrite and nitrosamines and risk of nasopharyngeal carcinoma in Taiwan. *Int J Cancer,* 86 (5)**,** 603-9.

Watanabe, N., Arai, H., Nishihara, Y., Taniguchi, M., Hunter, T. & Osada, H. (2004) M-phase kinases induce phospho-dependent ubiquitination of somatic Wee1 by SCFbeta-TrCP. *Proc Natl Acad Sci U S A,* 101 (13)**,** 4419-24.

Weiss, L.M., Movahed, L.A., Warnke, R.A. & Sklar, J. (1989) Detection of Epstein-Barr viral genomes in Reed-Sternberg cells of Hodgkin's disease. *N Engl J Med,* 320 (8)**,** 502-6.

Welburn, J.P., Tucker, J.A., Johnson, T., Lindert, L., Morgan, M., Willis, A., Noble, M.E. & Endicott, J.A. (2007) How tyrosine 15 phosphorylation inhibits the activity of cyclin-dependent kinase 2-cyclin A. *J Biol Chem,* 282 (5)**,** 3173-81.

Wheatley, S.P., Hinchcliffe, E.H., Glotzer, M., Hyman, A.A., Sluder, G. & Wang, Y. (1997) CDK1 inactivation regulates anaphase spindle dynamics and cytokinesis in vivo. *J Cell Biol,* 138 (2)**,** 385-93.

White, R.E., Groves, I.J., Turro, E., Yee, J., Kremmer, E. & Allday, M.J. (2010) Extensive co-operation between the Epstein-Barr virus EBNA3 proteins in the manipulation of host gene expression and epigenetic chromatin modification. *PLoS One,* 5 (11)**,** e13979.

Woisetschlaeger, M., Yandava, C.N., Furmanski, L.A., Strominger, J.L. & Speck, S.H. (1990) Promoter switching in Epstein-Barr virus during the initial stages of infection of B lymphocytes. *Proceedings of the National Academy of Sciences of the United States of America,* 87 (5)**,** 1725-1729.

Wood, C.D., Veenstra, H., Khasnis, S., Gunnell, A., Webb, H.M., Shannon-Lowe, C., Andrews, S., Osborne, C.S. & West, M.J. (2016) MYC activation and BCL2L11 silencing by a tumour virus through the large-scale reconfiguration of enhancer-promoter hubs. *eLife,* 5**,** e18270.

Wood, V.H., O'Neil, J.D., Wei, W., Stewart, S.E., Dawson, C.W. & Young, L.S. (2007) Epstein-Barr virus-encoded EBNA1 regulates cellular gene transcription and modulates the STAT1 and TGFbeta signaling pathways. *Oncogene,* 26 (28)**,** 4135-47.

Yam-Puc, J.C., Zhang, L., Zhang, Y. & Toellner, K.M. (2018) Role of B-cell receptors for B-cell development and antigen-induced differentiation. *F1000Res,* 7**,** 429.

Yandava, C.N. & Speck, S.H. (1992) Characterization of the deletion and rearrangement in the BamHI C region of the X50-7 Epstein-Barr virus genome, a mutant viral strain which exhibits constitutive BamHI W promoter activity. *J Virol,* 66 (9)**,** 5646-50.

Yang, Z.R., Thomson, R., McNeil, P. & Esnouf, R.M. (2005) RONN: the bio-basis function neural network technique applied to the detection of natively disordered regions in proteins. *Bioinformatics,* 21 (16)**,** 3369-76.

Yates, J.L., Camiolo, S.M. & Bashaw, J.M. (2000) The minimal replicator of Epstein-Barr virus oriP. *J Virol,* 74 (10)**,** 4512-22.

Yokoyama, A., Tanaka, M., Matsuda, G., Kato, K., Kanamori, M., Kawasaki, H., Hirano, H., Kitabayashi, I., Ohki, M., Hirai, K. & Kawaguchi, Y. (2001) Identification of major phosphorylation sites of Epstein-Barr virus nuclear antigen leader protein (EBNA-LP): ability of EBNA-LP to induce latent membrane protein 1 cooperatively with EBNA-2 is regulated by phosphorylation. *J Virol,* 75 (11)**,** 5119-28.

Young, L.S. & Dawson, C.W. (2014) Epstein-Barr virus and nasopharyngeal carcinoma. *Chin J Cancer,* 33 (12)**,** 581-90.

Young, L.S. & Murray, P.G. (2003) Epstein-Barr virus and oncogenesis: From latent genes to tumours. *Oncogene,* 22 (33 REV. ISS. 2)**,** 5108-5121.

Young, L.S. & Rickinson, A.B. (2004) Epstein-Barr virus: 40 years on. *Nature Reviews Cancer,* 4 (10)**,** 757-768.

Young, L.S., Yap, L.F. & Murray, P.G. (2016) Epstein-Barr virus: more than 50 years old and still providing surprises. *Nat Rev Cancer,* 16 (12)**,** 789-802.

Young, R.M. & Staudt, L.M. (2013) Targeting pathological B cell receptor signalling in lymphoid malignancies. *Nat Rev Drug Discov,* 12 (3)**,** 229-43.

Yu, M.C., Ho, J.H., Ross, R.K. & Henderson, B.E. (1981) Nasopharyngeal carcinoma in Chinese---salted fish or inhaled smoke? *Prev Med,* 10 (1)**,** 15-24.

Zech, L., Haglund, U., Nilsson, K. & Klein, G. (1976) Characteristic chromosomal abnormalities in biopsies and lymphoid-cell lines from patients with Burkitt and non-Burkitt lymphomas. *Int J Cancer,* 17 (1)**,** 47-56.

Zhan, F., Huang, Y., Colla, S., Stewart, J.P., Hanamura, I., Gupta, S., Epstein, J., Yaccoby, S., Sawyer, J., Burington, B., Anaissie, E., Hollmig, K., Pineda-Roman, M., Tricot, G., van Rhee, F., Walker, R., Zangari, M., Crowley, J., Barlogie, B. & Shaughnessy, J.D., Jr. (2006) The molecular classification of multiple myeloma. *Blood,* 108 (6)**,** 2020-8.

Zhang, H., Li, Y., Wang, H.B., Zhang, A., Chen, M.L., Fang, Z.X., Dong, X.D., Li, S.B., Du, Y., Xiong, D., He, J.Y., Li, M.Z., Liu, Y.M., Zhou, A.J., Zhong, Q., Zeng, Y.X., Kieff, E., Zhang, Z., Gewurz, B.E., Zhao, B. & Zeng, M.S. (2018) Ephrin receptor A2 is an epithelial cell receptor for Epstein-Barr virus entry. *Nat Microbiol,* 3 (2)**,** 1-8.

Zhang, Y., Lin, Y., Bowles, C. & Wang, F. (2004) Direct cell cycle regulation by the fibroblast growth factor receptor (FGFR) kinase through phosphorylation-dependent release of Cks1 from FGFR substrate 2. *J Biol Chem,* 279 (53)**,** 55348-54.

Zhang, Y., Liu, T., Meyer, C.A., Eeckhoute, J., Johnson, D.S., Bernstein, B.E., Nusbaum, C., Myers, R.M., Brown, M., Li, W. & Liu, X.S. (2008) Model-based analysis of ChIP-Seq (MACS). *Genome Biol,* 9 (9)**,** R137.

Zhao, B., Barrera, L.A., Ersing, I., Willox, B., Schmidt, S.C., Greenfeld, H., Zhou, H., Mollo, S.B., Shi, T.T., Takasaki, K., Jiang, S., Cahir-McFarland, E., Kellis, M., Bulyk, M.L., Kieff, E. & Gewurz, B.E. (2014) The NF-kappaB genomic landscape in lymphoblastoid B cells. *Cell Rep,* 8 (5)**,** 1595-606.

Zhao, B., Mar, J.C., Maruo, S., Lee, S., Gewurz, B.E., Johannsen, E., Holton, K., Rubio, R., Takada, K., Quackenbush, J. & Kieff, E. (2011a) Epstein-Barr virus nuclear antigen

3C regulated genes in lymphoblastoid cell lines. *Proc Natl Acad Sci U S A,* 108 (1)**,** 337-42.

Zhao, B., Maruo, S., Cooper, A., M, R.C., Johannsen, E., Kieff, E. & Cahir-McFarland, E. (2006) RNAs induced by Epstein-Barr virus nuclear antigen 2 in lymphoblastoid cell lines. *Proc Natl Acad Sci U S A,* 103 (6)**,** 1900-5.

Zhao, B., Zou, J., Wang, H., Johannsen, E., Peng, C.W., Quackenbush, J., Mar, J.C., Morton, C.C., Freedman, M.L., Blacklow, S.C., Aster, J.C., Bernstein, B.E. & Kieff, E. (2011b) Epstein-Barr virus exploits intrinsic B-lymphocyte transcription programs to achieve immortal cell growth. *Proc Natl Acad Sci U S A,* 108 (36)**,** 14902-7.

Zhou, P. & Wagner, G. (2010) Overcoming the solubility limit with solubility-enhancement tags: successful applications in biomolecular NMR studies. *J Biomol NMR,* 46 (1)**,** 23-31.